Faculty of Engineering and Science

Study of Different Acid Reaction Mechanisms during Matrix Acidizing

Mian Umer Shafiq

This thesis is presented for the Degree of
Doctor of Philosophy
of
Curtin University

October 2018

Declaration

To the best of my knowledge and belief, this thesis contains no material previously published by any other person except where due acknowledgment has been made.

This thesis contains no material which has been accepted for the award of any other degree or diploma in any university.

Signature: ……..

Date: 29/10/2018

List of Publications

- Shafiq M U., Ben Mahmud H K. and Arif M., 2018, "Mineralogy and Pore Topology Analysis during Matrix Acidizing of Tight Sandstone and Dolomite Formations Using Chelating Agents", Journal of Petroleum Science and Engineering, 167, 869–876, https://doi.org/10.1016/j.petrol.2018.02.057

- Shafiq M U., Ben Mahmud H K., 2018., "Integrated Mineral Analysis of Sandstone and Dolomite Formations Using Different Chelating Agents during Matrix Acidizing", Petroleum (KeAi), accepted, in press

- Shafiq M U., and Ben Mahmud H K., 2017., "Sandstone Matrix Acidizing Knowledge and Future Development: A Review", Journal of Petroleum Exploration and Production Technology, DOI 10.1007/s13202-017-0314-6

- Shafiq M U., Ben Mahmud H K., Rezaee R., and Testamanti N., 2017., "Investigation of Changing Pore Topology and Porosity During Matrix Acidizing using Different Chelating Agents", IOP Conf. Ser.: Mater. Sci. Eng. 217 012023, doi:10.1088/1757-899X/217/1/012023, IOP Publishing

- Shafiq M U., Ben Mahmud H K. and Rezaee R., 2017., "New Acid Combination for a successful sandstone Acidizing", IOP Conf. Ser.: Mater. Sci. Eng. 206 012010, doi:10.1088/1757-899X/206/1/012010, IOP Publishing

Abstract

To meet rising global demands for energy, the oil and gas industry continuously strives to develop innovative oilfield technologies. With the development of new enhanced oil recovery techniques, sandstone acidizing has been introduced and played a pivotal role in the petroleum industry. Different acid combinations have been applied to formation treatment, which results in minimizing the near wellbore damage and improving the well productivity. A combination of hydrofluoric acid and hydrochloric acid (HF: HCl) known as mud acid has proved to be effective in improving the porosity and permeability of the reservoir formation near to the wellbore. Hydrochloric acid (HCl) and acetic acid (CH_3COOH) are commonly used in dolomite matrix acidizing to remove damage around the wellbore and to create new pore spaces. Sandstone matrix acidizing is a complex and heterogeneous acid-rock reaction process. If improper acid treatment is implemented, further damage can be induced instead of removing the initial plug, particularly in high-temperature sandstone reservoirs. An efficient acid system is a key to successful acid treatment. High-temperature matrix acidizing is now growing since most of the wells nowadays become deeper and hotter temperature reservoirs, with a temperature higher than 150^{o}F. High-temperature sandstone treatment with conventional mud acid system faces problems including high acid-rock reaction rate which causes earlier consumption, short acid effective distance, susceptibility to secondary damage (formation of a precipitate), serious corrosion to pipelines and high change in pH value hence becoming less efficient. However, different acids have been developed to combat these problems where studies on retarded mud acids, organic-HF acids, emulsified acids and chelating agents (HEDTA, EDTA, and GLDA) have shown their effectiveness at different conditions. Using acids in core flooding acidizing in sandstone/dolomite formations is performed in the laboratory to observe different physical phenomena and to design acidizing stimulation jobs for the field. During the tests, some key parameters such as pore volume required for a breakthrough as well as pressure are analyzed. In this study, cylindrical samples with dimensions 0.0381 m. × 0.0762 m. of Berea sandstone, Colton sandstone, and Guelph dolomite underwent core flooding experiments using acids at a constant flow rate of 0.00006 m^3/sec. The core flooding experiments performed are aimed to dissolve sodium, potassium, magnesium, iron, aluminum and calcium particles from the core samples. These experiments were followed with determination of porosity, permeability of core samples and pH values of the acid samples as well analytical studies using lab-based benchtop machines, Nuclear Magnetic Resonance (NMR) logging, Inductively Coupled Plasma (ICP), Computed

Tomography (CT) scan, and Tescan Integrated Mineral Analysis (TIMA). Porosity and NMR logging analysis concluded that the 5% CH_3COOH: 10% HCl is more effective in increasing porosity while 5% HCl is more effective in increasing the permeability by creating fresh pore spaces in Berea sandstone while HEDTA is a more effective chelating agent in creating more spaces in dolomites and Colton and Berea sandstone. ICP analysis shows that more amount of positive ions (magnesium, potassium, sodium, calcium) have been dissolved by HEDTA compared to other chelates. On the other hand, GLDA was effective in dissolving more potassium and calcium from Berea sandstone. All the chelates were proved effective in dissolving iron ion. Mineralogy (TIMA analysis) concluded that (CH_3COOH: HCl) can dissolve more potassium and magnesium particles compared to the current conventional hydrochloric acid. Mineralogy analysis also concluded that chelating agents were very effective in dissolving iron minerals while HEDTA was effective in dissolving calcium minerals too. It can be concluded from these results that the combination of acetic-hydrochloric acid can also be used as a potential candidate for the preflush stage of sandstone acidizing at higher temperatures. The chelating agent (HEDTA) proved to be the best candidate for Berea sandstone, Colton sandstone, and Guelph dolomite formations. Logging (NMR analysis) established the fact that HEDTA was very effective in creating new and bigger pore paces after the acidizing. This study also explores the future development required for matrix acidizing treatments and new experimental techniques that can be useful for further development, which would provide better results and information on topology, morphology and mineral dissolution, and the challenges associated with implementing these "new" technologies.

Keywords: sandstone, acidizing, hydrocarbons, formation mineralogy, permeability, reaction mechanism

Acknowledgments

First of all, I would like to thank Allah Almighty for all blessings upon me.

I would like to express my deepest gratitude and sincere appreciation to my Supervisor Prof. Moses Tade for determined efforts to acquire core holder for my research. I would like to extend sincere appreciation to my Co-Supervisor Dr. Hisham Khaled ben Mahmud and Associate Supervisor Dr. Ali Saeedi for their constant support and guidance and encouragement during the research.

My gratitude also goes to Curtin University Malaysia for sponsoring my experimental trips to Bentley Campus, Perth. I acknowledge Curtin University Malaysia for providing me staff study support which supported me during the studies of Ph.D. without any financial tension. I am extremely grateful to the entire Petroleum Engineering Department for their contribution to my academic and intellectual development.

Needless to say, I am very thankful to all the laboratory technicians at Curtin University, Perth Australia, especially whom I worked with Bob Web and Karen Haynes, they all were very cooperative and always there for me. Special thanks to John De Laeter Center for TIMA analysis. The TESCAN Integrated Mineral Analysis (TIMA) instrument was funded by a grant from the Australian Research Council (LE140100150) and is operated by the John de Laeter Centre at Curtin University with the support of the Geological Survey of Western Australia, University of Western Australia and Murdoch University. Thanks to Sven and TSW Analytical Pty Ltd as an analyst and analytical service provider for ICP analysis.

Finally, thanks to my wife and my family for their love, prayers, understanding, and encouragement which made me work harder every day, without it, I would not be where I am now.

Contents

List of symbols

HF = Hydrofluoric acid

HCl = Hydrochloric acid

NMR = Nuclear Magnetic Resonance

ICP = Inductively Coupled Plasma

TIMA = TESCAN Integrated Mineral Analyser

CT scan = Computed Tomography

HEDTA = Hydroxyethylenediaminetetraacetic acid

EDTA = Ethylenediaminetetraacetic acid

GLDA = L-glutamic acid diacetic acid

OPEC = Organization of the Petroleum Exporting Countries

IEA = International Energy Agency

pH = Power of hydrogen ions

k_s = Stimulated permeability

k = Permeability

r_w = Wellbore radius

Ø = Porosity

HCOOH = Formic acid

H_3PO_4 = Phosphoric acid

HBF_4 = Fluoboric acid

CH_3COOH = Acetic acid

RHF= Retarded Hydrofluoric

H_3BO_3 = Boric acid

$AlCl_3$ = Aluminium chloride

KBF_4 = potassium tetrafluoroborate

ALRHF = Aluminum Retarded Hydrofluoric Acid

PRHF = Phosphonic Retarded Hydrofluoric Acid

EOR = Enhanced Oil Recovery

Na_3HEDTA = Trisodium HEDTA

HACA = Hydroxethylaminocarboxylic acid

DTPA = Diethylenetriaminepentaacetic acids

Na_2EDTA = Disodium EDTA

MIE = Multicomponent ion exchange

XRD = X-Ray Diffraction

SEM = Scanning Electron Microscope

MSA = Methanesulfonic acid

H_2SiF_6 = Fluosilicic acid

HV = Five-hydrogen complex

EDS = Energy-dispersive X-ray spectroscopy

CCS = Carbon Capture Storage

HPHT = High Pressure High Temperature conditions

HCH = Hydrostatic type Core Holders

HPLC = High Pressure Liquid chromatography

PPE = Personal Protective Equipment

P–T = Pressure - Temperature

ICP-AES = Inductively Coupled Plasma Atomic Emission Spectroscopy

PV = Pore Volume

S/V = Surface to Volume

BVI = Bulk Volume Irreducible

CBVI = Cutoff-BVI

FFI = Free Fluid Index

T_2 = Relaxation time

CBW = Clay Bound Water

NS = Number of Scans

RD = Relaxation Delay

BVM = Movable Bulk Volume

DSA = Drop Shape Analyzer

FESEM = Field Emission Scanning Electron Microscope

CL = Cathodoluminescence imaging

BSE = Backscattered Electron Imaging

SE = Secondary Electron Imaging

EDX = Energy-Dispersive X-ray

MOI = Minerals of Interest

List of Figures

List of Tables

Chapter 1
Introduction

In this research, the effect of different acids and chelating agents on dolomite and sandstone formations are discussed and evaluated. The main focus of this research is on the change of porosity, permeability, mineralogy, pore topology, pore size distribution, dissolution, particle size distribution, and wormhole propagation. In other words, determination of mechanism of acid reaction with formations. The first part of this chapter focuses on the background of matrix acidizing and significance of acids used in this research. This is followed by the outline of the problem statement, research objectives, scope and significance of this research. At the end of this chapter, a brief overview of the contents of this dissertation was presented.

1.1 Motivation for this research

According to OPEC (2016), it has been predicted that 14% more hydrocarbons maybe required by the year 2040 as compared to 2014. Table 1.1 shows the long-term reference case for the demand for oil, predicted by OPEC in 2016 (All values are MMb/d).

Table 1.1. IEA long-term reference case (OPEC, 2016)

	2015	**2020**	**2025**	**2030**	**2035**	**2040**
OECD	46.2	45.9	44.3	42.1	39.7	37.3
Developing Countries	41.5	46.8	52.2	57.4	62.0	66.1
Eurasia	5.3	5.6	5.8	6.0	6.1	6.0
World	93.0	98.3	102.3	105.5	107.8	109.4

Therefore, the production optimization from current reservoirs is inevitable. Well stimulation techniques are used to improve the flow of oil or gas from the reservoir by dissolving the rock or creating new channels around the wellbore. The most commonly applied stimulation techniques are matrix acidizing and hydraulic fracturing. In hydraulic fracturing, fluids are injected at a pressure greater than the formation failure pressure to create channels/fractures in the formation through which the production of oil or gas may increase. In acidizing, acids have been applied to the sandstone and dolomite formations to increase the formation permeability and porosity near the wellbore (Ituen et al, 2017). These acids have the ability to dissolve different minerals like quartz, dolomites, and feldspar present in reservoir rock which results

in increasing the permeability of the reservoir thus ultimately increases the flow rate of hydrocarbon fluid from the formation to the wellbore. Both of these operations (fracturing and acidizing) have their own advantages and limitations in sandstone stimulation (Shafiq & Ben Mahmud, 2017). Dolomite reservoirs are mostly soluble in acids, and acidizing in dolomite reservoirs generates conductive pathways known as "wormholes", whereas, in sandstone reservoirs, only a small portion of the rock is soluble by acids. Therefore, the goal of acidizing in sandstone formation is to dissolve minerals that are present in pores to enhance the formation permeability (Crowe et al., 1992). The choice between fracturing or acidizing a sandstone formation depends on various factors such as the geology of reservoir, its production history and well intervention objectives (Al-Harthy, 2009). A formation with high a permeability and porosity usually does not require fracturing in comparison with a tight formation with relatively low porosity and permeability, which requires hydraulic fracturing. Usually, the loosely bound formation can cause formation collapse due to the overburden pressure if posed to the hydraulic fracturing. Also, the damaged formation due to drilling and production process is not recommended to be stimulated with hydraulic fracturing instead of matrix acidizing (Shafiq & Ben Mahmud, 2017). Acid fracturing is more successful to be applied in carbonate formations with high natural fractures and high permeability (Economides et al., 2013). Figure 1.1 shows the matrix dissolution and acid fracturing during the acidizing operation.

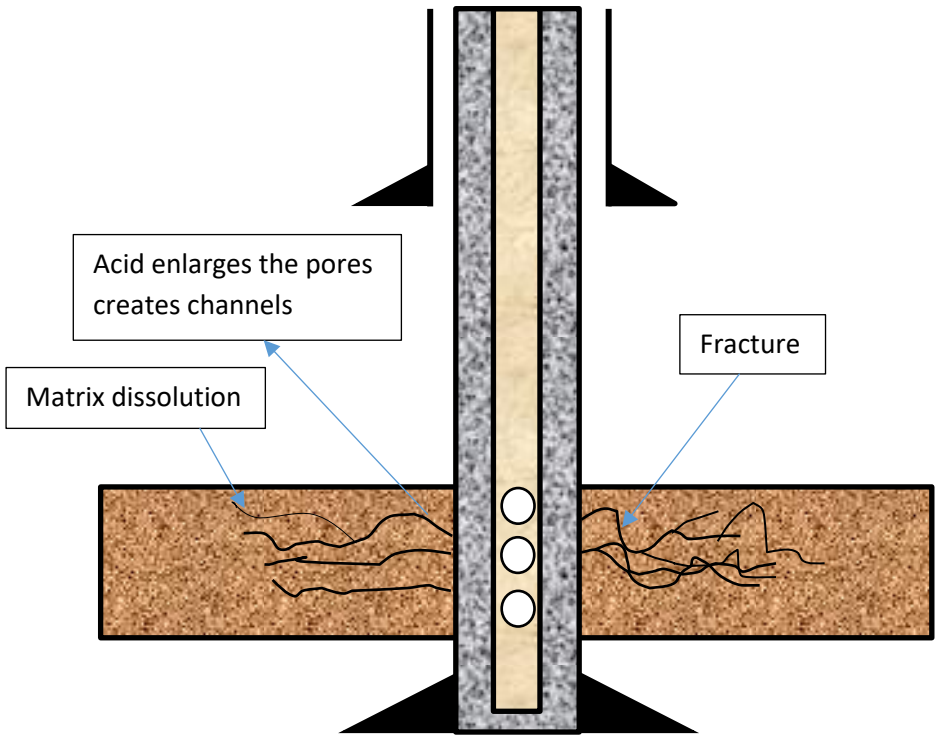

Figure 1.1. Acid fracturing and Matrix dissolution

Whenever the injection of acid is performed either at a pressure less or more than the fracture pressure of the formation, matrix dissolution occurs. Once the acid is injected with a pressure higher than the formation fracture pressure, it can create fractures (acid fracturing). Once the fractures are created, the acid then starts reacting with the formation to remove the minerals (matrix acidizing) present inside the formation and create new pore spaces and channels. In order to enhance the hydrocarbon reservoir productivity, acidizing is considered one of the most effective and common techniques in the industry (Sidaoui and Sultan., 2016). Acids play a key role in boosting production from hydrocarbon fields. Acidizing is a process in which injected fluid (mostly acid) in porous media causes reaction of minerals and chemicals. This may lead to the variation of permeability and porosity due to the dissolution of rock minerals and reprecipitation of reaction products. Different minerals like quartz, carbonates, and feldspar can be dissolved by the injection of acids. These reactions can cause dissolution of the rock matrix and formation of precipitates, which might bring about changes in the permeability and porosity of a reservoir (Shafiq et al., 2017). Drilling and production operations can cause formation damage i.e., migration of fines, mud invasion etc. (Shafiq et al., 2018). Formation damage is detrimental to the hydrocarbon recovery as it causes extra pressure drop around the vicinity of the wellbore. Therefore, the removal of formation damage is the main goal of sandstone and carbonate acidizing (Zhou et al., 2014). Thus, the original permeability of the formation can be restored or new pore spaces can be created by the application of acidizing. Therefore, the acidizing operation is performed in order to reduce the damage and maintain the productivity of the reservoir by allowing faster movement of the hydrocarbons (Zhao et al. 2015). This process can improve permeability by introducing high permeability flow paths and by removing the damage which enhances the well performance.

For many years, the most common acid in practice to acidize sandstone formation is mud acid and dolomite formations using hydrochloric acid. The mixture of hydrofluoric acid (HF) and hydrochloric acid (HCl), known as mud acid as described by Smith and Hendrickson (1965), and Abdelmoneim and Nasr-El-Din (2015), is normally applied during sandstone acidizing process to remove the damage around the wellbore, while hydrochloric acid is injected to create new wormholes in case of carbonate acidizing (Shafiq et al, 2017). Sandstone formation is usually acidized by using mud acid developed by Smith and Hendrickson (1965), and modified by Gidley (1985), while hydrochloric acid is applied on carbonate formation whose application was discussed by Buijse (1997) and Germino et al (2012) to dissolve carbonates and other

positive ions. However, the success rate of using these acids varies, even damages are reported by field studies (Thomas et al., 2002). The problems occurred are due to the disadvantages of hydrochloric acid. For example, HCl acid reacts with chlorite and precipitate iron, which may cause serious issues by choking the pore throat and thus decreasing the permeability and porosity. Secondly, corrosion may occur at high-temperature conditions, and precipitation reactions may occur due to the high reaction rate (Sepehrnoori et al., 1994). Since carbonate and sandstone formation pose different problems faced using HCl acid, it is inevitable to use other approaches as an alternative to HCl acid in carbonate and sandstone acidizing. Shafiq et al (2015 & 2016) used another acid where HCl acid has been replaced with another mineral acid to acidize sandstone formation. Unlike dolomite or carbonate acidizing, sandstone acidizing is very complex and challenging because of the involvement of a number of physical and chemical interactions between the injected acid and the formation. Therefore, appropriate selection of acid is essential to remove the damage or fines blocking the pore spaces (Nasr-El-Din et al. 2002). The complex nature of sandstone acidizing is due to the presence of some minerals which react with a specific acid only i.e., siliceous minerals can only react with hydrofluoric acid (HF) (Shafiq et al., 2018). This complexity can lead to secondary and tertiary reactions, where insoluble precipitates can form and can re-damage the formation.

It is known to be a challenging task to select an appropriate type of acid, its concentration and injection volume requirements. Different mineralogical environments and various temperature ranges influence the choice of acid to achieve specific objectives. Heterogeneous and complex nature of the sandstone formation further escalates this problem (Shafiq et al, 2018). Moreover, the chemical reaction or interactions between mineral and injected acid also depends on the morphology of the rock and the reservoir temperature in addition to chemical composition (Boyer and Wu,1983). One of the problems associated with the use of mud acid (HF: HCl) is corrosivity. Tubes made of low-carbon steel may contain rust and can be corroded by HCl acid. HCl can dissolve this rust and which in turn produces iron ions (Fe^{+3}), which can form a potential precipitate and damage the reservoir and the production well. Therefore, the corrosion inhibitor is required and the cost of inhibitor may increase up to 5% of the total cost of operation (Fredd and Fogler, 1998). Moreover, the problem with corrosion inhibitor is the change in the wettability of the rock as due to adsorption of the inhibitor on the rock surface, which becomes severe in low permeability reservoir. Gdanski (1998) and Nasr-El-Din et al. (2002), found that mud acid spent rapidly at the wellbore due to the fast reaction, which results in the creation of precipitates and less penetration of acid into the formation. The success rate of mud acid has

been reduced due to the problems like matrix unconsolidation and incompatibility of HCl with clays (like chlorite), which can cause further damage to the reservoir (Simon and Anderson 1990, Gdanski and Shuchart 1998, Nasr-El-Din et al. 2002).

During the well production, the largest pressure drop occurs in the zone around the wellbore, which is the major target for matrix acidizing. This zone usually extends (3 – 5 ft.) from the wellbore in dolomites and few inches in a sandstone formation. This zone is mainly damaged by drilling, production and completion operations like clay swelling, fines migration, drilling fluid invasion and deposition of scale during production (Al-Harthy., 2008;2009). Due to the presence of different minerals, sandstone acidizing process usually consists of multiple stages, which make it a very complicated and challenging task. During these stages, different acids react with different minerals and interactions of minerals with acids is an origin for precipitation reactions, which can be possibly dangerous and can cause a reduction in the reservoir permeability. During the process of sandstone acidizing, the resulting precipitation reactions can reduce the permeability and porosity due to damaging nature (Nasr-El-Din et al. 2011). These precipitates are: 1) Potassium and sodium silicates precipitate; 2) Calcium fluoride precipitate; 3) Precipitation of hydrated silica. Ammonium chloride (NH_4Cl) or hydrochloric acid (HCl) is used as a pre-flush ahead of the main acid in order to avoid the formation of silicates (Na_2SiF_6, K_2SiF_6) and fluorides (CaF_2). To prevent the hydrated silica precipitation; HCl or an organic acid is used in the main acid stage. However, this silica precipitates as hydrated colloid $Al_2Si_2O_5(OH)_4$ and causes a reduction in rock permeability. Therefore, three stages are conducted in sandstone matrix acidizing (Shafiq & Ben Mahmud, 2017):

1. A pre-flush stage: usually applied to remove any positive ions like (Na, K, Ca, Mg, or Fe), as these ions may react with silica especially Na and K ions to form insoluble silicates.
2. Main acid stage: usually applied to dissolve clay, feldspar and silicates and mobile fines of silica to improve permeability and porosity.
3. An after flush stage: applied to keep the wettability in original state (before acidizing) and clean the formation.

A single strong mineral acid has the ability to dissolve rock particles efficiently, by reducing formation damage, increase porosity and permeability and ultimately increase oil and gas

production. Conversely, well tabular expose to high risk of corrosions due to its high reactivity (Shepherd et al. 2016).

In this research, effects of acids and chelates on mineralogy, morphology, porosity, pore topology, pore size distribution, and permeability have been investigated at a constant temperature. Various acid combinations and chelates were examined to react with different sandstone and dolomite formations. The significance of this research is the application of new preflush acid combination followed by the application of environment-friendly chelating agents. The performed experiments are aimed to investigate the reaction mechanism of these acids and chelates with sandstone and dolomite formations. The experiments deployed have not been applied for acidizing investigation before. The successful application of chelating agents on conventional sandstones has raised interest in applying these chelates to dolomites and tight sandstone reservoirs. The impact of chelating agents on conventional sandstone, dolomite, and tight sandstone reservoirs can be understood by extensive study and research; and applying new techniques. Experimental techniques and analysis such as Tescan Integrated Mineral Analysis (TIMA), Nuclear Magnetic Resonance (NMR) Logging, and Inductively Coupled Plasma (ICP) Analysis have been used in this research to understand the effect of chelates on different formations. The main goal of this research is to overcome the problems associated with the use of hydrochloric acid. While the advantages of hydrochloric acid presented by McLeod (McLeod et al. 1983) should be maintained. In this study different analysis like NMR logging, TIMA analysis and CT scan have been performed to monitor alterations in rock at different stages of the acidizing process. In this research, NMR analysis has been applied by for the very first time on sandstone samples. This technique proved to be very useful in determining the pore space topology after acidizing (Shafiq et al, 2017).

1.2 Problem Statement

While many researchers have significantly contributed to the sandstone acidizing technology, yet many problems related to this complex phenomenon are still unsolved. These problems include fast spending of acid, corrosion of pipes due to acids, depth of penetration for the live and spent acid, and the nature of reaction products. Mud acid has been applied during sandstone matrix acidizing while hydrochloric acid (HCl) has been applied during conventional matrix acidizing in dolomite reservoirs. When the conventional acid is used in acidizing of soft formations, it may cause well enlargement due to dissolution which can lead to instability of the wellbore. In the sandstone reservoir, application of regular mud acid may cause weakening

of the clay minerals which promotes fine migration. The mobile fines are a reason for pore throat blockage and reduction in porosity and permeability by re-damaging. The formation of secondary and tertiary precipitates and inadequate penetration are due to the fast reaction of mud acid, pointing to the need to slow down the rate of acid reaction with the formation. The rapid spending of acid can lead to a condition where most of the acid reacted with the surface of the formation before penetrating into it. The main challenge for the design of sandstone acidizing lies in the complex nature of the sandstone formation. Therefore, a detailed study of the mechanisms of acid reacting with the sandstone formation is necessary for successful acidizing treatment. Moreover, due to this high reactivity acid not only poses a penetration problem but it also increases the cost of maintenance or imposes safety issues due to its corrosivity. Mostly due to the high reactivity, HF acid is used in a very low concentration (0.5% to 3% by volume) in the field to avoid fast reaction and corrosion. It has been applied to the formation or reservoir which mostly consists of quartz as HF acid can dissolve quartz.

1.3 Objectives of the Study

The purpose of this research is to study the reaction mechanisms and effects of new acid combination and chelates on sandstone and dolomite formations at elevated temperatures of 80^{o}C. This purpose is experimentally accomplished by achieving the following objectives:

1. To determine the effect of preflush acids and environment-friendly chelating agents on permeability, porosity, mineralogy, pore topology, pore size distribution and morphology of the sandstone and dolomite core samples.
2. To investigate the dissolution power of different chelates and acids towards various minerals present in the core samples.
3. To determine the reaction mechanisms of pre-flush acids with sandstone and different chelating agents with sandstone and dolomite core samples.
4. To determine the creation of wormholes in dolomite and sandstone formations using chelating agents.
5. To determine the effect of chelating agents on the wettability of the sandstone and dolomite formations.

1.4 Significance

- This research will help to furnish fresh information about sandstone and dolomite acidizing. Many hydrocarbon wells require acidizing at least once in their lifetime due

to different damages occur around the wellbore. This research will signify the importance of different chelating agents and techniques which can be applied during matrix acidizing.

- This research gives information about the role of mineralogy and pore size distribution during matrix acidizing.
- This research will investigate the importance of Nuclear Magnetic Resonance and Tescan Integrated Mineral Analysis application in matrix acidizing.

1.5 Scope of this Study

The scope of this thesis is to investigate the reaction mechanism of different acids and chelating agents with sandstone and dolomite formations by studying the change in porosity, permeability, mineralogy, pore topology, morphology and pore size distribution. In order to achieve this, core flooding experiments are to be performed first using acids and chelates on core samples followed by a series of analytical techniques like Tescan Integrated Mineral Analysis (TIMA), Nuclear Magnetic Resonance (NMR) logging, Inductively Coupled Plasma (ICP) analysis, pH value analysis and Computed Tomography (CT scan) analysis. These experiments were performed to determine the mineral dissolution, wormhole propagation, specific density particles dissolution and creation of fresh pores. Then based on these analyses most effective chelating agent for sandstone and dolomite matrix acidizing was determined. The combined results from all the techniques, methodologies and analysis applied will then be packaged together to determine the reaction mechanism in terms of mineral dissolution and pore structure by applied fluids.

1.6 Organization of the report

Chapter 1 consists of the introduction of the stimulation followed by problem statement, objectives, scope and significance. Chapter 2 consists of the theory and fundamentals of sandstone and dolomite acidizing. It also presents a detailed literature survey highlighting significant research gaps in the field of the sandstone acidizing. Advantages and limitations of different acids developed for the matrix acidizing are also discussed. Chapter 3 discusses the research methodology adopted to accomplish various objectives proposed for this study. In this chapter, materials, apparatus, and methods used are discussed in detail. Chapter 4 discusses the results and analysis of different experiments performed. This chapter includes results from ICP analysis, permeability, porosity, NMR Logging, wettability, CT scan and pH value analysis.

Chapter 5 discusses the analysis obtained by TIMA analysis which includes pore size distribution, particle size distribution, pore topology, and mineral and elemental analysis, Finally, Chapter 6 discusses the conclusion and future work which can be conducted in future for further research.

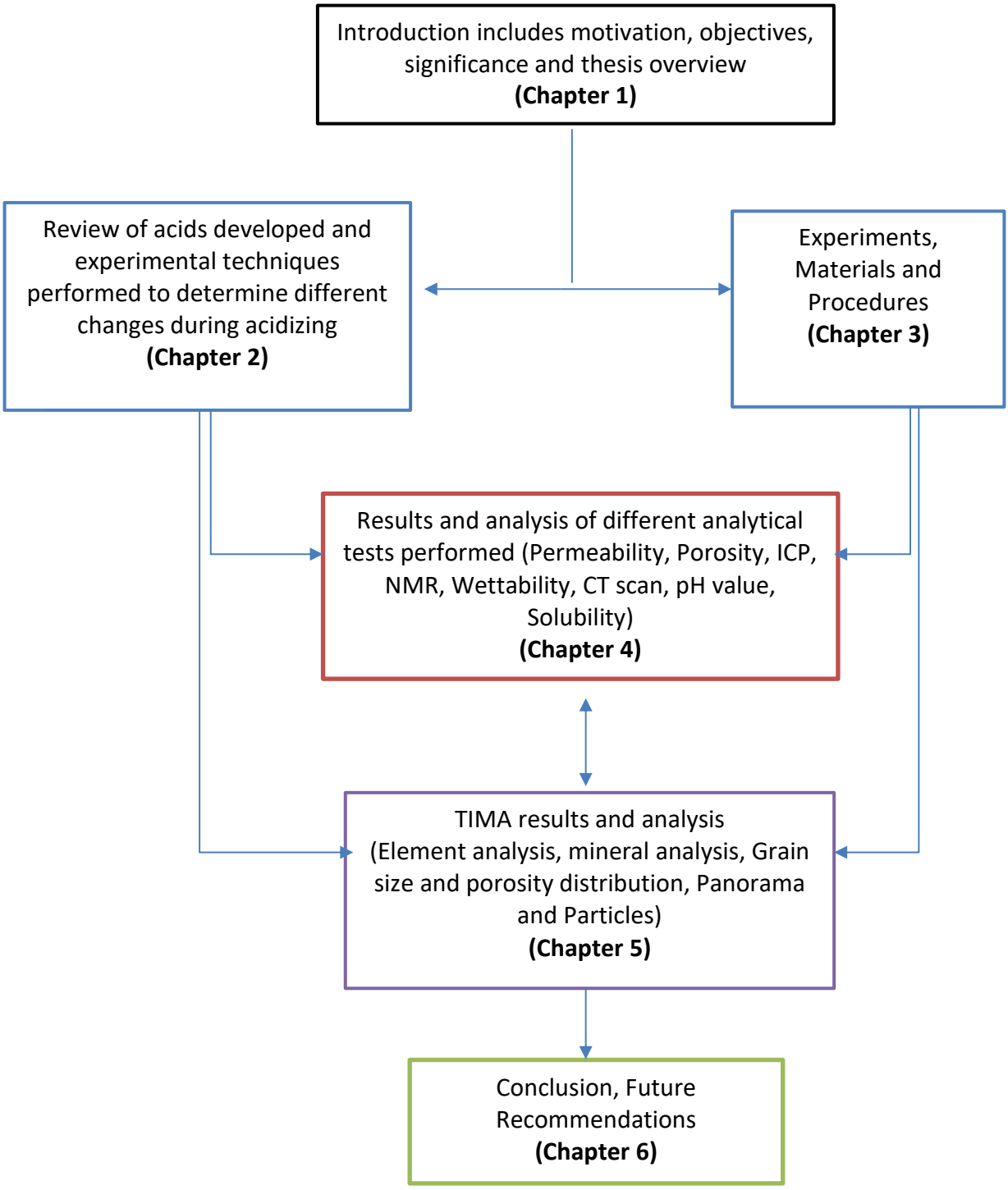

Figure 1.2. Mind map of the project

Chapter 2

Theory of Matrix Acidizing

This chapter discusses the basic fundamentals of the sandstone and carbonate matrix acidizing such as minerals present in the formation, fracture acidizing, matrix acidizing, sandstone acidizing mechanisms and reactions, stages of sandstone acidizing, carbonate/dolomite formation acidizing and aspects of additives during the acidizing operation. Creation of wormholes and conductive pathways during carbonate acidizing is also reviewed. The aspects of the successful acidizing operation are presented. Furthermore, this chapter provides information about the problems that may occur during the sandstone and carbonate matrix acidizing by the application of current technologies. In addition, the available guidelines for different acids and their field applications on different formations are also presented. This is followed by the background information on the acids developed to increase the production of hydrocarbons at different reservoir conditions and the effects of matrix acidizing on mineral dissolution in both carbonate and sandstone matrix acidizing. Finally, the relevant experimental techniques and their effects on matrix acidizing are described.

2.1 Introduction

The main aim of sandstone matrix acidizing is the dissolution of the damage around the wellbore. It is different from carbonate acidizing since it dissolves the damage around the wellbore or the fine particles which can chock or bridge the pore throats and pore spaces, thus the original permeability of the reservoir can be recovered. Hydrofluoric acid (HF) dissolves siliceous minerals and the interaction of the acid with these minerals is very complex compared to the carbonate reacting with HCl (Lund et al., 1973). It is always being a very confusing task to select an appropriate type of acid, its concentration, and volume needed for injection. Different mineralogical environment and various temperature ranges require different additives to be added with the acid. Heterogeneous and complex nature of the sandstone formation is the root cause of this problem. Moreover, the chemical reaction or interactions between the mineral and injected acid also depends on the morphology of the rock and the reservoir temperature in addition to the chemical composition (Shafiq et al., 2018). Mineralogy also plays an important role in the selection of acid for acidizing operation (Boyer and Wu., 1983).

2.1.1 Acidizing Treatment

Acidizing is one of the most commonly used techniques among all the stimulation methods applied in the oil and gas industry (Ituen., 2017). Drilling and production operations can cause the formation damage i.e., migration of fines, mud invasion etc. (Shafiq et al., 2018). While mechanical skin factor is induced by completion operations (Yildiz., 2006), the skin may be described as the variation in pressure and the flow rate in the wellbore from the original flow rate (Furui et al., 2008). The formation damage around the wellbore can cause an extra pressure drop in surrounding areas which have negative effects on the reservoir production. Therefore, the acidizing operation can be performed in order to reduce that damage and maintain the productivity of the reservoir by allowing faster movement of the hydrocarbons (Ghommem et al. 2015). This process can improve permeability by introducing high permeability flow paths and by removing the damage which enhances the well performance. There are two categories in which acidizing is divided which are fracture acidizing and matrix acidizing.

2.1.1.1 Fracturing Acidizing

When the acid is applied at a pressure higher than the fracture pressure of the formation. The pressure can create highly conductive and permeable channels by the deformation and cracking of the formation. Then, the injected acid flows through those permeable channels; can dissolve minerals and remove fine particles for the hydrocarbons to flow more rapidly to create permeable channels, is known as fracture acidizing (King., 1986). Acid fracturing based on the same concept as hydraulic fracturing which was applied in 1947, in Hugoton Field, Kansas for gas production enhancement (Veatch and Moschovidis., 1986). In recent years, well productivity has been improved by the application fracturing treatments applied in reservoirs with diverse geological settings. However, the complicated fracture formation has been evidenced due to heterogeneity and local properties of the formation (Adachi et al., 2007).

2.1.1.2 Matrix Acidizing

When reactive fluids such as acids are injected at a pressure less than the fracture pressure of the formation; the process is known as matrix acidizing. In sandstone acidizing, the main aim is to remove or dissolve the fine particles and the damage that is bridging or blocking the pore spaces. In carbonate reservoirs which are mostly acid soluble, acidizing operation creates conductive pathways known as “wormholes”, which are highly permeable and conductive flow paths for hydrocarbons (Ghommem et al; 2015, Wilson, 2016). Conversely, in sandstone acidizing, the acid can dissolve an only small portion of the rock. Thus, the removal of formation damage and restoring the permeability of the rock is the main focus of matrix

acidizing (Cruz-Maya et al; 2011, Zhou and Nasr-El-Din, 2016). This can be achieved by targeting the area near the wellbore (8 - 24 in) and improving its permeability (King 1986; Zerhboub et al., 1994). This area is mainly damaged by the clay swelling, fines migration and deposition of scale during the production as explained by (Al-Harthy, 2008;2009). Experimental studies showed the effect of several factors on matrix acidizing, including injection rate of acid, the rock properties reaction rate of acid with rock, permeability, porosity, mineralogy, pore structure and mineral distribution (Qiu et al. 2011; Maheshwari and Balakotaiah, 2013). In the past few decades, different formations especially low-temperature reservoirs (<100^{o}C), clean sandstones (< 10% dolomite), and clean dolomites were extensively treated with matrix acidizing (Morgenthaler, 2013). However, fields or reservoirs with these properties are few and now deep, hotter and heterogeneous reservoirs with complex mineralogy need acidizing treatment. To enhance the efficiency of sandstone or carbonate acidizing and to mitigate the damaging effects of precipitation, new technologies need to be developed.

2.1.2 Sandstone formation

Formation lithology and mineralogy plays an important role in matrix acidizing of any sandstone or carbonate formation. Major components of the sandstone formation are silica and silicate minerals. It also includes quartz, clays, feldspars, and zeolites (Muecke, 1982). Sandstone is a clastic sedimentary rock also known as arenite. Quartz also is known as silica, is the most common grain found in the sandstone formation, but it also contains other minerals such as feldspar and clay which are commonly cemented by silica, calcite or iron oxides (Shafiq & Ben Mahmud, 2017). Figure 2.1 represents the structure of different minerals present in the sandstone formation. The reservoir sandstone framework is usually consisting of quartz grains which are cemented by an overgrowth of dolomites (A), quartz (B), and feldspar (C). Kaolinite (D) and pore-lining clays such as illite (E) are usually responsible for the reduction in porosity and permeability.

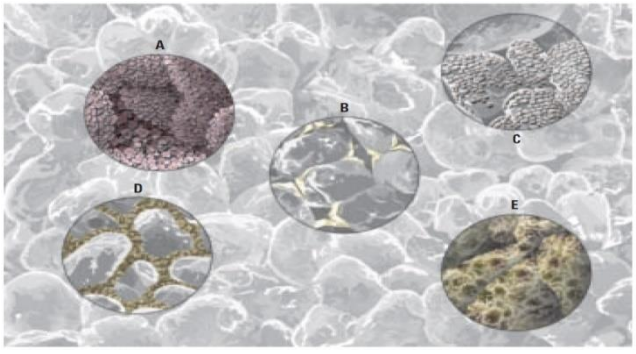

Figure 2.1. Sandstone matrix as described by (Al-Harthy, 2009).

2.2 Sandstone Acidizing

Acidizing the sandstone formation is a challenging task because of the presence of minerals like feldspar, zeolites, clays and alumino-silicates that may form undesired precipitate products when comes in contact with the mud acid. These products are formed due to secondary and tertiary reactions. For example, at a temperature ranging approximately 66^{o}C, instability of smectite and a mixed layer in the presence of HCl is a concern. While chlorite is unstable at temperatures above 52^{o}C in presence of HCl. Clay structures when comes in contact with HCl, may disintegrate, which results in the formation of iron precipitates (Rae and Di Lullo, 2002). Since the presence of hydrochloric acid causes the formation of an iron precipitate when it comes in contact with chlorite. Therefore, if acetic acid is present then formations having chlorite in high concentrations respond best instead of the presence of hydrochloric acid. As acetic acid can limit the liberation of the iron, therefore, it decreases the chances of iron precipitates formation from the reacted products (Hashem et al. 1999., Nasr-El-Din and Al-Humaidan, 2001). The high strength of HF acid is avoided if the formation consists of more than 20% feldspar. This is done to mitigate the fluorosilicate precipitation and other types of precipitates that may result from due to the unnecessary dissolution of rock minerals by acid (Coulter and Jennings, 1999).

The most imperative target of sandstone matrix acidizing is to dissolve/remove siliceous particles (clay, feldspar, and quartz) that restrict the flow of hydrocarbons and reducing permeability around the wellbore. This can be achieved by the injection of HF acid or its precursors (HBF_4) (Kalfayan and Metcalf, 2000). After the discovery of mud acid in 1935 (Smith and Hendrickson, 1965), it was extensively applied on sandstone formation to remove the damage and to solve problems related to the sandstone drilling and production damage. Initially, the main application of this acid was only limited to remove the mud filter cake but now it is also being applied to solve many problems such as removal of siliceous particles and damage around the wellbore. This acid proved to be very successful while treating the sandstone formations containing a small number of calcium minerals. Sandstone formation particles such as sand grains, feldspar, and clays react with HF acid because only Fluoride ion (F^-) has the capability to react with silica and clay. (Smith and Hendrickson (1965) Illustrated the reactive nature of HF acid with silica which makes it exceptional in the application of sandstone acidizing. Hydrochloric, sulfur and nitric acids do not react with the sandstone formation effectively (Smith and Hendrickson, 1965). In 1940, Dowel hit the idea of mixing HCl acid with HF acid to reduce the possibility of reaction products precipitation (Smith,

1965). The mixture is called mud acid and in sandstone acidizing, the common practice is to inject the mud acid with a concentration of 3% HF and 12% HCl (Smith and Hendrickson 1965; Abdelmoneim and Nasr-El-Din, 2015). Sandstone acidizing is an extremely difficult and challenging task due to multiple stages of fluids and their reactions with the minerals in the porous media. The fluid-mineral interactions can cause precipitation reactions, which can potentially reduce the reservoir permeability. Due to multiple stages of fluids-formation reactions during sandstone acidizing, the success rate to remove the damage is generally not according to the requirement. During sandstone acidizing, precipitation reactions may occur leading to formation damage and reduction in permeability and porosity (Shafiq & Ben Mahmud, 2017). When mud acid reacts with the formation to dissolve different minerals; the most important apprehensions are the reactions of dolomites with HCl and HF and the reactions of HF with silicates, quartz (equations 2.1 and 2.2) and feldspar.

$$4HF + SiO_2 \rightarrow SiF_4 + 2H_2O \quad (2.1)$$

$$6\,HF + SiO_2 \rightarrow H_2SiF_6 + 2\,H_2O \quad (2.2)$$

Soluble gas silicon tetra fluoride (SiF_4) formed behave just like CO_2 and can undergo additional reactions. It is held in the solution due to high pressure. Sandstone acidizing is usually performed using acids that contain Fluoride Ion (F^-) in some form**.** Such ion is very reactive and is the only ion that can react with quartz and clay expressively (Smith and Hendrickson, 1965). Stimulating carbonate rocks typically involves a reaction between an acid and minerals like calcite ($CaCO_3$) or dolomite $CaMg(CO_3)_2$. The primary reaction of carbonate with acid is presented in Equation 2.3 (Hill et al. 1994).

$$2HCl + CaCO_3 \rightarrow CaCl_2 + CO_2 + H_2O \quad (2.3)$$

2.2.1 Acidizing Mechanism

Hydrofluoric acid starts dissolution of minerals as soon as it enters a sandstone formation. The speed of reaction and dissolution of minerals depends on their reaction rate with acid and the exposed surface area (Shafiq & Ben Mahmud, 2017). The sandstone minerals are divided into two different categories: slow and fast reacting. “Quartz tends to act at a slower rate whereas feldspars and clays tend to react at a faster rate” (Plavnik et al. 1992). Figure 2.2 shows the types of reactions occurred when sandstone formation is exposed to mud acid.

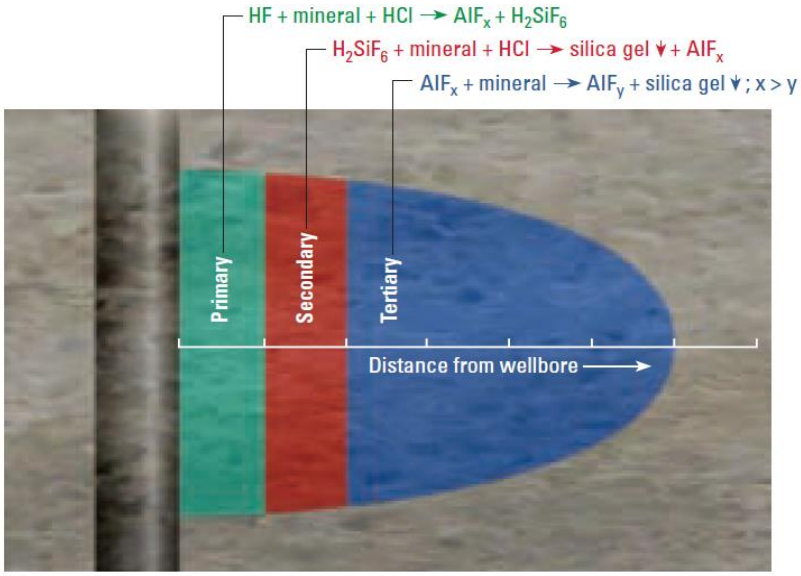

Figure 2.2. Sandstone Acidizing reactions (Al-Harthy, 2009).

When the sandstone formation is treated with the mud acid, usually three groups of reactions take place which is explained by (Al-Harthy, 2009). The primary reaction occurs close to the wellbore, results in the formation of aluminum and silica fluorides. In these reactions, minerals are usually dissolved rapidly and without any precipitation. Away from the wellbore, the secondary reaction takes place in which these primary products further reacted to form silica gel (slow reaction), which is a precipitate. At a greater distance from the injection zone, additional silica gel precipitates due to tertiary reactions. The sandstone acidizing treatment may fail due to the rapid kinetics of the secondary and tertiary reactions at higher temperatures. HF acid is the main reactant with formation rocks, while HCl acid is intentionally added into the mixture to reduce HF consumption and to maintain an acidic environment, which prevents precipitations of HF reaction by-products (Shafiq & Ben Mahmud, 2017).

Unlike dolomite acidizing, sandstone acidizing is very complex and challenging because the injected acid and rock minerals go through several physical and chemicals reactions. Therefore, appropriate selection of acid is required to remove the damage or fines blocking pore spaces (Thomas et al. 2002). Sandstone acidizing is complex due to the presence of some minerals like siliceous minerals, which can only react with a specific acid i.e., hydrofluoric acid (HF) (Shafiq et al, 2018). Moreover, the presence of acid-sensitive minerals like chlorite is also an issue. As discussed earlier, the secondary and tertiary reaction during sandstone acidizing can re-damage due to the formation of insoluble precipitates.

Silicates are formed due to the reaction of sodium and potassium ions with fluosilicic acid (H_2SiF_6), which is the primary reaction product as shown in Equation 2.2. Fluosilicic acid is water soluble but can form insoluble sodium fluosilicate and potassium fluosilicate precipitates when reacted with sodium and potassium ions Equation 2.4 and Equation 2.5 respectively (Ying-Hsiao et al., 1998).

$$SiF_6^{2-} + 2Na^+ \rightarrow Na_2SiF_6 \quad (2.4)$$

$$SiF_6^{2-} + 2K^+ \rightarrow K_2SiF_6 \quad (2.5)$$

Fluorides precipitates are formed due to the reaction between calcium and fluoride ions i.e., CaF_2. The solubility of this product is very low and it has the ability to form a precipitate, but it can be removed if adequate HCl pre-flush is applied (Shafiq et al, 2018). The reaction is shown in Equation 2.6 (Ying-Hsiao et al., 1998).

$$CaCO_3 + 2HF \rightarrow CaF_2 \downarrow + H_2O + CO_2 \quad (2.6)$$

Colloidal silica precipitate is formed due to the reaction of hydrofluoric acid (HF) with sandstone formation is very complex because of several interactions. Initially, HF acid reacts with silica to produce silica tetra-fluoride (SiF_4), which produce fluosilicic acid (H_2SiF_6) due to the further reaction between HF acid (Shafiq et al., 2018).

As soon as the concentration of reacting HF becomes very low, silica precipitates as explained by (Shaughnessy and Kunze, 1981). The reaction (Equation 2.7), that dissociated with the high concentration of HF dissolves silicate minerals.

$$6HF + SiO_2 \rightarrow H_2SiF_6 + 2H_2O \quad (2.7)$$

The reaction (Equation 2.8), reverses itself at a low concentration to regenerate HF acid and precipitates silica (Al-Harbi et al. 2011):

$$H_2SiF_6 + 4H_2O \rightarrow Si(OH)_4 + 6HF \quad (2.8)$$

These precipitation reactions may be avoided by following three stages of acidizing described by several researchers (Gidley, 1971; Kalfayan and Metcalf, 2000 and Shafiq et al., 2018).

- The preflush stage is employed to dissolve any Na, K and Ca ions that may produce insoluble silicates when reacted with the silica. Besides preventing the live HF acid to enter into a high pH region, preflush also provides a low pH region reducing the risk of precipitate formation.
- The main acid stage is applied to dissolve the quartz, clay, feldspar, and silicates. This acid may also dissolve the remains of dolomites present after the preflush stage.
- An after-flush stage is used to keep the wettability of the formation to the original state and it cleans the formation rapidly by removing the spent acid. Mutual solvents, diesel oil, NH_4Cl, acetic acid or HCl can be applied at this stage for the efficient displacement of the spent acids.

2.3 Carbonate Acidizing

Limited research has been performed on carbonate acidizing because of its less complex nature, but in recent years good understanding has been gained of this process (Bernadiner et al., 1992; Nasr-El-Din et al. 2011; Hassan and Al-Hashim, 2017 and Kankaria et al., 2017). The process of matrix acidizing in carbonate formation is significantly different from sandstone acidizing, primarily because of the fact that entire carbonate rock is reactive compared to sandstone where the only small portion is reactive. Due to this, large flow channels (depends on pore size) are created in carbonate acidizing in some areas of the rock, while the other areas remain unaffected. This type of dissolution pattern is due to the heterogeneous nature of carbonate formations. As the size of the pore is macroscopic in nature, therefore these conductive channels can conduct fluid at a high rate flow, which results in permeability increment of the rock. Contrary, in sandstone stimulation, there is homogeneous permeability increment throughout the sample because of pore-scale dissolution in entire rock (Bernadiner et al. 1992).

The response of dolomite to acidizing is different compared to limestone formation because the reaction of dolomite with HCl is dependent on temperature (Hoefner, 1987). Previous investigations have shown more dissolution in dolomite formations. Carbonate rock is a type of sedimentary rock which usually consists of carbonate minerals. Limestone ($CaCO_3$) and dolomite ($CaMg(CO_3)_2$ are two important minerals present in carbonate rocks. These minerals usually react rapidly with HCl or other acids to create wormholes even at low-temperature conditions. The network of wormhole creation is explained in Figure 2.3.

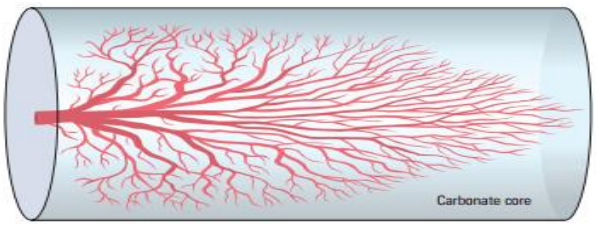

Figure 2.3. Wormhole pattern in dolomite acidizing (Al-Harthy, 2009).

Equation 2.3 represented the mechanism of reaction between HCl and limestone while Equation 2.9 shows the reaction between HCl and dolomite.

$$4HCl + CaMg(CO_3)_2 \rightarrow MgCl_2 + CaCl_2 + 2CO_2 + 2H_2O \quad (2.9)$$

Thus, the presence of wormholes in dolomite formation is the reason for productivity increment which is formed in the near wellbore region by formation dissolution and creation of new flow paths but not by removing the formation damage like in sandstone formation. According to Hawkins (1990), the formula for skin factor mentioned in Equation 2.10.

$$s = \left(\frac{k}{k_s}\text{-}1\right) \ln\left(\frac{r_s}{r_w}\right) \quad (2.10)$$

Where,

s = skin in the simulated or damaged area.

k_s and r_s = permeability and radius of the stimulated or damaged area around the wellbore, respectively.

If the value of k_s is very large compared to k, then k/k_s can be neglected. The value of wellbore radius (r_w) is constant for calculation, therefore, skin value is dependent on r_s. Therefore, high r_s value represents similar effect like negative skin which shows stimulated zone (Buijse and van Domelen, 1998). Conclusively, it can be said that narrow and long wormhole is better compared to wide and short one to enhance the reservoir production.

2.4 Aspect of additives and other factors

Some of the factors on which acidizing job failure and success depends are the concentration of acids, temperature, pressure, permeability, and porosity of the formations. Acid reaction rate

with the rock is directly proportional to the concentration, for example, double the acid concentration doubles the reaction rate (Gidley, 1971). Temperature and pressure also affect the acid spending rate. Reactivity between acid and rock minerals increased as a result of temperature increment. Under high pressure the solubility of by-product gases like CO_2 and SiF_4 increases. The increase in the silicon tetra fluoride solubility improves the reaction rate of silicate minerals with Fluosilicic acid. "Thus, the response of sandstone reservoir to matrix acidizing is very temperature-pressure dependent" (Farley, J. T. 1970). The reaction rate of acid with minerals if affected by the kinetics, other factors which influence the reaction rate are the concentration of acid and temperature. The acid-mineral reaction rates have a direct relationship to the concentration of HF acid during sandstone acidizing. The dissolution of minerals depends on thermal conditions; therefore, the increase in reaction rate observed with increase in temperature, and consequently the depth of penetration of live acid reduced (Plummer, 1978).

McCune et al. (1975), found out that the rock can be acidized successfully if permeability is less than 100 md and porosity is less than 20%. Based on mineral analysis of the rock and stimulation requirement some additives also added during sandstone acidizing. Frenier and Hill (2002) reported that these additives do not have an effect on acidizing results related to removal of damage and creating wormhole rather they are added to minimize some problems. For example, surfactants and corrosion inhibitors do not affect the stimulation process. They are added to minimize problems like corrosion and incompatibility of injected fluids. By adding surfactants to the main acid and pre-flush stages, incompatibility problems can be minimized. Metal integrity can be protected using corrosion inhibitors at concentrations of 0.1% uniformly throughout the acid stages (McLeod et al. 1983). Iron sequestrants are added if HCl is used during the main acid stage to stabilize any dissolved iron and to minimize the precipitation of iron compounds. A mutual solvent like Ethylene Glycol Monobutyl Ether (EGMBE) is usually included in the after-flush stage to restore the formation wettability and to reduce the surface tension of the returning spent acids (Sutton and Lasater, 1972).

2.5 Effect of clay minerals on acidizing

Presence of clay in sandstone or dolomite formation plays an important role in the selection of acid. Structure of illite clays consists of potassium which can cause trouble when reacted with acid. When dissolved, HF-alumino-silicate reaction products can react with readily available potassium, therefore, result in the formation of insoluble potassium hexa-fluosilicate. Also,

illite is found to be unstable at higher temperatures above 66^{o}C in HCl acid while Kaolinite clay found to be unstable in presence of HCl at temperatures higher than 93^{o}C. Kaolinite is also very important due to fines migration perspective (Coulter and Jennings, 1999). Zeolites minerals are secondary in nature and exist in the form of aluminum, calcium, sodium, and potassium hydrated silicates. Analcite (analcime) is the most important form of zeolites present in sedimentary rocks. They are significant because zeolites decompose in the presence of hydrochloric acid at temperatures higher than 24^{o}C (Coulter and Jennings, 1999).

2.6 Success and failure of acidizing

The major causes that may differentiate between a successful and unsuccessful operation of matrix acidizing, are described as follows:

- Poor choice of candidate acid
- Insufficient mineralogy data
- Incorrect acid design
- Inappropriate selection of acid additives
- Unsatisfactory iron control
- Usage of contaminated or dirty fluids
- Improper placement of acid
- Delay in application of post flush stage.

General guidelines followed to select the injected fluid are:

- At low temperatures, conventional mud acids are applied to clean sandstone formations with low concentrations to avoid precipitation and damaging reactions to maintain formation integrity. Mud acid is limited to treat the formation free of clay with high concentrations of calcite, zeolite, and feldspar at low temperatures.
- Clean sandstone formations with low clay content s are recommended to be treated with Organic acids.
- EDTA chelate or other reducing agents applied to Shaly formations that have high chlorite contents.
- The phosphonic acid blend is applied to Shaly formations having a low concentration of calcite and high concentrations of chlorite, zeolites, and feldspar.
- Acid chelate blends are usually used for formations which consist of high calcite content with low clay content, at high temperatures.

2.7 Problems associated with conventional acids

Despite the reasonable success of mud acid application on sandstone formation in recent years, still, some critical problems are associated with its use, which limits its effectiveness. Gdanski (1996) and Thomas et al. (2001) discovered that the most likely limitations of mud acid are rapid spending due to fast reaction; which results in consequent precipitations of reaction products followed by the secondary and tertiary reactions. This limits the acid penetration in the formation, especially at elevated temperatures. A combination of problems such as precipitations, matrix unconsolidation, high corrosion rate and incompatibility of hydrochloric (HCl) acid with sensitive clays (illite) resulted in the inconstant success rate or failure of stimulation treatments with mud acid (Simon and Anderson, 1990; Gdanski, 1998; Thomas, Thomas et al., 2002).

One of the problems associated with the use of HCl acid is corrosivity. Tubing made of low-carbon steel can comprise rust and can be corroded by HCl acid. HCl can dissolve this rust and which in turn produce iron ion (Fe^{+3}), which can form a potential precipitate and damage the reservoir. Therefore, the corrosion inhibitor is required and the cost of inhibitor may increase up to 5% of the total cost of operation (Shafiq et al, 2018). Moreover, the problem which corrosion inhibitor might arise is the change in the wettability of the rock as an inhibitor may adsorb on the rock surface. This problem becomes severe in case of low permeability reservoir (Fredd and Fogler, 1998a).

To avoid the formation of silicates and fluorides precipitates described by Simon and Anderson (1990), hydrochloric acid (HCl) was used it as a preflush ahead of the main acid stage by (Hill et al. 1994), while Yang et al. (2012) added ammonium chloride in organic acid and used it as a preflush. Shafiq and Shuker (2013) added acetic acid in hydrochloric acid and used as a preflush acid and found it more effective as compared to HCl acid. Nuclear Magnetic Resonance analysis has been applied on core samples obtained after core flooding using HCl and CH_3COOH: HCl and found the later one more effective, hence validated the results of previous analysis using this combination. Furthermore, to prevent the hydrated silica precipitation, HCl or an organic acid like citric acid, formic acid or acetic acid are added in the main acid stage with HF acid as reported by (Yang et al. 2012). McLeod (1983) presented the basic guidelines for sandstone acidizing mentioned in Table 2.1.

Table 2.1. Original McLeod's Sandstone Acidizing Use Guidelines (McLeod et al. 1983)

Formation	Main acid	Preflush
Solubility in HCl >20%	Use HCl only	
High Permeability (>100 mD)		
High quartz (> 80%); low clay (<5%)	12% HCl-3% HF	15% HCl
High feldspar (>20%)	13.5% HCl-1.5% HF	15% HCl
High clay (>10%)	6.5 HCl-1% HF	Sequestered 5% HCl
High iron chlorite clay	3% HCl-0.5% HF	Sequestered 5% HCl
Low Permeability (10 mD or less)		
Low clay (<5%)	6% HCl-1.5% HF	7.5% HCl or 10% acetic
High chlorite	3% HCl-0.5% HF	5% acetic

But due to the problems that associated with the use of mud acid, these guidelines are not effective in certain cases. The original McLeod guidelines were modified by himself (McLeod and Norman, 2000). The new guidelines mentioned in Table 2.2 have three sets: high, medium and low permeability. McLeod and Norman also recommended replacing HCl with an organic acid (acetic acid) for formations with chlorite and zeolite. These new guidelines covered two main limitations of McLeod previous guidelines. First of all, recommendations have been added for medium permeability reservoirs and second, they considered the sensitivity of HCl acid towards chlorite and zeolite. Abdelmoneim and Nasr-El-Din (2015) mentioned the drawback of these recommendations; that they are restricted to only three concentrations per permeability range.

Table 2.2. (McLeod, H. O. 2000) Updated guidelines

Mineralogy	> 100 md	20 to 100 md	< 20 md
<10% silt and <10% clay	12% HCl and 3% HF	8% HCl and 2% HF	6% HCl and 1.5% HF
>10% silt and >10% clay	13.5% HCl and 1.5% HF	9% HCl and 1% HF	4.5% HCl and 0.5% HF
>10% silt and <10% clay	12% HCl and 2% HF	9% HCl and 1.5% HF	6% HCl and 1% HF

<10% silt and >10% clay	12% HCl and 2% HF	9% HCl and 1.5% HF	6% HCl and 1% HF

Kalfayan (2001), modified the basic McLeod's guidelines presented in 1983 and 2000 to fill certain gaps. These guidelines are mentioned in Table 2.3. These guidelines recommended more than three concentrations per permeability range which were the drawback of McLeod and Norman's guidelines presented in 2000.

Table 2. Modified guidelines from (Kalfayan, 2001)

Formation	Main Acid	Preflush
Solubility in HCl > 15-20% Calcite or dolomite High iron dolomite (siderite, Ankerite)	Avoid use of HF, if possible 15% HCl only(1) 15% HCl + iron control(1,2)	5% NH_4Cl 5% NH_4Cl + 3% Acetic
High permeability (> 100 mD)(3,4) High quartz (>80%); low clay (<5%) Mod. Clay (5-8%); low feldspar (<10%) High clay (>10%) High feldspar (>15%) High feldspar (>15%) and clay (>10%) High iron chlorite (>8%)	12% HCl-3% HF 7.5% HCl-1.5% HF 6.5% HCl-1% HF 13.5% HCl-1.5% HF 9% HCl-1% HF 3% HCl-0.5% HF or, 10% acetic-0.5% HF	15% HCl 10% HCl 5-10% HCl 15% HCl 10% HCl 5% HCl 5% NH_4Cl + 10% Acetic
Medium permeability (10-100 mD)(3,4) High clay (>5-7%) low clay (<5-7%) High feldspar (>10-15%) High feldspar (>10-15%) and clay (>10%) High iron chlorite (>8%) High iron dolomite (>5-7%) K < 25 mD	6% HCl-1% HF 9% HCl-1% HF 12% HCl-1.5% HF 9% HCl-1.5% HF 3% HCl-0.5% HF or, 10% acetic-0.5% HF 9% HCl-1% HF 5% HCl-0.5% HF	10% HCl 10% HCl 10-15% HCl 10% HCl 5% HCl 5% NH_4Cl + 10% Acetic 5% HCl 10% HCl

Low permeability (1-10 mD)[3,4,5] High low clay (<5%); low HCl sol. (<10%) High clay (>8-10%) High feldspar (>10%) High iron chlorite (>5%)	6% HCl-1.5% HF 3% HCl-0.5% HF 9% HCl-1% HF 10% acetic-0.5% HF	5% HCl 5% HCl 10% HCl 5% NH_4Cl + 10% Acetic
Very low permeability (<1 mD)	Avoid HF acidizing; non-HF matrix stimulation (dictated by damage) or hydraulic fracturing is preferred.	

(1) Location of dolomite in the matrix is important; it may be possible to include HF in naturally fractured formations with high dolomite content.

(2) HCl can be replaced by acetic or formic acid- partially or completely-especially at higher temperatures (250 - 300 ^{o}F).

(3) If zeolites (analcime) are present (> 3%), consider replacing HCl with 10% citric acid or special service company organic acids.

(4) For higher temperatures (> 225-250 ^{o}F), consider replacing HCl with acetic or formic acid.

(5) Although fracturing may be preferable, low permeability, low clay containing sands may respond favorably to HF acidizing-contrary to conventional wisdom.

2.8 Effect of Mineralogy

Precipitates and emulsions may form in the area around the wellbore if a long residence time is given to the injected fluids in the reservoir (Barker et al., 2007). Therefore, careful mineral analysis of core samples is required before selecting the acid formulation. For example, if pore spaces of the sandstone contain authigenic iron chlorite clay, even with the low volume fraction, treatment with HF acid may not be effective as it may not respond to HF acid with any concentration, and can produce precipitate if reacted with HCl which is detrimental (Nwoke et al., 2004). On the other hand, treatment with the mild or moderate strength of HF acid is suggested by traditional guidelines which are based on bulk mineralogy regardless of its distribution in the formation (Coulter and Jennings, 1999).

2.9 Development of different acids

Mud acid and organic mud acid are the main focus in the presented guidelines (McLeod et al., 1983) while the guidelines of other acids have not been discussed due to less or minimal experimental investigation and analysis. For the preflush stage; hydrochloric acid and ammonium chloride were discussed in guidelines (Shafiq & Ben Mahmud, 2017).

Researchers have applied different combinations of acids with varying concentrations to get the best results for acidizing of sandstone formation in terms of permeability, porosity, and precipitation. Various approaches have been implemented to overcome the problems that are associated with the mud acid and conventional hydrochloric acid (Shafiq & Ben Mahmud, 2017). In most of the carbonate matrix or fracturing acidizing treatments, HCl acid is used as the main treatment fluid because it is cheap, high dissolution capability and most of the products formed are readily soluble. But the reaction of HCl acid with the carbonate is very fast, particularly at high-temperature ranges in the wellbore (Buijse et al., 2003). This fast reaction and rapid spending of acid prevent deep penetration which results in the creation of very small wormholes and compact dissolution accompanied with less skin decrease. Even complete dissolution of carbonates is expected at a slow injection rate near the wellbore (Fredd and Fogler, 1998b). Other disadvantages of using HCl acid in carbonate acidizing is excessive corrosion, poor etched length and tendency to form oil-sludge in asphaltenes crudes. Some of the acids developed during the last decades for matrix acidizing are discussed in coming sections with their benefits and limitations.

2.9.1 Mud Acid (HF: HCl)

Gomaa et al. (2013) carried out core flood test at 82^{o}C to investigate the effect of the different ratio of HF: HCl on the permeability of the sandstone core sample. Based on the results, all tested ratios of HF: HCl acids successfully enhanced the permeability of the core samples. However, they observed that better permeability enhancement can be achieved with increasing HF: HCl ratio (Shafiq & Ben Mahmud, 2017).

Al-Harthy (2009), stated that combination of HF: HCl acid was consumed too early during the acidizing process due to rapid reaction rates at temperatures above 93^{o}C. Although mud acid was proved to be efficient and had been widely used, the inefficiency of the acidizing process at high temperature limit its success. It was an indisputable fact that mud acid is very hazardous and can cause corrosion to wellbore equipment. Therefore, in the view of the shortcomings related to mud acid and by considering all of these disadvantages new acid combinations (HF: H_3PO_4 and HBF_4: HCOOH) seems to be a better choice. These combinations used previously by Shafiq and Shuker (2013) inferred to not only be having better permeability improvement, but also less corrosive.

2.9.2 Retarded Mud acids

Gdanski (1998); Thomas et al. (2002) and Gomaa et al. (2013) applied retarded mud acids during the main acid stage, which are supposed to decrease the reaction rate between acids and minerals. Three Retarded Hydrofluoric acids (RHF acids) based on boric acid (H_3BO_3), Aluminum Chloride ($AlCl_3$) and phosphonic acid were tested. However, these methods also posed similar problems at high temperatures. For example, when RHF acid was applied: some minerals form precipitates that were not formed when normal mud acid was used. For example, Al-Dahlan et al. (2001) investigated the formation of potassium tetrafluoroborate (KBF_4) precipitate when the fluoboric acid reacted with feldspar. Fluoboric acid has been produced when a boric acid reacts with HF acid, presented in Equations 2.11 & 2.12 respectively.

Fast reaction

$$H_3BO_3 + 3HF \rightarrow HBF_3OH + 2H_2O \quad (2.11)$$

Slow Reaction

$$HBF_3OH + 2H_2O \rightarrow HBF_4 + H_2O \quad (2.12)$$

The second system Aluminum Retarded Hydrofluoric Acid (ALRHF) consists of aluminum chloride ($AlCl_3$). Aluminum fluoride species formed when aluminum chloride reacts with HF (Equation 2.13). Ji et al., (2014) added $AlCl_3$ as a retarding agent for regular mud acid and found it suitable for controlling AlF_3 precipitation.

$$AlCl_3 + 4HF + H_2O \rightarrow AlF_4 + 3HCl + H_3O^+ \quad (2.13)$$

When HF acid spends while reacting with siliceous minerals, AlF_4 hydrolyzes to regenerate HF acid (Equation 2.14).

$$AlF_4 + 3H_3O^+ \rightarrow AlF_2{}^+ + 3H_2O + 3HF \quad (2.14)$$

The third system Phosphonic Retarded Hydrofluoric Acid (PRHF) is based on a phosphonic acid complex which contains five hydrogen atoms. Ji et al. (2014) described “This acid reacts with ammonium bifluoride to produce an ammonium phosphonate salt and HF acid. The fluoride ions are provided by the ionization of dissolved ammonium bifluoride”. In comparison to mud acid, phosphonic-based HF acid system shows the significantly better performance of permeability enhancement up to 177.86% at 300^{o}F (Shafiq & Ben Mahmud, 2017).

Shafiq and Shuker (2013) and Shafiq et al, (2014) performed an experimental study with different acid combinations, replacing conventional mud acid. These studies focused on the combinations of HF: H_3PO_4, and HBF_4: HCOOH. The Berea sandstone core samples were reacted with these acid combinations and were analyzed in terms of the porosity, permeability, mineralogy, pH change, and compressive strength. According to the findings, although all these acid combinations can be used as the main acid in sandstone acidizing, yet the best acid combination is 3% HF: 9%H_3PO_4. The permeability increment using this acid combination is up to 135.32%, even better than standard mud acid, which showed a permeability increase of 101.76%. However, these experiments were performed at ambient temperature conditions, which is not representative at real field condition. Initial experiments revealed that these combinations are less corrosive, stable and allow deep penetration due to the slow hydrolytic reaction. Then, these results can be compared with the results of mud acid at the same temperature. Therefore, it can be concluded that the experimental procedures and outcomes from the studied literature have provided some productive approaches to the selection of acid and experimental design. Tables 2.4 through 2.6 represent some of the findings and comparison between these acids and mud acid. Berea Sandstone core samples were used consist of following composition 93% quartz, 4% feldspar and 3% other constituents.

Table 2.4. Porosity Results from (Shafiq et al., 2014)

Sample	**Combinations**	**Initial Porosity (%)**	**Final Porosity (%)**	**% change**
Sandstone	3%HF: 12%HCl	10.28	16.85	**63.91**
Sandstone	3%HF: 9% H_3PO_4	9.17	18.10	**97.38**
Sandstone	1.5%HF: 9% H_3PO_4	10.01	17.73	**77.12**
Sandstone	3%HBF_4 : 12%HCOOH	10.56	17.79	**68.47**
Sandstone	3%HBF_4 : 9%HCOOH	10.44	17.85	**70.98**
Sandstone	1.5%HBF_4 : 9%HCOOH	10.75	17.99	**67.35**

Table 2.5. Permeability Results (Shafiq et al., 2014)

Sample No	**Combinations**	**Initial Permeability (md)**	**Final Permeability (md)**	**% change**
Sandstone	3%HF: 12%HCl	70.26	141.76	101.76

Sandstone	3%HF: 9% H_3PO_4	70.5	165.90	**135.3**
Sandstone	3%HBF_4 : 12%HCOOH	71.81	164.96	**129.7**
Sandstone	3%HBF_4 : 9%HCOOH	71.82	162.32	**126.0**

Table 2.6. Mineralogy Results (Shafiq et al., 2014)

	Initial composition		**Main Acid**	**New Combinations**	
	Elements	% weight	HF + HCl	HF + H_3PO_4	HBF_4 + HCOOH
1	Oxygen (O)	55.90	51.03	50.97	55.96
2	Silicon (Si)	37.80	27.02	34.27	36.35
3	Aluminium (Al)	2.60	1.89	2.49	2.30
4	Potassium (K)	1.00	0.90	0.86	0.95
5	Iron (Fe)	0.95	1.28	0.78	2.36
6	Fluorine (F)	0.00	0.00	7.28	0.00
7	Phosphorus (P)	0.00	0.00	1.12	0.00
8	Chlorine (Cl)	0.00	1.17	0.87	0.96
9	Calcium (Ca)	1.75	0.81	1.36	1.12
10	Carbon (C)	0.00	15.92	0.00	0.00

2.9.3 Chelating Agents

Chelating agents were applied as an alternative to the strong acids in order to mitigate the problems associated with their use. It is highly admirable that many types of research had focused on the development of chelating agents which can be applied in high-temperature reservoirs. Suitable acids for high-temperature formations are proposed in few studies, however, clay-rich sandstones and heterogeneous dolomites are more suitable for acidizing using chelating agents (Fredd et al. 1997; Nasr-El-Din et al. 1998; Fredd and Fogler, 1998a; Fredd, 1998b; Fredd and Fogler, 1999 and Almubarak et al. 2017). The application of chelating agents on sandstone and carbonate formations has emerged as an effective enhanced oil recovery (EOR) technique (Hassan and Al-Hashim, 2017). The thorough recovery mechanisms which are leading to significant oil recovery due to use of these chemicals is not fully understood. However environmental issues and less dissolving power of these agents is the point of concern (Almubarak et al. 2017).

In the petroleum industry, chelating agents have been applied to control the unnecessary reactions of metals, therefore, preventing insoluble solids precipitates when acids react with the formation (Frenier et al. 2002). The capability of chelates in removing cations such as $Fe^{3+,}$ Ca^{2+}, Na^{+} or Al^{3+} is due to the presence of carboxyl and hydroxyl functional group. Thus these chelating agents form stable precipitate under various temperature conditions (Mahmoud and Abdelgawad, 2015).

The decrease in metal ion reactivity with other acids and chemicals is due to the bonding between chelate and the metal. For example, when EDTA is applied, the reactive tendency of Ca^{+2} towards HCO^{3-} decreases and it reacts with or makes bonds with EDTA. Hence, there is less precipitation of calcium carbonate $CaCO_3$ observed.

The ratio of MY^{-2} (chelated ions) to M^{2+} (unchelated metal ions) is directly proportional to K_{eff}, which indicates the bonding affinity between the chelate and metal ions as shown in Equation 2.15.

$$K_{eff} = \frac{[MY^{-2}]}{[M^{2+}][Y_{free}]} \qquad (2.15)$$

The chelating agent has a tendency to fully ionized at very low pH values and producing hydrogen ions (H+) which may lead to the decrease in efficiency of the chelating agent. And also at high pH values, the presence of hydroxide ions (OH-) can form precipitates of insoluble metal hydroxides (Equation 2.16) which can result in the decrease in the ratio of chelated to unchelated metal ions (Equation 2.15).

$$MY^{-2} + 2OH^{-} \leftrightarrow M(OH)_2 + Y^{-4} \qquad (2.16)$$

Chelating agents may be used to stimulate sandstone formations entirely without using any HF-containing chemical. Different chelating agents have been used at high-temperature conditions. Ethylenediaminetetraacetic acid (EDTA) and Hydroxyethylenediaminetetraacetic acid (HEDTA) used at a high temperature resulted in the increase of gas production without the use of HF-containing fluids. Wormholes can be formed by EDTA and HEDTA at temperatures up to 205ºC. Frenier et al. (2002) and Nasr-El-Din et al. (2011) used chelating agent Na_3HEDTA and found it more effective in sandstone acidizing as compared to mud acid. Using trisodium HEDTA (Na_3HEDTA) has given better results in stimulating sandstone as compared to HCl. Various stimulating studies on sandstone formation using HEDTA chelating agent have been conducted by (Ermel et al. 2008; Nasr-El-Din et al. 2011) and showed that it gave better results

in increasing permeability compared to mud acid especially at high temperatures. Hydroxethylaminocarboxylic acid (HACA) group of chelating agents can be used as an alternative to the mud acid. Nasr-El-Din et al. (2011) also showed that HEDTA, Diethylenetriaminepentaacetic acids (DTPA), and Disodium EDTA (Na_2EDTA) are effective in acidizing sandstone formations. Single stage sandstone acid has been developed by Gomaa et al. (2013), consists of boric acid (H_3BO_3), ammonium bifluoride ($NH_4H.HF$) and HCl to generate fluoboric acid. This system eliminates the use of pre-flush and after-flush stages. Iron precipitation is controlled effectively by EDTA and it's also effective in removing scales. Shaughnessy and Kline, (1983) applied EDTA successfully in Prudhoe field where in 19 out of 25 wells, the productivity has shown significant improvement. Chelate-based hydrofluoric acid (APCA/HF) have been applied successfully by (Sopngwi et al. 2014), in one of the wells in Ewing Bank 973 Field, where a significant increase in the oil production has been reported by approximately 305% increment in production by removing the formation damage. It has been reported by Frenier et al. (2004) that HEDTA has the ability to dissolve clay and other fine minerals which are the common reason to clog the pore throat inside the sandstone formation and proved impressive in dissolution. At elevated temperature 177°C, the effects of Mud acid, HCl acid, and Na3HEDTA, were studied on the undamaged core sample. From the results, chelating agent Na3HEDTA proved to be effective in stimulating Berea sandstone core samples compared to HCl and 9/1 mud acid (9% HCl: 1% HF).

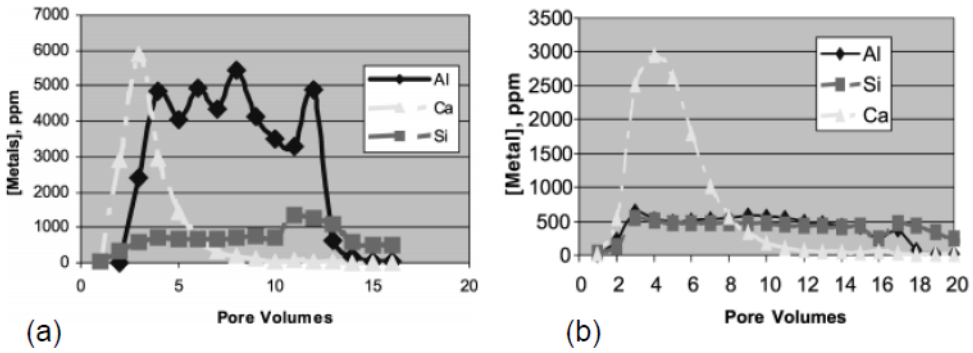

Figure 2.4. Metal ions concentration during core flood of Berea core sample using (a) 9/1 mud acid and (b) Na_3HEDTA (Frenier et al., 2004).

Fredd and Fogler (1997), Fredd et al. (1997), Fredd and Fogler (1998), Fredd (1998b), Fredd and Fogler (1999), stimulate carbonate core samples by applying ethylenediaminetetraacetic acid (EDTA) and diethylenetriamine pentaacetic acid (DTPA). Fredd and Fogler (1997), investigated that EDTA is very effective in creating wormholes in a limestone formation. Fredd and Fogler (1998) studied the effect of (EDTA) as an alternative fluid for carbonate stimulation.

He founded that effective wormholes have been created when EDTA is applied in limestone formation at low flow rates, where face dissolution may occur only, even when pH value of injected chelate is moderate or non-acidic (4 to 13). Sludge tests showed that the asphaltenes precipitation could not occur from crude oil when EDTA is used as a stimulation fluid, even when the concentration of ferric iron is 3000 ppm. Fredd and Fogler, (1998), discovered that EDTA can form a stable chelate in the ferric or ferrous iron environment. They showed that no hydrogen is required during the process as EDTA has the ability to chelate calcium (II) ion directly from the carbonate rock. If EDTA and HAc are injected at a higher rate, both can stimulate carbonate rock efficiently compared to HCl if the rate is greater than 0.000006 m^3/sec (Fredd and Fogler, 1998). At less flow rate HC consumed very rapidly at the face of the core and most of the dissolution occurs there. The low diffusion coefficient of EDTA and HAc compared to HCl is responsible for this ability of these chelates to create wormholes at slow injection rates (Fredd and Fogler, 1998). EDTA, Optimum injection rate to have a breakthrough by injecting a certain volume of pore volume depends on the diffusion coefficient. Diffusion coefficient for HCl is maximum and decreased from HCl to HAc to EDTA. Moreover, the corrosion inhibitor is not required when EDTA is applied up to 204°C. As EDTA can chelate both ferric and ferrous irons, therefore, the reducing agent is not required. Thus, usage of EDTA as a stimulation fluid does not require these costly additives. Sludge precipitation was very significant when crude oil comes in contact with 15% HCl. However, only a small amount sludge was precipitated by EDTA and HAc, despite the presence of 3000 ppm of ferric oxide, when comes in contact with the same oil. This ability of EDTA to form a trace amount of sludge precipitate is due to its power to chelate iron and moderate acidity. The effectiveness of HAc is apparently due to its ability to chelate ferric iron.

Hassan and Al-Hashim (2017), used Indiana limestone during research; core flooded them under reservoir conditions with different concentrations of chelating agents. It has been observed that permeability has been increased significantly in all core samples which showed the significant dissolution of the rock. The investigation of the effects of the chelating agent on rock dissolution properties had been carried out by (Fredd and Fogler, 1997). Computed tomography (CT) scan and nuclear magnetic resonance (NMR) logging experiments were applied to the core samples before and after the core flooding experiments. It has been analyzed from experimental results that, permeable pathways/channels have been created inside the core samples that can cause more oil production. Absolute permeability of the core sample has been increased significantly whereas the maximum increment in the permeability had been observed

near the entry point of the core and small improvement in the porosity of the rock also observed. Hassan and Al-Hashim (2017), applied ICP analysis to determine the ion concentrations in the reacted sample to evaluate the rock dissolution happened due to core flooding of chelating agents. Considerable rock dissolution had been observed because of the significant increase in calcium ions concentrations. These results revealed that the leaching of calcium needs to be controlled and optimized to modify the wettability of the rock in order to produce more oil and to prevent or mitigate excessive rock dissolution. By controlling the concentration of the chelate at a small level and pH value of the chelating agent at a moderate level (towards a less acidic solution), it can be achieved. Another important test performed by Hassan and Al-Hashim, (2017) is a multicomponent ion exchange (MIE) phenomenon. It is investigated by measuring the Mg^{+2} concentration, where the decrease in the Mg^{+2} concentration below the reference point during chelating agent core flooding is the indication of replacement of calcium ions by the adsorbed magnesium on the rock surface.

Almubarak et al. (2017) summarize the application and theory of different chelating agents in the removal of damage during the acidizing. It has been investigated that the application of various chelating agents in the field of matrix acidizing, where he included the chelating agents latest field applications and developments. This knowledge can be used by the investigators to enhance the application of chelating agents in the oil and gas industry.

Several organic acids were proposed to solve the issues related to conventional acids. However, even the use of organic acids has issues with the solubility and incompatibility. Almubarak et al. (2017), performed various laboratory tests in order to find the interactions of chelating agents with the formation and the fluids present inside. These tests include compatibility of acids with the formation, dissolution, X-Ray Diffraction (XRD), Scanning Electron Microscope (SEM) and Inductively Coupled Plasma (ICP). Considering these shortcomings, Almubarak et al. (2017) showed that the chelating agents have good dissolving power, less corrosive and do not form excessive sludging, iron controlling power and environmentally friendly. Oil field scales which are detrimental to production due to their insolubility in HCl can be dissolved using chelating agents.

L-glutamic acid diacetic acid (GLDA), an environment friendly chemical, is used as a replacement for stimulation treatment in deeper and hotter reservoirs. Nasr-El-Din et al. (1952), performed core flooding first time using chelating agents and analyzed the concentration of calcium ion in the effluent sample. It is found that GLDA has the ability to chelate a significant

amount of calcium in carbonate samples. GLDA can dissolve more amount of calcium compared to ethanoldiglycinic acid (EDG) but less compared to hydroxyethyl ethylenediamine triacetic acid (HEDTA). GLDA is very effective to create wormholes at low injection rates and is thermally stable up to 177ºC. EDTA has the ability to form a stable chelate when reacted with divalent ions or trivalent ions such as calcium and iron (Martell, 1952).

Successful matrix acidizing of carbonate reservoirs depends on the selection of optimal stimulation fluids. Due to several disadvantages of the presence of HCl acid as stimulation fluid. Nasr-El-Din et al. (2017), applied and investigated methanesulfonic acid (MSA) as an alternative to the HCl acid. This acid is viable in terms of less corrosive and environmentally benign. Conversely, MSA is a very expensive acid. Therefore, in order to reduce the cost of stimulation, blend of HCl and MSA has been proposed to be applied during for carbonate stimulation. This blend can be helpful to enhance the properties of HCl. Nasr-El-Din et al. (2017) performed core flooding experiments using MSA, HCl separately and as a blend also and results were compared. Core flooding experiments were conducted on 0.1524 m long core sample (Indiana Limestone) using three different ratios of HCl and MSA at 121°C. The breakthrough volume of acid required was recorded and CT scan analysis was performed on the core samples to identify the wormhole structures. Unconsumed acid concentration, pH value, and calcium concentration can be analyzed using effluent samples. The effluent samples were analyzed for pH value, calcium (II) ion concentration, and unconsumed acid concentration. 5% HCl: 5% MSA by wt% blend was found to be a more suitable candidate from core flooding experiments for carbonate matrix acidizing where three blends were tested with the ratio (2.5% HCl: 7.5% MSA, 2.5% HCl: 7.5% MSA by wt%). They discovered that at a higher flow rate or injection rate of 0.00045 m^3/sec, the mixture needs lesser pore volume and achieved breakthrough earlier as compared to single acid. When the acid blend is applied; a single, dominant and straight wormhole was created without any branch while single acids created branches whereas MSA created wormholes. 5:5 wt% dissolve the least amount of calcium compared to other ratios. Also, the minimum amount of acid has been consumed in the case of 5:5 wt% blend compare to others. This is promising for deeper penetration of acid with less amount of pore volume required. The other blend in which the percentage of HCl is high required the same amount of pore volume to create a wormhole as single HCl acid and it was more enlarged and tortuous compared to the blend in which MSA concentration high. The new acid blend gives following advantages like deeper wormhole creation which can result in enhanced oil recovery, followed by cost-effectiveness and less corrosivity.

2.9.3.1 Importance of Chelating Agents

These are organic compounds that consist of an electron donating group. Because of this electron donation, these groups can perform as a Lewis base and has the ability to connect to the central metal atom by forming coordinate bonds. When multiple coordinate bonds are connected with each other; a single molecule formed consist of one or more chelate rings or heterocyclic ring, therefore, named as chelating agents. For interested ion, the stability constant is usually the indicator of chelating agent strength. For example, if chelating agents show a higher stability value with Fe (III) ion compared to one chelate, they will also have the same trend with other metal ions. In the oil and gas industry, the chelating agent term is used or referred to one kind of subgroup of chelating agents (aminopolycarboxylic acid). This group includes acids such as EDTA, HEDTA, DTPA, and NTA. These can be applied to sandstone and carbonate formations to remove damage and iron control.

Considering experimental works and field applications of chelating agents, they proved to be capable of improving the well performance. They are less corrosive, stable and retarded in nature even under high-temperature conditions, which allowed them to be applied to high-temperature formations. Moreover, the nature of chelating agents is also environmentally friendly compared to other acids applied during matrix acidizing like mineral and organic acids (Frenier et al. 2004). Therefore, three basic chelating agents (HEDTA, EDTA, and GLDA) are selected for this project.

Ethylenediaminetetraacetic Acid (EDTA):

In the oil and gas industry, EDTA has been applied for stimulation and iron control applications but still, there are some problems related to its application. First of all, it is not readily biodegradable and is prohibited in some countries. Secondly, its solubility in acidic environment decreases because of its ampholytic nature (Almubarak et al. 2017).

Hydroxyethylethylenediaminetriacetic Acid (HEDTA):

It was first used by Frenier et al. (2000); Rainey et al. (2003) in place of EDTA acid for stimulation application. It is another type of aminopolycarboxylic acid and same in a structure like EDTA nut it has one hydroxyl group instead of an acetic acid group (Almubarak et al. 2017). The addition of this hydroxyl group improves its stability but still faces the

biodegradability issue like EDTA. HEDTA has been used in the petroleum industry for oil scale removal and as iron control agent (Frenier, 1986 and Frenier, 2001).

Glutamic Acid (GLDA):

It's a new chelating agent and has been applied by (Heus, 2008), highly soluble in water and acidic solutions (LePage et al. 2009) due to the presence of iminodiacetic acid part and is highly biodegradable. In oil and gas industry it has been applied for iron control and stimulation of sandstone and carbonate reservoirs. Figure 2.5 represents the structure of chelating agents used in this project.

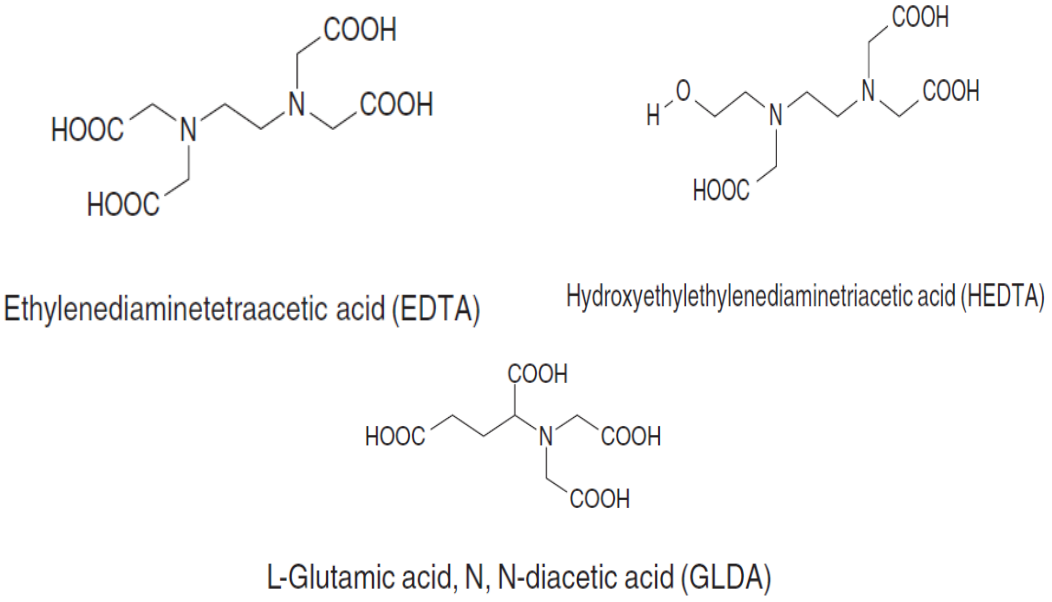

Figure 2 5. Structure of GLDA, EDTA, and HEDTA (Nasr-El-Din et al. 2011)

2.9.4 Organic-HF system

Organic-HF acid has been applied to mitigate the problems faced during sandstone matrix acidizing. Slow reaction rate and less corrosivity have allowed the petroleum industry to apply formic and acetic acids for many years as alternatives to HCl in carbonate acidizing. The rapid HCl spending prevents deep penetration of acid into the formation. Studies on sandstone acidizing using mud acid have shown that the presence of HCl acid is effective in maintaining the acidic environment and solubility of reaction products. However, the use of HCI can cause damage such as corrosion, crude oil sludging and unpredictability of formation minerals. These problems become more severe at high temperatures. Therefore, Shuchart (1997); Gdanski and Shuchart (1998); Al-Khaldi et al. (2011) and Nasr-El-Din et al. (2012) applied Organic-HF in sandstone matrix acidizing to overcome the problems. Due to less corrosion rate and retarded

nature of organic acids, these acids provide better results, especially at elevated temperatures and considered as an excellent alternative compared to mud acid in sandstone acidizing. These acids proved to be very useful when HCl sensitive clay (can cause damage to the formation when reacts with HCl), such as illite is present in the formation. The two organic acids used commonly are acetic acid and formic acid; a combination of HF with HCOOH also known as organic mud acid (Blake R.E, 1999). These acids also possessed some problems similar to mud acids like fast reaction rates and formation of precipitates (Shafiq & Ben Mahmud, 2017).

Shafiq and Shuker (2013) and Shafiq et al. (2014), used organic mud acid to acidize sandstone formation in comparison with mud acid and presented their results in terms of acid pH value change. The results revealed that the pH value change after the acidizing is not much when organic mud acid is used as compared to standard mud acid, and this change is even less when fluoboric acid was added in place of hydrofluoric acid. It shows the effective buffer effect and slow reaction rate which can be useful for deep penetration of acid into the formation.

Buijse et al. (2003), discussed the application of organic acid by replacing it with mineral acid during the acidizing of carbonate formations. Organic acids (acetic or formic acid) due to their low corrosive nature have been applied to carbonate formations for many years as an alternative to HCl acid. These acids possess retarded reaction rate and also less tendency to form acid-oil sludge in crudes which are rich in asphaltenes. Organic acids have been tested as a fracturing fluid in deep hot limestone formations by (Buijse et al. 2003). Some other case studies have been discussed too and in fact, the success rate is high but design optimization was hindered because the models to predict organic acid spending on carbonate formation did not exist.

Buijse et al. (2003), proposed a model for strong mineral acids and for weak organic acids and can be used for acid mixtures too. He added the element of acid dissociation constant compared to existing models, which helps in describing the differences between strong and weak acids. Validation was done by using the experimental results which are compared with simulation results. In laboratory rotating, disk experiments were performed to measure the rate of dissociation of the acid. He also discusses the results of acid fracture simulations, comparison of etched length and width when organic acid was applied against HCl acid.

2.9.5 Emulsified Acid system

De Groote in 1933 was the first who introduced the emulsified acid to the oil and gas industry. Two immiscible phases exist in the emulsified acid system usually consists of two immiscible i.e., diesel and acid; where diesel exists as the continuous phase and acid as dispersed phase (Fattah, 2010). Therefore, in place of acid, well tabular and reservoir rock directly contact with the diesel. Contact of acid with the rock also delayed because diesel can be a barrier between the rock and the acid reaction. No effect of emulsion has been observed on the reaction rate between the rock and the plain acid (Crowe and Miller, 1974; Touboul et al, 1989). In order to react with the rock, acid need to cross strong interfacial tension which helps in the delay of the reaction between the acid and the rock (Peters and Saxon, 1989). This resulted in deep penetration of the acid into the formation of the dispersed acid which is trapped in the emulsion will be released slowly. This deeper penetration allows longer wormholes, which are high permeability conductive pathways (Buijse and van Domelen 2000; Al-Anazi et al. 2000 and Hill et al. 2008). Larger flow channels will be created in naturally fractured dolomite reservoirs because the wormholes created during matrix acidizing can connect with the existing fractures. On the contrary, reservoir without natural fractures, the length of created wormholes will be small compared to the naturally fractured reservoir but still quite significant and can range up to several feet. Therefore, the effective wellbore radius increased and permeability improved due to the creation of these wormholes. Negative skin factor of -2 to -4 can be achieved by applying matrix stimulation (Jennings et al. 1992 and Lietard, 1994).

Emulsified acids are basically retarded acids, which are extensively used in acid fracturing and matrix stimulation. Several studies (De Rozieres 1994; Navarrete et al. 1998; Conway et al. 1999; Kasza et al. 2006 and Nasr-El-Din et al. 2009) examined the reaction rate of emulsified acid with dolomites. Navarrete et al. (1998) indicated that the reaction rate of 28 wt% HCl emulsified acid with limestone was 8.5 times slower than that of regular acid that contained 28 wt% HCl with limestone.

(Xiong, 2010), applied a novel emulsified acid in the Chinese oil fields. The significance of this emulsified acid is that increases the permeability of oil-saturated cores by 96.1% while by only 10.1% for water-saturated cores. (Pandya and Wadekar, 2013), applied emulsified acids on high-temperature reservoirs ranging from 135 to 190^{o}C compared to nonretarded and gelled acids. He studied the stability of emulsified acids when the corrosion inhibitor is added in. It

has been found that only emulsified acid system sustained this high-temperature range as compared to other acids (Cairns et al., 2016), studied deeper well stimulation using improved emulsified acid systems at a high temperature up to 149^{o}C. The CT images for the treated core samples show that the stabilized acid system had less face dissolution and had the desired wormhole characteristics, i.e. narrow and directional propagation behavior with deeper penetration into the core sample. He concluded that the stabilized system achieve up to three times increment in core permeability as compared to the conventional acid system.

The emulsified acid not only efficient in creating big wormholes and prevent rapid spending but it also protects the well and tubing integrity from corrosion issues. Deep penetration into the reservoir can be enhanced because of the high viscosity of the emulsified acid which ultimately decreases the acid leak-off rate from the wormhole (Maheshwari et al., 2016). Low viscosity acids (conventional plain acids) can flow towards more permeable areas if applied in a highly heterogeneous reservoir, leaving the intervals with low permeability and high skin values. Thus, the non-uniform acid coverage in target zone resulted in unsuccessful acid treatment. Therefore, acid with higher viscosity if designed carefully can enhance the acid diversion and wellbore coverage (Jones and Dovle, 1996; and Jones and Davies, 1998). The viscosity of emulsified acid is found to be almost 50cp, which is considered very high compared to the viscosity of the reservoir fluid, therefore, sweep efficiency, zonal coverage, acid distribution and penetration of acid heterogeneous reservoirs can be improved (Buijse and van Domelen, 2000).

Apart from uniform zonal coverage, the occurrence of compact dissolution can also be minimized using the emulsified acid. It is a phenomenon in which wormholes are not formed because of the fast reaction and rapid spending of the acid when comes in contact with the formation surface. Usually, to create wormholes, it is required to inject acid at a high rate when dealing with tight formations. When average injection rate is used during acidizing of a highly heterogeneous formation having a high difference in permeability, it becomes difficult to create wormholes in tight areas. The acid will be spent on the formation surface without penetrating into the formation. Thus, emulsified acid can be very useful to avoid compact dissolution and it can improve the efficiency of creating wormholes due to deeper penetration of acid (Buijse and van Domelen, 2000). Above advantages can be achieved even using high viscous emulsified acid, some researchers investigated that due to the high viscosity of emulsified acid

the pumping pressure and injection rate can be restricted, especially in the tight reservoir (Carpenter, 2015).

Stable emulsified acid can be prepared by adding additives like chelating agents, surfactants, and emulsifiers in the mixture to reduce interfacial tension between the phases. The stability of the emulsified acid is of critical importance because the success or efficiency of an emulsified acid depends on its stability. Instability of emulsified acid can separate the phases before it reaches the desired target, therefore, causing the failure of the job.

2.9.6 In-situ foam

Behavior of the foam and its effect in porous carbonate formation has been studied extensively (Bernard and Holm, 1964; Bernard and Jacobs, 1965; Holm, 1968; Owete and Brigham, 1987; Radke et al. 1991 and Ettinger and Radke, 1992), applied in-situ generation of foam during carbonate acidizing of 0.3048 m long sample, which helps in allowing deeper penetration into the formation and create deeper wormholes; therefore uses less amount of acid compared to conventional techniques. This technique was used to increase the wormholing process (Thompson et al., 1986). Moreover, low acid flow rates can be used where there are chances of face dissolution. This in-situ process is also very suitable for the formations where low acid injection rates are required or also in cases where heterogeneity comes into play and some zones do accept acid slowly. Specific characteristics related to acidizing are:

1. Uniform and thin wormholes are produced in the presence of foam and only little branching is observed. This represents efficient dissolution by this system.
2. There is no acid leak off from sides of the wormhole formed, which allows uniform distribution and channel formation. It states that almost all acid spent in the creation of the primary effective channel.
3. The efficient wormhole has been produced by a nonfoamed gas/acid system but the amount of branching is increased.
4. Acidizing efficiency has been dropped when a higher concentration of acid has been used in this system because extra acid can produce radial dissolution instead of increasing the wormhole length.
5. In dolomite formations, foamed acidizing was very effective and created structured wormholes. Spending of acid is relatively slow in dolomite, causing in a more or less matrix-type dissolution. The wormhole structure is almost similar to limestone because

acid reaction rate is slow which causes extensive reactions. When the foam is present, the acid flow rate can be slow enough to allow extensive reaction in the primary flow path.

The foam system described above is very well suited for low permeability formation especially dolomite (Hoefner, 1987) as it confines the acid to the primary channel and makes it sure that it is well spent in primary channel. Table 4 shows the effectiveness of this system in low permeability dolomite. At a flow rate of 0.0000025 m^3/sec, conventional stimulation resulted in the dissolution of most of the core which causes a large increase in permeability. Therefore, the use of the foam system is very efficient in creating wormholes.

2.9.7 Other acids

Hartman et al. (2003), applied 10% acetic acid which proved to be useful in sandstone acidizing at a higher temperature and showed better results compared to 10% HCl. This acid is only effective at low temperature. Martin (2004), insisted on using the non HF-based system because of the damaging nature of this acid and complex reaction mechanism. Fluosilicic acid (H_2SiF_6) plays an important role in removing the formation damage. It was applied successfully to stimulate sandstone in two injector wells in off-shore Brazil in 1999 by (Da Motta and C.M. Dos Santos, 1999). Kalfayan and Metcalf (2000), achieved 200% increment in permeability by applying the same acid. During sodium fluoride manufacturing, H_2SiF_6 formed as a byproduct, which is also considered as a viable option for sandstone acidizing operations because of its low cost. This acid can cause precipitation reactions at high temperatures. Table 2.7 shows the summary of acids development with time.

In order to get better results from the acidizing job and to extend the life of the acidizing treatment, one of the alternative technique used as a remedy is the acid blends instead of conventional HCl-HF acid systems. Phosphonic acid complex replaced HCl acid in one of the improved chemistry systems. A number of available hydrogen ions in phosphonic acid are five, which can dissociate at different stoichiometric conditions. Therefore, this Phosphonic acid complex can also be named as five-hydrogen (HV) complex (Nwoke et al. 2004; Rae and Lullo, 2007 and Nasr-El-Din, 2016). The HF acid can be obtained by reacting HV acid with ammonium bifluoride (NH_4HF_2). 1000 gal of water mixed with 20 gals of HV when reacted with almost 123 lbs of NH_4HF_2 can produce 1% HF acid solution (Uchendu et al. 2006). HBF_4 is the retarded acid where this self-generating reaction of HF acid lessen the rate acid of reaction with the rock and therefore, allows live HF acid to penetrate deep into the formation. Due to

this slow reaction, the risk of formation deconsolidation decreases, unlike conventional acids which are the reason for the deconsolidation of rock near the wellbore.

In past 30 years, several research publications have appeared which are related to the development of an expert system for designing sandstone acidizing (Abel et al. 1990; Van Domelen et al. 1992; Chiu et al. 1993, and Nitters et al. 2000). Robust rule-based systems have been introduced by (Van Domelen et al., 1992 and Xiong and Holditch, 1995) specifically for damage type formations acid fluid selection but depend predominantly on the fluid injected and the reservoir rock mineralogy. A matrix stimulation model has been developed by (Bartko et al. 1996) that helps in diagnosing the type of formation damage, optimization of acidizing treatment and pressure differential due to skin acid treatment. All these guidelines and systems developed, however, do not include or describe the recent technology development in acidizing like a phosphonic acid blend or chelating agents developed. Instead, mostly the selection of acid through guidelines based on mud acid and organic mud acid. Also, in the discussed rule-based systems, the presence of clay and the interaction of oil and acid in the rock has been totally ignored.

(Nasr-El-Din et al. 2002; Nasr-El-Din et al. 2007; Rae and Lullo, 2007 and Urraca, 2009), developed another acidic chelate-based blend to mitigate secondary and tertiary reactions and satisfy long-lasting effects of simulation in sensitive sandstone formations. But the application of these chelates is restricted to high-temperature formations with a high content of dolomite and low clay. Table 2.7 represents the summary of different acids developed during the last few decades.

Table 2.7. Summary of acids developed and under active research

Name, year, author	Experiments performed	Advantages	Disadvantages / Gaps
Mud acid (HF – HCl) 1965 - Smith and Hendrickson	F^o NMR, ICP, CT scan, solubility, SEM, XRD, EDS, core flooding on Berea sandstone	Dissolves quartz, Removes damage, HF acid dissolves silicates while HCl helps in controlling precipitation reaction	Corrosive, precipitation reactions, fast reaction, inefficient due to early consumption especially at temperatures higher than 200^{o}F.
Retarded mud acids 1996 - Al-Dahlan 2012 – Al-harbi	F^o NMR, ICP, solubility, SEM, XRD, EDS, Core flooding on Berea sandstone	Reduces the reaction rate for penetration	Same problems as mud acid at high temperatures and formation of precipitates (KBF_4)
HCOOH-HF acid (Organic mud acid) 1996 - Shuchart	F^o NMR, ICP, CT scan, solubility, SEM, XRD, EDS, core flooding on Berea sandstone	Less corrosion rate, useful in HCl sensitive clay at temperatures more than 350^{o}F	Expensive, some precipitates formed at high temperature
CH_3COOH – HF acid 2003 - Hartman	Core flooding, SEM, ICP analysis	Good results at a higher temperature – more than 100^{o}F	Only applicable where dolomite percentage is high, mostly applied in carbonate acidizing
Na_3HEDTA and HEDTA 2002 – Ali and Frenier	F^o NMR, ICP, CT scan, solubility, SEM, XRD, EDS, core flooding on Berea sandstone	Better acidizing results at high temperature (400^{o}F)	No fluoride ion, no dissolution of quartz, only applicable where quartz percentage is less

Fluosilicic acid 1999 - Da Motta	Permeability, porosity, corrosion tests, core flooding	Decent permeability increment, Byproduct of HF acid and silica reaction	Not used at high temperature, corrosive, can form a precipitate at high temperatures
Single stage acid 2013 – Goma and Cutler	Core flooding, corrosion, productivity	Eliminates the use of preflush and after flush stages	Expensive, reaction mechanism is not clear
Phosphoric-HF & Fluoboric-formic 2013 - Shafiq	Porosity, permeability, strength, SEM, EDS, saturation, solubility	More permeability increment and less corrosion	Not used at high temperature, reaction mechanism unknown
Emulsified Acids 1933 – De Groote	Core flooding, permeability, CT scan	Slow reaction rate, stable at high temperature	Not applied to a sandstone formation
GLDA 2008 – Heus	F^o NMR, ICP, CT scan, solubility, SEM, XRD, EDS, core flooding on Berea sandstone	Environment-friendly, iron controlling agent, applied at high temperatures successfully	No fluoride ion, no dissolution of quartz, only applicable where quartz percentage is less
EDTA and HAc 1997 – Fredd and Fogler	F^o NMR, ICP, CT scan, solubility, SEM, XRD, EDS, core flooding on Berea sandstone	Effective in creating wormholes, less corrosive, control iron precipitates and remove scales	Not soluble in the less acidic environment, not readily biodegradable
MSA 2017 - Kankaria	Core flooding, corrosion, CT scan, ICP	Applied at high temperatures, suitable in the form of a blend	Expensive, not effective when quartz percentage is high
In-Situ foam 1964 - Bernard and Holm	Core flooding, CT scan	Create uniform wormholes in carbonates, effective in dolomite	No fluoride ion, no dissolution of quartz, only applicable where quartz percentage is less

		acidizing, effective in low permeability formation also	
HV complex Nwoke, Uchendu et al. 2004	Core flooding, strength, complexation of ions	Slow reaction rate, more penetration of acid into the reservoir, less formation deconsolidation	No fluoride ion, no dissolution of quartz, only applicable where quartz percentage is less

2.10 Why acidizing is preferred over hydraulic fracturing

Acidizing may, in fact, be the oldest stimulation technique and still in modern use. Still, researchers are trying to develop acids that can be used at different temperatures and pressures because of the advantages of acidizing over hydraulic fracturing (Abdelmoneim and Nasr-El-Din, 2015). Acidizing can be used instead of hydraulic fracturing in many cases like high permeability formation with loose packing, naturally fractured reservoirs and removing damage around the wellbore. Moreover, sandstone acidizing can be utilized in depleted sandstone reservoirs for Carbon Capture Storage (CCS), where hydraulic fracturing cannot be implemented (Shafiq & Ben Mahmud, 2017).

The increase in well stimulation activity (acid and frac jobs) has been increased in recent years with the double number of treatments performed more than through the 1990s. In 1994, 79% of the stimulation jobs were acid treatments, but since they are a low cost, low volume operation than hydraulic fracturing treatment, they only consumed 20% of the money spent for well stimulation. For acid jobs, the observed failure rate was 32%. The failure rate is less frequent but more expensive hydraulic fracturing treatments was much lower, only 5% (Collier, 2013). There are a limited number of reasons why sandstone acidizing treatments do not succeed. The six-step process to succeed sandstone acidizing are as follows (Shafiq & Ben Mahmud, 2017):

- Determine the presence of acid-removal skin damage;
- Determine appropriate fluids, acid types, concentrations, and treatment volumes;
- Determine a proper treatment additive program;
- Determine a treatment placement method;
- Ensure a proper treatment execution and quality control;
- Evaluate the treatment.

Some oil companies have found acidizing more effective in the Monterey Shale than fracking. Conventional fracking, in which water and other chemicals are pumped at a high pressure to create fissures in the rocks, reportedly it does not work well in many parts of the Monterey Shale – a rock formation known for its complexity and low permeability, which makes fracking less effective. In drought-prone California, acidizing with HF works much better than fracking in the Golden State because the oil-bearing shale is already naturally fractured and buckled from tectonic activity (Collier, 2013).

2.11 Effect of Mineral Dissolution

Dissolution of calcium dolomite and anorthite minerals releases free calcium ions which can be used for CO_2 storage later on described by (Kumar et al. 2004). Hence, acidizing can be helpful in a way for CO_2 storage also. Taron (2009), studied chemical precipitation/dissolution using TOUGHREACT simulator and indicates that mineral precipitation plays a large role in reservoir evolution. Calcite can be dissolved by the addition of chelates. Chemical changes and the effectiveness of chemical treatments depends on hydro-mechanical fracture flow properties. Precipitation and dissolution of calcite and amorphous silica are responsible for initial permeability change. Other likely minerals, such as potassium feldspar and quartz, are also followed in order to see the effect of their precipitates.

As minerals precipitate due to the reaction between and injected fluid and the rock, changes are experienced in the porosity and permeability of the fracture system. In currently operating geothermal systems, calcite and amorphous silica precipitation have posed problems at recovery and injection wells, respectively. Calcite precipitation can successfully be inhibit using acidic injection. Other problems due to acidizing include the potential for corrosion of casings, although corrosion inhibitors can often be added to avoid this problem. Another alternative for calcium dissolution is chelating agents, which reduce the activity of metal ions (through binding) whereas, inhibiting the precipitation of amorphous silica has proven to be more difficult (Shafiq & Ben Mahmud, 2017). Acidizing using HF acid is currently the preferred method, but some have suggested that amorphous silica can be dissolved using chelating agents at high pH to prevent calcite deposition (which would be favored at high pH). This research is, however, relatively recent, and uncertainty remains as to the effects of these treatments on the host rock (Taron, 2009). The potential for porosity loss due to the formation of anhydrite will also need to be assessed.

Pore-level imaging is very important to know the change in mineralogy due to dissolution (Khishvand, 2016). Mapping the pore space of synthetic and natural porous media can be analyzed significantly by recent advances in pore-level imaging. Three-dimensional snapshots of fluid occupancy can be obtained by researchers/scientists during flow experiments, which enables the investigations of rock/fluid interactions on a pore-by-pore basis. During last decade, a large number of studies have been performed concentrating on the use of pore-level

imaging techniques to study complications associated with a wide range of flow through porous media problems (Shafiq & Ben Mahmud, 2017).

High-resolution X-ray images have been used for characterization of relative permeability changes due to gel injection, capillary pressure calculation, and quantification of porosity changes during mineral dissolution, pore- scale contact angle measurement, mapping of pore-scale fluid distribution during drainage, and investigation of trapped non- wetting phase distribution in the pore space. (Khishvand, 2013 and Wildenschild, 2013), have provided a detailed discussion on the applications of micro-CT imaging in this area of research.

2.12 Experimental work

Different type of experiments was carried out by researchers to investigate the effect of acid combinations on sandstone and carbonate formations applied during the matrix acidizing. Al-harbi et al. (2012) and Zhou and Nasr-El-Din, (2013), applied FNMR, ICP, and SEM analysis to identify the reaction products and to explore the possibility of any precipitations. While Al-Harbi et al. (2011) applied XRD and SEM technology to explore the reaction products. Krebs et al. (2014), used CT scan technology to investigate the acid reaction path during sandstone acidizing. So, in the view of this, most of these experiments are included in this project in order to find the reaction mechanism of acids and chelates with sandstone and carbonates. Some new experiments are introduced in this research like Nuclear Magnetic Resonance Logging (NMR Logging) and Tescan Integrated Mineral Analysis (TIMA). NMR Logging is very useful in the determination of pore topology and pore size distribution. It helped to analyze the number of small and large pores within the core sample. This technique can prove to be very important for analyzing acidizing results. TIMA, on the other hand, can be very useful in the determination of change in mineral composition due to acidizing. Elemental concentration, mineral concentration, mineral locking, and pore size distribution can be determined using this technique. TIMA will be very useful to determine the relationship between acidizing and CO_2 storage as mineral analysis can review the dissolution of different minerals which can help in increasing CO_2 storage.

2.13 Summary

Matrix or Fracture Acidizing in sandstone or carbonate reservoirs is very important to remove damage or by introducing new pathways to ensure high production of the reservoir. Many

studies have been performed so far highlights the importance of acidizing in sandstone formations. Many researchers developed different acid combinations to get the best results related to permeability, porosity, and change in mineralogy but still, there are some limitations like fast spending of acid, precipitation reactions, less penetration of acids, sludge formation and corrosion of pipelines. New acid combinations are required for future matrix acidizing aspect and further study is needed on current technology because of the limitations of present acid combinations at high-temperature wells and limited study of these combinations on different sandstone and carbonate formations. Techniques applied to study the changes in the reservoir are also of very importance. New techniques need to be applied to investigate deep changes in the properties of the sample. Mineral Dissolution plays an important role in matrix acidizing where precipitation reactions and other products formed can be analyzed using types of reactions occurred. Dissolution of certain minerals can help in storage of carbon dioxide (CO_2), thus geosequestration of CO_2 can also be discussed as a part of matrix acidizing.

.

Chapter 3

Experimental Setup, Material and Procedures

In this chapter, components and specifications of different parts of the core flooding setup will be discussed which is capable of dealing with the necessary conditions of experimental work i.e., size of the core sample, temperature, flow rate, corrosivity, and pressure. As the major section of the experimental work performed during this research consists of core flooding experiments, which were performed using a core flooding apparatus (High-Pressure High-Temperature conditions (HPHT) compatible), present at the main campus of Curtin University, Department of Petroleum Engineering. The first section of this chapter consists of a detailed description of the core flooding apparatus and its supporting parts. The second section gives the detailed description of materials lie acids and core samples used during the project. This section is followed by the experimental procedures of performing various laboratory experiments carried out before and after the core flooding experiments. These experiments include pH value, permeability, porosity, pore volume, solubility and breakthrough volume. At the end of this chapter, a brief introduction of specialized equipment used to analyze pore topology, pore size distribution, mineral and effluent properties is presented. Moreover, mineral composition, pore topology, pore size distribution, particle size distribution and high-quality images analysis are obtained using Tescan Integrated Mineral Analysis (TIMA), effluent samples are analyzed using Inductively Coupled Plasma (ICP), immobile and mobile pore spaces analyzed using Nuclear Magnetic Resonance and finally flow pathways are investigated using Computed Tomography (CT scan).

3.1 System requirements

The main parts and functions of core flooding setup essential to perform acidizing experiments are:

- The pump which can pump the fluids at broad rates and is able to work at either constant pressure or constant flow rate modes.
- The setup should be developed which can be run at a steady rate and linear flow.
- High-Pressure Liquid Chromatography flow system to inject fluids like brine and acids. The required flow rate is 0.00006 m^3/sec.

- Corrosion resistant core holder made up of Hastelloy material which can prevent acid corrosion and can withstand at high pressure and temperature conditions for a long time. There should be two inlets and one outlet for acid flow while at least two inlets for the confining pressure.
- Temperature controllers and heating tape to increase temperature according to field conditions or at a desired value. The maximum temperature attained using the controller should be 260^{o}C.
- Data acquisition system connected with pressure transducers to monitor pressure changes at the inlet and outlet of setup.
- Hydraulic syringe pump used to create the needed confining pressure within the core holder to confine the core sample. It uses fresh water to create a high pressure which can reach up to 138 Mpa.

3.2 Core Flooding Setup

Figures 3.1 and 3.2 show the core-flooding experimental setup and schematic diagram respectively, considering the requirements mentioned in section 3.1. This setup was used for the core flooding of Berea sandstone, Colton sandstone and Guelph dolomite core samples with acids and chelates. This core flooding setup is capable of handling a pressure up to 68 MPa and a temperature up to 260^{o}C. The wetted parts of the apparatus which probably comes in contact with acids and chelates are made of corrosion resistive material (e.g., Hastelloy), therefore, even higher concentrations of acids will not cause any corrosion or rusting. Fluids are injected at a rate of 0.00006 m^3/sec. The experimental setup consists of six basic parts which are listed below where the function of each part is described below:

- Core holder
- HPLC pump
- Syringe Pump
- Temperature Controller
- Pressure Transducers
- Piping, network, valves and fittings

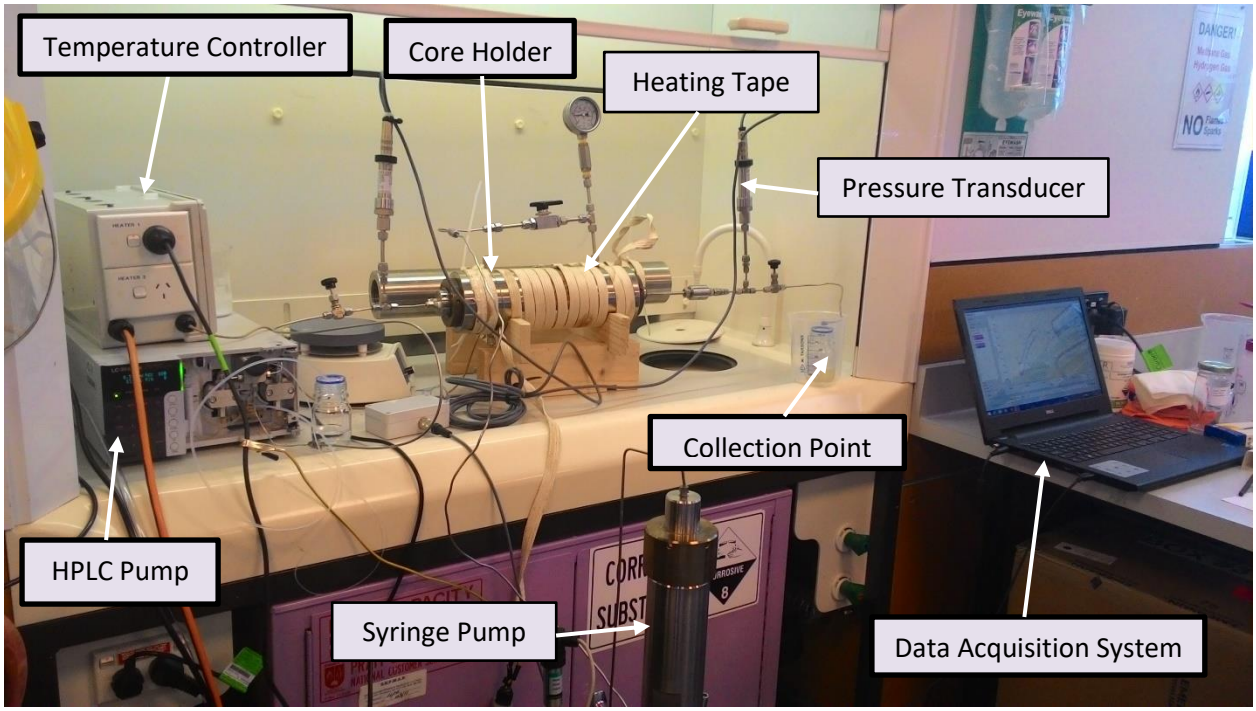

Figure 3.1. Core Flooding Setup

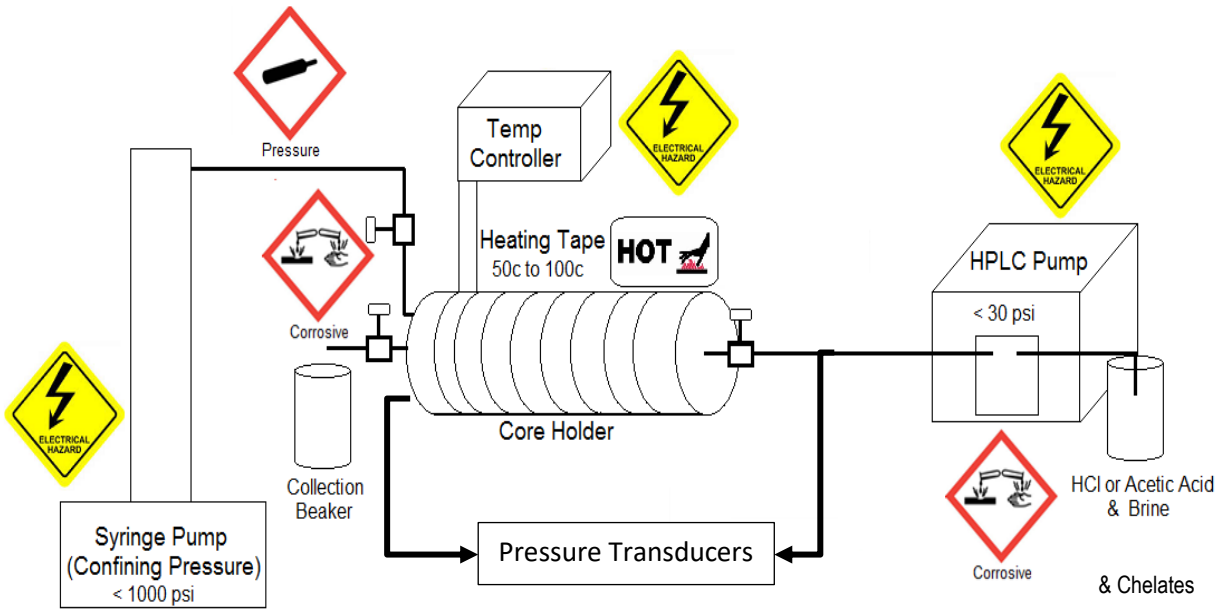

Figure 3.2. Schematic Diagram of core flooding setup

3.2.1 Core holder

The core holder (as shown in Figure 3.1) is commonly used in core flooding experiment and is used to confine the core sample at desired pressure and temperature. The material of this core holder is Hastelloy which protects it from corrosion. It has two inlets and one outlet. HCH Series core holders consist of Hydrostatic or standard Biaxial, type core holders. Biaxial type

core holder is a core holder which experienced common radial and axial pressure. Gas and liquid permeability can be measured using this type of core holder. Unconsolidated core samples are usually tested using HCH type core holders. Biaxial type core holder is recommended for high-temperature core flooding operations and can be used for full diameter core samples. This design is less in weight and is more compact compared to other models. Using sleeves this type of core holder can be used to core flood different diameter core samples too.

For HCH Series core holders, the axial pressure is applied at the outer diameter of the core while the radial pressure is applied through the end of the core sample. To displace the air and to fill the annulus properly, two confining pressure ports are provided. 0.00635 meter tube is used to connect the distribution plug, which floats inside the end cap. This allows the back and forth movement of the distribution plug within the core holder which allows a constant contact of the distribution plug with the core sample during compression and confining. Due to this flexibility, the core holder can be used for cores with different lengths. One or more outlets can be made available to distribution plugs, depends on the requirement. Minimum volume is kept at ports and flow lines to accurately determine flow data and to improve the accuracy of volume measurement. Spiderweb type groove is used at the end of distribution plugs as shown in Figure 3.3. To make sure the even distribution of the fluid at the core sample face (before entering or leaving), this groove type structure is furnished. This type of groove pattern proved to be effective in creating the inlet and outlet capillary effect, usually experienced while performing displacement experiments.

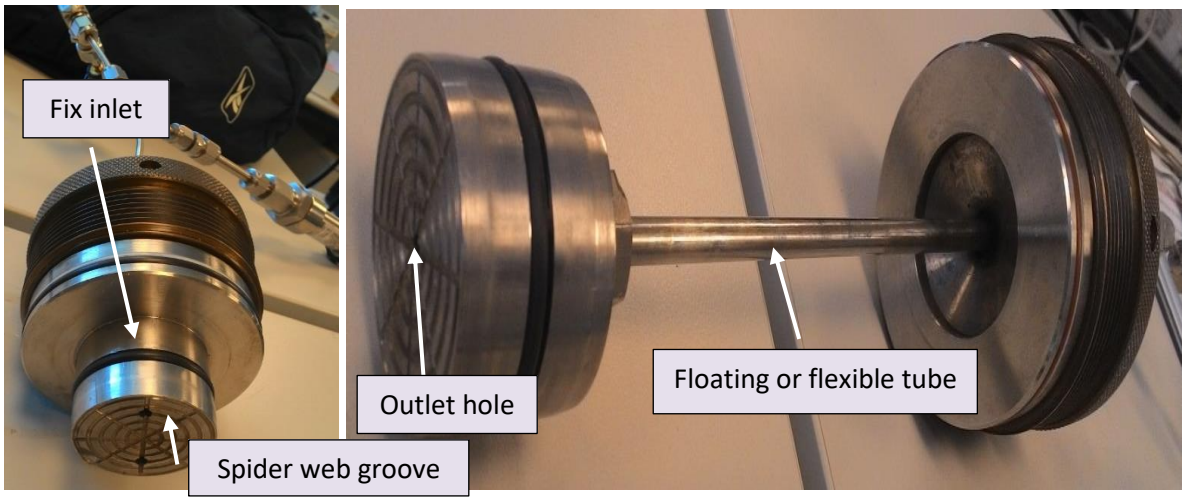

Figure 3.3. Core Holder Inlet and outlet ports

The core holder is connected to HPLC pump, syringe pump and outlet system using piping of 1/8-inch diameter. This pipe is then connected to transducers at the outlet and inlet ports. Valves are placed at the inlet and outlet to control any unrequired pressure conditions that may occur during the core flooding procedure. The schematic diagrams of core holder set up and spider web groove are shown in Figures 3.4 and 3.5 respectively:

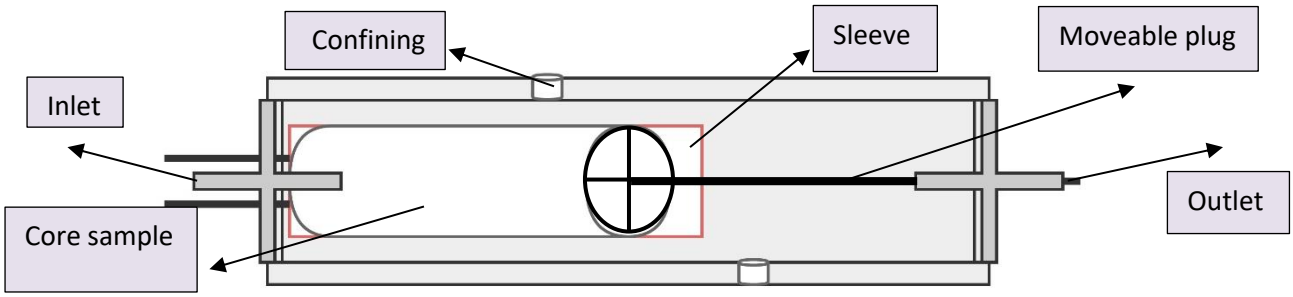

Figure 3.4. Core holder schematic diagram

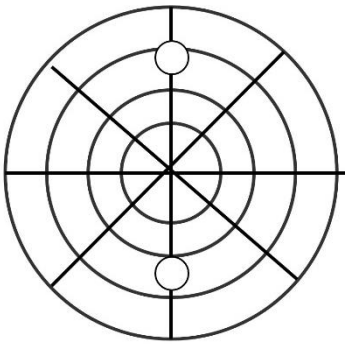

Figure 3.5. Core holder spider web groove

3.2.2 HPLC pump

The High-Performance Liquid Chromatography pump as shown in Figure 3.6, is used to inject the acid into the core holder at a desired and controlled rate. It can inject a liquid at a maximum rate of 0.36 m^3/sec. The injection rate for this research is 0.00006 m^3/sec. The less injection rate is used in order to avoid high back pressure during the experiment. Less reaction rate also allows the acid to react effectively with the surface of the core sample, which can help in creating wormhole structures. As the chelate solution is viscous and experiments also involved tight samples, therefore, less injection rate is necessary to avoid high pressure at the inlet face. If the pressure increases to more than 6.9 MPa (confining pressure), the chelate may bypass the core sample which is not desirable phenomena during the core flooding. The schematic diagram of the HPLC pump used is shown in Figure 3.7.

Figure 3.6. HPLC Pump Parallel Double Micro Plunger Type

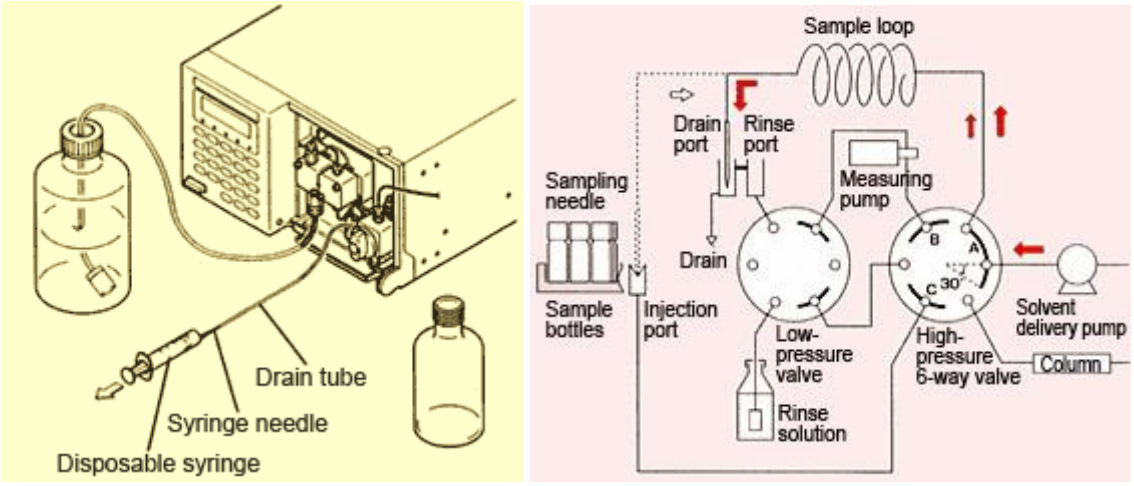

Figure 3.7. Schematic Diagram of LC-20AD HPLC pump (Shimadzu technical Manual)

The LC-20AD is one of the most stable systems for the injection of the solvent in the world. This pump is equipped with the automatic pulsation-correction mechanism and it can achieve pulse free delivery of solvent because of high-speed micro parallel type double plunger drive. It is called double micro plunger as it consists of one low-pressure valve and one high-pressure valve (Figure 3.7). The capacity of the plunger is $0.01m^3$ and the maximum discharge pressure of this pump is almost 40MPa. It can inject up to 0.00001 m^3/sec where the minimum flow rate is set at 0.00000001 m^3/sec. It can be operated in a temperature range of 4ºC to 35ºC. The maximum pressure indicated the pressure above which the pump will automatically stop. The value of this pressure should be kept less than the confining pressure to avoid acid bypassing the core sample.

3.2.3 Temperature Controller

The temperature is one of the most important and relevant factors that can affect the reaction rate and chemical reactions kinetics between acids and the minerals. Therefore, the temperature considered to be an important aspect of stimulation; and acidizing experiments are conducted at elevated temperature conditions as the fact that the actual temperature of the reservoir is much higher than atmospheric or room temperature. To study the effect of temperature on wormhole creation and minerals dissolution, the core holder is completely insulated using heating tape. Heating tape is used to cover the core holder in the laboratory setup, shown in Figure 3.7. This heating tape is capable to wrap around the core holder of any size, as small as 0.003175 m and can be used in either nonconductive or conductive surfaces.

The Temperature controller (Figure 3.8) is used to heat the core holder at the desired temperature value. This is a high-temperature heating tape with a maximum exposure temperature of 260^{o}C is used, it consumes 500 watts of electricity and is 6.096 meters long. This tape provides excellent flexibility and durability due to the multi-stranded resistance wire heating element. To avoid electrical conductivity and safe use through conductive surfaces, the outer sheath is provided for electrical insulation. Whenever required, accurate heat is provided through rapid thermal response. This heating tape and controller are ideal for laboratory application like heating for valves, core flooding and more. To make the operation safe, the temperature controller is used with the heating tape.

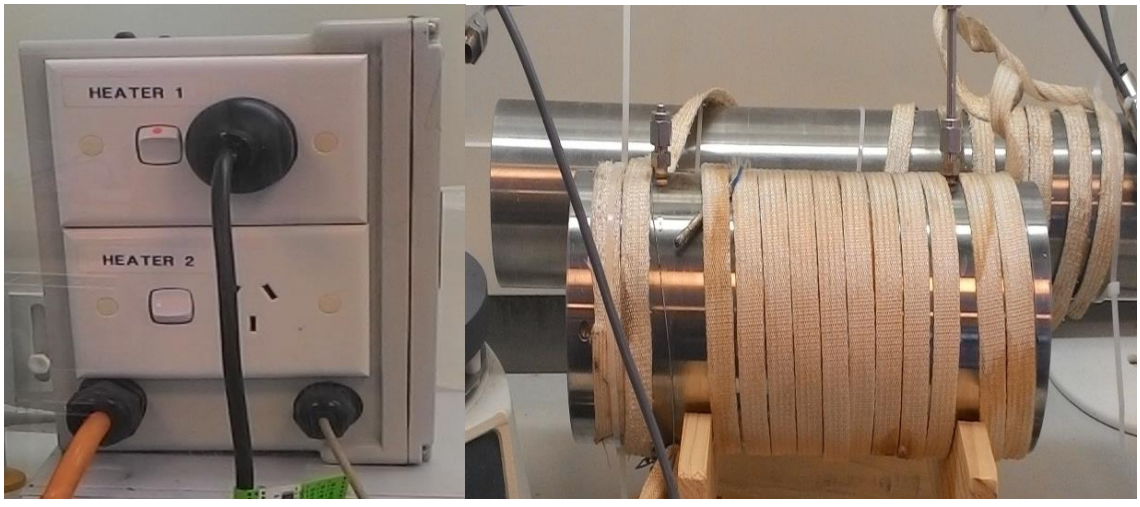

Figure 3.8. Temperature Controller (left) and heating tape (right)

The temperature of the heating tape wrapping the core holder is controlled by using the temperature controller, which utilizes selectable control mode temperature control. Digital

output, which is a 4-digit display is the main feature of this controller which indicates the processing/core flooding temperature. The front panel of the temperature controller consists of the electric plug where heating tape can be connected. While on the side of the controller there is the digital panel where up and down keys are provided to set the temperature in °C or ^{o}F. The resolution of this controller is 0.1^{o} and it uses a thermocouple type K and two outputs, with an accuracy of ±0.25% full scale ±1°C.

3.2.4 Syringe pump

The syringe pump (Figure 3.9) is used to create a high pressure inside the core holder. It uses fresh water to create high pressure and can create up to 137 MPa. The confining pressure used in this study is 6.89 MPa, this is applied not to allow the acid to bypass or overflow the core sample matrix. The Isco Tedelyen 65D syringe pump is one of the best pumps which can be used for very high-pressure ranges or very low flow rates. It also proved in this research as the pressure was maintained accurately with very less variation during the core flooding.

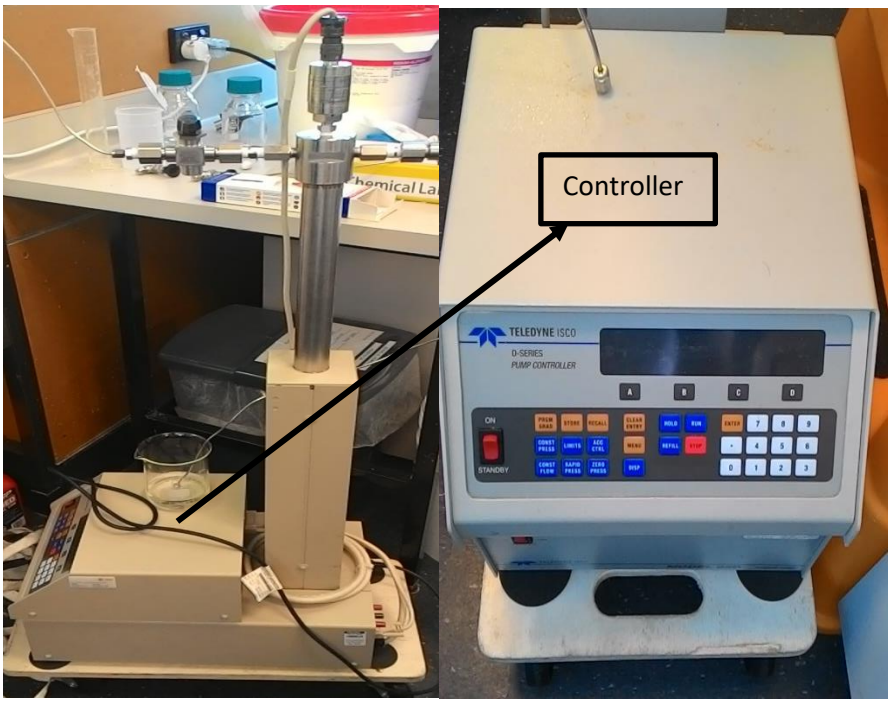

Figure 3.9. Isco Tedelyen 65D syringe pump

Standard Features

- 1/4" F-250 has been provided to 65D pump for secure high-pressure connections.

- Long life and low maintenance of the pump has been assured by providing auto lubricating gears.

"Smart Key" controller is installed in this pump and it includes following modules:

- Constant pressure or flow (Single pump independent)
- Ramp programming (Single pump pressure or flow)
- Dispensing (Single pump)
- Constant pressure or flow (Dual pump continuous)
- Concentration gradients (Dual pump)
- Configured systems (Three-pump)

For monitoring of operating parameters or the computer control; RS-232/485 serial interface is provided. The pump is corrosion resistance due to the presence of Nitronic-50 material (austenitic stainless steel) which is standard for preparing different parts of the pump like caps, cylinders, and pistons. This material has outstanding strength and can withstand high pressure and is corrosion resistive.

Applications

- For High-pressure experiments which require precision control
- Can be used for core analysis to study hydrocarbon recovery in core flooding experiments for high temperature and pressure reservoirs.
- Can be used for Chemical/reactant feed during chemical process development.

Options and Accessories

- Hastelloy can be used in the construction of this instrument
- Temperature control jacket is installed for cooling of fluids like liquefied gas
- When ultra-low flow rates were used; thermal stabilization can be provided
- High accuracy pressure transducers are installed with 0.1% linear accuracy,
- Drivers for LabVIEW graphical programming software from National Instruments can be installed.

3.2.5 Pressure Transducers

The pressure transducer senses the difference in pressure between two points and produces electric signals as an output according to calibrated the pressure range. It is often known as a pressure transmitter; it is a transducer which can produce the analogue electrical signal by converting pressure signals. Different types of pressure transducers are available but most often used is the strain-gage base transducer.

The electrical signals are obtained by converting the pressure which can be achieved by the strain gages physical deformation, connected to the pressure transducer diaphragm while Wheatstone bridge configuration is wired. The pressure transducer is affected by the pressure applied which in turn produces diaphragm deflection; this deflection produces strain to the gauges. Electrical resistance is produced by the strain which is proportional to the pressure.

Core flood setup in this project is installed with the pressure transducer (Figure 3.10), which can measure pressure difference across the core holder and coveys the signals to the computer during the experiments. The transducer engaged is PR-23SEi manufactured by Keller, with an accuracy of 0.001%. The pressure range is 0 – 2 MPa with the efficiency of 0.01%. Two transducers were connected with the setup to measure pressure at inlet and outlet ports.

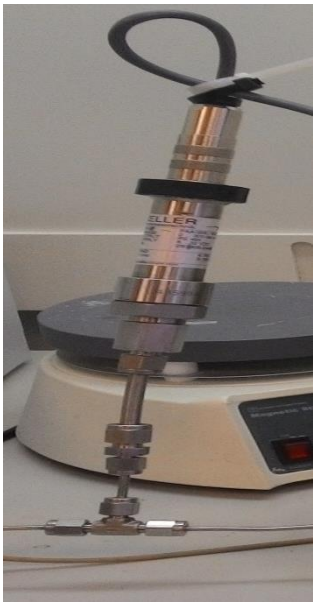

Figure 3.10. Pressure Transducer

3.2.6 Piping network, valves, and fittings

Acids and brines are displaced during the operation using the tubing pipes of 0.003175 m diameter having wall thickness of 0.000762 m. The significant inner diameter will allow the

maximum flow rates of acids and brine provided by the HPLC pump and ISCO 65D pumps respectively. Because the fluids used during this project consists of acids, therefore, the tubing connected with HPLC pump is made of Hastelloy, which is acid resistive material. Regular stainless steel tubing of 0.003175 m is connected with the syringe pump where brine is used. Needle type valves (figure 3.11) are installed in the core flooding piping set up; Hastelloy material is used to made needle valves taper seal, as acid is used in this project. There is a sliding sleeve in the valve which attaches metal to metal as a compression fitting. They are designed in such a way that can tolerate pressures up to 103 MPa and temperatures as high as 232^{o}C.

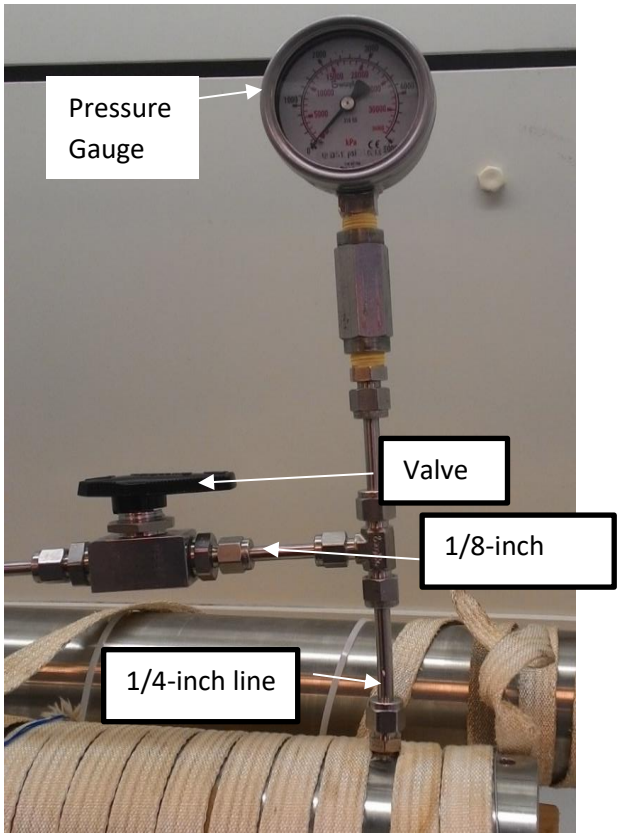

Figure 3.11. Gauge, piping, and valves

3.3 The Materials

3.3.1 Fluids

During various stages of experimental work which were conducted during this project, six different types of fluids were utilized. These fluids used are dead brine (brine without any content of dissolved gas), acetic acid (CH_3COOH), hydrochloric acid (HCl) and different chelating agents like GLDA, HEDTA, and EDTA. 5% NaCl brine solution was also used to

saturate the sample for Nuclear Magnetic Resonance experiments. Properties and description of acids used in this project are mentioned in Table 3.1.

Table 3.1. Acids and their properties

Acid	Properties and Description
Acetic Acid 	The colorless liquid organic compound, CH_3COOH, also known as a glacial acetic acid when undiluted. It has a sour taste and pungent smell, it's a weak acid but if concentrated can be corrosive. Widely used in petroleum industry during acidizing due to its less corrosivity. Density: 1.049 g/cm^3, Boiling point: 118 to 119°C
Hydrochloric Acid 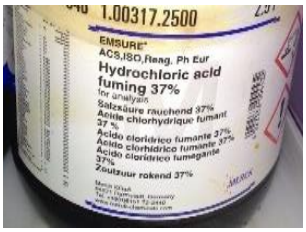	It's a strong mineral acid, HCl, corrosive, colorless and pungent smell. It is highly reactive acid and widely used in acidizing operations due to its reactivity and ability to dissolve several minerals. Density: 1.19 g/cm^3, Boiling point: 40^{o}C
EDTA 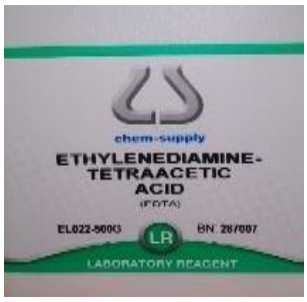	It is colorless amino polycarboxylic acid and is water soluble. It is used to remove limescale and it has the ability to sequester metal ions such as calcium and iron. It is being applied during acidizing due to stability and less corrosive nature at high temperatures. The most widely used, strong, cost-effective and general purpose chelating agent. EDTA Disodium salt Density: 860 mg/mL[1] (at 20 °C), Formula: $C_{10}H_{16}N_2O_8$
HEDTA 	It is colorless aminopolycarboxylic acid. A chelating agent with similar effectiveness like EDTA. Very useful in petroleum industry acidizing procedure to stabilize iron at high pH value and is soluble in low pH value. It has less corrosivity at high temperatures. Formula: $C_{10}H_{18}N_2O_7$

GLDA 	The latest, strong and green chelate. It is readily biodegradable and safe, that can be used in cleaning applications, as an alternative to EDTA, phosphates, NTA, and phosphonates, It is high solubility over a wide pH range. It usually originates from a natural sustainable source. Formula: $C_9H_9NO_8Na_4$

3.3.2 Acid Selection

This section illustrates different acid combinations and chelating agents proposed for matrix acidizing. These combinations and chelates are selected; based on the previous studies and research discussed in chapter 2. Table 3.2 shows the acids and chelates prepared for this study.

Table 3.2. Fluids prepared for acidizing

FLUIDS / ACIDS	**PURPOSE**
15%HCl: 2.5%CH_3COOH 10%HCl: 5%CH_3COOH 12%HCl: 3%CH_3COOH 10% HCl	Used to dissolve positive ions like calcium, sodium, potassium, magnesium and act as a buffer for the main acid stage.
GLDA HEDTA EDTA	To increase the porosity and permeability of the reservoir by removing different minerals inside the formation without corrosion and precipitation.

3.3.2.1 Acid preparation

Different acid mixtures with various concentrations have been prepared for different acidizing treatments. In sandstone matrix acidizing usually a mixture of HF and HCl acid is applied, and their concentrations usually vary depends on the required effect. While during the preflush stage usually HCl acid is used to remove positive ions like calcium, magnesium, and sodium. In sandstone acidizing HCl acid is applied with different concentrations. Acid volume can be calculated using formula mentioned in Equation 3.1:

$$M_1V_1 = M_2V_2 \qquad (3.1)$$

Concentrations of acids are already given by the supplier (acids in liquid form):

- HCl is 37%,
- CH_3COOH is 100%.

For Example: To prepare a combination of 7.5% HCl: 2.5%CH_3COOH, the calculations are as follows (Table 3.3):

Table 3.3. Calculation of Acid-water volume for pre-flush stage

HCl	**CH_3COOH**
$M_1V_1 = M_2V_2$	$M_1V_1 = M_2V_2$
(37) V_1 = (7.5) (175)	(100) V_1 = (2.5) (175)
V_1 = 35.47 ml	V_1 = 4.375 ml
The total amount of solution is 175ml; the remaining volume is filled in by the brine water. Volume of water = 175-35.47-4.375= 135.55 ml	

3.3.2.2 Preparation of chelating agents

The saturated solutions of chelating agents (figure 3.12) have been prepared in distilled water. The chelating agent's structures are already mentioned in chapter 2, while the equilibrium constant and stability constants of acids and chelates are mentioned in table 3.4 and table 3.5 respectively below. These chelates are basically complex acids and dissociation in water is important for the acidizing purpose. The dissociation is expressed in terms of equilibrium constant pK_a. The theoretical values of pK_a obtained are mentioned in table 3.4. These values can be used to determine the distribution of GLDA as a function of pH. These chemicals in purified solid form are purchased from the chemical supply. Tokyo Chemical Industry Co. LTD (TCI) provided GLDA and HEDTA. As can be seen in Figure 3.12, the HEDTA and GLDA are soluble in deionized water and showed acidic properties when the 20% wt. a saturated solution is prepared. While EDTA is less soluble, therefore, 5% wt. a solution of EDTA is prepared in deionized water. The solubility of EDTA in deionized water is increased and 20% wt. the saturated solution can be prepared.

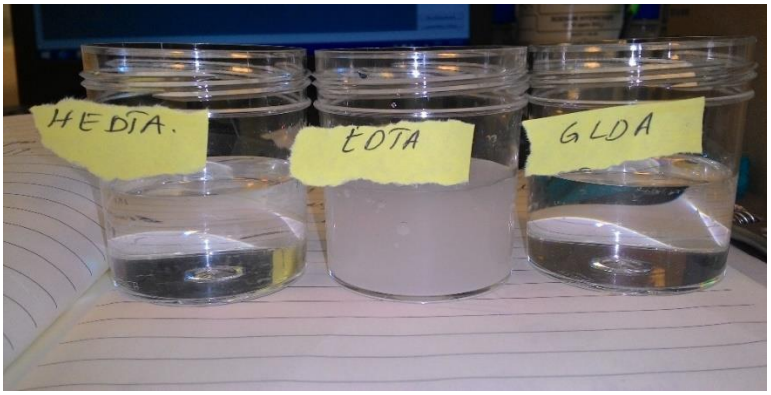

Figure 3.12. Prepared Chelating agents

Table 3.4. Equilibrium constants of acids and chelates (Martel and Smith, 2004; Begum et al. 2012a and 2012b; Frenier 2001; Shuler et al. 2002)

Acid	MW	pKa values				
		pK1	pK2	pK3	pK4	pK5
Acetic Acid	60	4.5				
Hydrochloric acid	37.5	-4				
EDTA	292	10.2	6.2	2.7	2.0	1.5
GLDA	185	9.4	5	3.5	2.6	
HEDTA	278	9.8	5.4	2.6		

Table 3.5. Stability Constant (Martel and Smith, 2004; Begum et al. 2012b, Anderegg at al. 2005)

Ion	Acetic Acid	Hydrochloric acid	EDTA	GLDA	HEDTA
Al (III)	1.51	Not available	16.5	12.2	14.4
Fe (II)	1.4	Not available	14.2	8.7	12.2
Fe (III)	3.4	Not available	25.0	15.2	19.8
Cu (II)	1.8	Not available	18.8	13.03	17.4
Mg (II)	1.27	Not available	8.83	5.2	7.0
Ba (II)	1.07	Not available	7.8	3.5	6.2
Ca (II)	1.18	Not available	10.7	4.8	8.4

3.3.3 Core Samples

Figure 3.13 represents Berea sister grey core sample, which is one of the samples used in this project. The size of each core sample is 0.0381 m in diameter and 0.0762 m in height. The properties of each core sample are mentioned in the table.

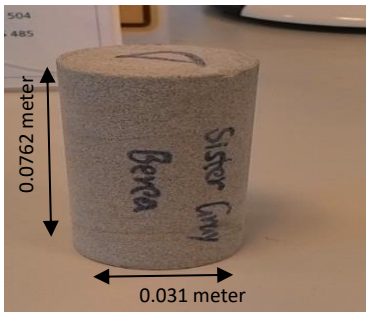

Figure 3.13. Core Sample dimensions

Sedimentary rocks consist of 46%, shale, 32% sandstone and 22% carbonates (Leet LD 1971). Therefore, a huge amount of hydrocarbons has been stored in sandstones and carbonate formations around the world. Whereas deeper and hooter sandstone and carbonates aquifers are considered to store oil and gas all around the world and present a large storage capacity available. The core samples used in this experimental work mainly consisted of different types of sandstones and dolomites in terms of permeability and porosity. The core samples could be divided into three different groups based on their origin, porosity and permeability ranges.

The first type of core sample having moderate permeability to high permeability and moderate porosity values, which are the characteristics of Berea sandstone. The second type of sandstone formation having very low permeability and moderate porosity are usual characteristics of a Colton Sandstone. The third type is carbonate with variable permeability and porosity due to heterogeneity are known as Guelph dolomite.

The Berea Sandstone core samples purchased from Vermilion, Ohio, USA. All core plugs are homogeneous and having the same absolute permeability (60 – 100 md) and porosity (19 – 20%) as requested. The Berea core sample has following characteristics: well-sorted, clean having medium to fine size grains with moderate porosity and high to moderate permeability. Berea sandstone mostly consists of quartz (90 - 93%) and feldspar (3–5%) and small quantities of calcite and aluminosilicates. Cementing material in Berea sandstone is predominantly quartz (85 – 90%), clays (6–8%), dolomite (1–2%) and some traces of iron sulfide. These samples

were denoted by word Berea followed by sample number like A, B, for example (Berea A, Berea B).

The Colton sandstone samples were purchased from Kocurek Industries INC. Hard Rock Division, Caldwell, Texas, USA. These samples are also homogeneous having porosity and permeability as requested. These samples have the following characteristics: well sorted, the clean formation having a moderate porosity (7 – 14%) and very low permeability (1 – 2md). Colton sandstones mostly consist of quartz (90 - 93%) and feldspar (3–5%) and small quantities of calcite and aluminosilicates. Cementing material in Berea sandstone is predominantly quartz (85 – 90%), clays (6–8%), dolomite (1–2%) and some traces of iron sulfide. These samples were denoted by word Colton followed by sample number like A, B, for example (Colton A, Colton B).

The Guelph dolomite samples were purchased from Kocurek Industries INC. Hard Rock Division, Caldwell, Texas, USA. These samples are heterogeneous in nature having porosity and permeability as requested. These samples have the following characteristics: well sorted, the clean formation having a moderate porosity (17%) and very low permeability (10 md). But these values can be different from plug to plug due to heterogeneity. Guelph dolomite mostly consists of ankerite (93 - 95%) and feldspar (3–5%) and small quantities of calcite and aluminosilicates. Cementing material in Guelph dolomite is predominantly quartz (85 – 90%), clays (6–8%), dolomite (1–2%) and some traces of iron sulfide. These samples were denoted by word Dolomite followed by sample number like A, B, for example (Dolomite A, Dolomite B). Table 3.6 represents the properties of core samples used during the project.

Table 3.6. Core samples and their properties

Properties / Core sample	**Berea (Conventional Sandstone)**	**Colton (Tight Sandstone)**	**Guelph dolomite**
			
Company	Cleveland queries, Vermilion, Ohio, USA	Kocurek Industries INC. Hard Rock Division, Caldwell, Texas, USA	Kocurek Industries INC. Hard Rock Division, Caldwell, Texas, USA

Properties	Homogenous, Clear sandstone	Homogenous, Dirty sandstone	Heterogeneous, Clean formation
Minerals	93-96% Quartz 3-5% Feldspar	59% Quartz 10% Albite 8% Calcite 4% Ankerite 3% Orthoclase	97% Ankerite 2.5% dolomite
Porosity	16 - 19 %	10 - 12 %	14 – 15%
Permeability	60 – 100 mD	0.1 - 2 mD	9 – 500 mD

3.3.4 Core sample preparation and description

Core samples used in this project are Berea sandstone, Colton sandstone (Tight sandstone), carbonates (Guelph Dolomite). Core cutting machine was used to cut the desired length of core samples. For core flooding experiments the length of the core required was 0.038 m diameter by 0.0762 m long. While for TIMA and Wettability analysis the small size of the sample was required as shown in the figures 3.14 and 3.15. The figure 3.14 shows the smallest size of a sample obtained from Berea sandstone, Colton sandstone, and Guelph dolomite. All the samples have been dried and vacuumed inside the vacuum oven to remove any liquid or gas particle present inside.

Figure 3.14. Samples prepared for wettability analysis

Figure 3.15. Samples prepared for TIMA analysis

3.4 Experimental Procedure

Standard protocols and procedures that have been outlined in literature have been applied to all experiments performed in this research. Other than core flooding experiments which are the core experiment of this research several other laboratory procedures were performed as well, which include the following:

- Cutting of core-plugs according to the desired length for experiments.
- Cleaning of core-plugs to remove any liquid or salt present inside.
- Drying of core samples before and after acidizing at 80^{o}C for 24 hours in a vacuum oven (figure 3.16).

Figure 3.16. Vacuum Oven

- Measuring the weight of the core sample before and after acidizing to check solubility.
- Measuring porosity and permeability of the core-plugs before and after acidizing using AP-608 automated Permeameter-Porosimeter.
- Analyze mineralogy of the core sample before and after acidizing using Tescan Integrated Mineral Analysis (TIMA).
- Measuring the concentration of different metals in effluent samples using ICP analysis.
- Finding the change in wettability state of core sample due to acidizing using Wettability apparatus.
- Cutting small size core samples for micro-Ct scan analysis
- Saturating core samples with 5% brine solution for NMR analysis
- Running NMR tests on all samples before and after each core flooding test.
- Measuring pH value of acid solutions before and after core flooding tests using pH meter (figure 3.17).

Figure 3.17. pH meter

3.4.1 Initial Measurements and Core-Plug Preparation

The core holder has the ability to hold a core of 0.0381 m diameter and 0.3048 m in length. Therefore, an appropriate size color plug has been used. The size of the core plug used in this research is 0.0381 diameter and 0.0762 m length. Brine water is used as a fluid during the coring operations because freshwater or oil base mud can cause swelling of the clay and ultimately damage the core sample properties such as porosity, permeability, and wettability alteration. To avoid capillary discontinuity due to the presence of a rough surface at the end of the core sample, the core surface is smoothened to make sure proper contact between the core and core holder.

The maximum length of the core plug that porosity measurement instrument can accommodate is 0.0990, therefore, the plug is cut accordingly. After cutting, methanol and toluene were used to clean the core plugs from any salts and fluids respectively during the dean stark experiment (Gluyas, 2004) (Figure 3.18). The permeability of the sample controls the cleaning time which ranges from 15 to 48 hours. Special care was taken while cleaning the sample to not expose it to a very high temperature as it may damage the core sample. After cleaning, all the core plugs were dried in an oven under 80^{o}C for 24 hours. Stabilized weight is the indication of complete drying of core samples. The 80^{o}C temperature was selected to avoid evaporation of water bounded by clay. The removal of such water may cause damage to clay minerals present in the core samples (Byrne, 2004). After cleaning and drying process, the core samples were cooled down to room temperature under desiccator to perform other analysis. Once cooled, Vernier caliper is used to measure the dimensions like diameter and length.

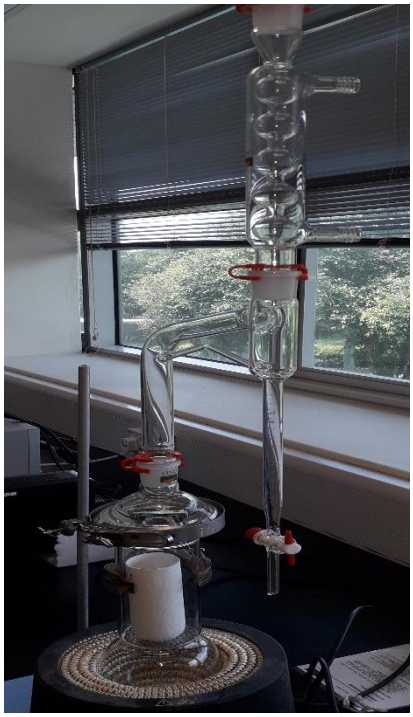

Figure 3.18. Dean-stark apparatus

3.4.2 Sample Restoration

Wettability of the porous rock plays an important role in the fluid displacement of during core-flooding experiments. Moreover, wettability conditions of the porous media also influence the NMR analysis that is carried out on core samples before and after the core flooding experiments (Fleury, 2003 and Chen, 2006). The Strong water-wet condition is the characteristic of a cleaned dry sandstone (Anderson, 1987; Wendell et al., 1987). In order to achieve the desired rock characteristics and reservoir conditions, if there was a change in wettability during the core handling procedures (contact with drilling fluids, with fluids on the rig floor, and by contact of the air with the core). Moreover, for most reliable measurements of wettability, laboratory fluids should also be at reservoir conditions. it is required to be restored to the original water-wet condition. Therefore, after measuring the porosity of the core sample, the formation brine was prepared using distilled water and NaCl salt to saturate the samples by immersing them in brine inside a vacuum desiccator (Figure 3.19). According to the time range recommended in the literature, the samples were kept saturated in the brine under vacuum conditions for about 2 weeks (Mungan, 1966; Anderson, 1987 and Wendell et al., 1987). This is to ensure that the adsorption equilibrium is reached and the water wetness is restored. Brine level was continuously monitored during this 2-week period to observe any evaporation and if

there is any drop in the level of brine, an appropriate amount of distilled water is added to the solution.

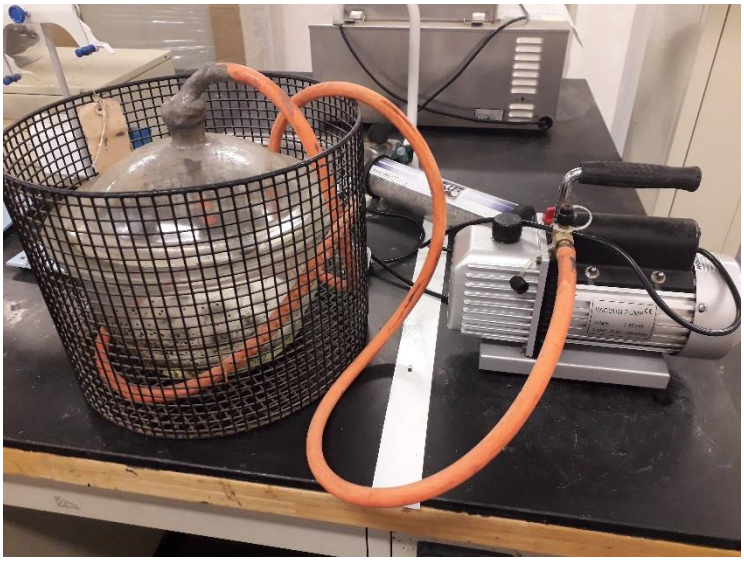

Figure 3.19. Vacuum pump and desiccator

3.5 Core flooding procedure

The effect of acids on different types of core samples can be mimicked by acid core-flooding technique. Acid-mineral interaction is a diverse phenomenon during linear core flooding experiments. Performing linear core flooding acidizing in the laboratory is quite useful to understand the complex acid mineral interaction process especially in matrix acidizing.

One of the aims of this project is to design a reliable cost-effective core flooding acidizing setup to conduct core flooding experiments at different conditions and to investigate different effects on core samples once acidized. In carbonate rocks formation of highly conductive pathways (wormholes) is the indication of effective matrix stimulation which is the result of flow and reaction of acids.

The injection rate, fluid, and rock properties affect the structure of wormholes (Fredd et al. 1997). Complete dissolution of wormhole structure can occur at inlet face at low injection rates i.e., less than 0.00012 m^3/sec while uniform dissolution may occur at higher flow rates and intermediate flow rates may create a single a dominant wormhole.

After the type of rock and treatment fluids characteristics are defined along with the requirement of setups, the beaker is filled with appropriate fluids, then the core flooding can be carried out. The detailed procedure of whole core flooding is as follows:

- First of all, the core was inserted inside the core sleeve and was placed inside the core holder and the inlet and outlet wings of the core holder were closed. The flow lines from the inlet, outlet and HPLC were connected. It was made sure that all the connections were tightened and valves were placed in proper positions. The inlet flow line was connected to the HPLC pump to inject the fluids into the core sample. Set the flow rate at 0.00006 m^3/sec and 6.55 MPa pressure range was selected to disconnect the injected flow of acid.
- The core holder was filled with the water with the help of a syringe. It was then connected with a syringe pump and connections were tight carefully; pressure was then increased to confine the core sample. The confining pressure was set at 6.89 MPa. Then the discharge valve of the syringe pump was opened which was filled with water to confine the core sample. The front panel of the syringe pump was used to select the pressure value and flow rate of the water.
- Core holder was wrapped with the heating tape completely and the temperature controller was connected to the heating tape. The heating tape only started operation after the core sample was confined under pressure. Pressure and temperature were monitored constantly. The syringe pump was kept connected and the valve was kept open during heating of the core holder as the increase in temperature can cause the expansion of the fluid. The temperature of the core flooding experiments was set at 80^{o}C. The core sample and confining fluid inside the core holder was heated for 24 hours before starting the acid injection. This was done to make sure that the whole system should attain the same temperature of 80^{o}C. The acid was heated to the temperature of 180^{o}F with the help of magnetic stirrer and heater before injection; to make sure there was no temperature difference between the acid and the core sample.
- Pressure transducers were connected with the data acquisition system. The pressure transducers monitored the pressure values at the inlet and outlet of the core sample.
- The inlet and outlet valves were kept opened to allow the fluids to be displaced through the core and collected at the outlet. Once confined and heated; the core flooding experiments were started, once the lab exhaust system was turned on

- The pore volume injected and the change in the volume in injection beaker was kept noted once the reacted fluid started coming out of the outlet flow line. It was made sure that there was no leakage in the flow lines where high pressure was applied.
- The acid flow continued until the constant pressure drop was observed which indicated the completion of the reaction.
- Once the reaction was completed, acid flow was stopped and the water post flush injection was started to remove the unwanted reaction products.
- When the post flush with water was finished, HPLC pump was switched off and the inlet valve was closed. After sometime when no flow was coming out of the outlet line, confining pressure was released.
- After the completion of the core flooding, all the fittings were disconnected and the core was taken out. All the fittings and the parts of the core holder were rinsed with the distilled water and the core samples were placed in an oven at 80^{o}C for 24 hours to dry.
- The reacted acids and core samples collected were used for different analysis mentioned in table 3.7.

3.5.1 Core sample saturation

The core samples were saturated with brine sample before using them in NMR analysis. The saturation can be done by using the Trident system as shown in Figure (3.20). The 5% NaCl brine sample was prepared to saturate the core samples. Firstly, the vacuum pump was connected to the Trident system to remove all the air present inside the vessels and core samples because the presence of bubbles can affect the saturation process with brine. The vacuum pump was then connected to the vacuum lines, glass vessel, trident, and the switch. The Trident system consisted of three vessels in which three different samples can be saturated with brine. The trident was connected to the vacuum pump with the help of needle valves while three relief valves were present at the outlet. The confining pressure was applied by the syringe pump to the core samples with the help of these relief valves. The relief valves were kept open when the pressure was applied to the core samples present inside the vessels. These valves were kept open until the stabilized reading was achieved at the syringe pump. Stabilize pressure showed that there was no air inside the sample and sample was fully saturated. Once saturated, the valves were closed and the syringe pump was disconnected. Then, the syringe pump was removed and the samples were saturated for more 24 hours. Then the core samples were taken

out from the vessel after 24 hours of saturation and placed in the container filled with the similar type of brine to avoid contact with air after the saturation.

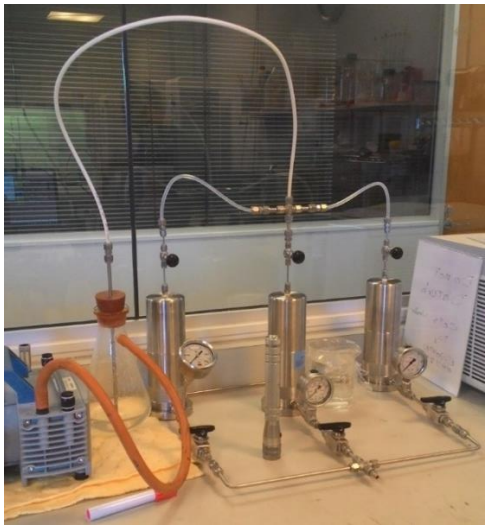

Figure 3.20. Trident for saturation

3.5.2 Sources of Errors

3.5.2.1 Environmental errors

Environmental errors are caused by the environmental conditions where the temperature is the main factor that can disturb the acidizing experiments, especially during the core flooding. The core holder was heated using the heating tape, where some of the heat could be dissipated into the environment as the setup was placed in open air. The water inside the core holder may not reach the specified value but this error was minimized by giving enough time for the heating tape to heat the water to a specified temperature. An environmental error can also occur during the NMR analysis when placing the saturated core sample into the core chamber as the sample needs to be wrapped inside the plastic sheet. Extra care was used during this process to avoid any dehydration into the air.

3.5.2.2 Personal Errors

The personal error may occur due to recording the wrong value of measurements or adding the wrong amount of acid to the mixture. This error may occur when recording the volume of acid which is required to be mixed with water but this error was reduced by using instruments/beakers with more precise labels.

3.5.2.3 Equipment Errors

Some of the equipment can measure different readings every time when the sample is run. This is due to the environment conditions (such as temperature, pressure) that surround the apparatus. Such an error is minimized by recording extra readings (at least three values) and the mean value is presented in the results and analysis chapter. During the research project, most of the apparatus/equipment that are involved in giving different readings are automatic (such as porosimeter permeameter (to calculate porosity and permeability), electronic weighing balance (to determine the weight of the core sample) and pH meter (to find pH value of acids).

3.5.3 Safety Precautions

- The acidizing procedure includes the usage of highly dangerous acids like CH_3COOH, HCl etc., therefore, while performing, one must be aware of how to deal with these dangerous fluids and acids. Thus, while performing experiments especially at high temperature and pressure, special attention needs to be given to safety and proper Personal Protective Equipment (PPE) should be used. The experimental procedures should be planned carefully and deserve special attention.
- Due to the very high reactivity of HF acid and its fatal characteristics discussed in Chemical Risk Assessment form and HAZOP form, it was advised not to use that acid in the laboratory.
- Personal Protective Equipment includes Acid resistive gloves (nitrile or natural rubber glove), Laboratory coat, Googles and Closed shoes. All these equipment should be used while performing experiments and all experiments including acids and chelates should be performed inside the fume cupboard.
- Avoid working alone while doing experiments with acids and chelates. Try to isolate the area of the laboratory where experiments are performed to keep others safe.
- Calcium gluconate gel used to be used as first aid as it is a topical antidote for acid skin exposure.
- Store all acids, chelates and their waste product in labeled chemically compatible containers (e.g., polyethylene or Teflon).

3.6 Methodology Summary

The methodology for this research work is described in Figure 3.21 below:

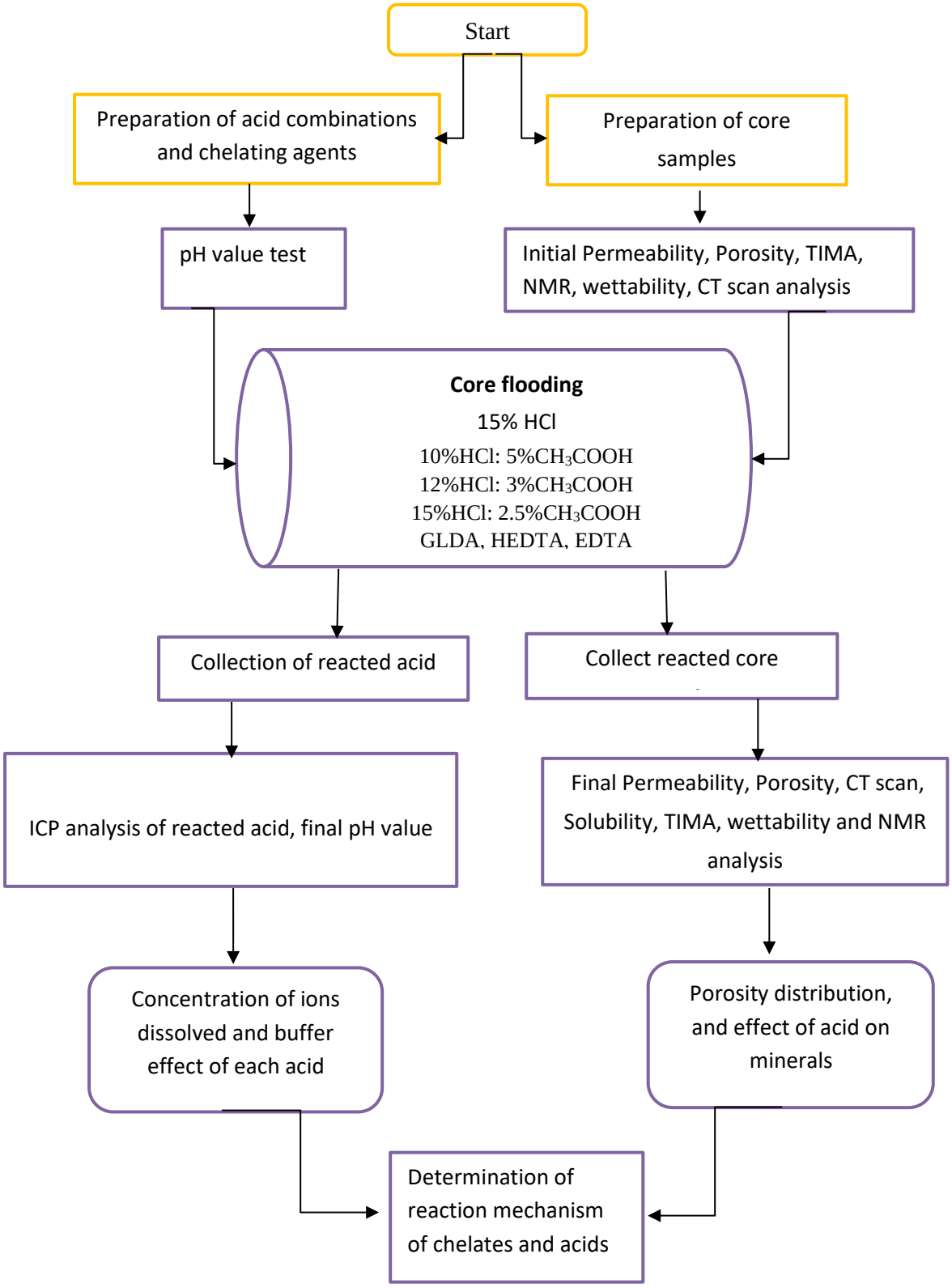

Figure 3.21. Flow chart of experiments

Table 3.7. Apparatus and their purpose

No	Apparatus	Purpose
1	Weighing balance	To measure the weight of core samples
2	Automatic Porosimeter and permeameter	To measure porosity and permeability of the core samples
3	Tescan Integrated Mineral Analysis (TIMA)	To find the effect of acid on the mineralogy of core sample
4	ICP (Inductively Coupled Plasma)	ICP emission spectroscopy is used to analyze for Na, K, Ca, Mg, Fe, Si, and Al
5	NMR (Nuclear Magnetic Resonance)	NMR logging provides porosity distribution
6	pH meter	To find pH of the acid solution
7	CT Scan (Computed Tomography Scan)	To find the effect of acid on the morphology of the sample
8	Heating Oven	To dry the core sample
9	Manual Saturator	To saturate the core sample
10	Wettability	To determine the contact angle

Chapter 4

Results and discussion

4.1 Introduction

To achieve the objectives of this study, various types of laboratory experiments and analysis were conducted. The laboratory work was carried out ranged from the acid and the core sample preparation, routine core analysis to core-flooding tests while the analysis includes Tescan Integrated Mineral Analysis (TIMA), Inductively Coupled Plasma (ICP), micro-CT scan, Wettability, and Nuclear Magnetic Resonance (NMR) logging. This chapter discusses in detail the results of various experimental works and analysis performed on the core and reacted acid samples. This chapter starts with the presentation of the results which are related to permeability and porosity performed before and after acidizing. This is followed by a presentation of different analysis results which includes ICP (to determine dissolved ions), pH value (to determine completion of reaction), and NMR analysis (determination of immobile and mobile pores). In the end, wettability (change in wetting state) and micro-CT scan analyses (to evaluate the acid reaction path) were presented, then TIMA analysis (pore size distribution, mineralogy and surface topology) presented in chapter 5 followed by the description of the mechanism of each chelating agent.

4.1.1 P-T Conditions, Core Properties, and Core Flood Data

Table 4.1 shows the values of laboratory conditions used during the experiments which were carried out under elevated pressure and temperature. These values were selected based on the risk assessment and hazard identification in the laboratories during the experiments. While Table 4.2 lists the properties of core samples used during the project.

Table 4.1. Reservoir P–T conditions during the experiments

Reservoir Parameter	Value
Confining Pressure	6.89 MPa
Temperature	80^{o}C

Table 4.2. Properties of the core samples used for the experiments

Sr No	Group No	Sample ID	Length (m)	Diameter (m)	Weight (kg)	Lithology
1	1	Berea A	0.0628	0.0375	0.153	Sandstone
2	1	Berea B	0.0766	0.0376	0.179	Sandstone
3	1	Berea C	0.0767	0.0376	0.179	Sandstone
4	1	Berea D	0.0766	0.0377	0.180	Sandstone
5	2	Berea B	0.0766	0.0375	0.177	Sandstone
6	2	Berea D	0.0767	0.0377	0.178	Sandstone
7	2	Berea E	0.0763	0.0377	0.180	Sandstone
8	2	Colton A	0.0760	0.0376	0.202	Tight Sandstone
9	2	Colton B	0.0761	0.0375	0.199	Tight Sandstone
10	2	Colton C	0.0761	0.0375	0.197	Tight Sandstone
11	2	Dolomite A	0.0762	0.0375	0.200	Dolomite
12	2	Dolomite B	0.0764	0.0375	0.207	Dolomite
13	2	Dolomite C	0.0764	0.0375	0.190	Dolomite

Tables 4.3 and 4.4 illustrate the core flood data used during the acidizing with conventional acids (pre-flush stage) and with chelates respectively.

Table 4.3. Core flood data for pre-flush stage

Sample ID	Berea A	Berea B	Berea C	Berea D
Solvent	15% HCl	2.5% CH_3COOH: 15% HCl	5% CH_3COOH: 10% HCl	3% CH_3COOH: 12%HCl
Initial Permeability (md)	122.76	166.32	113.23	124.53
Flow rate (m^3/sec)	0.0006	0.00006	0.00006	0.00006
Temperature (^oC)	80	80	80	80
Initial Porosity (%)	19.56	19.65	19.52	19.03

Confining pressure (psi)	1,000	1,000	1,000	1,000
pH value	0.06	0.055	0.09	0.067

Table 4.4. Core flood data for chelates

Sample ID	**Colton B, Dolomite B, Berea B (Group 2)**	**Colton A, Dolomite A, Berea A (Group 2)**	**Colton C, Dolomite C, Berea C (Group 2)**
Solvent	**HEDTA**	**EDTA**	**GLDA**
Initial Permeability (md)	Colton B = 0.4633 Dolomite B = 9.80 Berea B = 165.12	Colton A = 0.7120 Dolomite A = 104.27 Berea D = 124.53	Colton C = 0.8069 Dolomite C = 405.55 Berea E = 80.41
Flow rate (m^3 / sec)	0.00006	0.00006	0.00006
Temperature (^oC)	80	80	80
Initial Porosity (%)	Colton B = 11.49 Dolomite B = 14.19 Berea B = 19.70	Colton A = 10.56 Dolomite A = 16.80 Berea D = 19.04	Colton C = 12.13 Dolomite C = 21.20 Berea E = 18.98
Confining pressure (psi)	1,000	1,000	1,000
concentration	20 wt%	5 wt%	20 wt%
pH value	1.85	2.7	1.25

4.2 Porosity and permeability

The porosity is a measure of void spaces and gives information about the storage capacity of the reservoir rock. The permeability is defined as the capacity of the rock to conduct the fluid through its matrix. These properties are very important for understanding the oil and gas initial in place and the ability of the rock to transmit a fluid. The porosity can be determined by applying certain techniques like saturation method or determination using automatic porosity analysis apparatus. In this research, porosity and permeability are measured before and after core flooding experiments using the Automated Permeameter-Porosimeter (AP-608) from Coretest system Inc. as shown in Figure 4.1 (a). The installation of hydrostatic core holder is shown in Figure 4.1 (b). AP-608 instrument is cost-effective and applied Boyle's law to

measure the porosity and Klinkenberg effect to measure the permeability. Figure 4.2 shows the schematic diagram of AP-608 automated porosimeter permeameter.

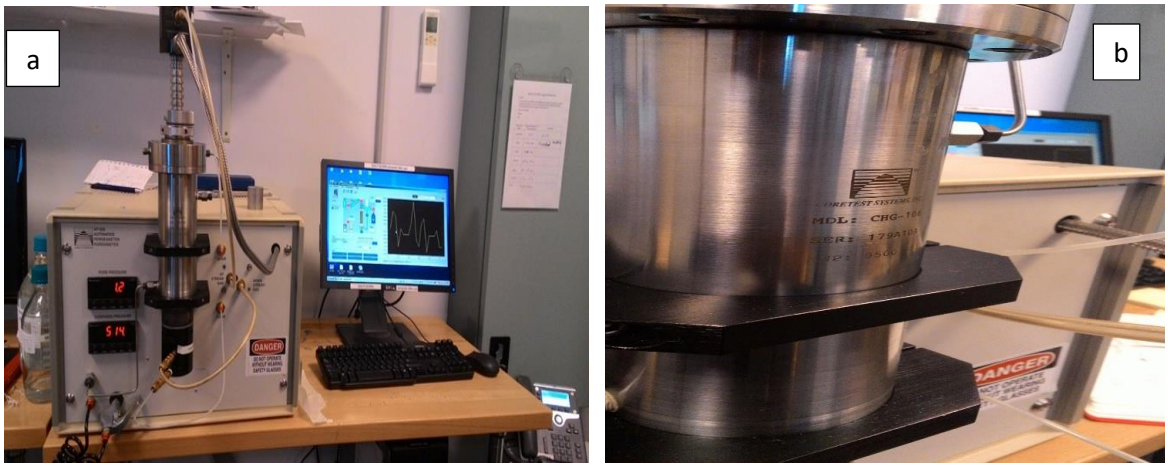

Figure 4.1. (a) Automated Permeameter Porosimeter (b) core holder

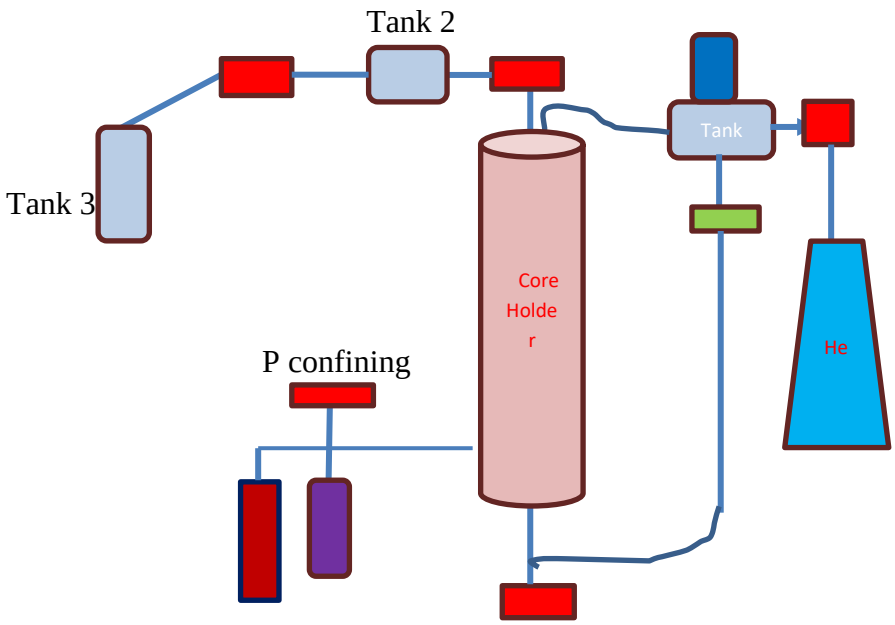

Figure 4.2. Schematic Setup of Automated Permeameter Porosimeter

Helium gas is a non-toxic and non-damaging gas to the core samples, and because of its high diffusivity was used as the pore fluid to measure porosity and permeability. Klinkenberg-corrected permeability can be measured using AP-608 systems. Using automated permeameter porosimeter, porosity can be calculated at different confining pressure ranges. During this research, the porosity values at 3.44 MPa, and 6.89 MPa pressure are measured because the confining pressure during the core flooding experiments was 6.89 MPa maximum. The permeability measured range is 0.001 mD to >10, depending on the sample while the porosity

range is 0.1% to > 40%. Along with the porosity and permeability, a pore volume of each core sample was also measured as an important parameter to determine the breakthrough and used to understand the reaction completion. This apparatus can be used to carry out measurements up to 65.8 MPa pressure.

4.2.1 Preflush Analysis

The main aim of the preflush stage is to remove the calcium, sodium, magnesium and potassium ions that are present in the core samples. The removal of these ions is very necessary in order to get better acidizing results because these minerals can cause precipitation later during the main acid stage. By dissolving these minerals the new pores are created which may increase the porosity of the formation but may have a little effect on the permeability. Because the pores created are usually small or capillary sized as these ions are present in very small quantity. Moreover, due to their small quantity, the observed change in porosity is also less. Table 4.5 represents the acid combinations that were prepared to react with Berea sandstone formation during the pre-flush stage to determine the best combination.

Table 4.5. Acid combinations for pre-flush stage

Acid Combination	Sample name
15% HCl	A
2.5% CH_3COOH: 15% HCl	B
5% CH_3COOH: 10% HCl	C
3% CH_3COOH: 12%HCl	D

15% HCl is the base case as this is the standard acid used in the industry for the pre-flush stage of sandstone acidizing. The permeability increased by almost 24% when 15% HCl was applied during acidizing as shown in Figure 4.3, while very less variation in permeability has been observed using a newly proposed acid combination (HCl: CH_3COOH). The less change in the permeability can be attributed to the reaction products formed due to the reaction of minerals with acids and consequently blocking the pore spaces. However, permeability was not the major concern at this stage of acidizing as it does not show the dissolution of minerals effectively. On the other hand, the porosity results are quite favorable where the change in the porosity when the new combination (5% CH_3COOH: 10% HCl) applied was 6.2% as shown in Figure 4.4, which is almost 1% more than the base case. Table A1 and Table A2 (Appendix A)

characterize the initial and final permeability and porosity values, respectively. The initial values were obtained before the core flooding treatment while the final values were recorded after the core flooding.

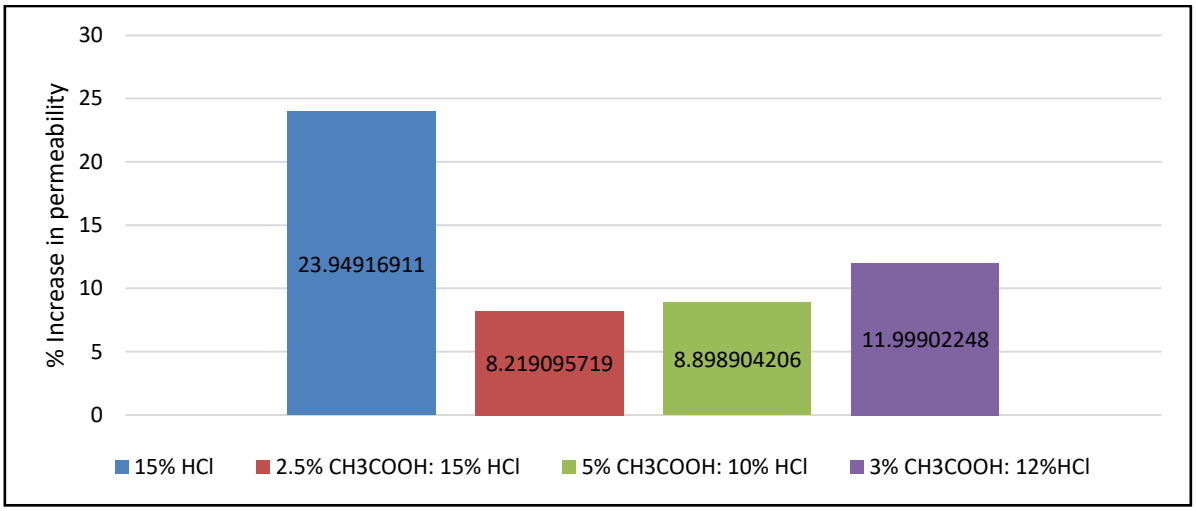

Figure 4.3. Permeability Analysis before and after pre-flush

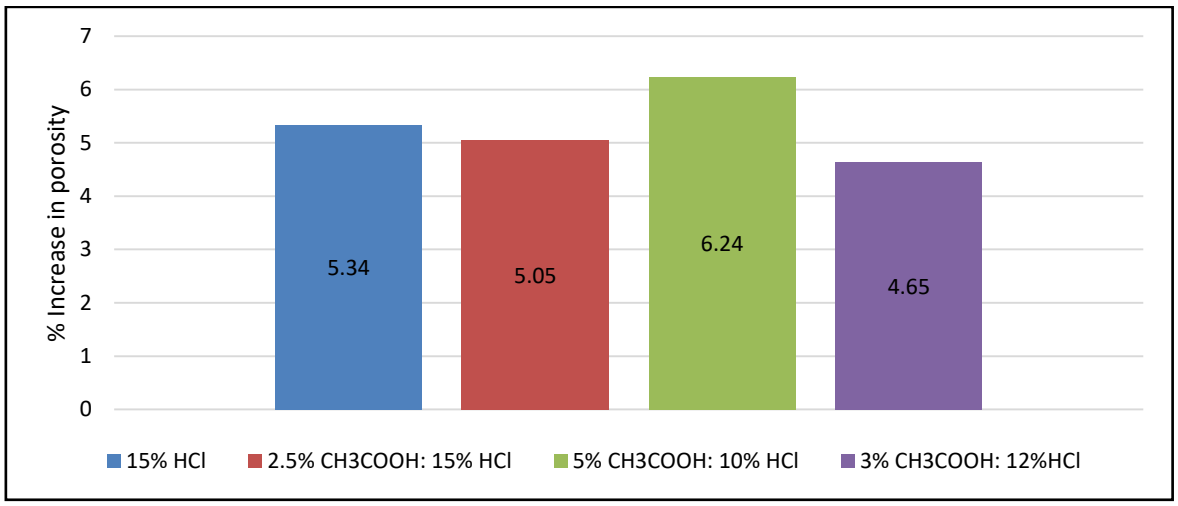

Figure 4.4. Porosity Analysis before and after pre-flush

4.2.2 Main Acid Stage

Chelating agents have been applied during the main acid stage of matrix acidizing to increase the porosity of the formation. List of samples which reacted with different types of chelates is presented in Table 4.6. While the results are presented in Figure 4.5 and Figure 4.6. The maximum change in porosity has been observed when HEDTA is applied to core samples. There is 10.10%, 6.3% and 6.8% increment in the porosity of Colton sandstone, Guelph Dolomite and Berea sandstone core samples respectively which is higher than the application

of other chelates. EDTA and GLDA also proved efficient in increasing the porosity of Colton sandstone and Berea sandstone samples while they are not that effective in increasing porosity of dolomite samples. These results will be further discussed at TIMA porosity distribution analysis.

Permeability is the representative of oil and gas conductivity in the reservoir. More permeability indicates effective well productivity. Figure 4.6 represents the increase in permeability of the core samples when all three chelates have been applied on Colton sandstone (tight sandstone), Berea sandstone and Guelph dolomite core samples. HEDTA proved to be the most effective chelate and increases the permeability by almost 100% when applied to dolomite and tight sandstone core samples. Other chelates are not effective in increasing the permeability of the samples maybe due to precipitation inside the pores. These precipitates might be blocking the small pore through present inside the tight sandstone sample. In tight sandstone samples, the size of pore throat is very small which resulted in low permeability of these type of rocks. Therefore, the formation of precipitates when GLDA and EDTA reacted with dolomite and sandstone formations blocking the pore throats is the possible cause for the less increase in permeability even after stimulation. One possible reason for less change in permeability can be due to less biodegradability of these chelates compared to HEDTA. Other reasons can be their effectiveness in dissolving different positive ions from the core samples which will be discussed later in ICP and TIMA analysis, section 4.4 and chapter 5 respectively.

Table 4.6. Sample name and composition

Sample Name	**Type of rock**	**Chelate**
Sample A	Colton Sandstone	EDTA
Sample B		HEDTA
Sample C		GLDA
Sample A	Guelph Dolomite	EDTA
Sample B		HEDTA
Sample C		GLDA
Sample A	Berea Sandstone	EDTA
Sample B		HEDTA
Sample C		GLDA

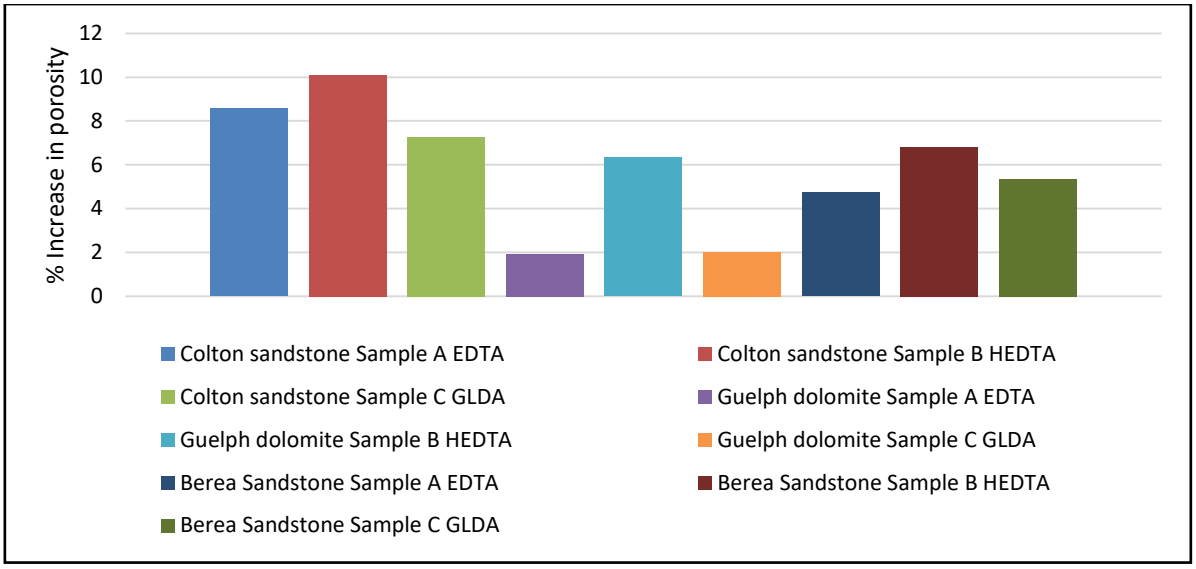

Figure 4.5. Porosity Analysis before and after reaction with chelates

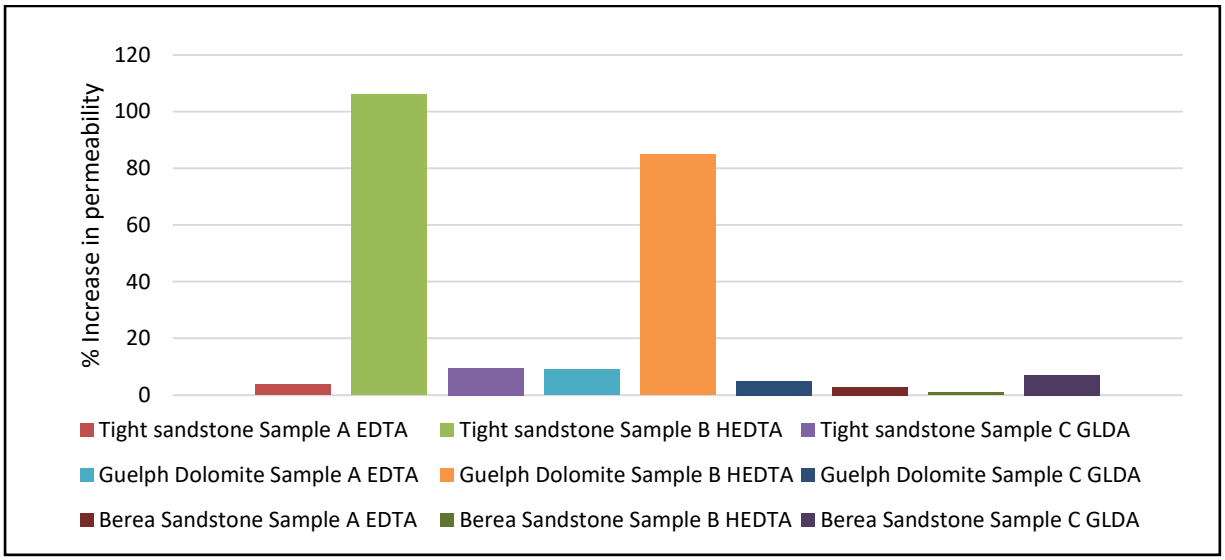

Figure 4.6. Permeability Analysis before and after reaction with chelates

4.3 pH Value Test

pH value determination versus pore volume is also one of the important parameters considered during the acidizing procedure. It can determine the buffer effect of acids and can give the indication of penetration power of the acids. More change in pH value describes the fast reaction of acid which subsequently leads to less penetration. Less change in pH value is favorable, but it may also indicate no reaction of the acid with a rock at later stages of acidizing. It indicates that most of the minerals present in the core sample may be consumed during the early stage of reaction and the remaining acid is coming out without reacting. This may result

in the low pH value of the reacted acid sample. The results of the pH value variation during the pre-flush acidizing stage are presented in Figures 4.7 and 4.8.

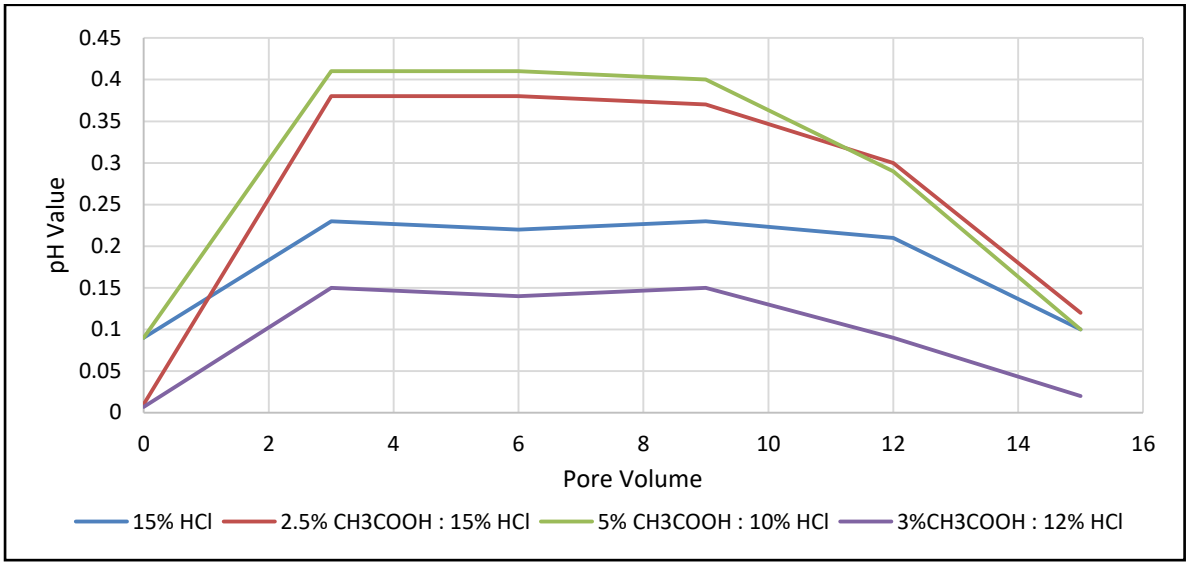

Figure 4.7. pH value curve during the pre-flush stage

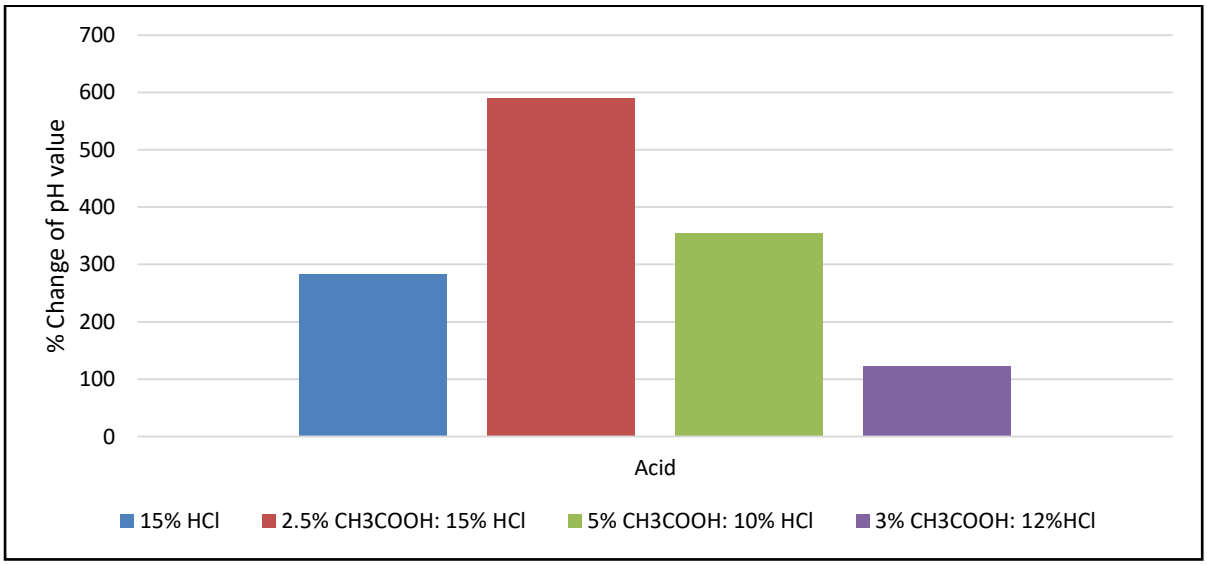

Figure 4.8. The final change in pH value during the pre-flush stage

Sample D (in Table 4.5) showed less pH value change as compared to other samples of acid. This condition is favorable and an indication that the acid coming out is not fully reacted and can go further deep into the formation. Porosity analysis in Figures 4.3 and 4.4 showed that this combination was good in increasing porosity and permeability of the sandstone sample respectively. The change in sample C is also almost equal to the change in sample A which is the base case. This change is not high nor low, likewise permeability and porosity change also

favorable. This illustrates that acid (5% CH_3COOH: 10% HCl) was reacting and meanwhile keeping the reaction products in the solution. The maximum pH value change was observed in sample B (2.5%CH_3COOH: 15% HCl) and this was confirmed by permeability and porosity analysis where the change was less compared to other acids. This pH change is the reason behind less porosity and permeability change because the fast reaction can cause precipitation reactions which consequently block the pore spaces.

The results of the pH value variation during the chelating agent acidizing stage are presented in Figures 4.9 and 4.10. The pH value is measured constantly after every 3 pore volumes injection. The first volume of collected spent acid showed the maximum value of pH (Figure 4.7, pH value after 3PV). This is because, in the spent acid, the acid was neutralized due to reaction with the minerals. Then, the next volumes collected almost showed the constant value (Figure 4.7, pH value from 3PV to 9PV), as the acid was reacting continuously with the minerals. The decrease in the pH value (Figure 4.7, after 9PV) indicates that the acid coming at the outlet also consists of unreacted acid as the reactive minerals inside the core sample are already dissolved by the initially injected volumes of acids. Therefore, the pH value reaches a plateau first and then start decreasing due to unreacted low-value pH acid collected at the outlet.

- Figure 4.9b shows that in case of Guelph dolomite the pH value of EDTA started dropping after about 9 pore volumes which shows that the chelate is coming out with no reaction. But for HEDTA, the pH value started decreasing after about 12 pore volumes. This implies that HEDTA took more volume to remove the required product and it also implies that the reaction rate of chelate with the rock sample is slow. GLDA shows the same trend as EDTA.
- For Colton sandstone samples (Figure 4.9a), the trend is more or less the same as in Guelph dolomite, where the change in pH value of EDTA started after the injection of 9 pore volumes while for HEDTA and GLDA the change started after 12 pore volumes injections.
- For Berea sandstone samples (Figure 4.9c), the trend is more or less the same as in Guelph dolomite, where the change in pH value of EDTA and GLDA started after the injection of 9 pore volumes while for HEDTA the change started after 12 pore volumes injections.

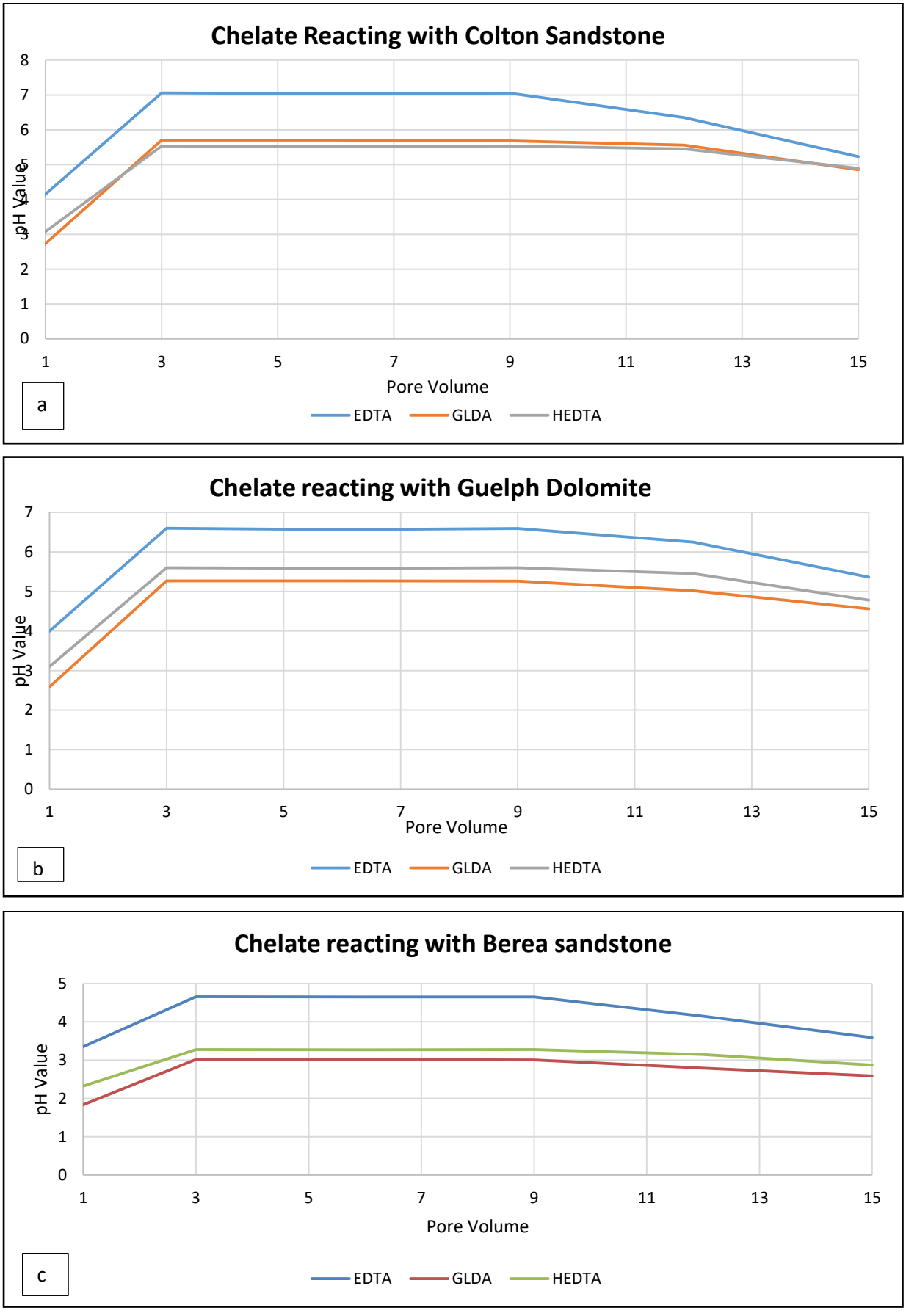

Figure 4.9. pH Value Vs Pore volume injection of different chelates

Moreover, one trend is very notable, where the maximum change in pH was observed when GLDA reacted with all three types of core samples (Figure 4.10), followed by HEDTA and then EDTA. This can be the reason why the change in the porosity and permeability of the core sample was less when reacted with GLDA. Because more change in the pH value shows fast reaction which can ultimately lead to the foundation of precipitates. However, the change in the pH value in case of EDTA was less but still, the permeability and porosity change was not high. This may be due to the factor that EDTA is not readily biodegradable and not reacting with the core samples effectively. The maximum permeability and porosity change were observed in the case of HEDTA (Figures 4.5 and 4.6) and pH value test also validated this result.

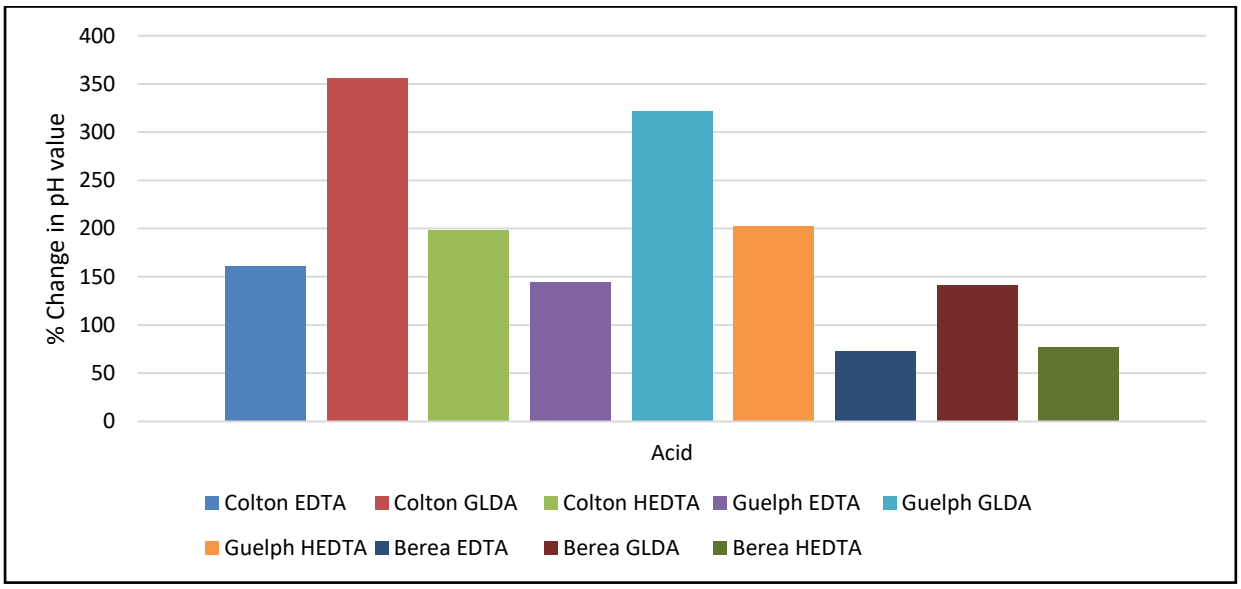

Figure 4.10. Final change in pH value after reaction with chelates

4.4 Inductively Coupled Plasma (ICP) Analysis

The type of analytical technique is used to detect the trace metals and is known as inductively coupled plasma atomic emission spectroscopy (ICP-AES), or inductively coupled plasma optical emission spectrometry (ICP-OES) as shown in Figure 4.11. The trace metals can be detected using an analytical technique whereby excited atoms have been emitted using inductively coupled plasma, and ions that can emit radiation wavelength of particular ions are also emitted. The temperature ranges from 5727^{o}C to 9727^{o}C and is known as a flame technique temperature. The concentration of the element present in the sample is indicated by the intensity of this emission. The concentration of each element is presented in parts per millions (ppm). However, the minerals or compounds settled at the bottom of the sample cannot be detected by

this technique. Different samples were collected during the core flooding experiments based on the pore volume injected. The results are presented in tables A7 to A10 (Appendix A).

Figure 4.11. Inductively Coupled Plasma Machine

4.4.1 Theory

It is a powerful and useful tool to measure the dissolved concentration of different cations present in the samples collected from dissolution reactions and core flood effluents sample. It provides the total amount of ion of interest. The advantage of using plasma in comparison to other techniques is that it is performed in a chemically inert environment which prevents the formation of oxides, therefore, a complete ionization occurs. There are several ways in which the sample can be introduced into the system but the purpose of each is same; to sweep the sample into the ICP torch in aerosol form for analysis.

Generally, the samples used in ICP-Ms are in liquid form. But when they are introduced into the system, the sample should be in aerosol or gaseous form. One of the most fundamental aspects of ICP-MS that can be stated as both strength and weakness is that the elements are quantified and detected in total. In other words, it can be described as, no separation of compounds containing the elements of interests occurred.

It is an analytical technique where the ions absorb the energy and jumped to higher energy state from a stable state and become excited. When these ions decay back to the original stable state, energy is emitted in the form of a specific wavelength of each element. Mass spectrometry is used and can provide elemental composition information of samples, organic and biological molecules structures, the quantitative and qualitative composition of different complex mixtures and the structure of solid materials.

This analysis is used to validate the porosity results. This test investigates the concentration of different ions dissolved by the acid during the reaction. In this test core effluent samples (reacted acid) were utilized to determine the concentrations of Si, Ca, Na, K, Fe and Mg present in acid after the reaction. The results presented are in parts per million (ppm). The acid samples are collected after every 5 pore volumes injection of acids or chelates and results are presented in tables A7 through A10 (Appendix A). Figure 4.12 shows the collected sample at the outlet of the core flooding setup.

Figure 4.12. Reacted acid Samples for ICP analysis

4.4.2 Pre-flush stage analysis

Figures 4.13 through 4.15 show the comparison of ICP data at the pre-flushed stage and presented in Table A7 (Appendix A). Figure 4.13 represents those minerals which are present in abundance in the sandstone core sample and have been dissolved by applied acids in large quantities.

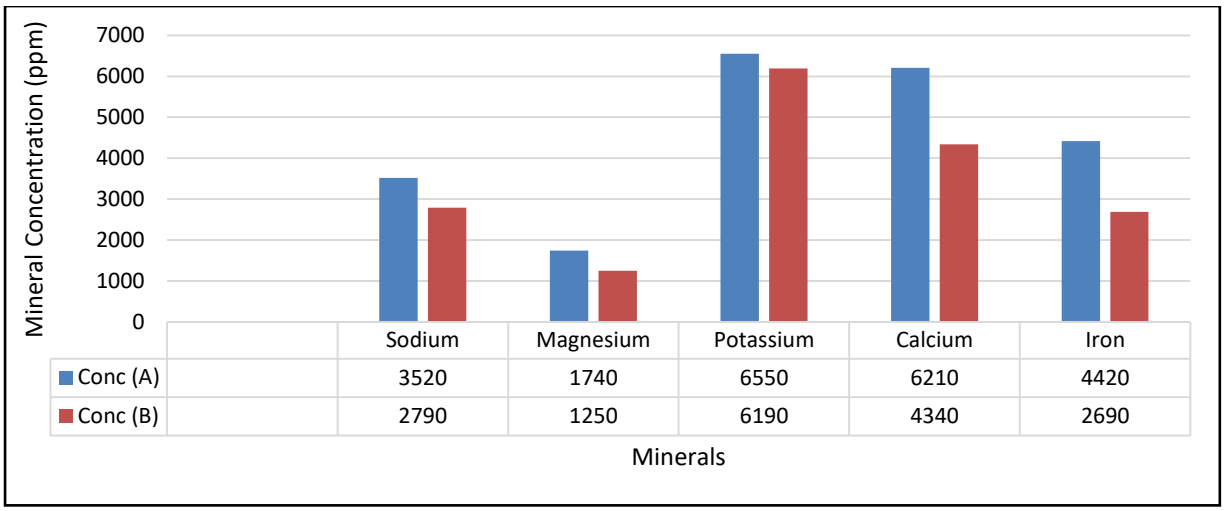

Figure 4.13. Comparison of minerals present in abundance quantity

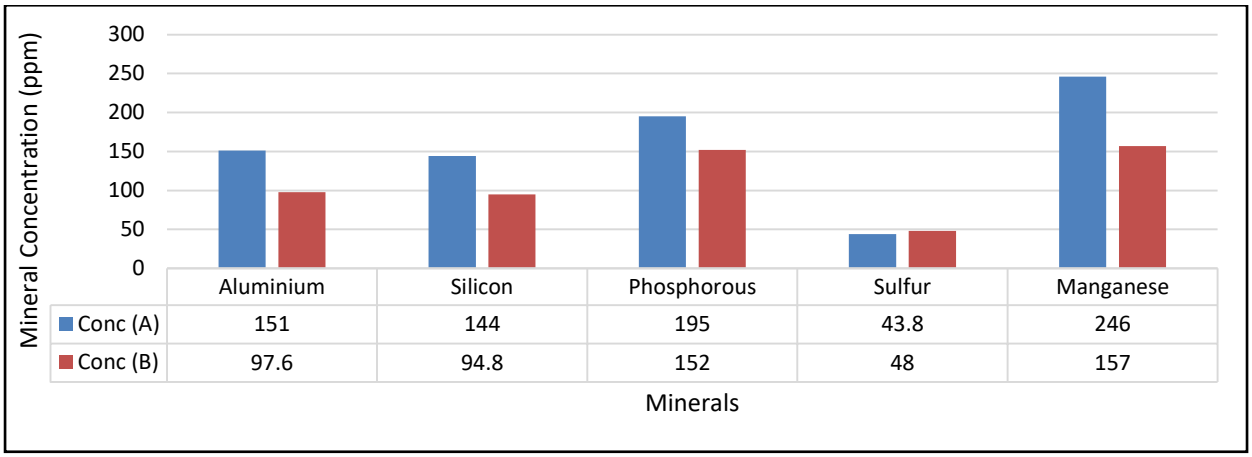

Figure 4.14. Comparison of minerals present in average quantity

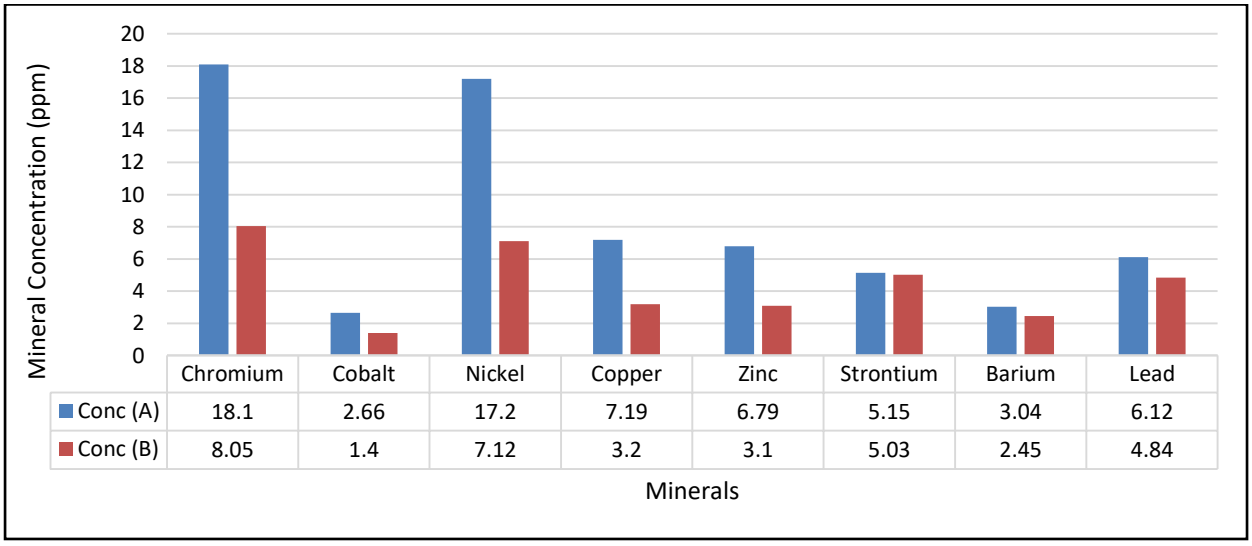

Figure 4.15. Comparison of minerals present in less quantity

Where,

Conc (A) = 5 %CH_3COOH: 10% HCl

Conc (B) = 15% HCl

The acid combination of 5% CH_3COOH: 10% HCl can dissolve 730 ppm of more sodium, 490 ppm of more magnesium, 360 ppm of more potassium, 1870 ppm of more calcium and 1730 ppm of more iron as compared to 15% HCl. The rest of the minerals are not in abundance and their effect on porosity and permeability can be neglected. These results are validating the porosity analysis discussed previously in Figure 4.3, which showed that the increase in porosity is more when 5% CH_3COOH: 10% HCl was applied as compared to 15% HCl.

4.4.3 Main Acid Stage Analysis

Colton Sandstone

- After injection of 5 Pore volumes, HEDTA dissolved maximum amount of sodium from the core sample; 3221 ppm (Figure 4.16), while EDTA dissolved 3000 ppm (Figure 4.18) and GLDA 2410 ppm (Figure 4.20). After 15 PV, HEDTA still managed to increase dissolve concentration of sodium by almost 1000 ppm (1069 ppm) and reached the total concentration of 4290 ppm. HEDTA is equally effective in case of magnesium (Figure 4.16) and aluminium (Figure 4.17) where it dissolved 1370 ppm and 136 ppm respectively, where dissolution of aluminium is negligible by other chelates.
- chelate (HEDTA) is also very effective in the dissolution of Calcium (4600 ppm) and Strontium (78 ppm) mentioned in Figure 4.16 and 4.17 respectively, compared to other chelates where calcium dissolution is 2640 ppm by GLDA (Figure 4.20) and 1090 ppm by EDTA (Figure 4.18).
- 207 ppm Iron and 98 ppm silicon have been dissolved after injecting 15 PV of chelate HEDTA (Figure 4.17). However, the dissolution of these ions is negligible when EDTA and GLDA are injected.

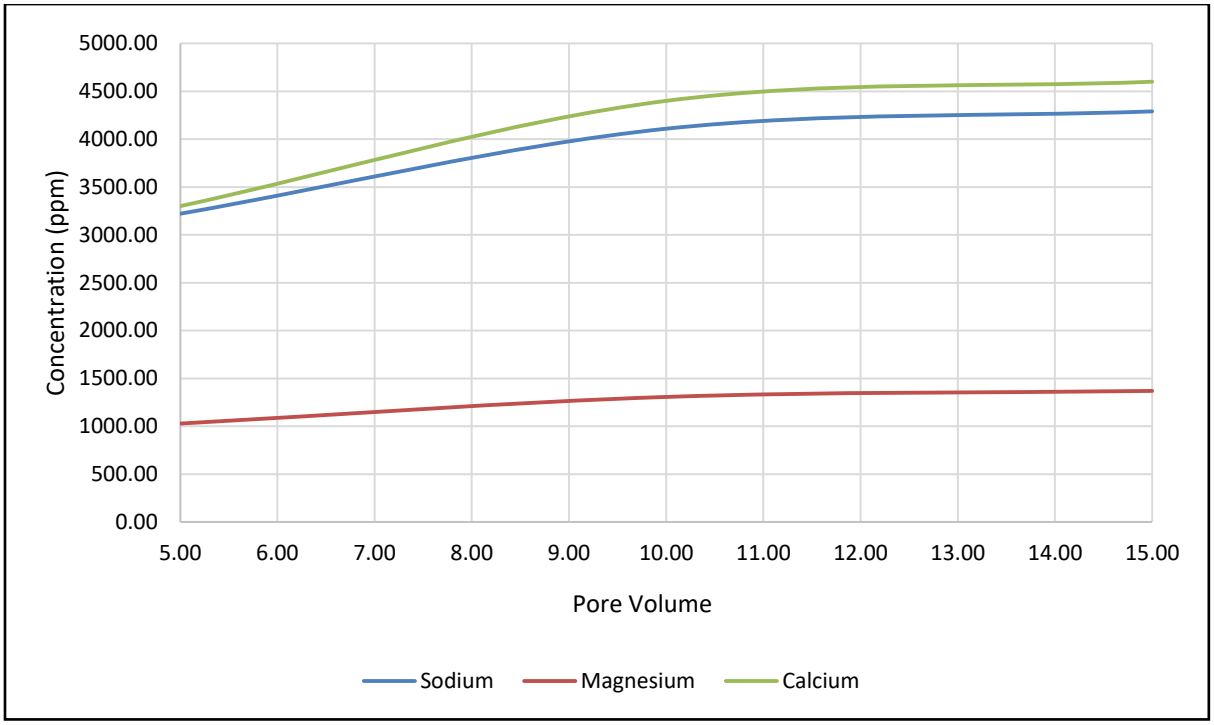

Figure 4.16. Dissolution of minerals by HEDTA from Colton sandstone in high quantity

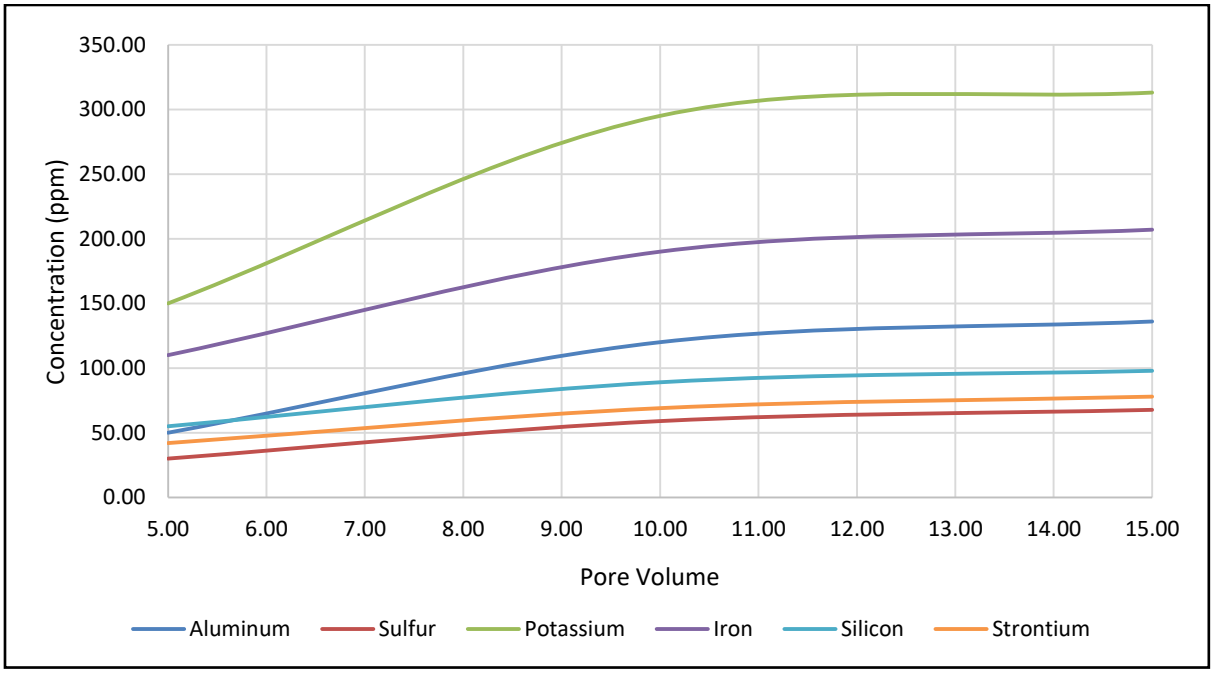

Figure 4.17. Dissolution of minerals by HEDTA from Colton sandstone in low quantity

- Chelate (EDTA) proved to be effective in the dissolution of Sulphur (Figure 4.19) and potassium (Figure 4.18) where it dissolves 105 ppm and 869 ppm respectively after 15 PV of injection.

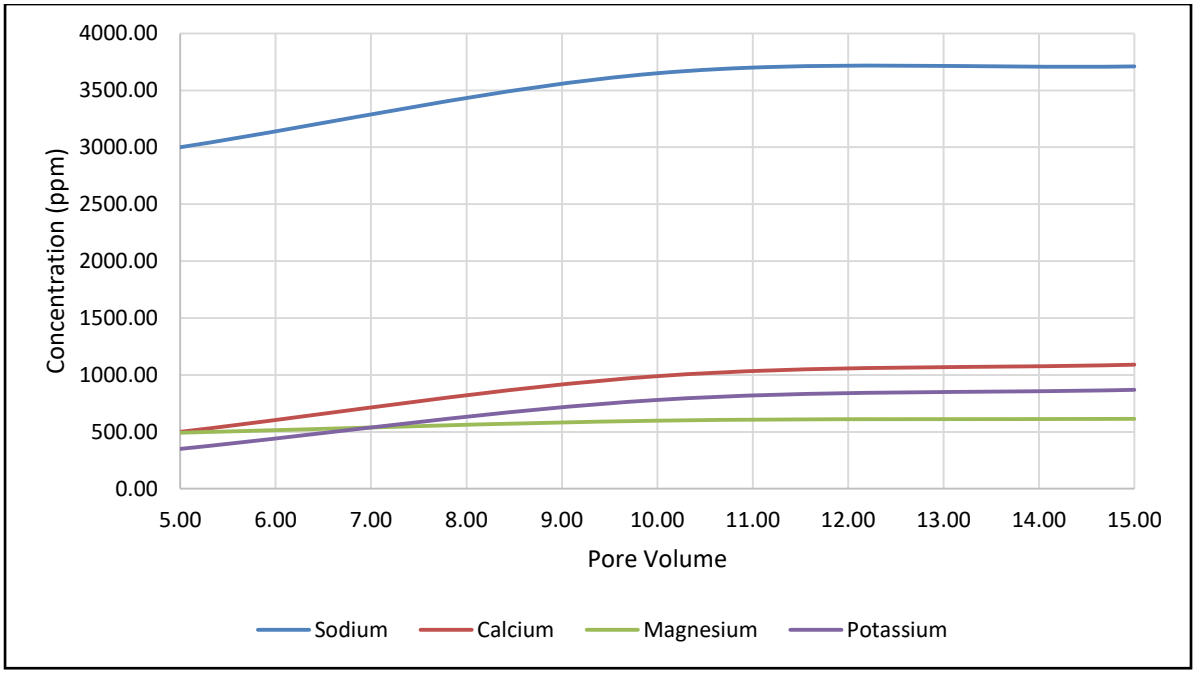

Figure 4.18. Dissolution of minerals by EDTA from Colton sandstone in high quantity

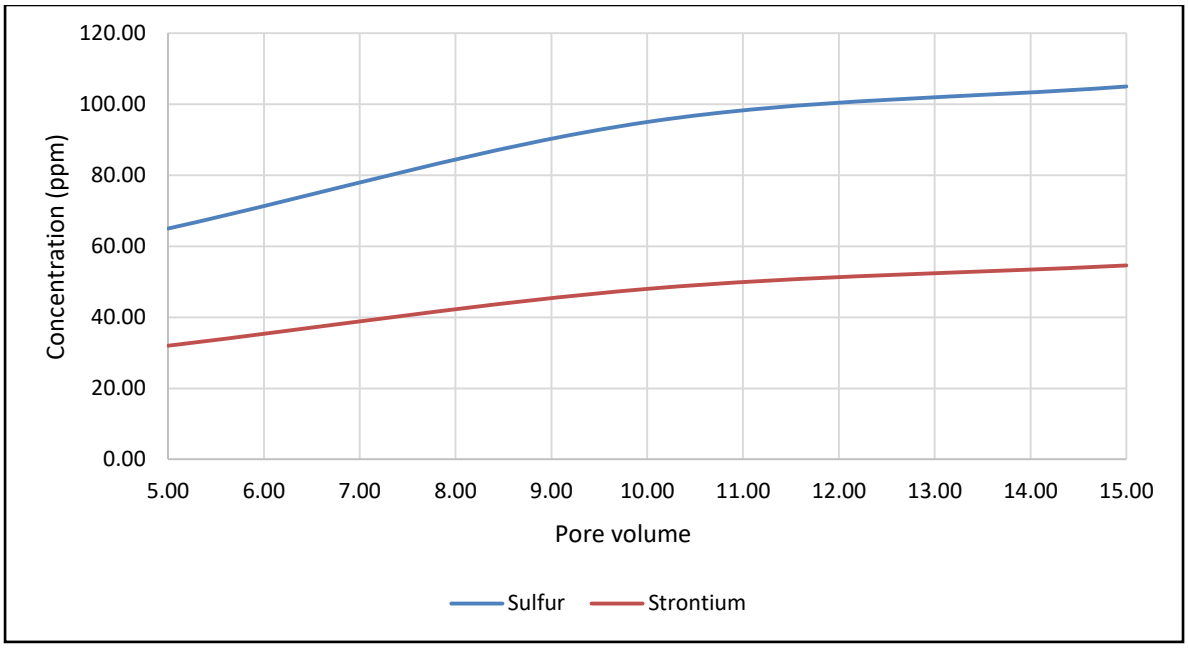

Figure 4.19. Dissolution of minerals by EDTA from Colton sandstone in low quantity

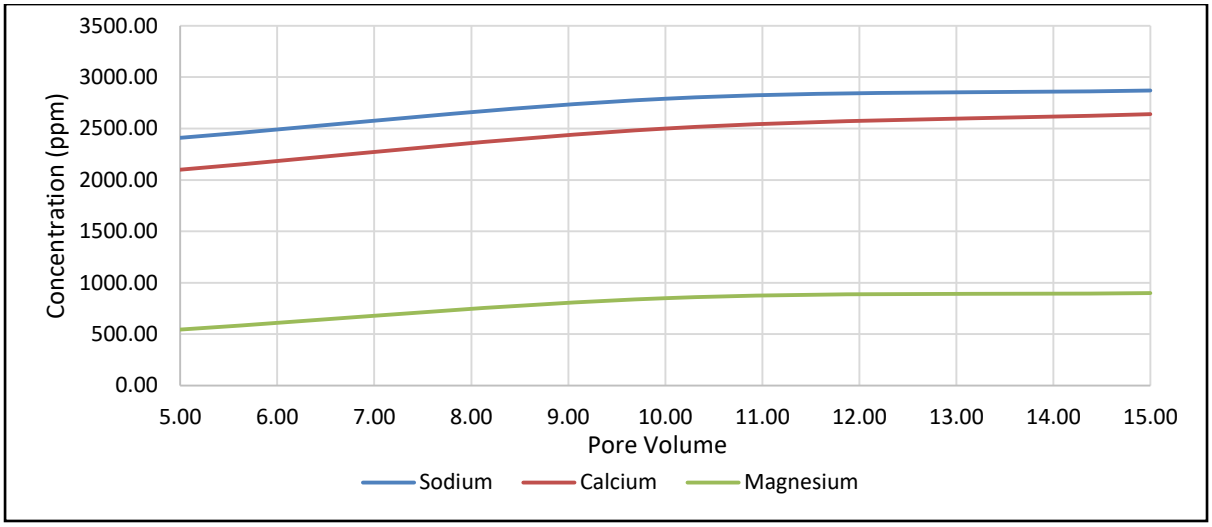

Figure 4.20. Dissolution of minerals by GLDA from Colton sandstone in high quantity

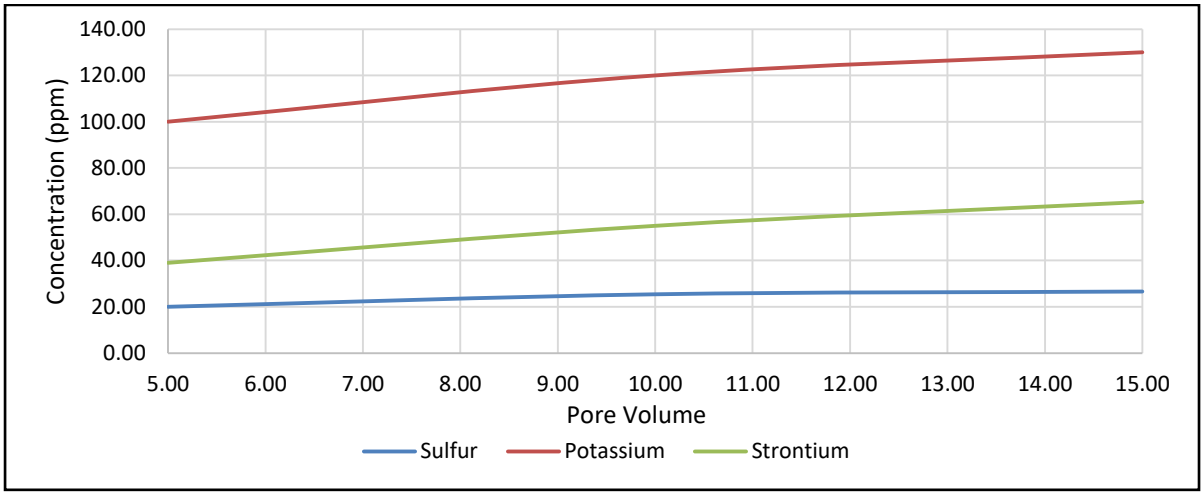

Figure 4.21. Dissolution of minerals by GLDA from Colton sandstone in low quantity

Concluding remarks

- Chelate (HEDTA) proved to be effective in dissolving sodium ions where it dissolves 580 ppm more sodium than EDTA, magnesium (470 ppm more than GLDA), and calcium (1960 ppm more than GLDA) ions from Colton sandstone core samples while EDTA is effective in dissolving potassium (556 pm more than HEDTA) indicated in Figure 4.22a and 4.22b. HEDTA also dissolved the fair amount of Aluminum (136 ppm) and iron (207 ppm). These results indicate that HEDTA is a good chelate with the power to dissolve magnesium, sodium, iron, aluminum and calcium ions in tight sandstone acidizing.
- Chelates (EDTA) and (GLDA) are also good in the dissolution of sodium where they dissolved 3710 ppm and 2870 ppm of sodium respectively.

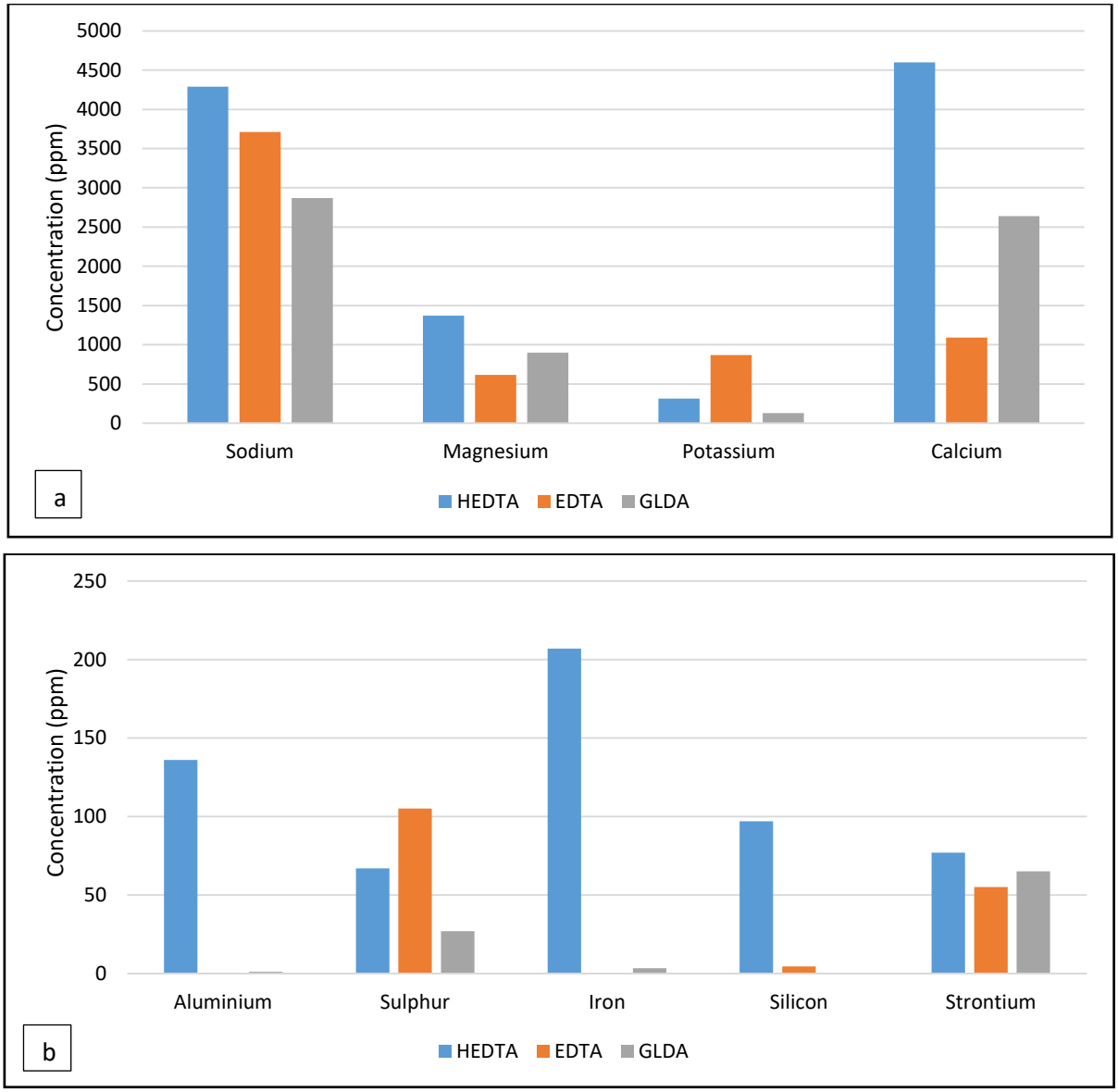

Figure 4.22. Comparison of dissolution of minerals by chelating agents from Colton sandstone

Guelph dolomite

- After injection of 5 Pore volume, GLDA dissolved maximum amount of sodium from the core sample; 3300 ppm (Figure 4.27), while EDTA dissolved 3210 ppm (Figure 4.25) and HEDTA 3200 ppm (Figure 4.23). After 15 PV, GLDA still managed to increase dissolve concentration of sodium by almost 2000 ppm and reached the total concentration of 5440 ppm. EDTA and HEDTA are also good in the dissolution of sodium where they dissolved 4930 ppm and 4440 ppm of sodium respectively.
- Chelate (GLDA) is equally effective in case of magnesium where it dissolved 1570 ppm (Figure 4.27). Likewise, HEDTA dissolved 2570 ppm of magnesium (Figure 4.23). GLDA

proved to be effective in the dissolution of aluminium compared to EDTA.

- Chelate (HEDTA) is equally effective in the dissolution of Calcium, Potassium, Iron, and Strontium. Where 2310 ppm of potassium and 4320 ppm of calcium has been chelated after injecting 15 PV of acid (Figure 4.24). EDTA managed to chelate 1970 ppm of potassium (Figure 4.26) and GLDA chelated 1130 ppm of potassium (Figure 4.27). Compared to HEDTA, dissolution of calcium by EDTA is negligible while GLDA dissolves 2640 ppm. Good amount of iron is only dissolved by HEDTA where almost 55 ppm has been dissolved which is far better than other chelates.

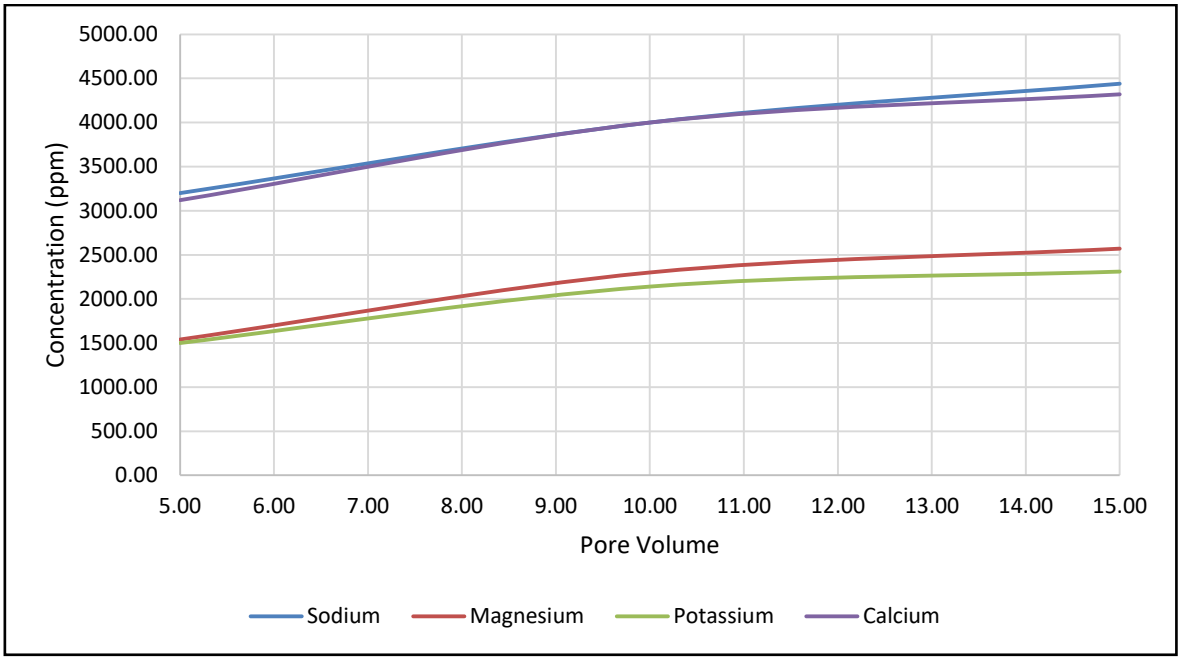

Figure 4.23. Dissolution of minerals by HEDTA from Guelph dolomite in high quantity

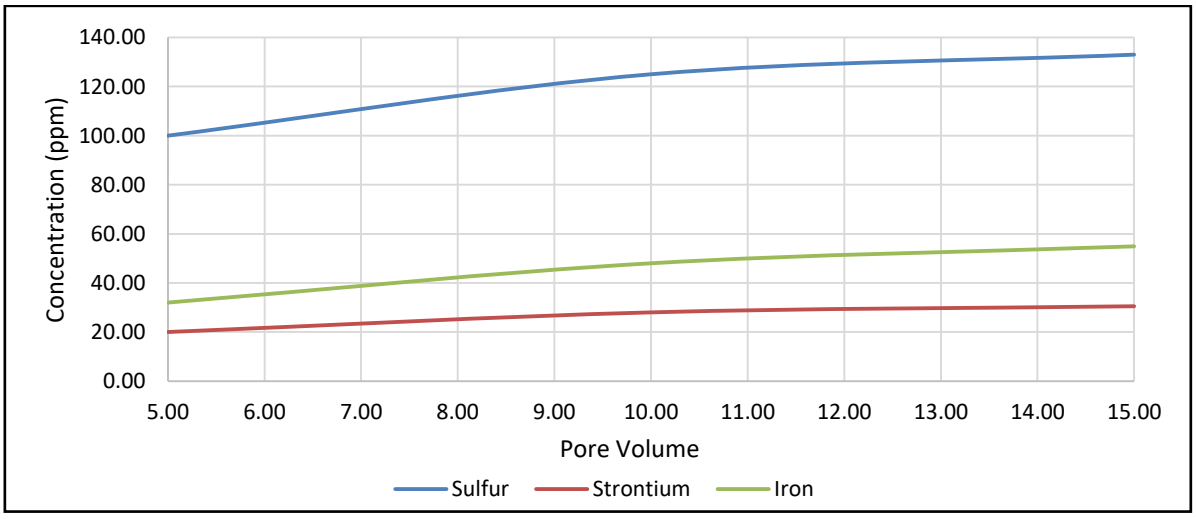

Figure 4.24. Dissolution of minerals by HEDTA from Guelph dolomite in low quantity

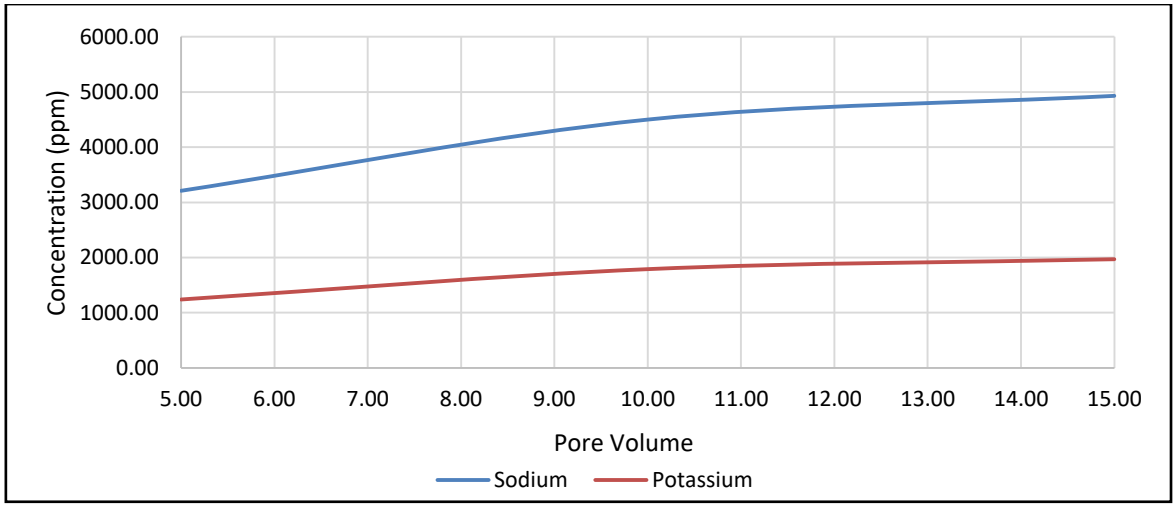

Figure 4.25. Dissolution of minerals by EDTA from Guelph dolomite in high quantity

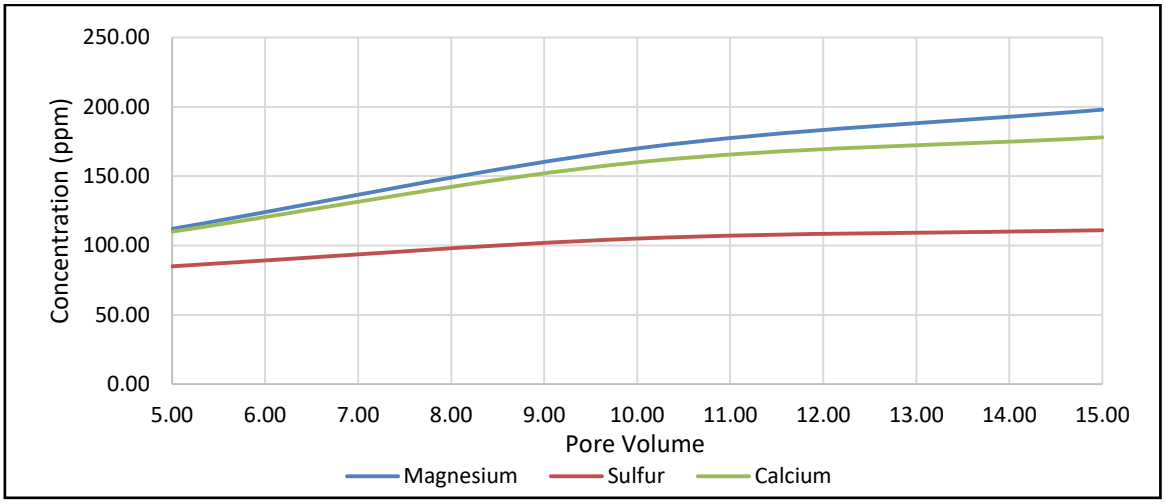

Figure 4.26. Dissolution of minerals by EDTA from Guelph dolomite in low quantity

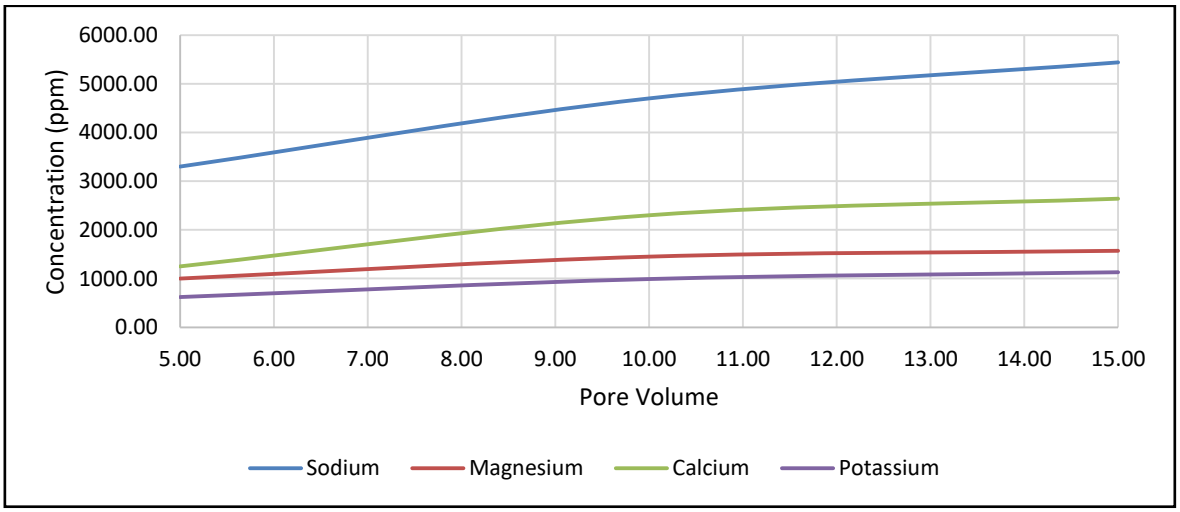

Figure 2Figure 4.27. Dissolution of minerals by GLDA from Guelph dolomite

Concluding Remarks

- Chelate (HEDTA) dissolved 1000 ppm more magnesium ions than GLDA, and calcium (1680 ppm more than GLDA) from dolomite samples while GLDA is effective in dissolving sodium (510 ppm more than EDTA) as shown in Figure 4.28. These results are indicating that HEDTA is a good chelate with the power to dissolve magnesium, calcium and iron ions in dolomite acidizing. EDTA and GLDA are also effective in dissolving some ions like sodium and potassium.

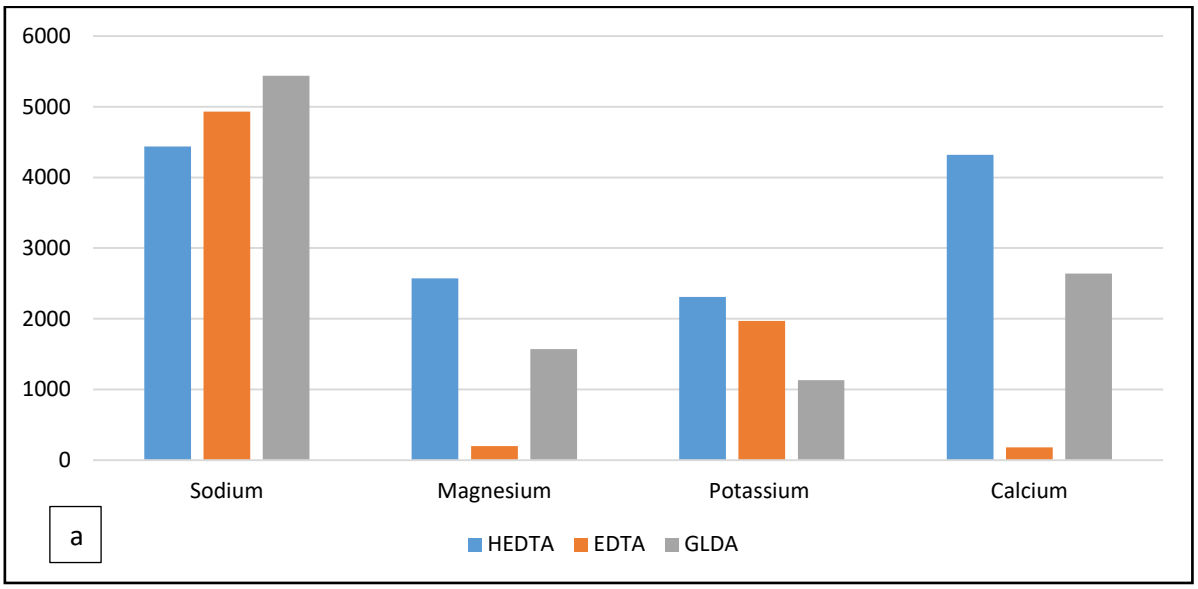

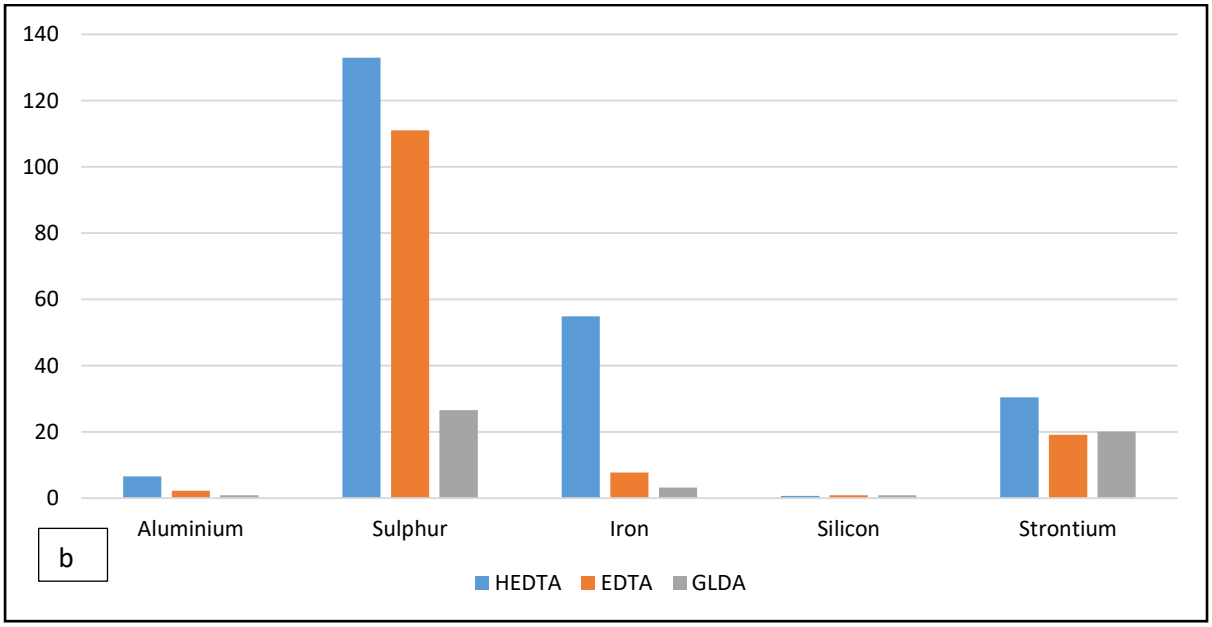

Figure 4.28. Comparison of dissolution of minerals by chelating agents from Guelph Dolomite

Berea sandstone

- After injection of 5 Pore volume, HEDTA dissolved the maximum amount of sodium from the core sample; 4500 ppm while EDTA dissolved 4400 ppm and GLDA 4150 ppm. After 15 PV, HEDTA still managed to increase dissolve concentration of sodium by almost 1700 pm and reached the total concentration of 6200 ppm (Figure 4.29). EDTA and HEDTA are also good in the dissolution of sodium where they dissolved 5990 ppm (Figure 4.31) and 5610 ppm (Figure 4.33) of sodium respectively.
- Chelate (HEDTA) is equally effective in case of potassium, calcium, and iron where it dissolved 6612 ppm, 6364 ppm (Figure 4.29) and 4782 ppm (Figure 4.29) respectively.
- Chelate (GLDA) proved to be more effective in the dissolution of Magnesium, potassium, and calcium where 2702 ppm of magnesium, 8220 ppm of calcium and 9160 ppm of potassium have been chelated after injecting 15 PV of chelate (Figure 4.33). EDTA managed to chelate 6629 ppm of potassium, 6262 ppm of calcium (Figure 4.31). Good amount of iron is dissolved by EDTA (4467 ppm) and GLDA (4565 ppm).

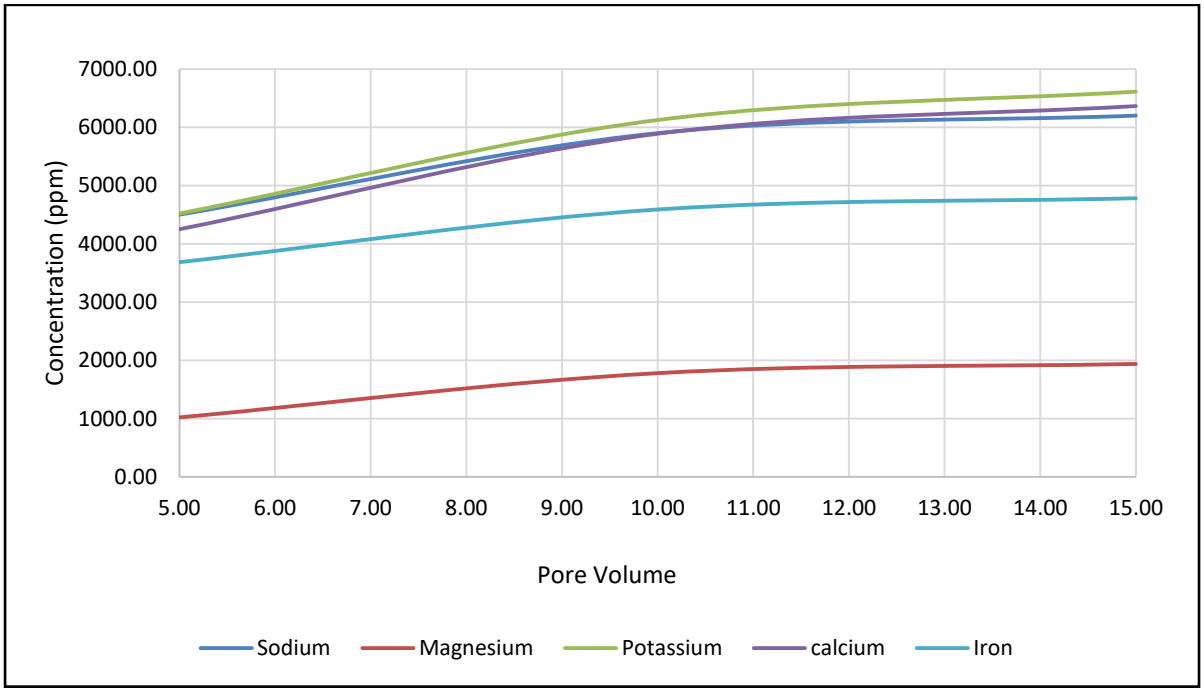

Figure 4.29. Dissolution of minerals by HEDTA from Berea Sandstone in high quantity

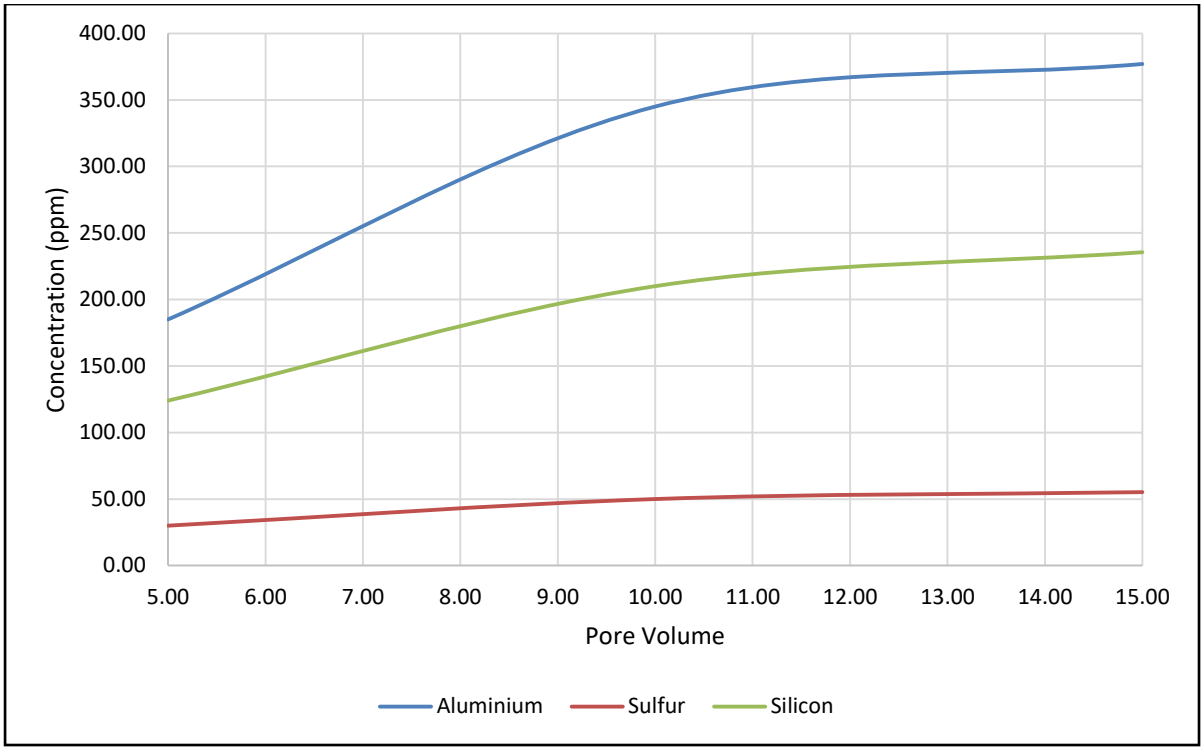

Figure 4.30. Dissolution of minerals by HEDTA from Berea Sandstone in low quantity

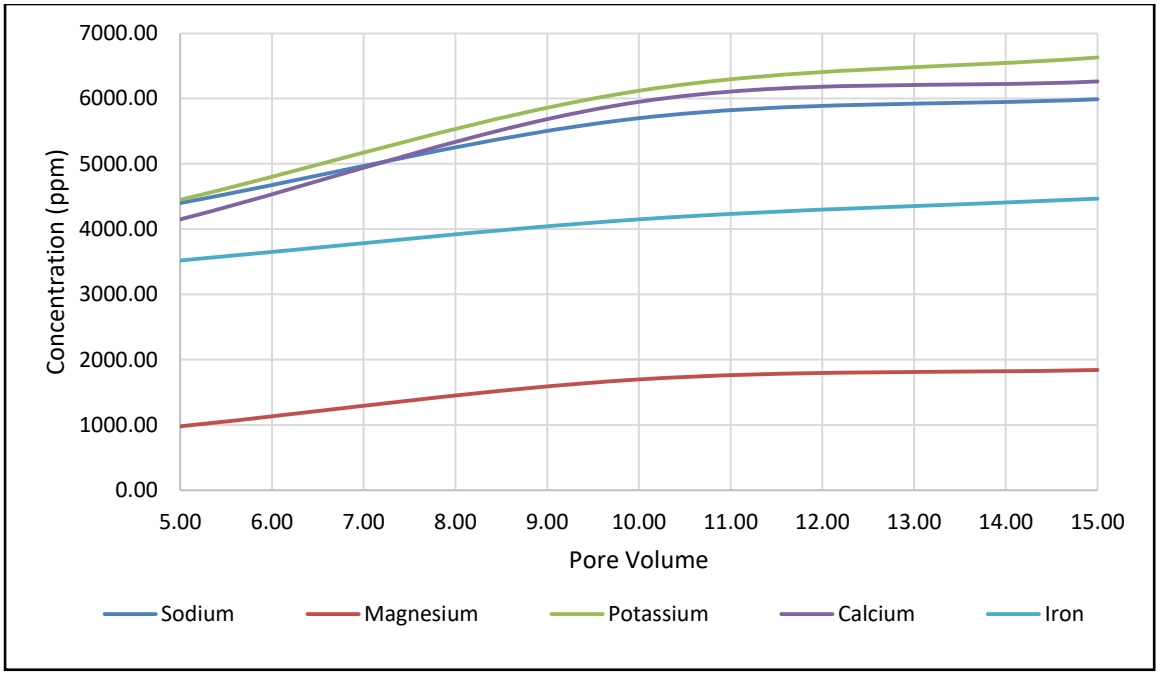

Figure 4.31. Dissolution of minerals by EDTA from Berea Sandstone in high quantity

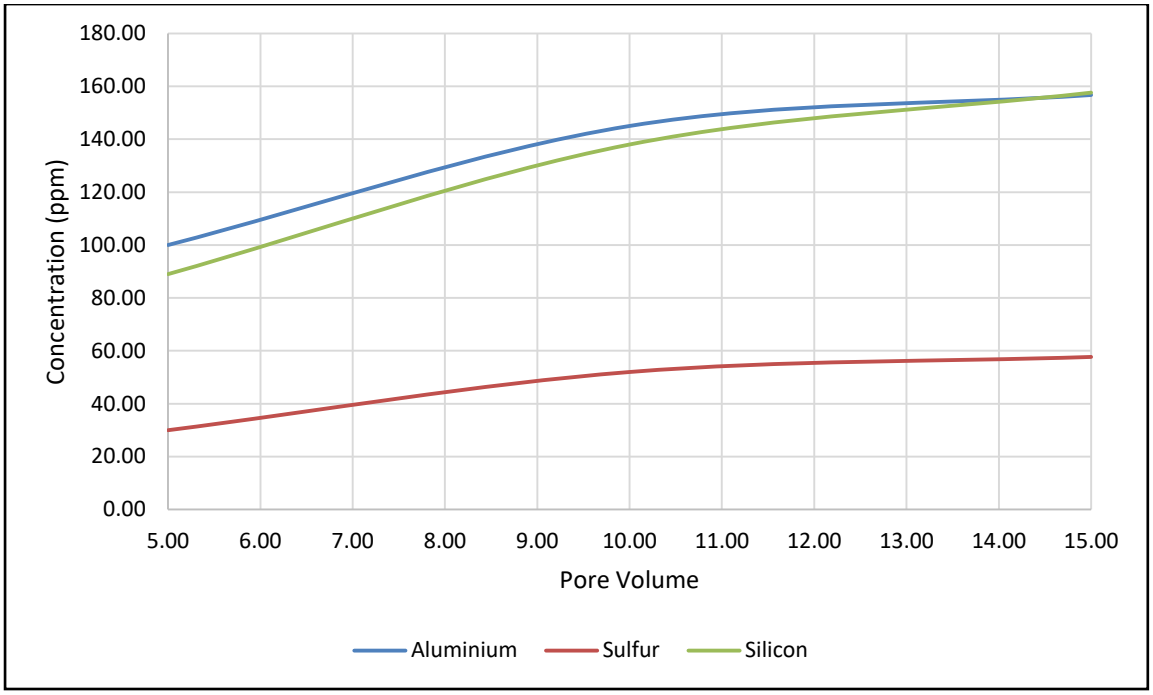

Figure 4.32. Dissolution of minerals by EDTA from Berea Sandstone in low quantity

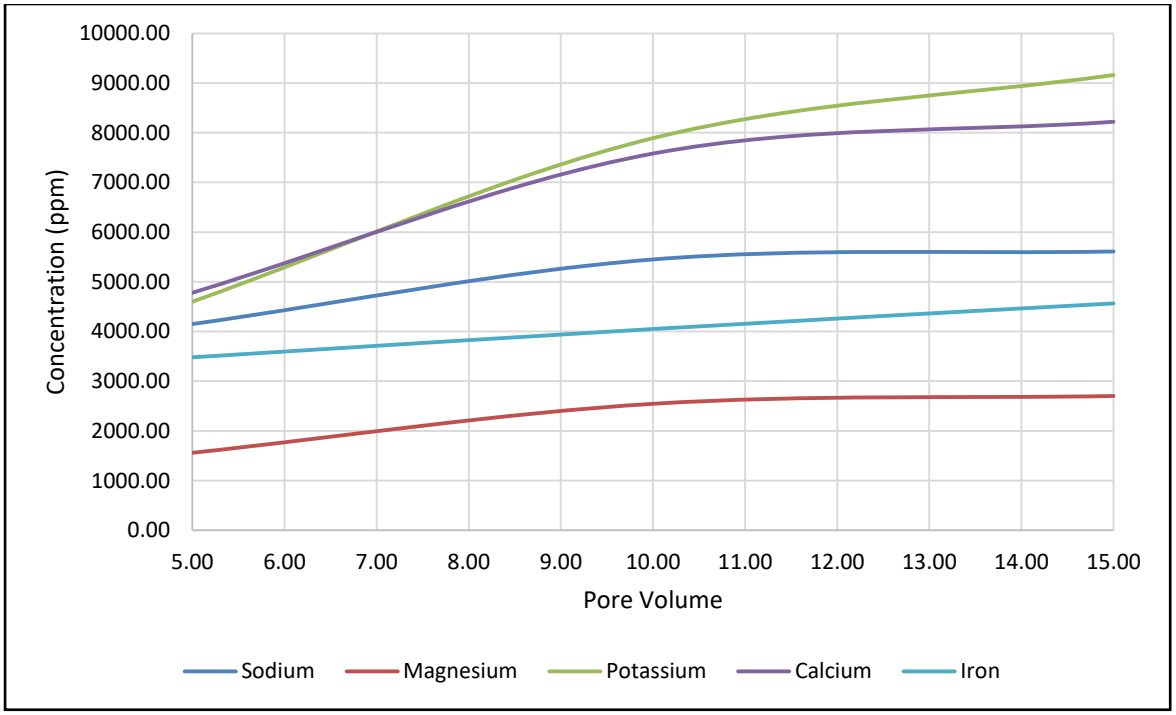

Figure 4.33. Dissolution of minerals by GLDA from Berea Sandstone in high quantity

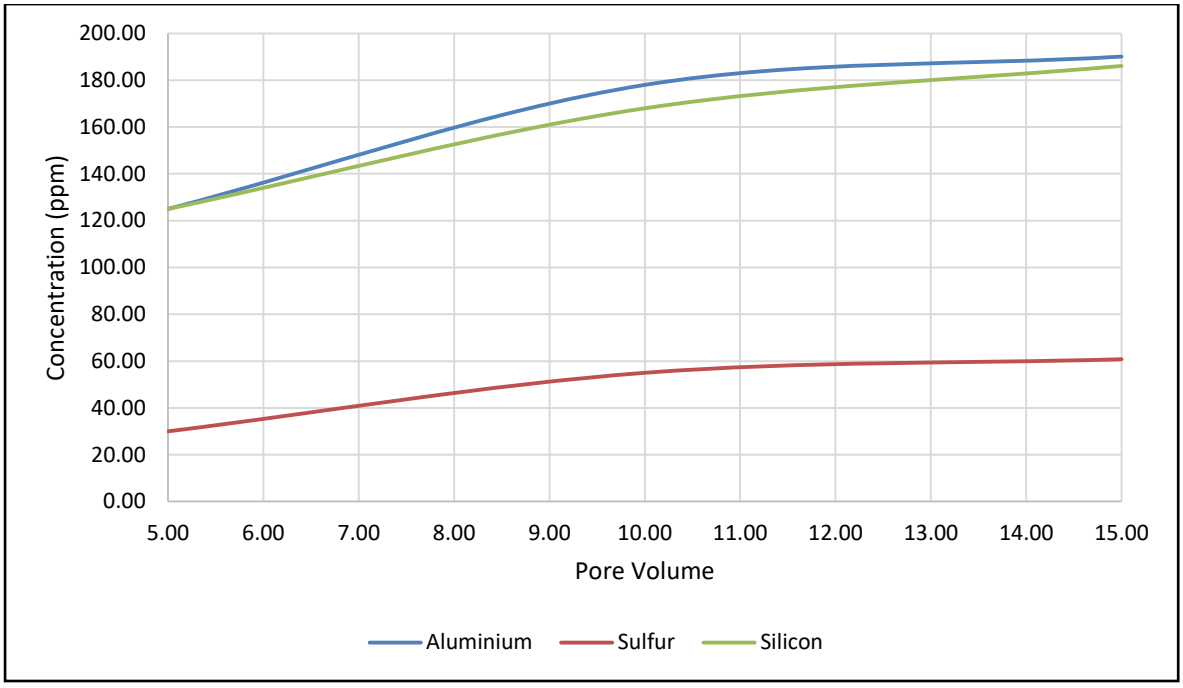

Figure 4.34. Dissolution of minerals by GLDA from Berea Sandstone in low quantity

Concluding remarks

Chelate (HEDTA) proved to be effective in the dissolution of aluminium compared to EDTA and GLDA. All chelates proved effective in the dissolution of sodium ions from Berea sandstone sample but most effective is HEDTA where it dissolves 210 ppm more ions than EDTA. HEDTA also proved to be effective in dissolving aluminium (187 ppm more than GLDA), silicon (49 ppm more than GLDA), and iron (217 ppm more than GLDA). While GLDA is effective in the dissolution of magnesium (764 ppm more than HEDTA), potassium (2531 ppm more than EDTA) and calcium (1856 ppm more than HEDTA) ions from the Berea sandstone core samples as mentioned in Figure 4.35.

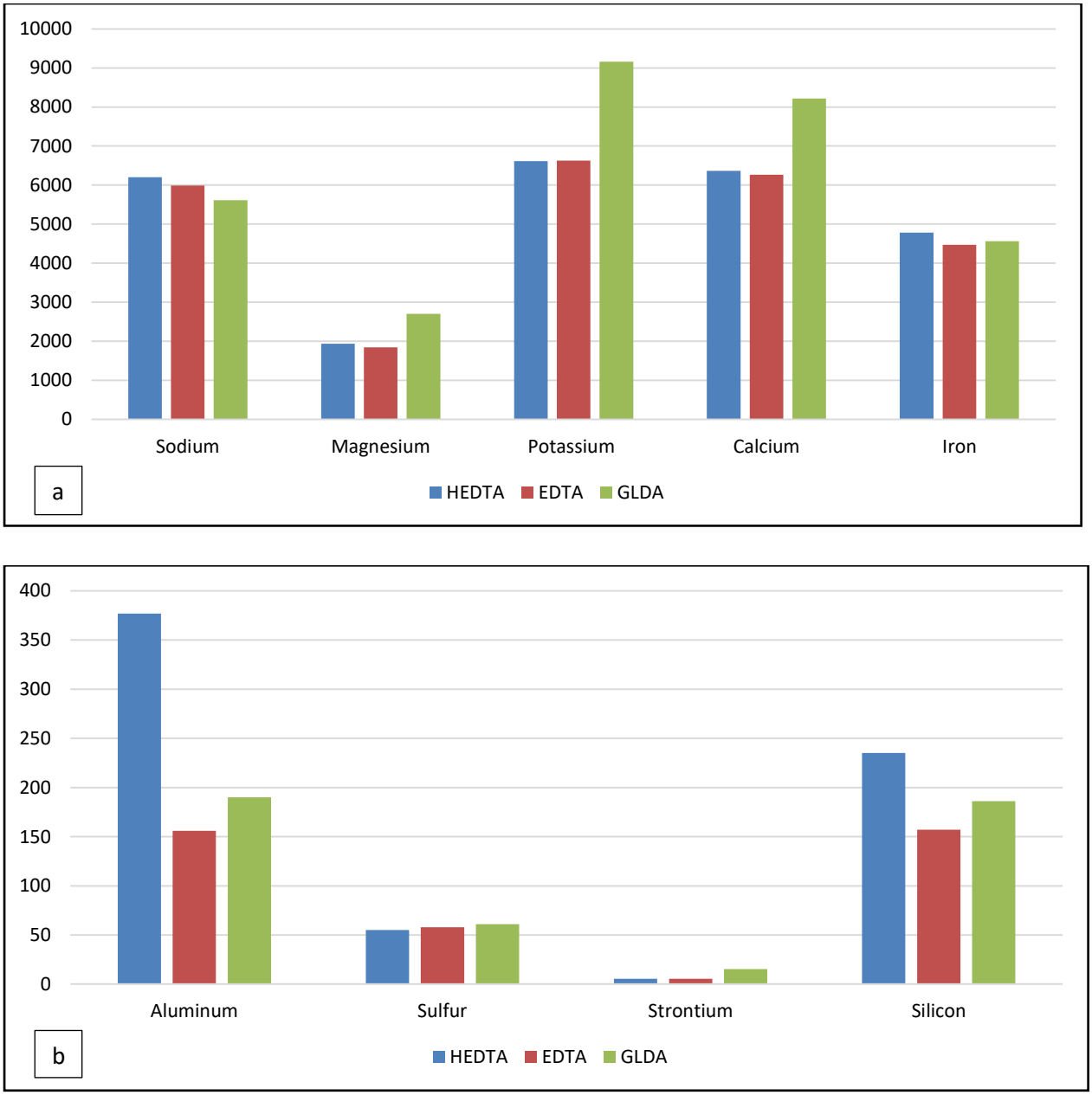

Figure 4.35. Comparison of dissolution of minerals by chelating agents from Berea sandstone

4.5 Nuclear Magnetic Resonance (NMR) Analysis

Nuclear Magnetic Resonance analysis has been widely used in chemistry, physics, and biomedicine and in clinical diagnosis for imaging the internal structure of the human body. The same principle applied in clinical imaging can also be applied for the imaging of fluid-saturated porous rock, such as reservoir rock. "NMR logging is a subcategory of electromagnetic logging (Marschall, 2000), that can measure the induced magnet moment of hydrogen nuclei (protons) contained within the fluid-filled pore space of porous media (reservoir rocks)". The conventional logging measurements (e.g., acoustic, density, neutron, and resistivity), respond

to both rock matrix and fluid properties, which are strongly mineralogy dependent while NMR-logging responds to the presence of hydrogen protons. NMR analysis can be used to obtain the information related to the quantities of fluids present, the properties of these fluids, and the sizes of the pores containing these fluids. From this information, it is possible to infer or estimate.

- The volume (porosity) and distribution (permeability) of the rock pore space
- Rock composition
- Type and quantity of fluid hydrocarbons
- Hydrocarbon producibility

4.5.1 Bulk volume irreducible (BVI) determination

Determination of (BVI) of water in the rock sample is one of the most widely used applications of NMR logging. BVI is the representative of immovable or bound water in a formation. BVI is a function of pore-throat size distribution, where smaller pore throat is responsible for high threshold pressure which retains the fluids in the pores. Figure 4.36 and 4.37 explain the different aspects of NMR logging corresponding to T_2 time decay. T_2 distribution for rocks with different porosity type (same geometric shape but different sizes) and fully saturated with water. The largest pores have the lowest surface to volume (S/V) and thus the longest T_2 whereas the smallest pores have the highest S/V (Coates et al., 1999).

BVI can be used for representing or assessing the permeability and producibility of the formation. There are two methods currently used for BVI determination. The first one is the cutoff-BVI (CBVI) model, based on a fixed-T_2 value ($T_{2cutoff}$). The porosity measured by NMR tools can be divided into two components: pores reflecting free fluid index (FFI, associated with large pores), and Bulk Volume Irreducible (BVI) associated with capillary pores (Figure 4.36). Figure 4.37 illustrates the T2cutoff which is used to divide the NMR calculated porosity into mobile and immobile components in the CBVI model. The second method is the spectral BVI (SBVI) model, in which the coexistence between the free and bound fluids is assumed in any pore space defined by the T_2 distribution at water saturation (Sw) = 100% (Marshall, 2000). The SBVI method is used primarily for quantifying movable water and, secondarily, for estimating permeability. This research based on the CBVI model which divides BVI and FFI. FFI is the amount of porosity associated with fluids that are free to flow (mobile fluid) and BVI

is the amount of porosity associated with fluids that will not flow (immobile fluid). An NMR pore size distribution can be used to divide the fluid content into producible fluids (FFI) that are mobile and capillary bound water fluids that are immobile (BVI). These divisions are made using a relaxation time cut off.

$$Ø_{NMR} = FFI + BVI \quad (4.1)$$

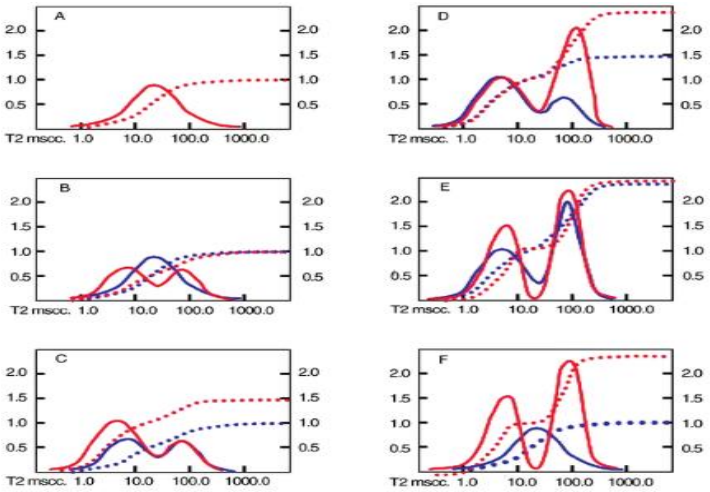

Figure 4.36. Dependence of T2 distribution on NMR-acquisition parameters (Marshall, 2000).

In Figures 4.36, previous results are presented in blue, while new results are represented by red. Solid lines are representative of incremental T_2 (left axis), while the dashed lines show cumulative T_2 vs. T_2 relaxation time (right axis) (Marshall, 2000).

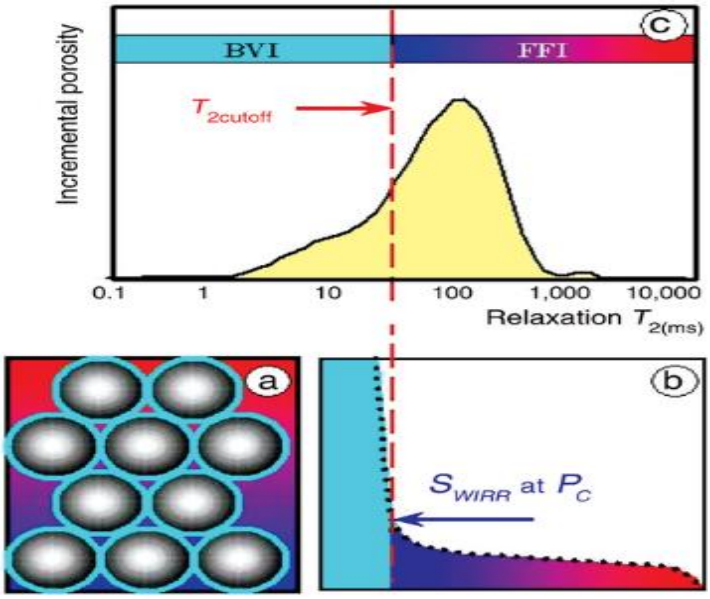

Figure 4.37. Correlating NMR T2cutoff to capillary pressure (Marshall, 2000).

In Figure 4.37, (a) gray color represents grains, light blue color show capillary-bound water (BVI), while gradient tone blue/red represents free fluids; (b) defines capillary pressure (P_c), black dots represent capillary pressure curve, shows irreducible water saturation (S_{wirr}); (c) a single-porosity cutoff value on theT_2 distribution, corresponding to this pressure (Marshall, 2000). The importance of NMR logging in matrix acidizing can be attributed to this ability of NMR logging to tool to determine FFI and BVI. FFI represents the pore spaces where oil can move and matrix acidizing main objective or goal is to create more pore spaces. Successful matrix acidizing can increase FFI where if damaged occur during acidizing BVI area will increase.

4.5.2 CBVI (cutoff) model

The T2 signal from the rock matrix is very difficult to detect even by modern logging tools due to its speed. Therefore, the only parameters recorded by T2 distribution are the porosity occupied by immovable Bulk Volume (BVI), movable water (Free Fluid Index, FFI) and clay-bound-water (CBW) components. If it is assumed that the mobility of fluids present in the reservoir is mainly controlled by the pore size (i.e., the large pores usually house producible fluids while the small pores contain immobile fluids), a fixed-T_2 value can be assigned related directly to the pore size depends whether fluid flow or not. T_2 distribution between producible and immovable fluids is divided using this value (T2cutoff) as shown in Figure 4.38 (Timur, 1969). T_2 cutoff is a value that may vary from one formation to another and can be affected by lots of factors such as: Capillary pressure, Lithology, Grain size, Compaction, Pore characteristics.

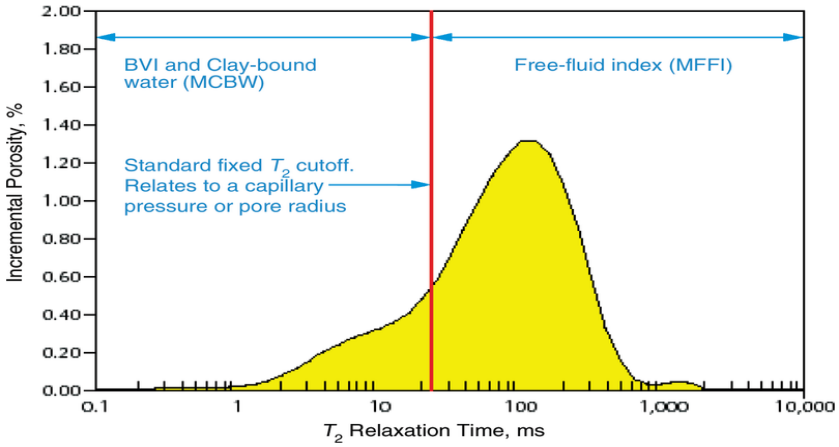

Figure 4.38. Illustration of the T2cutoff used in the CBVI model to divide NMR porosity into movable and immovable components (Timur, 1969).

4.5.3 Procedure

Maran-Ultra 2 MHz bench-top spectrometer (a resonance instrument) as shown in Figure 4.39 was utilized to conduct the NMR experiments and analysis. NMR analysis was carried out on almost all the samples which were used during the core-flooding procedure. On these samples, the NMR measurements were conducted twice (before and after the core flooding experiments). To generate the T_2 relaxation time for the samples tested, a hard pulse CPMG sequence was used. Meanwhile, the difference in the porosities and permeabilities of samples used were not much different, a constant combination of parameters was considered acceptable in the generation of T2 distribution spectrum which represents the pore-size distribution inside the core samples. Table B5 (Appendix B) shows that the number of scans (NS) was set at 8, which is good and can help to produce very high-quality spectrum by attaining high signal-to-noise ratio. Relaxation delay (RD) was set at 30 seconds which also assures full polarization for precise measurements.

In Nuclear Magnetic Resonance hydrogen nuclei can be exposed to the oscillating one when immersed in a static magnetic field. Useful information can be investigated by using NMR relaxation response measurements like clay-bound water volume (CBW), irreducible bulk volume (BVI), and movable bulk volume (BVM). This information helps in determining effective porosity, total porosity, and permeability index (Coates et al., 1999).

Figure 4.39. Resonance Instruments Maran-Ultra 2 MHz bench-top spectrometer

Longitudinal relaxation time (T1) and transverse relaxation time (T2) are the other properties of the pore fluids that may affect or influence the obtained NMR measurements. T1 measures the speed of the protons that how fast they are relaxed longitudinally when exposed to the external magnetic in the fluid (relative to the axis of the static magnetic field). On the other hand, T2 tells that how fast the protons can relax transversely (relative to the axis of the static magnetic field) (Coates et al., 1999).

Pore size, pore fluid, and mineralogy of the formation effects T2 relaxation time. When T2 time is encountered with the same rock type and the pore filling fluid; pore size will be the most important parameter to control. A direct relationship exists between pore size and T2 relaxation time. Means, if the size of porous media increases hydrogen nuclei takes more time to relax thus T2 will increase. While rocks having small pore sizes show smaller T2 relaxation time.

Nuclear Magnetic Resonance analysis tests were conducted before and after each flooding experiments on a number of saturated core plugs with 5% brine. NMR experiments were conducted using a Resonance Instruments Maran-Ultra 2 MHz bench-top spectrometer which consists of a standard homogeneous field probe and an additional gradient coil set. The following steps were followed for each NMR test:

1. Saturation of core samples using brine (5% NaCl) for NMR analysis using trident shown in Figure 3.20. Using this trident setup, 3 core samples can be saturated at one time at high confining pressure which can be created suing syringe pump. First of all, the vacuum is created inside the core holder using a vacuum pump, after that syringe pump us connected and brine is injected and high pressure is created to ensure maximum saturation. The core sample is left inside the Trident under high pressure until the gauge shows a constant reading.
2. When core samples are saturated, removed them one by one from the trident and weighed them to determine the weight of the saturated sample. Weight them quickly to avoid any loss of water vapors due to the explosion to air.
3. The saturated weighed samples were immersed in the brine inside glass jars and then heated to 35^{o}C. This preheating is done to avoid any experimental error as the temperature inside the NMR machine chamber is also 35^{o}C.

4. Three to four hours' time was allowed to equilibrate the temperature of the water inside the bath. After that, the core sample was taken out of the jar and wrapped in clean plastic film. This wrapping is done to avoid evaporation of water during the experiment. As soon as possible, the wrapping was performed again very quickly in order to avoid the evaporation of water to the air from the exposed sample pores. Also, it was kept in mind not to have any free water on the surface of the core sample as it will cause an error in the measurement.
5. The wrapped sample was then inserted into the sample chamber of the NMR machine. Before running any NMR test is worth to notify that the machine needs to be calibrated first. The calibration was done between signal amplitude and water content using 15 cc of water contained in a small jar. Nickel chloride was usually added to the water sample used for calibration. It helps to make it comparable to the relaxation time of the bounded water in the pore space by reduces the water relaxation time. T2 relaxation spectrum was generated using a hard pulse CPMG (Carr–Purcell–Meiboom–Gill) on all the core samples. In the down-hole environment, one of the most commonly employed NMR measurement is CMPG-T2 and it is one of the easiest low-field methods to implement and to interpret (Clennell et al., 2006).
6. At the end of each NMR run, the echo decays were converted to T2 spectra by the means of DXP programme which was provided by the Resonance Instruments in combination with MARAN2 spectrometer software. The pore size distribution of the pores filled with brine can be measured using this T2 distribution attained from the NMR measurements (Clennell et al. 2006., and Chen et al., 2002).

4.5.4 NMR measurements during Pre-slush stage

Nuclear Magnetic Resonance logging technique has been applied to all four core samples before and after core flooding to investigate the change in pore size distribution using CBVI model. Figures 4.40 and 4.41 represent the T_2 spectrum and commulative T_2 spectrum for each core sample before and after acidizing respectively.

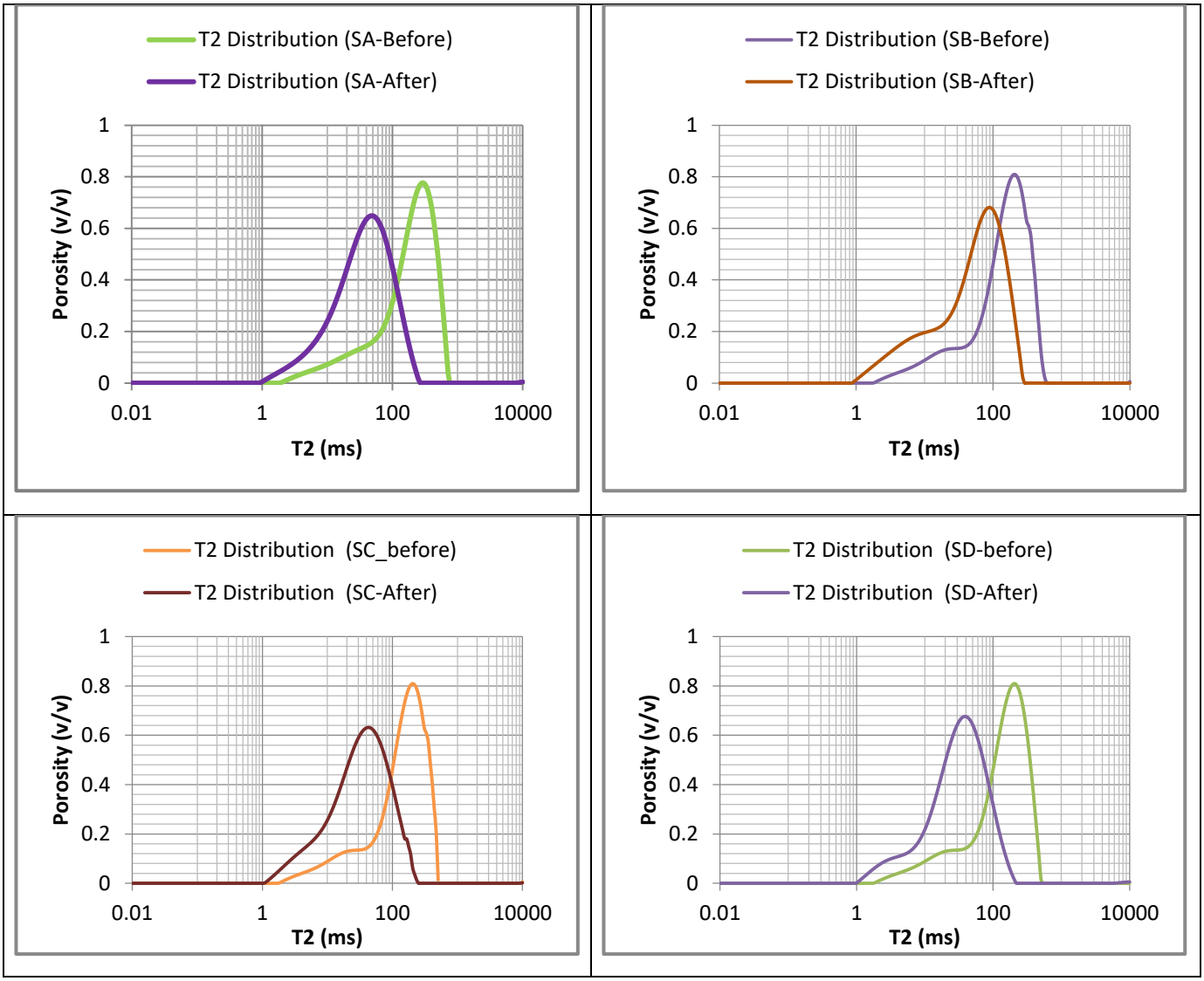

Figure 4.40: T2 spectrum of all core samples before and after acidizing

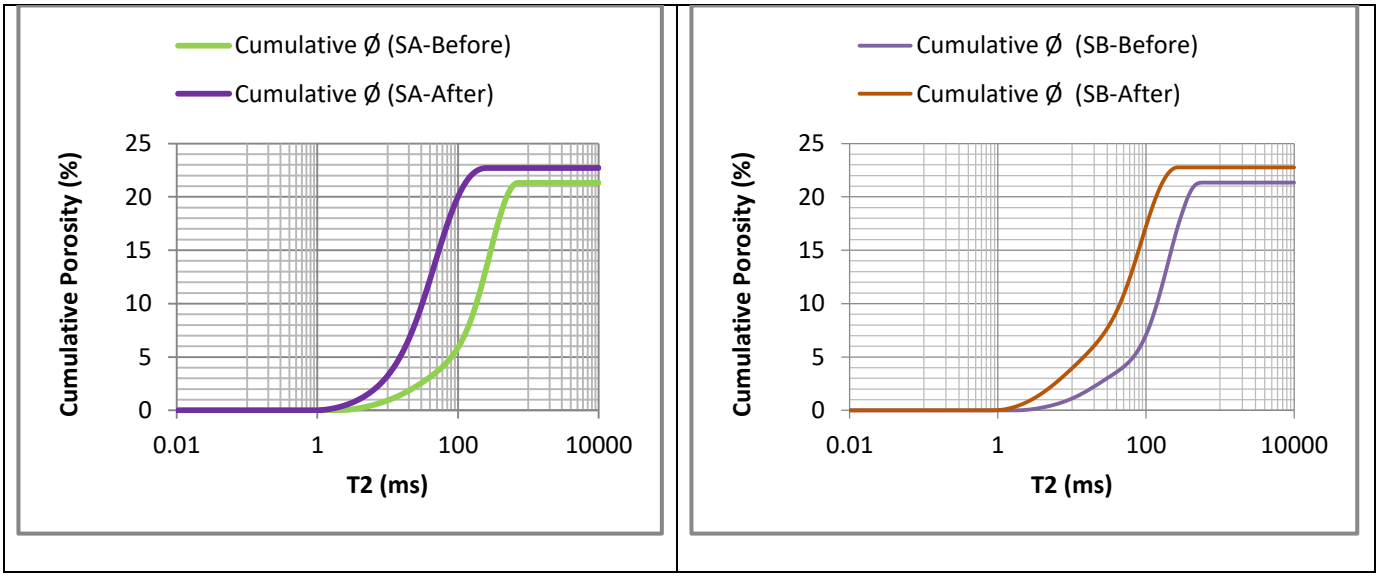

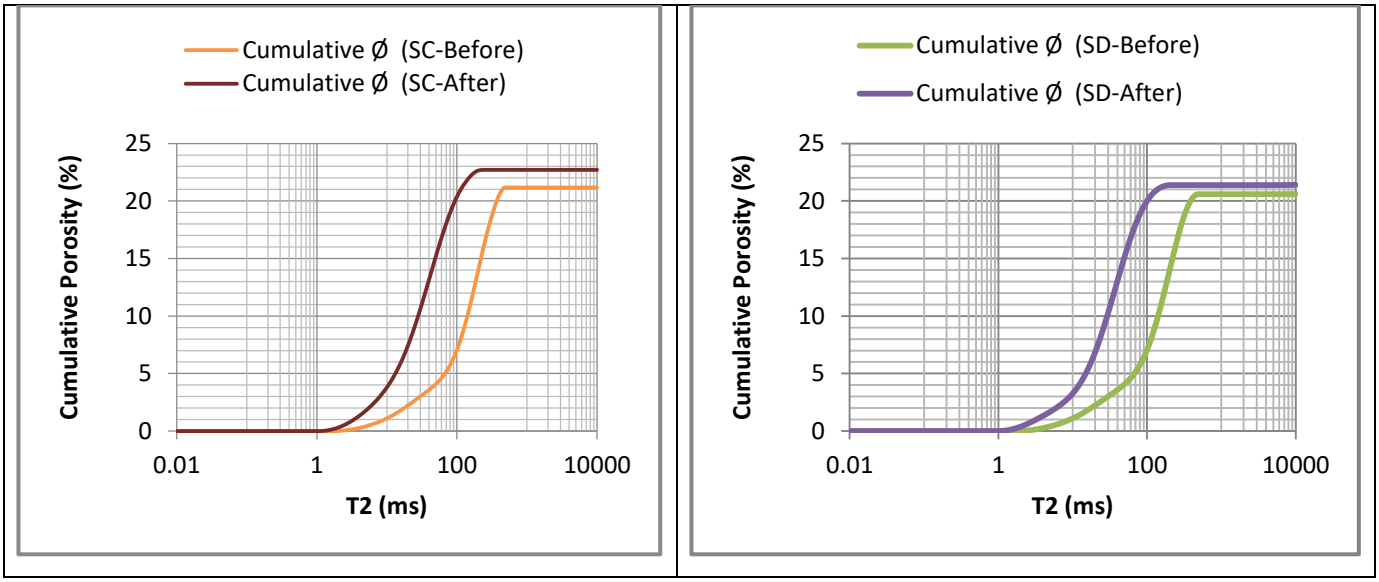

Figure 4.41. T2 commulative spectrum of all core samples before and after acidizing

Spectrum analysis of each sample presented in Figure 4.40 represents the shift in the curve towards the left side. It means that new small pores have been created and now the small pores are dominating the porosity distribution. Although there was an increase in pore space volume for all samples studied NMR T2 distributions indicate that pore sizes have been decreased for all samples analyzed. The reduction of pore space sizes can be attributed to dissolution of minerals and re-precipitation in larger pores. However, overall porosity has been increased which represent the creation of small pores. These results are validating the previously discussed results of porosity and ICP. Commulative T_2 spectrum (Figure 4.41) clearly represents the increase in the total amount of pores in the sample before and after acidizing with the least change in commulative spectrum in sample D; validating porosity results discussed in Figure 4.3. Based on the NMR analysis, the number of pore spaces has been increased for all samples studied. The maximum increase in porosity observed for Sample C, where the porosity was increased from about 20% to 23% (Figure 4.41).

Table 4.5 shows the porosity results obtained from NMR analysis. Figure 4.41 is based on these results. These results are validating the porosity results obtained previously mentioned in table A1 (Appendix A), where the maximum change in the porosity was noted within sample C. The advantage of NMR porosity measurement over general porosity measurement is the knowledge of pore distribution which has been explained and analyzed using Figure 4.40.

Table 4.5. Porosity Results using NMR analysis

Sample name	Initial Porosity (%)	Final Porosity (%)	% Change
Sample A	21.31	22.71	6.57
Sample B	21.34	22.76	6.65
Sample C	21.17	22.70	7.22
Sample D	20.59	21.40	3.94

4.5.5 NMR measurements during chelating agent stage

NMR measurement has been applied to all core samples before and after acidizing to investigate the change in pore size distribution and change in pore topology. Figure 4.42 represents T_2 spectrum for each dolomite core sample reacted with chelates.

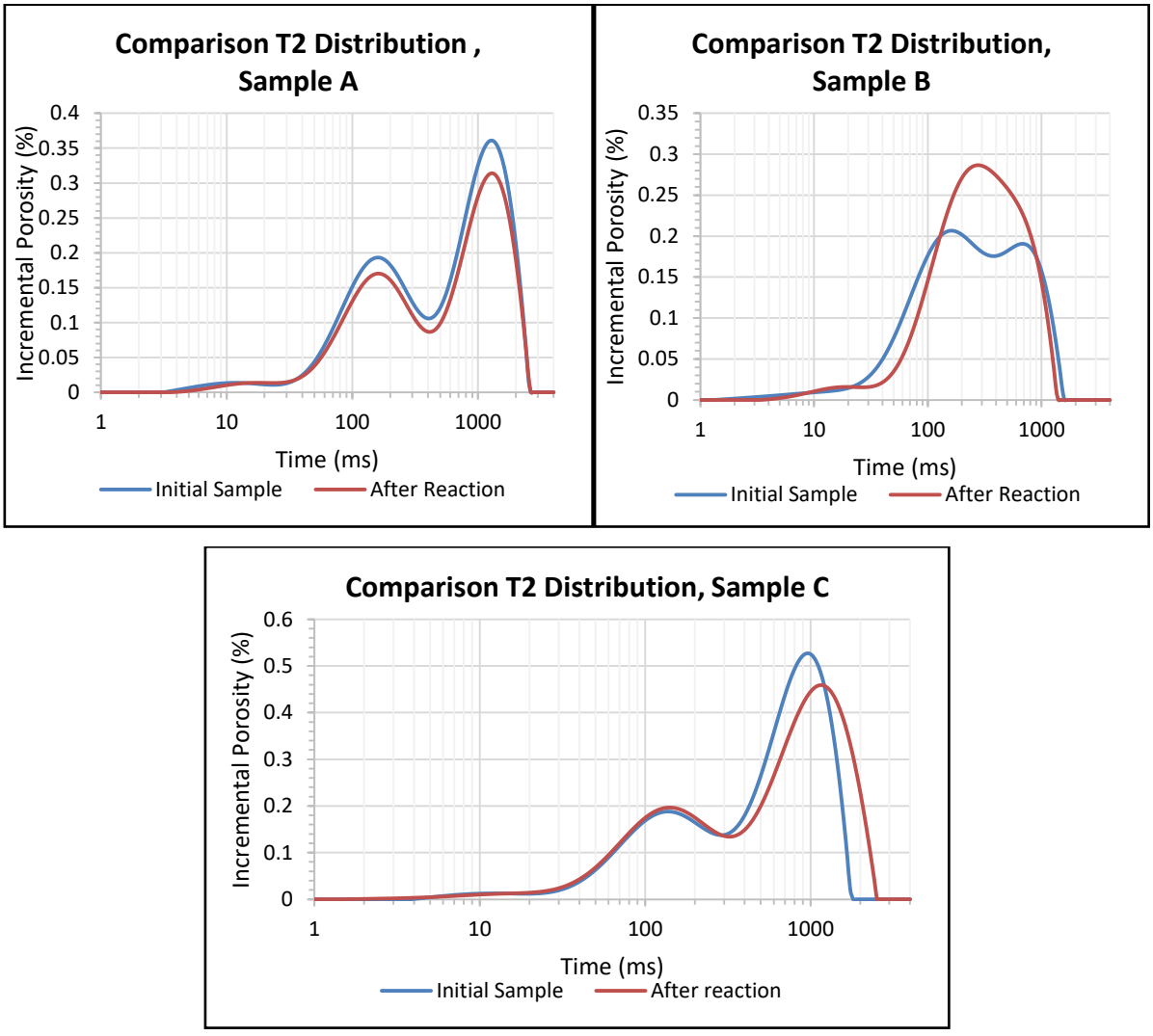

Figure 4.42. T2 spectrum of Guelph dolomite samples before and after reaction with chelates

Change in pore size distribution can be seen clearly in the spectrum of sample C and B, it indicates that the new pores have been created while the spectrum of sample A represents a decrease in the pore space sizes. This reduction of pore space sizes can be attributed to the dissolution of the minerals and reprecipitation in the pores. These precipitates can be formed due to ineffective acidizing by chelate and can reduce the porosity. Sample B (reacted with HEDTA) spectrum showed a maximum increase in a number of large pore spaces, validating permeability and porosity results discussed in Figures 4.5 and 4.6.

Figure 4.43 represents the spectrum analysis of each Colton sandstone core sample. The spectrum clearly represents the increase in the total amount of pore spaces in the sandstone core samples after acidizing, where maximum change in a number of pore spaces has been observed in sample B reacted with HEDTA, validating porosity and permeability results Figures 4.5 and 4.6.

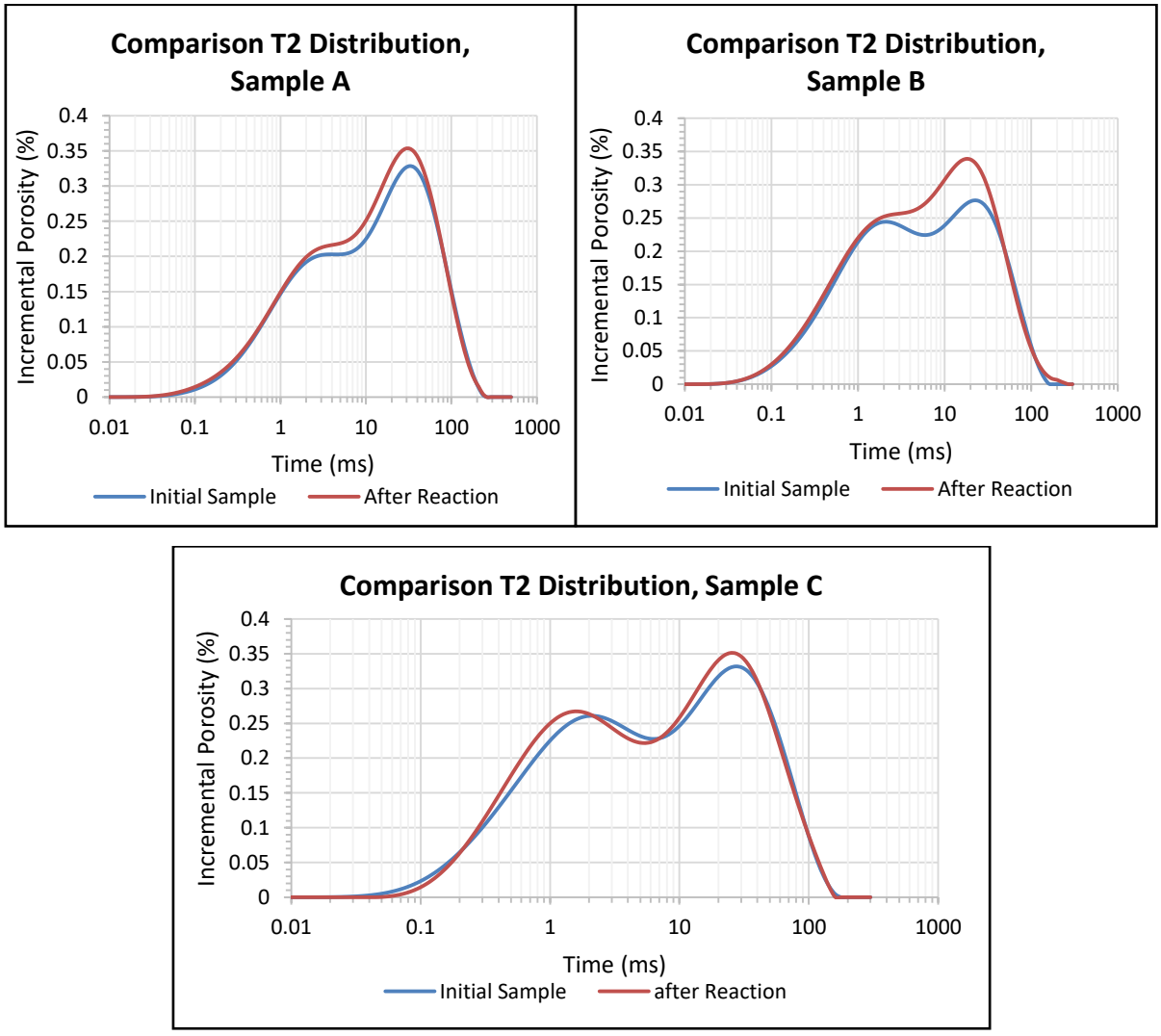

Figure 4.43. T2 spectrum of Colton sandstone samples before and after reaction with chelates

The increase in porosity after acidizing can be attributed to the effective action of chelate on the core sample. Sample A reacted with EDTA and there is an only a slight increase in porosity which can be attributed to the ineffectiveness of EDTA on the sandstone core sample. HEDTA proved to be very effective in creating more spaces in both sandstone and carbonate samples.

Figure 4.44 represents the spectrum analysis of each Berea sandstone core sample. The spectrum clearly represents the increase in the total amount of pore spaces in the sandstone core samples after acidizing, where maximum change in a number of pore spaces has been observed in sample B reacted with HEDTA, validating porosity and permeability results (Figures 4.5 and 4.6).

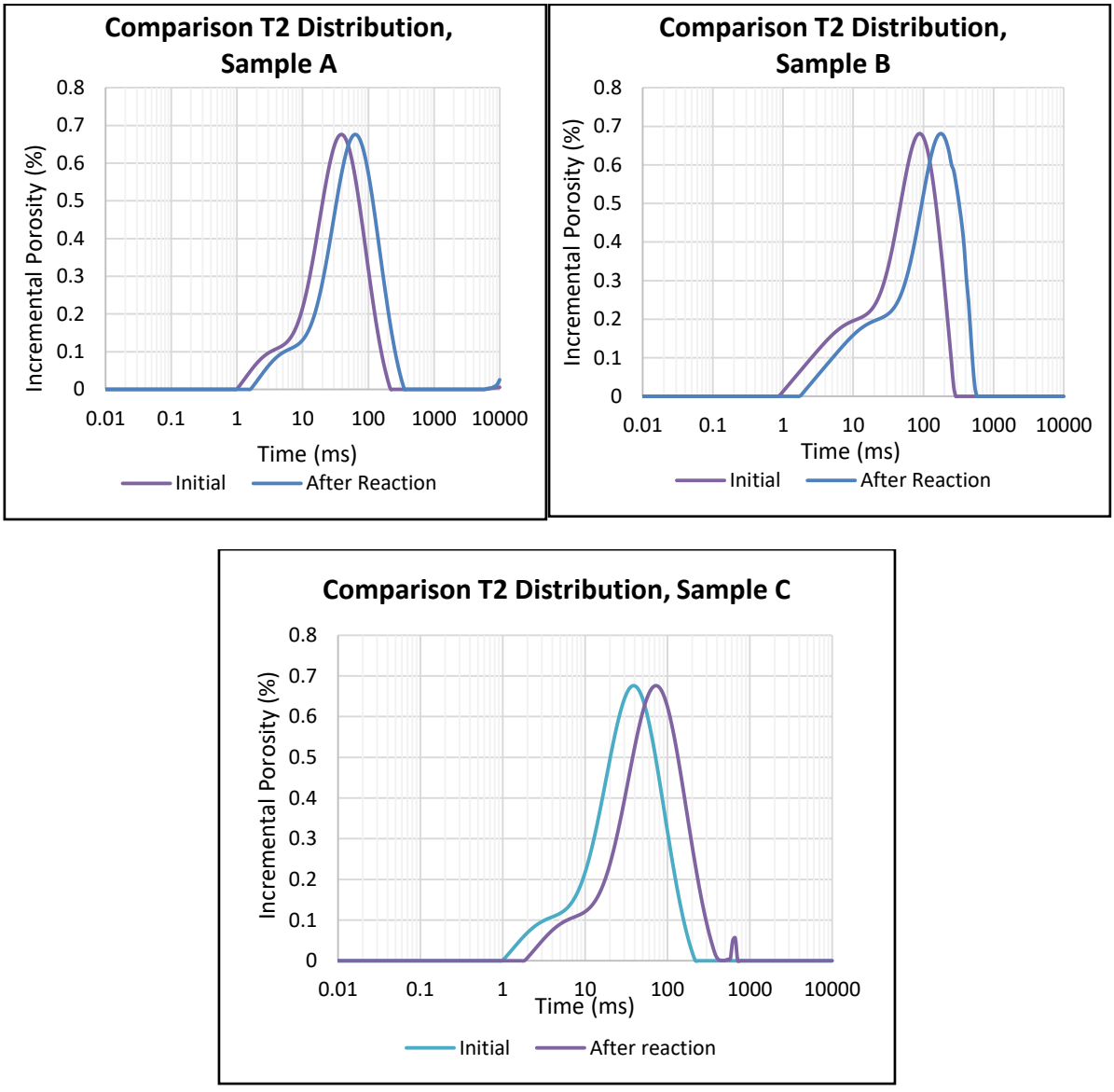

Figure 4.44. T2 spectrum of Berea sandstone samples before and after reaction with chelates

The increase in porosity after acidizing can be attributed to the effective action of chelate on the core sample. Sample A reacted with EDTA and there is an only a slight increase in porosity which can be attributed to the ineffectiveness of EDTA on the sandstone core sample. HEDTA and GLDA both proved to be very effective in creating more spaces in Berea sandstone samples.

Commulative T_2 spectrum (Figure 4.45) clearly represents the increase in the total amount of pores in the Colton sandstone samples before and after acidizing with chelates. The less change in commulative spectrum is observed in sample A and C; validating porosity results. Based on the NMR analysis, pore spaces have been increased for all samples studied. The maximum increase in porosity is for Sample B where the porosity is increased from about 12.5% to 14% (Figure 4.45).

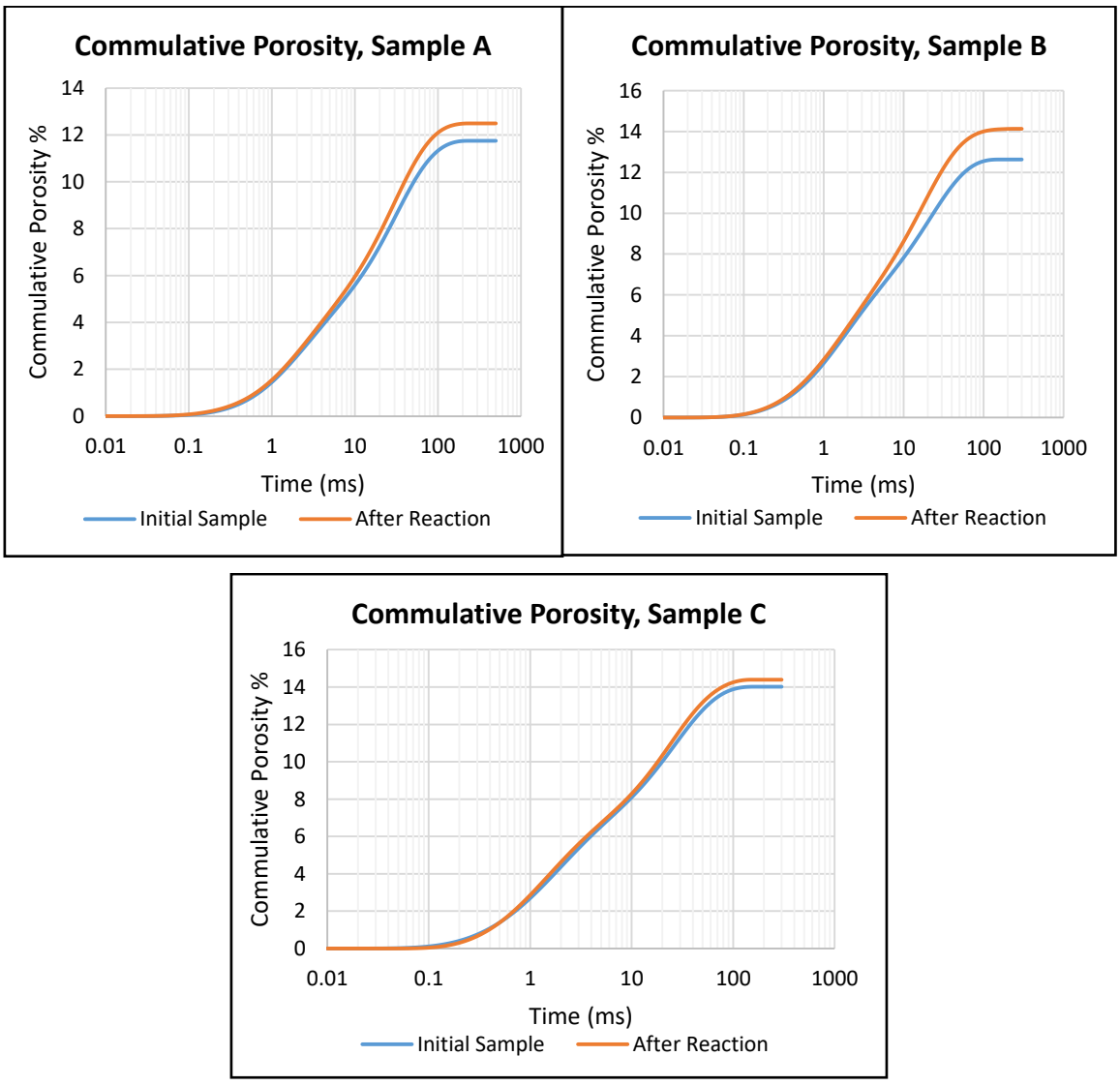

Figure 4.45. T2 commulative spectrum of all Colton sandstone core samples before and after reaction with chelates

Commulative T_2 spectrum (Figure 4.46) clearly represents the increase in the total amount of pores in the Guelph dolomite samples before and after acidizing with chelates. The decrease in commulative spectrum is observed in sample A; validating porosity results. Based on the NMR analysis, pore spaces have been increased for samples B and C. The maximum increase in porosity is for Sample B where the porosity is increased from about 14.5% to 16% (Figure 4.46).

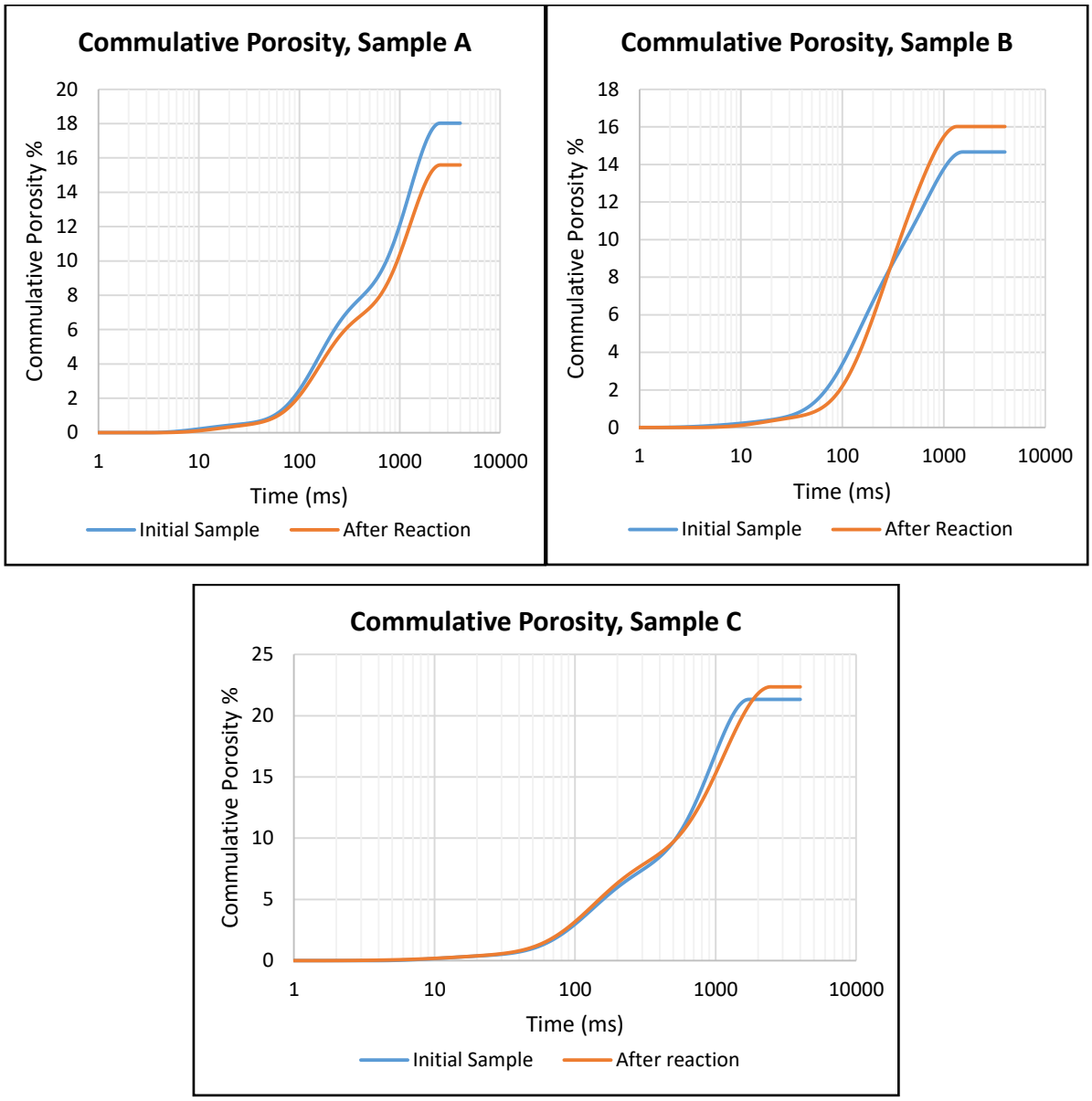

Figure 4.46. T2 commulative spectrum of all Guelph dolomite core samples before and after reaction with chelates

Commulative T_2 spectrum (Figure 4.47) clearly represents the increase in the total amount of pores in the Berea sandstone samples before and after acidizing with chelates. Based on these

analysis, pore spaces have been increased for all samples. The maximum increase in porosity is for Sample B where the porosity is increased from about 22% to 24% (Figure 4.47).

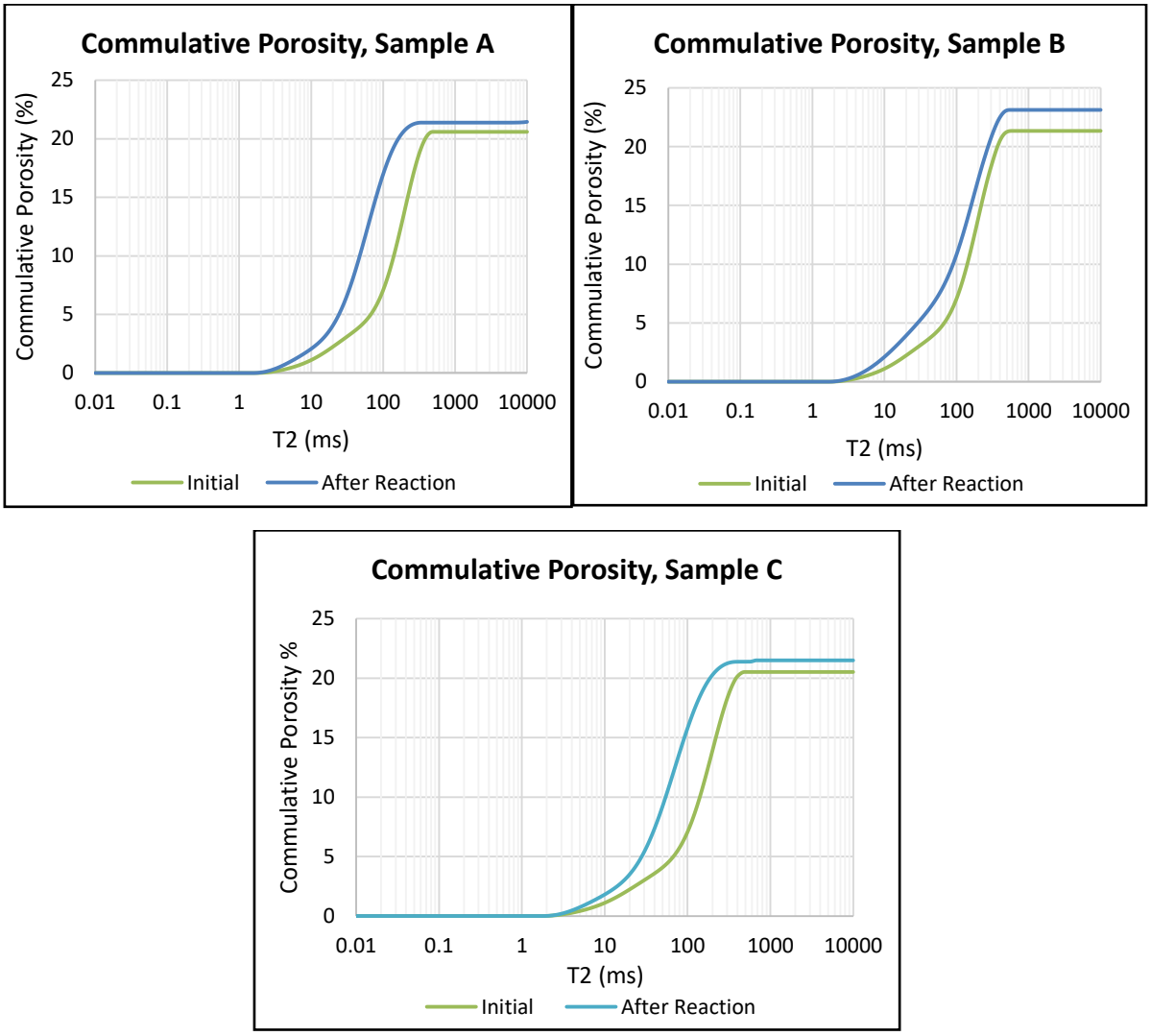

Figure 4.47. T2 commulative spectrum of Berea sandstone samples core samples before and after reaction with chelates.

Table 4.6. Porosity Results using NMR analysis during chelating agent stage

Lithology	**Sample name**	**Chelate used**	**Initial Porosity (%)**	**Final Porosity (%)**	**% change**
Colton Sandstone	Sample A	EDTA	11.75	12.49	6.39
	Sample B	HEDTA	12.63	14.13	11.87
	Sample C	GLDA	14.02	14.39	2.63
Guelph Dolomite	Sample A	EDTA	18.02	15.59	-13.48
	Sample B	HEDTA	14.66	16.02	9.27
	Sample C	GLDA	21.33	22.35	4.78
Berea Sandstone	Sample A	EDTA	20.61	21.49	4.26
	Sample B	HEDTA	21.23	23.02	8.43
	Sample C	GLDA	20.35	21.65	6.38

Table 4.6 explains the porosity results obtained from NMR analysis. Figures 4.45 through 4.47 are based on these results. These results are validating the porosity results obtained previously mentioned in tables A3 and A4; where the maximum change in the porosity has been observed when carbonate sand sandstone samples were reacted with HEDTA. The advantage of NMR porosity measurement over general porosity measurement is the knowledge of pore distribution which has been explained and analyzed using Figures 4.42 through 4.44.

4.6 Wettability Test

Wettability is the ability of the fluid to cover the surface area of the rock sample. Wettability test can be performed to recognize the wetting behavior of fluids (oil and water), on the rock surface. Wettability is usually determined with the help of contact angle. The contact angle of the liquid with a rock in the range of 0° to 75° usually represents water-wetting conditions. While 115° to 180° indicates oil-wetting conditions. On the other hand, the angle from 75° to 115° indicates neutral wettability, which shows that the rock surface is neither wetted by oil nor by water (Alotaibi et al., 2011). Figure 4.48 illustrates the water-wet and oil-wet conditions and their corresponding contact angles Θ_c.

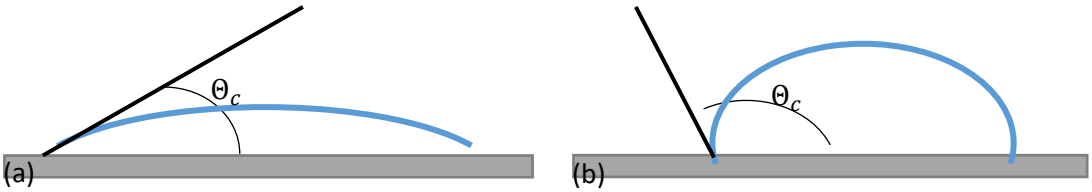

Figure 4.48. Contact angles of an (a) water-wet and (b) oil-wet surface (Alotaibi et al., 2011)

The ability of the wetting phase to stick to the rock surface and inhabit the smaller pore spaces within the reservoir is due to the capillary pressure inside the rock. Consequently, the wetting phase has the lower mobility due to its trapping inside the small pores compared to non-wetting phase, therefore, non-wetting phase move and produced easily compared to wetting phase. However, in the case of a tight reservoir, the fluid used for stimulation like an acid, usually trapped and accumulated in the small pore throats of the reservoir due to the high capillary pressure. This can be the reason for blocking of the hydrocarbons flow path and water banking. The hydrocarbons must overcome this very high capillary pressure created by the blocking of fluids which in turn can considerably reduce the production of hydrocarbon, most importantly gas (Saneifar et al., 2010; 2011). Thus, wettability conditions are different in different

reservoirs based on production methods, reservoir conditions and Enhanced Oil Recovery (EOR) techniques applied (Mohammadi et al., 2009). In conventional sandstone reservoirs, usually, water-wet conditions are favorable to optimize the production of hydrocarbons. In this project, the wettability of the different core samples has been measured by recording the contact angles from the Drop Shape Analyzer (DSA) apparatus. The DSA is equipped with aperture, illumination, sample table, prism, dosing unit, and camera. The liquid was dropped by the dosing unit which was then detected by the camera. Later the image was sent to the computer for further analysis. Then, the contact angle of that drop of liquid was interpreted, generated and analyzed. The results are mentioned in table 4.7 and the pictures taken during wettability test are attached in Appendix B. Drop Shape Analyzer is shown in Figure 4.49 while the workflow to record the contact angle is presented in Figure 4.50.

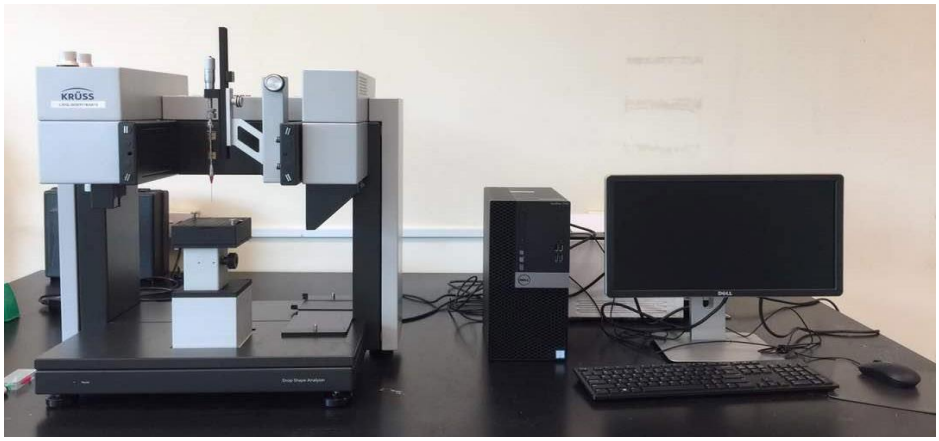

Figure 4.49. Drop Shape analyzer (DSA100).

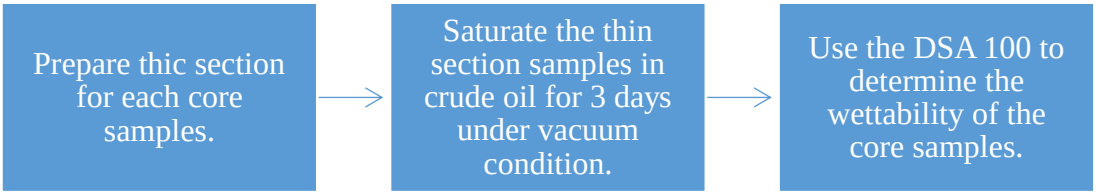

Figure 4.50. Workflow of DSA

4.6.1 List of Equipment

The equipment used for the measurement of wettability are shown in Figures 4.51 through 4.54.

Figure 4.51 shows the Vacuum Oven. The main purpose for the use of the vacuum oven was to increase the saturation efficiency of the core sample by creating pressurized conditions. 0.05MPa pressure has been set as a standard for saturation of both formation water and crude oil.

Figure 4.51. Vacuum Oven

To ensure a flat and smooth surface of the core sample along with correct size, several types of equipment were utilized such as Lortone 8” Bench Trim Saw (Figure 4.52), Hillquist Thin Section Grinder (Figure 4.53), hotplate and Ingram Ward Thin Section Saw / Grinder (Figure 4.54). The smooth surface of the core sample was required because roughness can affect the wettability analysis.

Figure 4.52. Lortone 8” Bench Trim Saw

Figure 4.53. Hillquist Thin Section Grinder

Figure 4.54. Ingram Ward Thin Section Saw / Grinder

4.6.2 Procedure

KRUSS instrument was switched on 30 minutes before the experimental measurement to make it warm and ready for measurements. All the necessary information was entered using the ADVANCE software, under the text boxes of NAME and DETAILS. Also, the temperature range was entered in the software at which the experiment was carried out. Then, the liquid used by the dosing unit was selected (distilled water in this case) under the section CONFIGURE DOSING and afterward fill the syringe with that liquid. Later, a thin section of the core sample was placed beneath the syringe and calibration was performed on ADVANCE software. After calibration, put a drop of brine on the core sample placed and recorded the contact angle by using the ADVANCE software. Figure 4.55 shows all the samples that were analyzed for wettability conditions.

Figure 4.55. Samples used for wettability measurement

4.6.3 Wettability Analysis

As seen from table 4.7, the change in wettability of Berea sandstone samples shifts towards more water-wet condition, which is favorable for the oil and gas production. The initial contact angle of Berea sandstone core sample was 71.94; nearly neutral wetting conditions. But after reacting with the chelating agents, the contact angle decreased to 69.92 in case of EDTA (2.8% change), 62.86 in case of HEDTA (12.6% change) and 60.95 in case of GLDA (15.3% change) as mentioned in Figure 4.56.

Table 4.7. Contact angles of the core samples.

Core Samples	**Contact Angles, Θ_c (°)**
Dolomite A (EDTA)	87.55
Dolomite B (HEDTA)	83.89
Dolomite C (GLDA)	83.75
Berea A (EDTA)	69.92
Berea B (HEDTA)	62.86
Berea C (GLDA)	60.95
Berea E (Initial)	71.94
Colton A (EDTA)	76.54
Colton B (HEDTA)	73.90
Colton C (GLDA)	73.42
Colton E (Initial)	78.74

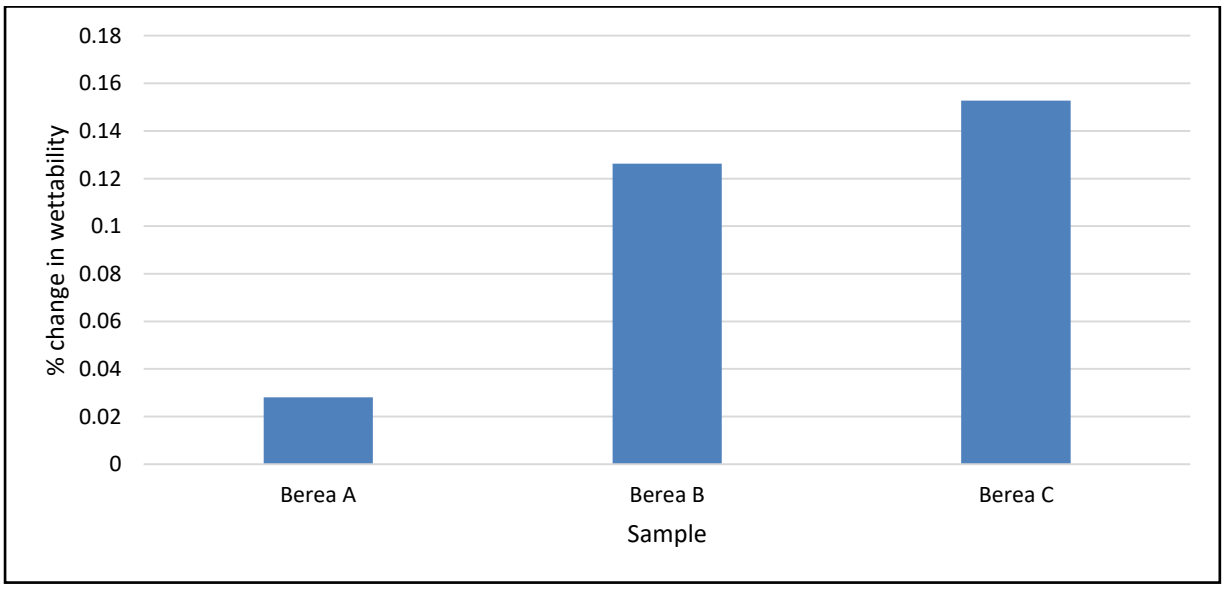

Figure 4.56. Wettability changes in Berea sandstone after acidizing

As seen from table 4.7, the change in wettability of Colton sandstone samples shifted towards more water wet conditions, which is favorable for the oil and gas production. The initial contact angle of Colton sandstone core sample was 78.74; neutral wetting conditions. But after reacting with the chelating agents, the contact angle has been decreased to 76.54 in case of EDTA (2.7% change), 73.90 in case of HEDTA (6.1% change) and 73.42 in case of GLDA (6.7% change) as mentioned in Figure 4.57. From the analysis of sandstone sample, one trend is very clear where the maximum change in wettability was observed when GLDA reacted with sandstone formation. On the other hand, the minimum change in wettability was observed when the core sample reacted with EDTA. A similar trend has been observed in case of dolomite samples also, where the contact angle value is towards higher side when reacted with EDTA compared to other chelates where the contact angle has been decreased and shifted towards water wet conditions as seen in Table 4.7. Therefore, chelating agents are not only increasing the permeability and porosity of the reservoirs but also change the wettability of the sandstone core sample. From Table 4.7, it was observed that the potential change in the wettability of the reservoir rock towards more water-wet. Therefore, this wettability change can increase the imbibition of water into the hydrocarbon reservoir, consequently optimizing the oil recovery (Xu et al., 2008).

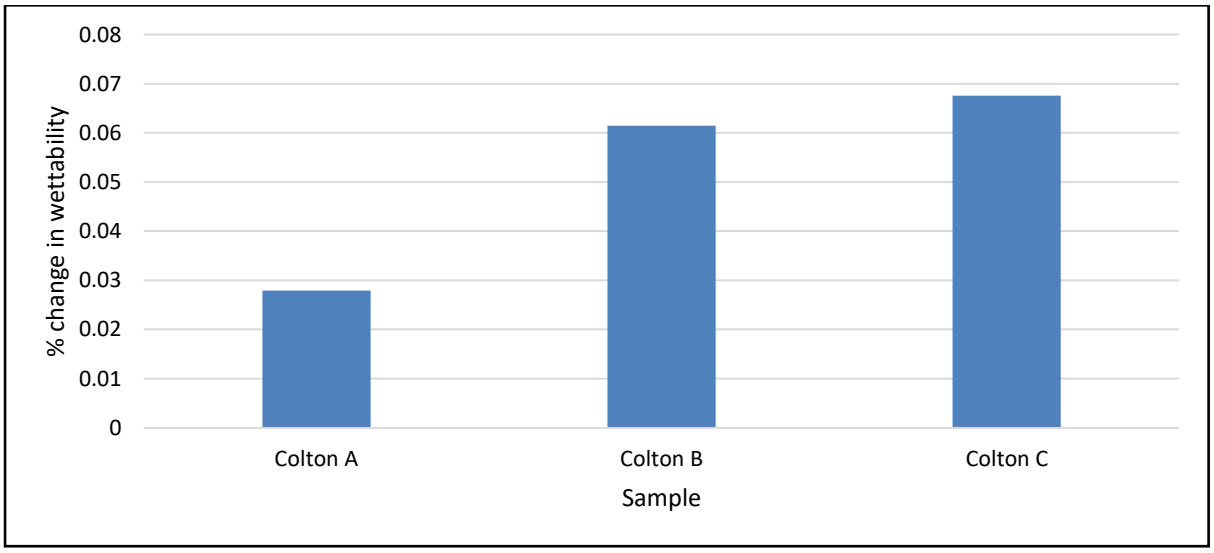

Figure 4.57. Wettability changes in Colton sandstone after acidizing

Wettability of the formation is affected by the presence of the pore structures. It has been investigated already by (Saneifar et al., 2010) that application of acids does not change the wettability of the core samples, which directly shows that even if pore paces are created the wettability remains the same as it is the property of the grain surface. Wettability analysis was

not performed during the pre-flush stage because the acid does not affect the wettability of core samples. The results are verified by the experimental work carried out by (Saneifar et al., 2010). In this work, they showed that the 15% HCl spent acid didn't significantly affect the wettability of the core samples. They also investigated that increasing or decreasing the concentration of acid also did not affect the wettability of the formation.

4.7 Solubility and Pore Volume analysis

The solubility test describes the power of chelating agent or acid during acidizing. This test can use to validate the porosity and permeability analysis discussed earlier. On the other hand, pore volume measurement can investigate the volume of acid or chelate required for the acidizing. As the flow rate is constant for all the tests (0.00006 m^3/sec) and the total volume to be injected is also constant for all samples (15 PV). Therefore, Pore volume analysis, on one hand, can investigate the volume of acid required while the change in pore volume after acidizing can validate porosity analysis discussed earlier. Table 4.8 and 4.9 represent the pore volume and weight changes respectively of all the core samples after acidizing.

It has been observed that the maximum pore volume increment is created by 5% CH_3COOH: 10% HCl in case of Berea sandstone (5.9%), by HEDTA in Colton sandstone (10.85%), by HEDTA in dolomite (5.6%) and by HEDTA in Berea sandstone (5.6%). These changes validating the porosity and permeability analysis discussed in earlier sections.

Table 4.8. The pore volume of core samples before and after acidizing

Sample	Description	Initial Pore Volume (ml)	Final Pore Volume (ml)	% Change
Berea	Sample A	14.265	15.027	0.053417
	Sample B	16.76	17.593	0.049702
	Sample C	16.70	17.686	0.059042
	Sample D	16.32	17.082	0.046691
Colton	Sample A	8.908	9.827	0.103166
	Sample B	9.66	10.709	0.108592
	Sample C	10.193	11.052	0.084274
Dolomite	Sample A	14.155	14.292	0.009679

	Sample B	12.101	12.637	0.044294
	Sample C	18.057	18.336	0.015451
Berea (Group 2)	Sample A	16.98	17.708	0.042874
	Sample B	16.19	17.096	0.05596
	Sample C	16.28	17.19	0.055897

Table 4.9 represents the change in the dry weight of the core sample before and after acidizing. The maximum decrease in weight of Berea sandstone, Colton sandstone, and Guelph dolomite have been observed when they were reacted with HEDTA (1.1%, 1.8 % and 1.7% decrement respectively). Likewise, maximum decrement has been observed when Berea sandstone reacted with 5% CH_3COOH: 10% HCl; hence validating porosity, permeability, and pore volume analysis.

Table 4.9. The weight of core samples before and after acidizing

Sample	**Description**	**Initial weight (kg)**	**Final weight (kg)**	**% Change**
Berea	Sample A	0.15328	0.15090	0.015527
	Sample B	0.17914	0.17664	0.013956
	Sample C	0.17962	0.17660	0.016813
	Sample D	0.18076	0.17827	0.013775
Colton	Sample A	0.20210	0.20080	0.006432
	Sample B	0.19970	0.19611	0.018027
	Sample C	0.19770	0.19652	0.005928
Dolomite	Sample A	0.20030	0.19980	0.002496
	Sample B	0.20710	0.20340	0.017866
	Sample C	0.19010	0.18813	0.010363
Berea (Group 2)	Sample A	0.17827	0.17712	0.006451
	Sample B	0.17664	0.17464	0.011322
	Sample C	0.18071	0.17987	0.004648

4.8 CT Scan Analysis

The cores were photographed and reweighted after the core flooding experiments were finished, to determine the wormhole creation and weight loss. The weight loss was already discussed in Table 4.9 while photographed cores with wormholes can be seen in Figures 4.58 (a, b, c, d). Figure 4.58a shows the core sample inlet face before acidizing. On the other hand, Figures 4.58b to 4.58d show the core samples inlet face after acidizing with GLDA, HEDTA, and EDTA respectively. All the chelating agents successfully created new wormholes in the dolomite core samples. However, face dissolution was maximum in case of HEDTA (Figure 4.58c) compared to other chelates. That is why the change in porosity and permeability when dolomite sample reacted with HEDTA was a maximum. It is worth noted that good wormhole structures are usually formed in the carbonate samples compared to the sandstone samples. Therefore, Figures 4.58a to 4.58d only showed dolomite core samples as no wormhole structure has been observed in sandstone samples.

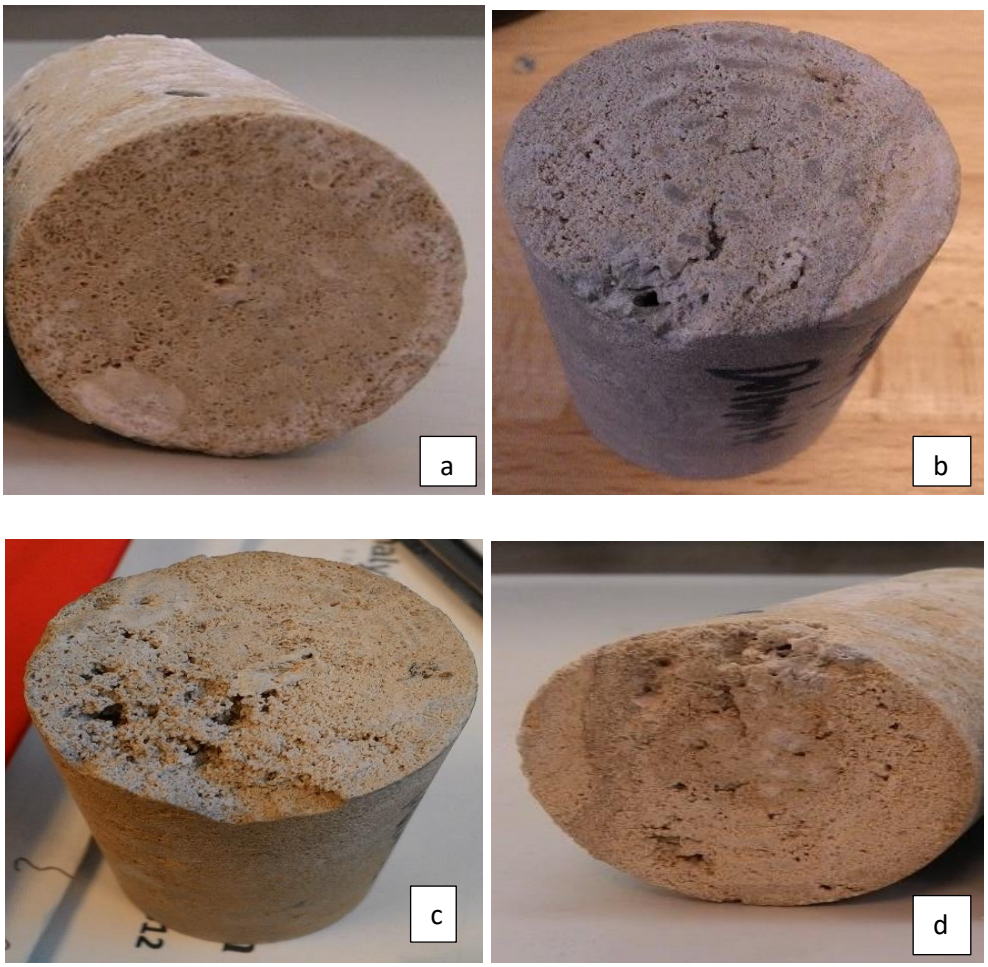

Figure 4.58. Photographed dolomite core samples and creation of wormholes

To further investigate the pore structure of the core samples, micro CT scan analysis were conducted on a small section of core samples (6mm × 8 mm) reacted with HEDTA.

4.8.1 CT scan

Micro-CT scan is just like X-ray vision but with better resolution. Without destroying the subject it allows seeing inside of the subject. It is just like medical CT system where one can get slice by slice images without destroying the sample (Carlson, 2006). 2-D images tell us what is in an object but 3-D images obtained using micro-CT can tell us where those things are present inside the object.

4.8.1.1 Broad overview of Micro-CT

Micro-Computed tomography is a technique in which X-rays are emitted from an X-ray generator. These X-rays travel through the sample, and on the other side recorded by a detector to produce a radiograph also known as a projection image. Then another projection image at a new position will be taken by rotating the sample by a fraction of a degree. Series of projection images have been taken by rotating the sample by 180 or 360 degrees with continuous iterations. One of the major advantages of CT scan technique is that it can characterize the three dimensions rock internal structure without destroying it. It can provide a stack of 1000 or more 2D cross-sectional images of the investigated sample non-destructively; which is much faster than performing serial sectioning. On the contrary, only small samples can be analyzed using this technique which therefore required many samples to be scanned to get the correct volume. To determine the properties like electrical conductivity and permeability, the complex internal microstructure needs to be described properly. X-ray microtomography is very useful but is not readily available and 2D thin sections are the most adequate source of information for pore structure analysis (Øren and Bakke, 2002). Accordingly, the most appropriate approach was to make a 3D structure from already available 2D images by using statistical models (Joshi, 1974; Adler et al., 1990; Adler et al., 1992; Hazlett, 1997; Yeong and Torquato, 1998a; 1998b). However, during the beginning, the CT scan was mostly applied for medical purposes, but soon it was realized that it had good potential in many other fields and application like paleontology (Fourie, 1974), soil science (Allan et al., 2002), and fluid-flow research (Wellington and Vinegar, 1987). Image analysis of 3D structure starts with high-quality images because it is useful to get valuable information from the true images. Image analysis usually consists of complex image processing and advanced calculations (Starkey and Samantaray, 1994; Pirard, 1994). Image analysis consists of few steps which include noise reduction followed by

segmentation and then binary image editing. However, 2D original images need to be processed before performing image analysis. This image analysis is mainly done in order to enhance the appearance of the images. Figure 4.59 shows the initial raw image and processed segmented image of one of the core sample used during this research. For each sandstone and dolomite core samples, around 700 2D raw images were obtained, segmented and then converted into a 3D image. The initial 2D sandstone image obtained was very dark and very hard to determine the pore spaces while after image analysis, the quality of the image improved a lot as shown in Figure 4.60. The segmented image shows different minerals present inside the Berea sandstone core sample represented by different numbers in Figure 4.60, while the segmented image of dolomite core sample mostly shows ankerite mineral which is around 97% of total matrix. In both segmented images shown in Figure 4.59, the blue color represents the pore spaces.

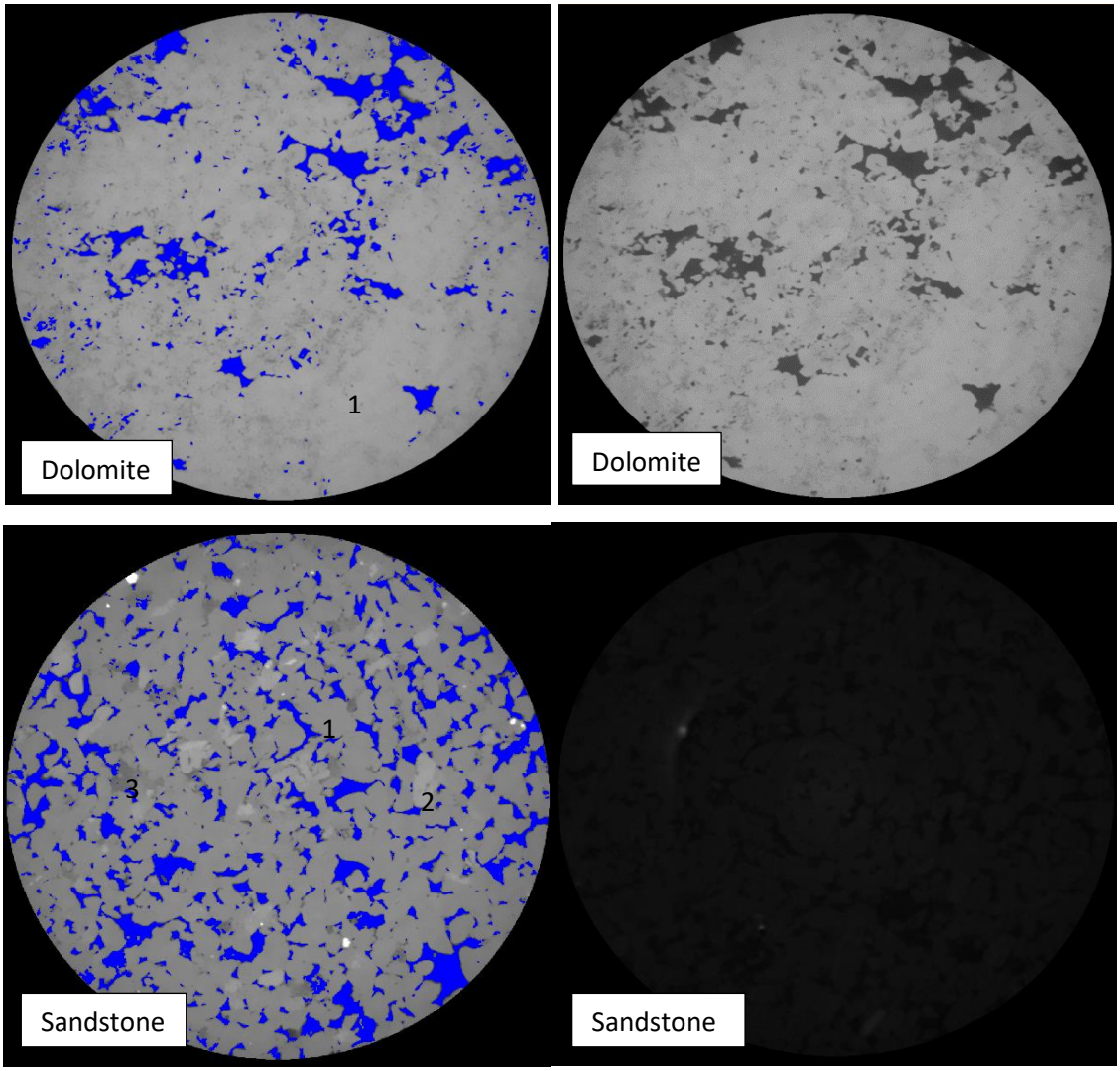

Figure 4.59. Dolomite and Sandstone Fomration (left) Segmented images (right) Raw Image

Figures 4.60 show the pore structure of sandstone and dolomite core samples respectively before and after the acidizing procedure. These samples are reacted with HEDTA chelate and porosity of 3-D core samples have been calculated for each sample. Increase in the pore spaces have been observed in both cases and porosity for sandstone sample was changed from (13.96% to 17.20%) while for carbonate the porosity increased from (8.66% to 10.93%).

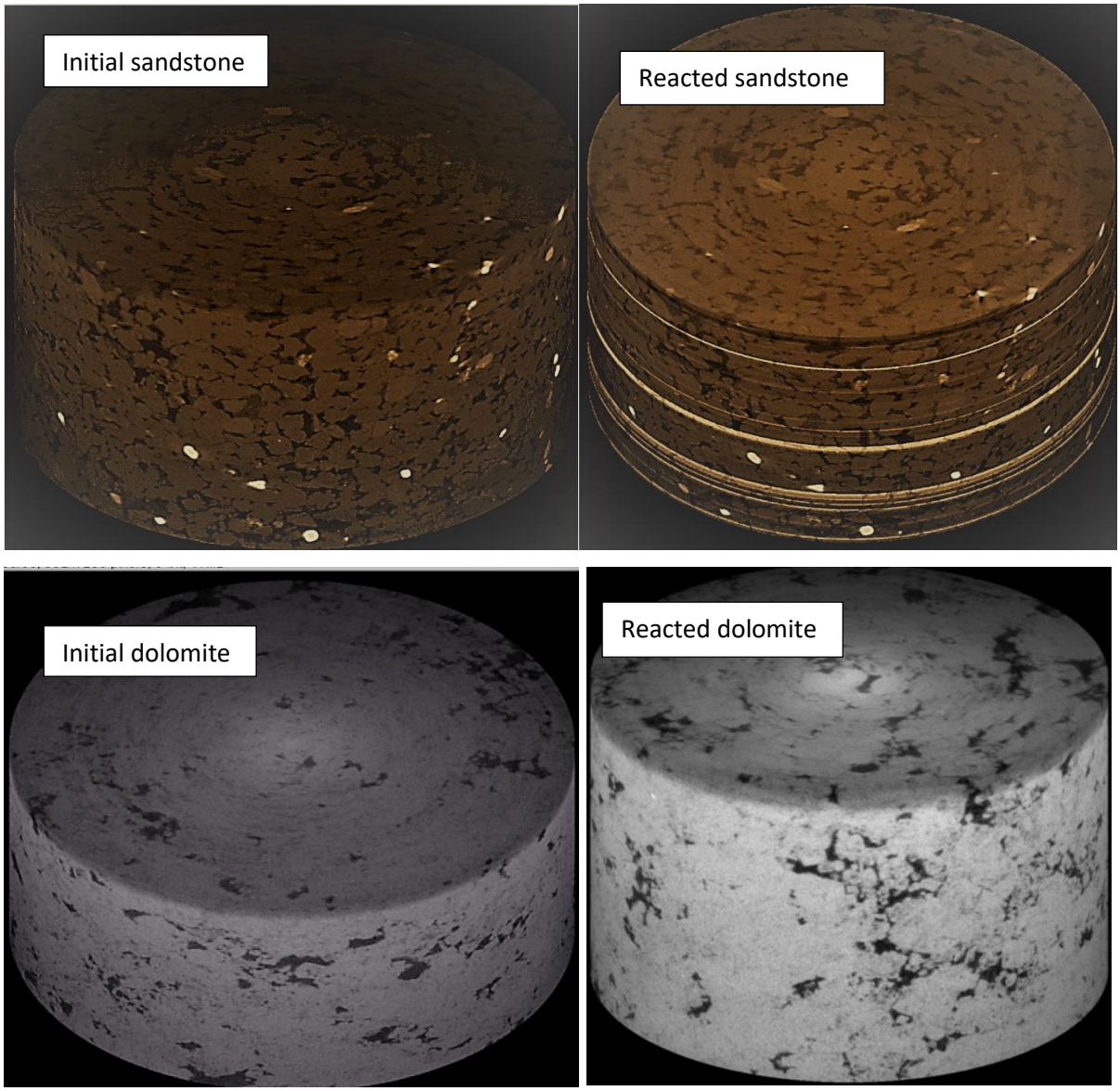

Figure 4.60. 3-D CT scan image of Berea Sandstone and Guelph Dolomite formation reacted with HEDTA

Chapter 5

TIMA Analysis

The Tescan Integrated Mineral Analyser (TIMA) is an analytical technique which is related to Field Emission Scanning Electron Microscope (FESEM). This technique is high throughput and effective for analysis of sample mineral composition and morphology. This chapter explains the results and analysis related to TIMA technology. These results are related to elemental mass, element deportment, mineral mass, mineral locking, porosity distribution, grain size distribution, pore size distribution, particle size distribution, and particles density of the core samples reacted with acids and chelates. These results together with the results discussed in chapter four helped in investigating the reaction mechanisms of different acids and chelates with a different type of reservoirs rocks.

5.1 Introduction

The TIMA can deliver particle by particle mineralogical data (quantitative) of inorganic materials, is an automated scanning electron microscope (Ward et al., 2017). It follows the same operation as other scanning electron microscopy-energy dispersive spectroscopy (SEM-EDS) techniques (e.g. QEMSCAN) proposed by (Pirrie et al., 2004; Haberlah et al., 2011).

SEM-EDS is provided with ultra-fast data acquisition expert software that can combine 100,000 minerals analyzed per hours which are obtained by collecting 600,000 x-rays per second. According to (Haberlah et al., 2011), this expert system can convert mineral quantitative and textural data obtained to a single particle.

Due to the presence of a high-resolution beam (1– 5 μm), the measurement obtained can be custom-made to the specific investigation, which allows <10 μm grain of minerals to be identified which cannot be seen by the human eye. SEM-EDS techniques have been mainly applied to the mineral analysis and petroleum research (Sutherland & Gottlieb 1991; Liu et al., 2005; Santoro et al., 2015).

5.1.1 Importance

Fast and quick analysis can be performed because the equipment is equipped with BSE, color CL, and four energy dispersive X-ray Spectroscopy (EDS) detectors. Mineral composition in

the sample can be analyzed quickly by using this technique. This is an SEM-based automated mineralogy solution. Some of the key capabilities of TIMA are mineral and element mapping, mineral abundance, mineral association, particle size, porosity distribution, and size by size liberation. The application includes characterization, process optimization etc.

1. FESEM
2. Energy Dispersive Spectroscopy
3. Modal, liberation and bright phase
4. RGB color Cathodoluminescence
5. SE and BSE detectors

A most important use of automated SEM-EDS analysis is within the petroleum and minerals industry, while its use in other areas of the Earth and environmental sciences is not that significant. The case study performed by (Ward et al., 2017) on Boodie cave is the first study that demonstrated the analytical technique used to thoroughly measure the changes in mineral chemistry, mineralogy, grain size, and texture. The technique developed for characterization of cave sediments that is very generic in nature and can be applied equally to other sites and sediments. This technique major significance is the ability to separate trends of a particular mineral which is not possible otherwise. Mineral mapping used in this automated mineralogy technique can also be applied to identify depositional environments. This technique is limited to inorganic materials and its application in inorganic compounds and carbon species is not well known. A pilot study using automated analysis demonstrated the significance of this technique in the characterization and analysis of anthropogenic processes that usually make up the sedimentation record of the globally important archaeological site. Automated Mineral integrated application with unique characterization techniques i.e., reflectance spectroscopy, will be a desirable technique in future worldwide.

Figure 5.1 shows the apparatus used by (Ward et al., 2017) for Boodie cave analysis and for this project mineral and elemental analysis, located at John De Laeter Centre (JDLC), Curtin University, Australia.

Figure 5.1. TIMA analysis apparatus

5.1.2 Application

- Fast throughput method to analyze the mineralogy
- Determine important minerals present on the surface
- Methodology to determine ore liberation using particle size analysis
- Location of minerals for element distribution
- Determine the size of mineral grains

5.1.3 Key capabilities

- Backscattered Electron Imaging (BSE)
- Secondary Electron Imaging (SE).
- Grain size and locking analysis
- Cathodoluminescence (CL) imaging
- Mineral analysis
- Mineral mapping

5.1.4 Procedure

Figure 5.2 shows the schematic workflow of TIMA analysis explained by (Ward et al., 2017). Individual mineral grains can be identified from a thin section by generating a backscattered electron image (BSE) and Energy-Dispersive X-ray (EDX). Multiple - EDX detectors used the pre-defined resolution to scan each mineral particle. EDX spectra formed automatically is examined against the classification scheme of TIMA, assigning each gain a certain mineral phase through mineral definition, which allows very accurate mineral mapping for each mineral.

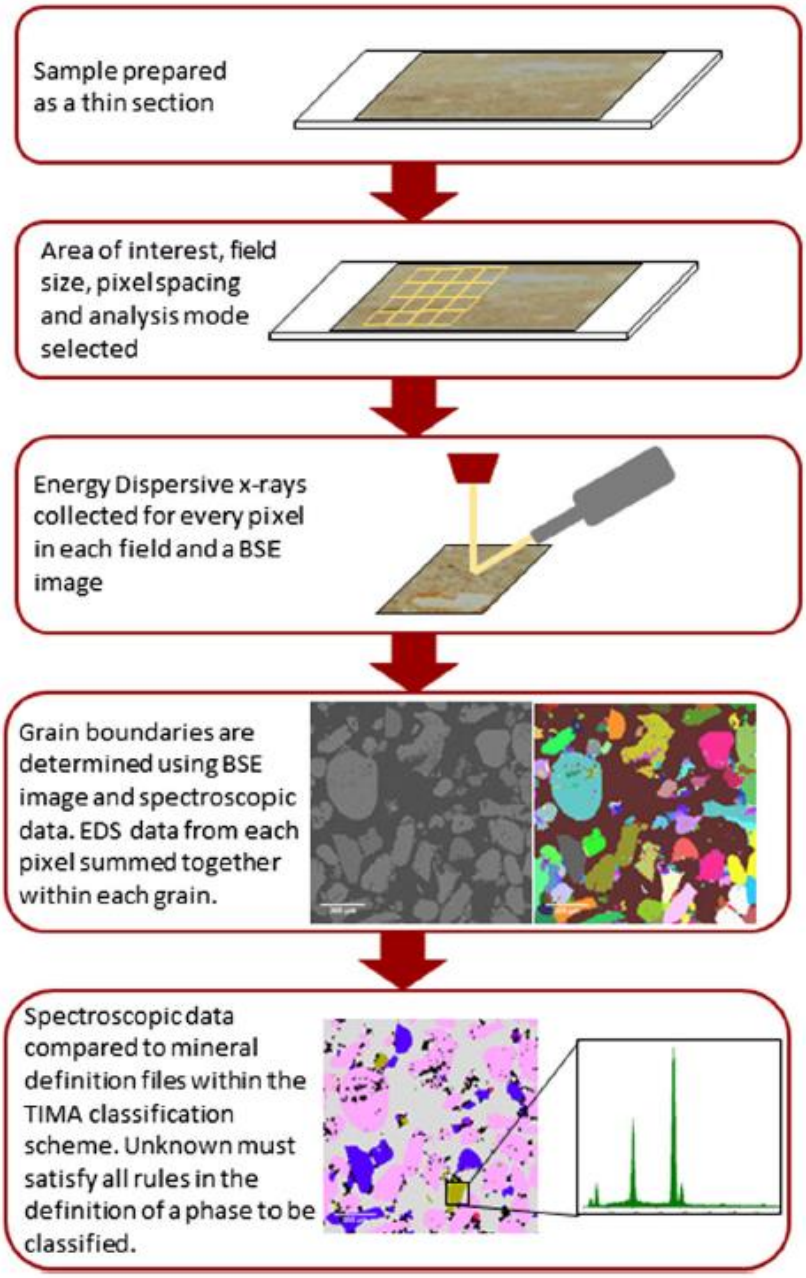

Figure 5.2. Schematic workflow of a TIMA analysis using resolution liberation analysis mode (Ward et al., 2017)

5.2 Analysis

The analyses which were performed using TIMA technique during this project consist of elemental mass analysis, element deportment, mineral mass analysis, mineral locking analysis, grain size analysis, mineral location (panorama), density distribution analysis, particle size distribution analysis and finally porosity distribution analysis. These analyses were performed using two types of acids on sandstone and dolomite formations. The first section of analysis consists of the interaction of pre-flush stage acids while in the second section, the interaction of chelating agents with rocks was analyzed. The section below gives a brief introduction to each analysis performed.

5.2.1 Elemental Analysis

The element mass report shows mass fractions of chemical elements. The data are valid only if the minerals have got elemental compositions.

5.2.2 Element Deportment

The elemental deportment describes the distribution of one chemical element in phases. The data are valid only if the minerals have got elemental compositions.

5.2.3 Mineral mass analysis

Mineral analysis was applied to analyze the change in the mineralogy of the core samples before and after the acidizing. Mineralogy describes the mineral composition of the core sample which is very important in the analysis of acidizing experiments. The change in mineralogy shows the relative decrease or increase of specific minerals present inside the core sample.

5.2.4 Mineral Locking

The ‘Mineral locking’ express minerals of interest (MOI) locked in. It is related to tab ‘Mineral liberation’ which express how much a mineral of interest is liberated. The program takes each particle and it computes the mass of mineral of interest that the particle consists of and also it determines the FREE surface area of each mineral in that particle (free perimeter of the particle). The mass of MOI is then divided into bins based on fractions of the surface area of minerals. There is one special bin called Free surface which expresses the fraction of MOI that is free (it is found on the particle perimeter). Figure 5.3 represents the example of free surface and locked minerals.

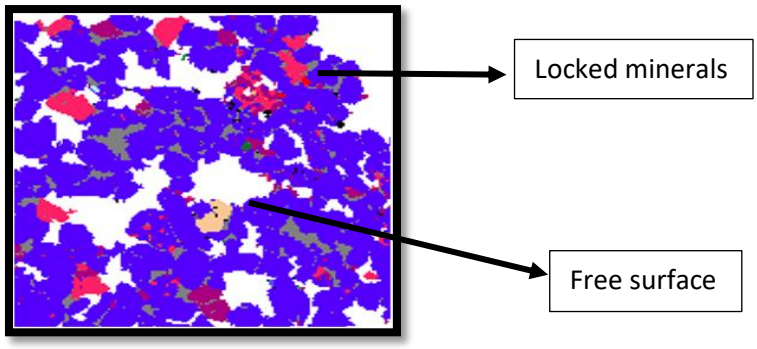

Figure 5.3. Mineral Locking

5.2.5 Grain Size Distribution

The 'Grain size' shows the population of grains of selected minerals in size categories. The grain size (d) is defined as the diameter of a circle with the same area as the sectional area (number of pixels on its cross-section) of the grain:

$$d = \sqrt[2]{\frac{A}{\pi}}. \text{ pixel spacing} \qquad (5.1)$$

Where A is a number of pixels inside the particle (on its cross-section) and pixel spacing is an analysis parameter. The results are presented in a table and histogram. The basic statistic values can be also shown. It is possible to filter data by phases.

5.2.6 Panorama Images (Mineral location)

The 'Panorama' report shows a mosaic image created from all acquired fields. A mosaic image can show a SEM image (BSE, SE, CL, etc.), color-coded phase maps or elemental maps.

5.2.7 Porosity Distribution

The tab 'Porosity' shows also basic statistic values computed from the population of detected holes. A percentile P is a size in microns below which a certain percent by volume of holes fall.

5.2.8 Particles

Particle viewer is a report that shows particles (cf. Grain viewer) that were found in the sample. Unlike the Fields report that shows the true spatial arrangement of particles on fields, the Particle Viewer report presents the particles side-by-side, sorted by a selected property (size, mineral content etc.); it means that two particles from different fields or data sets can be displayed next to each other if they have similar value of a selected property.

5.3 Pre-flush stage results

During the pre-flush stage, Berea sandstone core samples were allowed to react with two acid combinations consisting of hydrochloric acid and acetic acids. The results obtained using the TIMA technique are discussed and analyzed in next sections.

5.3.1 Elemental analysis

Figure 5.4 represents the change in the concentration of each element present in the Berea sandstone core sample after reaction with acids applied. Both applied acids caused change (decrease) in the concentration of potassium, calcium, sodium, iron and magnesium ions. Especially the power of 5%CH_3COOH: 10% HCl was better to dissolve calcium ion. This combination was equally good in dissolving iron, magnesium, carbon, sodium and heavy elements like manganese, zirconium, and titanium. Standard acid combination (15% HCl) was more effective in dissolving sodium, iron, titanium, carbon, zirconium, magnesium and manganese compared to 5%CH_3COOH: 10% HCl. To avoid silica precipitation during the acidizing, effective removal of sodium, potassium, and calcium is essential. But still, the less removal or dissolution of these elements was due to the presence of complex minerals (mentioned in section 5.3.4) and strong bonding (covalent and metallic bonds) between them. Increase in the mass of aluminum showed that this element was not dissolved by the applied acids. The elements or ions dissolved usually were present in free state inside the core sample and are a source of reactions. Due to less reactivity of the applied acids, the ions from the complex minerals were not soluble and remained in the form of minerals. The major element present was silicon but not soluble by the applied acids as shown in Appendix C (Table C1).

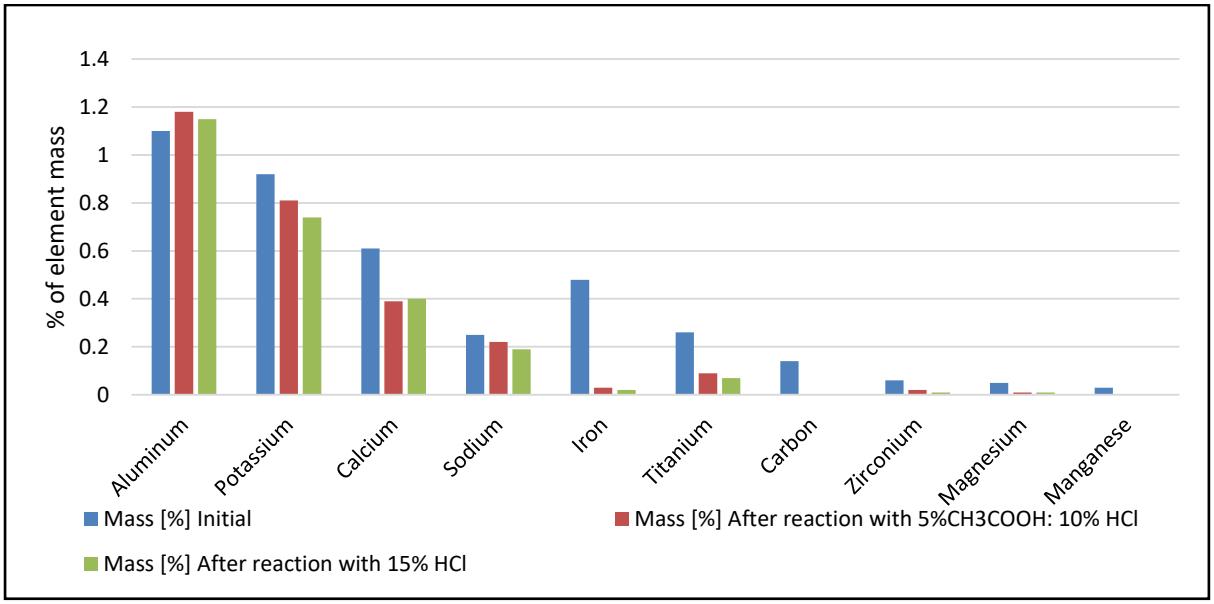

Figure 5.4. Elemental mass analysis of Berea sandstone before and after Pre-flush stage

5.3.2 Element Deportment

Figures 5.5 through 5.10 represent the presence of different elements in different minerals before and after the pre-flush acidizing stage. Element deportment is effective in describing the presence of a concentration of certain elements inside the minerals. By analyzing the deportment of elements, dissolution of different minerals can be analyzed effectively. For example, Figure 5.5 represents the presence of an iron element in the form ankerite ($Ca(Fe, Mg, Mn)(CO_3)_2$), magnetite (Fe_3O_4) and pyrite (FeS_2). Ankerite is a complex mineral of magnesium, calcium, manganese and iron carbonate. It is almost similar to the composition of dolomite but magnesium is replaced by manganese and iron. Figure 5.5 clearly showed that ankerite and magnetite iron minerals present in the Berea sandstone were dissolved by the acids applied, while only trace amount of pyrite was present which was dissolved completely by 15% HCl.

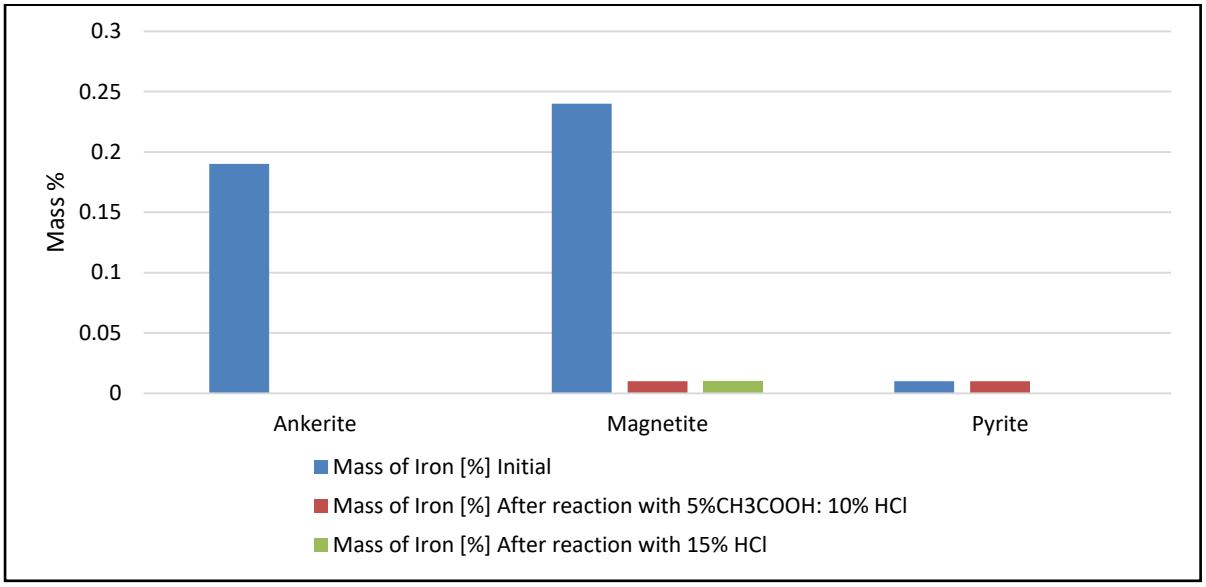

Figure 5.5. Iron deportment in Berea sandstone before and after Pre-flush

Figure 5.6 shows the presence of potassium element in the form of orthoclase and muscovite minerals inside Berea sandstone core samples. 15% HCl proved to be more effective in the dissolution of potassium element from orthoclase mineral ($KAlSi_3O_8$). A small amount of Muscovite was also present inside the core sample which was not dissolved by both acids due to complex nature of muscovite ($KAl_2(AlSi_3O_{10})(F, OH)_2$), where a lot of elements are bounded together to form a mineral.

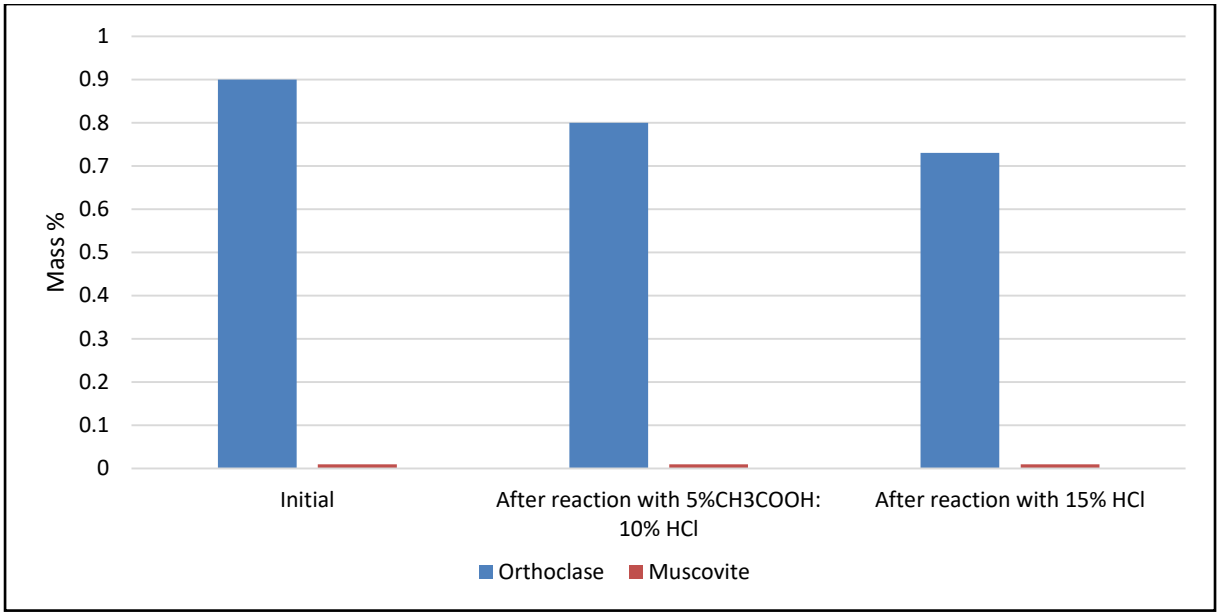

Figure 5.6. Potassium deportment in Berea sandstone before and after Pre-flush

Figure 5.7 represents the presence of silicon in the form of various minerals like orthoclase, plagioclase ($NaAlSi_3O_8 – CaAl_2Si_2O_8$), kaolinite ($Al_2Si_2O_5(OH)_4$), zircon ($ZrSiO_4$) and quartz ($SiO_2$). Both acids were effective in the dissolution of silicon from quartz mentioned in Appendix C (table C.4), while only trace amount of silicon had been dissolved from kaolinite and zircon. Both acids also proved to be effective in dissolving small quantities of silicon from orthoclase and plagioclase, where 15% HCl dissolved more amount of silicon compared to 5%CH_3COOH: 10% HCl from plagioclase and orthoclase. Less solubility of plagioclase is due to its complex nature where different elements are bounded together to form a mineral.

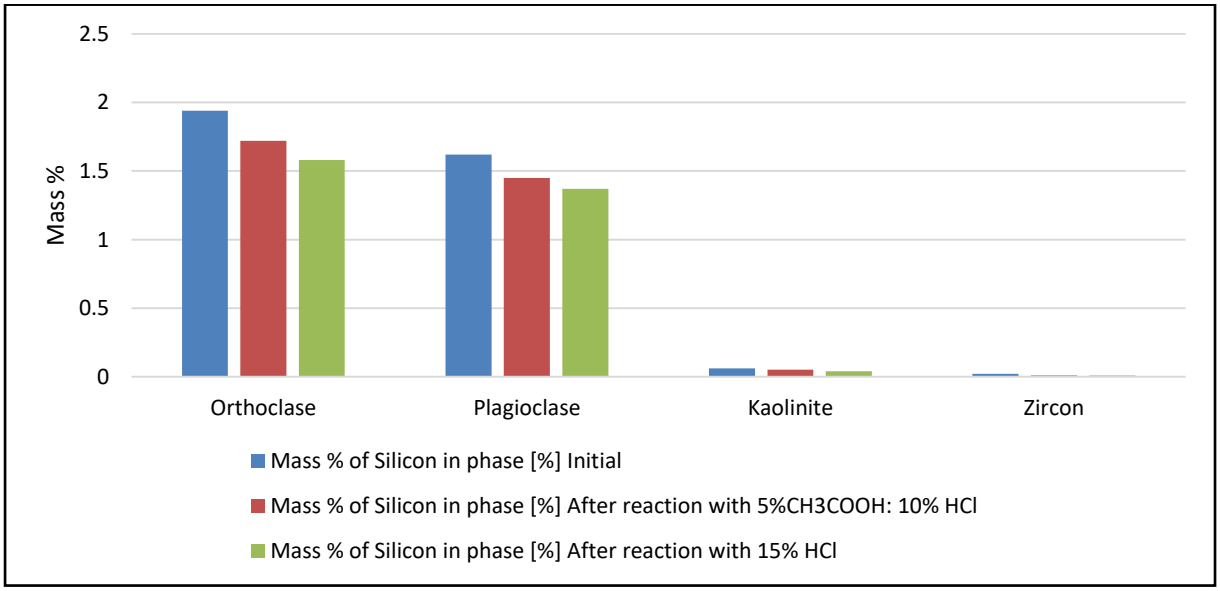

Figure 5.7. Silicon deportment in Berea sandstone before and after Pre-flush

Figure 5.8 represents the presence of titanium in the form of heavy mineral rutile (TiO_2). Both acids proved to be effective in dissolving titanium which showed their ability to dissolve heavy elements and minerals. As, the rutile is not a complex mineral having simple formula TiO_2, which allowed these acids to dissolve it and consequently titanium was dissolved.

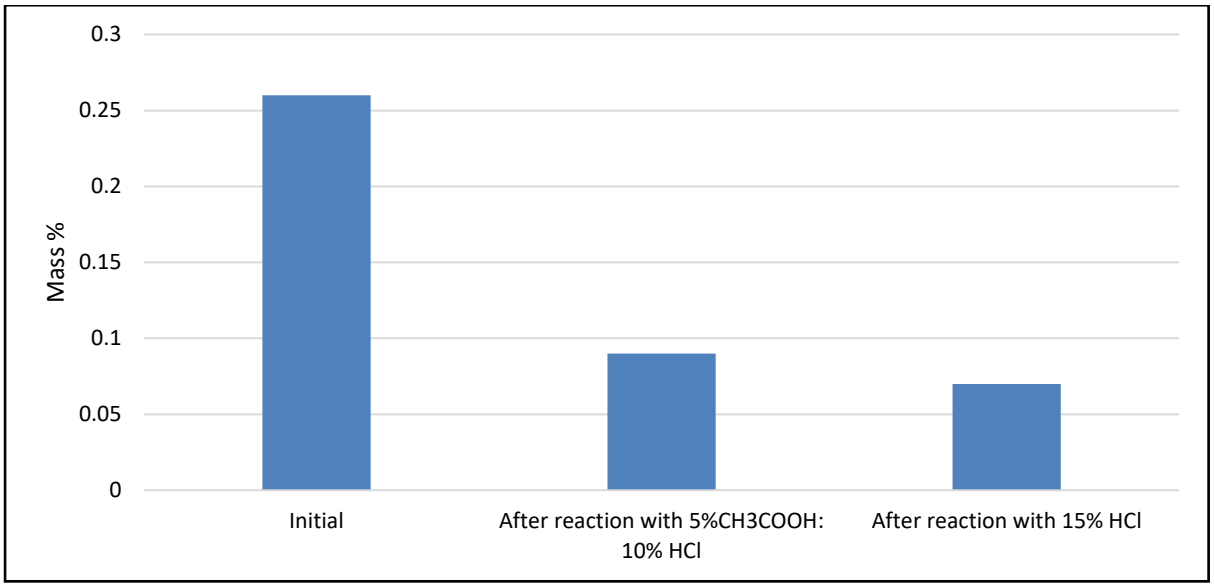

Figure 5.8. Titanium deportment in Berea sandstone before and after Pre-flush

Calcium is usually present in the form of carbonates but in Berea sandstone, its presence was established in the form of ankerite and plagioclase minerals. Ankerite was readily soluble by these acids, therefore, the concentration of calcium became zero as shown in Figure 5.9, while a small amount of calcium had been dissolved from plagioclase as it was not readily soluble by these acids due to complex bonding discussed earlier in Figure 5.7.

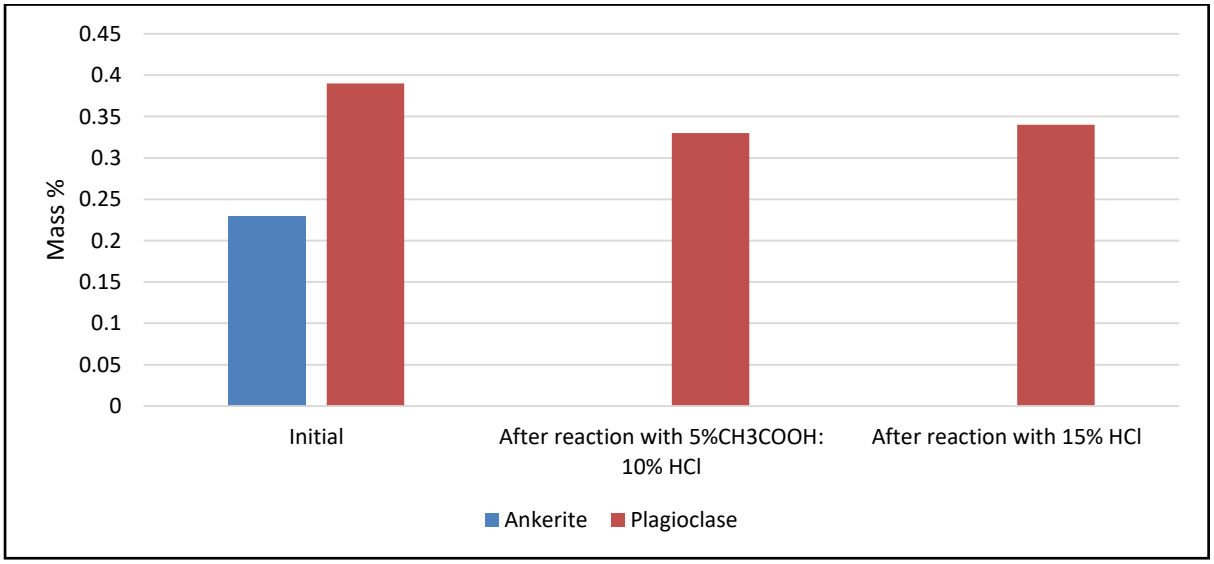

Figure 5.9. Calcium deportment in Berea sandstone before and after Pre-flush

Figure 5.10 shows the presence of magnesium in the form of ankerite mineral which was readily soluble by these acids as described previously in Figure 5.5. The solubility of ankerite mineral in applied acids is due to the fact that this mineral consists of the element which are readily soluble by the applied acids and due to its less complex nature where elements are bounded together by week metallic forces.

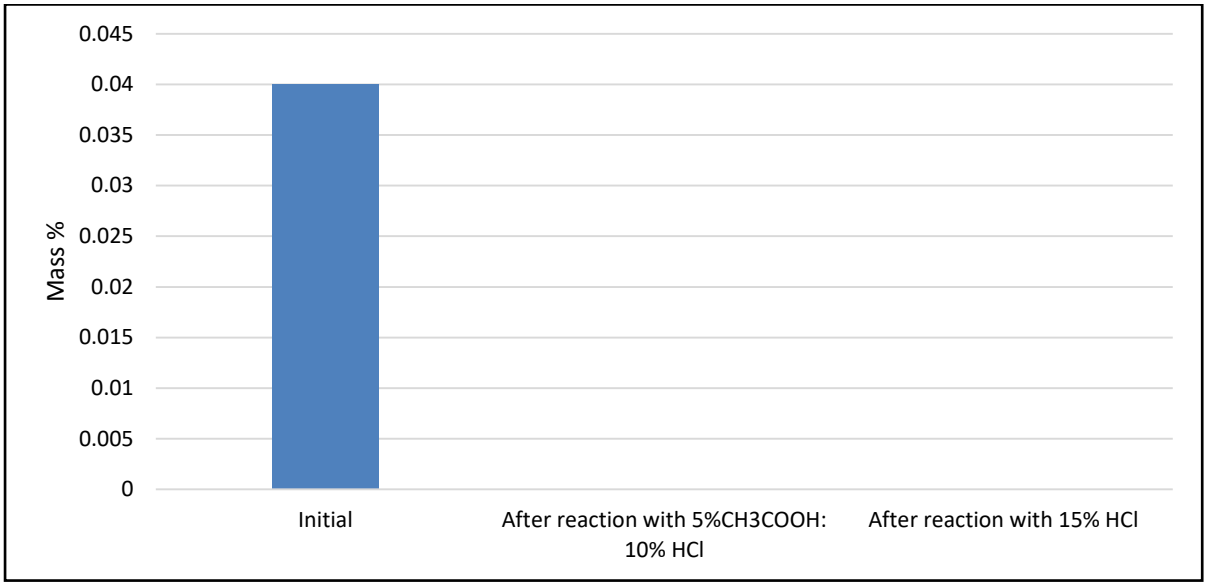

Figure 5.10. Magnesium deportment in Berea sandstone before and after Pre-flush

Elemental analysis established the fact that acetic and hydrochloric acids can dissolved iron, calcium, magnesium, titanium ions effectively. While potassium and silicon were not dissolved by these acids effectively due to complex bonding within the minerals (strong metallic bonding). Strong acids are required to break these bondings whereas these chelates are not as strong as plain mineral acids. These results can be validated by mineral mass analysis and mineral locking analysis; explained in next sections.

5.3.3 Mineral Analysis

A mineral is a naturally occurring substance and is formed due to the combinations of different elements present in the reservoir. Mineral mass shows the percentage of each mineral in the core sample. As the Berea sandstone core sample is homogeneous in nature, therefore, the initial mass percentage of each mineral was considered constant. The mineral mass was represented in terms of relative mineral mass, where the total percentage remains constant (100%). If the mass of one mineral is decreased as a result of dissolution, the relative mass of undissolved mineral increased consequently.

Figure 5.11 represents different types of minerals present and their contribution to the total mass in the Berea core sample. Ankerite mineral which is a combination of calcium, iron, magnesium, manganese, and dolomite had been dissolved completely by these acids. Orthoclase and plagioclase are rock-forming minerals and are a part of the feldspar group. These minerals consist of potassium, aluminum, and silicon locked together. The acids used during pre-flush stage were not able to react with silicon due to the absence of fluoride ion (F^-). As a result, these minerals are not soluble and there was an increase in the relative mass of these minerals when reacted with 5%CH_3COOH: 10% HCl as mentioned in Appendix C (Table C.8). Likewise, an increase in the mass of quartz and orthoclase minerals after reaction showed that they were not dissolved by these applied acids. However, an only a small amount of plagioclase and kaolinite were dissolved by 15% HCl, while a little amount of muscovite was dissolved by 15% HCl acid only.

Ankerite and magnetite were completely dissolved by both acids and these acids also showed good solubility towards rutile, schorl, and zircon. Further, not so complex nature of these minerals was responsible towards the dissolution of these minerals with the applied acids.

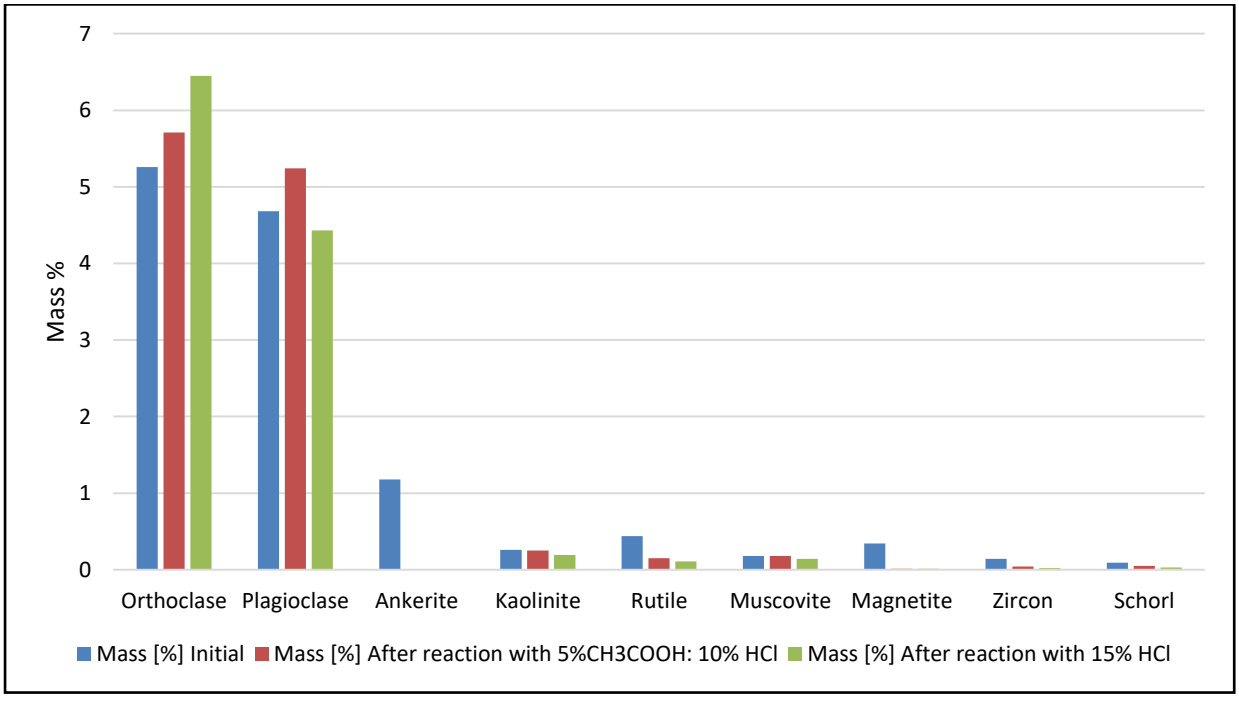

Figure 5.11. Mineral mass in Berea sandstone before and after Pre-flush

5.3.4 Mineral Locking

Figure 5.12 shows that magnetite mineral was locked with quartz, plagioclase, and orthoclase. The initial value of mineral locking was considered the same for both samples initially due to

the homogeneous nature of the sample. 76.5% of magnetite was locked with quartz as mentioned in Figure 5.12. Moreover, a small quantity was also locked with orthoclase and plagioclase. Mineral locking of magnetite with quartz has been completely disappeared after the reaction. This occurred due to the dissolution of magnetite mineral which was also the cementing material of the core sample because it was locked with quartz. Percentage locking was calculated by dividing each mineral locking by total locking. For example, in the case of quartz mentioned in Figure 5.12 or Table C9 (Appendix C), it was calculated as mentioned in Equation 5.2:

$$\text{Mineral Locking} = \text{locked mineral mass \%} / \text{total locking} \quad (5.2)$$

$$\text{Mineral locking of ankerite with quartz} = 0.26 / 0.34 = 0.765 = 76.5\%$$

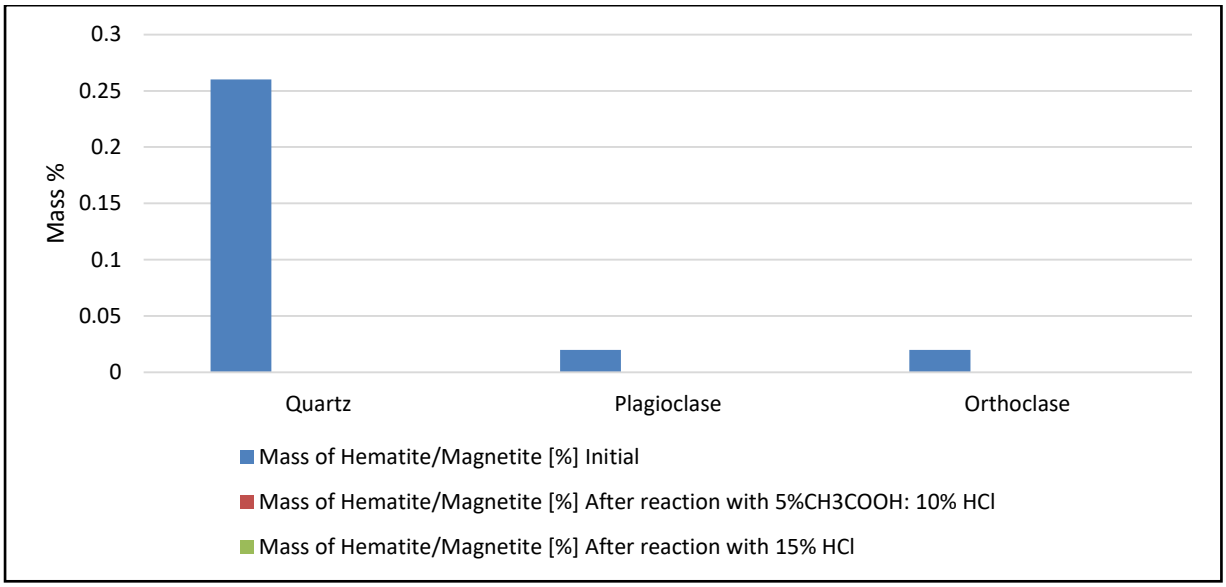

Figure 5.12. Magnetite Mineral Locking in Berea sandstone before and after Pre-flush

Figure 5.13 shows the locking of quartz mineral with different other minerals present in the Berea sandstone core sample. Mostly it was present in the form of the free surface (appendix C, table C.10), which means that the boundary or perimeter of the grain was not locked with any other mineral. Zircon, magnetite, ankerite, and rutile locking with quartz almost disappeared after reaction with the applied acids. This showed the ability of the applied acids to dissolve these minerals and also validated the previous results discussed in elemental locking and mineral analysis sections.

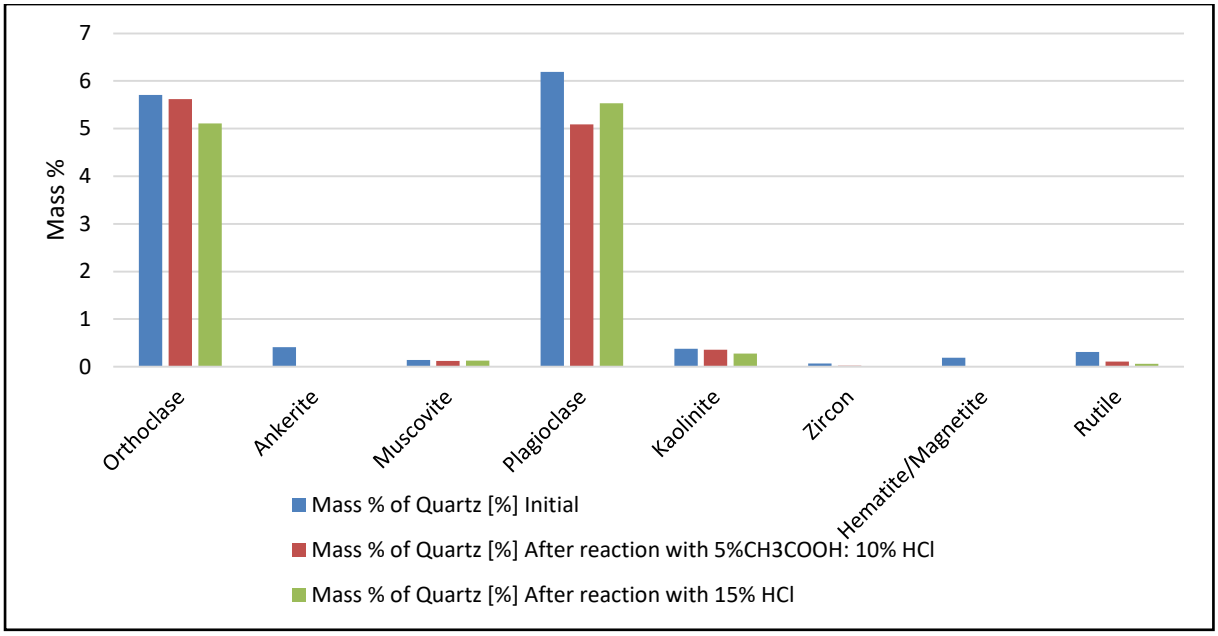

Figure 5.13. Quartz Mineral Locking in Berea sandstone before and after Pre-flush

Figure 5.14 represents the locking of orthoclase mineral with plagioclase. It's locking with quartz was already mentioned in Figure 5.13. Despite locking with quartz, most of the orthoclase exists as a free surface and there was an increase in the free surface after reaction with acids, indicting that some amount of locking minerals (quartz and plagioclase) with orthoclase have been dissolved and pore spaces have been created. Free surface indicates that the perimeter of the grain is surrounded by the pore spaces. Figure 5.13 established the fact that orthoclase locking with quartz has been decreased by a small amount.

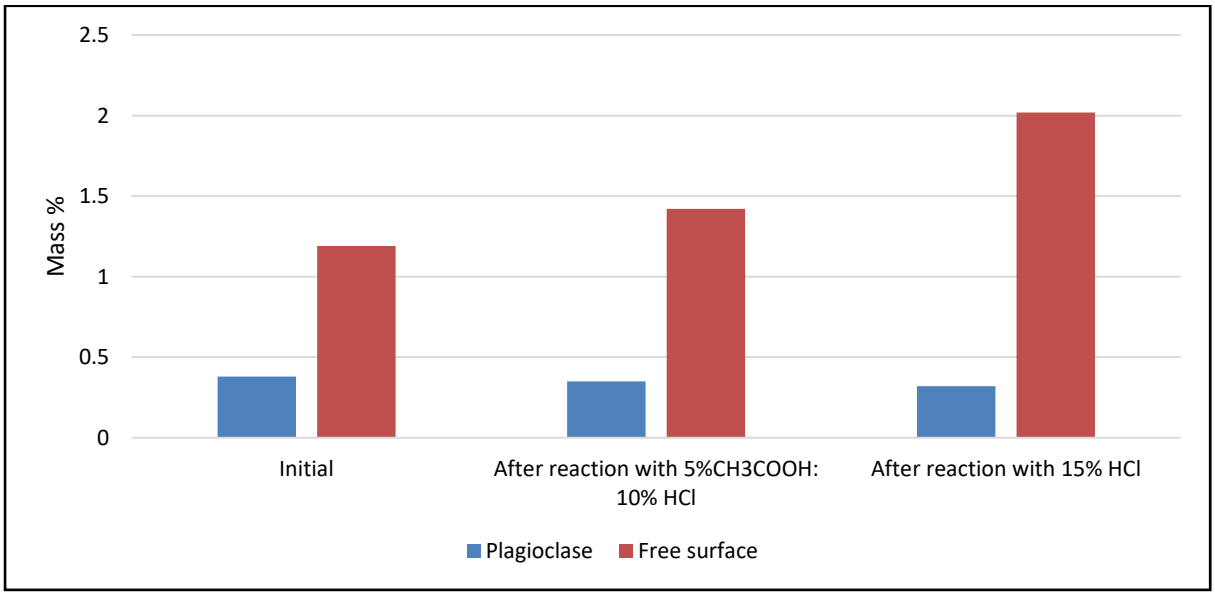

Figure 5.14. Orthoclase Mineral Locking in Berea sandstone before and after Pre-flush

Figure 5.15 shows the locking of plagioclase mineral with different minerals. A small quantity of plagioclase has been locked with ankerite, which was disappeared completely after reaction with the applied acids. Some grains of plagioclase were locked with orthoclase and quartz but most of it was exist as a free surface. However, an only a small amount of plagioclase free surface has been increased after reacting with applied acids, which can be credited to the dissolution of ankerite mineral.

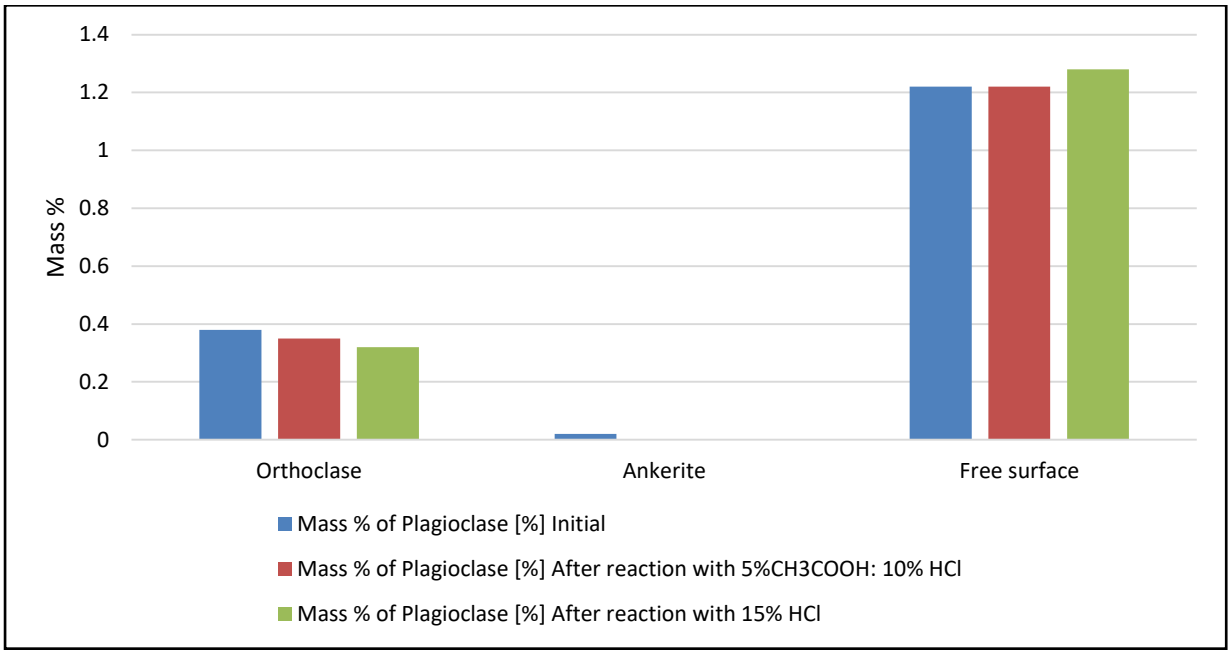

Figure 5.15. Plagioclase Mineral Locking in Berea sandstone before and after Pre-flush

Figure 5.16 showed the complete dissolution of ankerite mineral from the core sample, where the mineral locking has been completely wiped out after reacting with the acids. Most of the ankerite mineral was locked with quartz initially. After reaction, no evidence of ankerite mineral locking with quartz was observed which was the reason for the increment of porosity and permeability as discussed earlier in section 4.2.1. Figure 5.16 only showed the initial values because after reaction there was no ankerite locking with any other mineral present inside the sample.

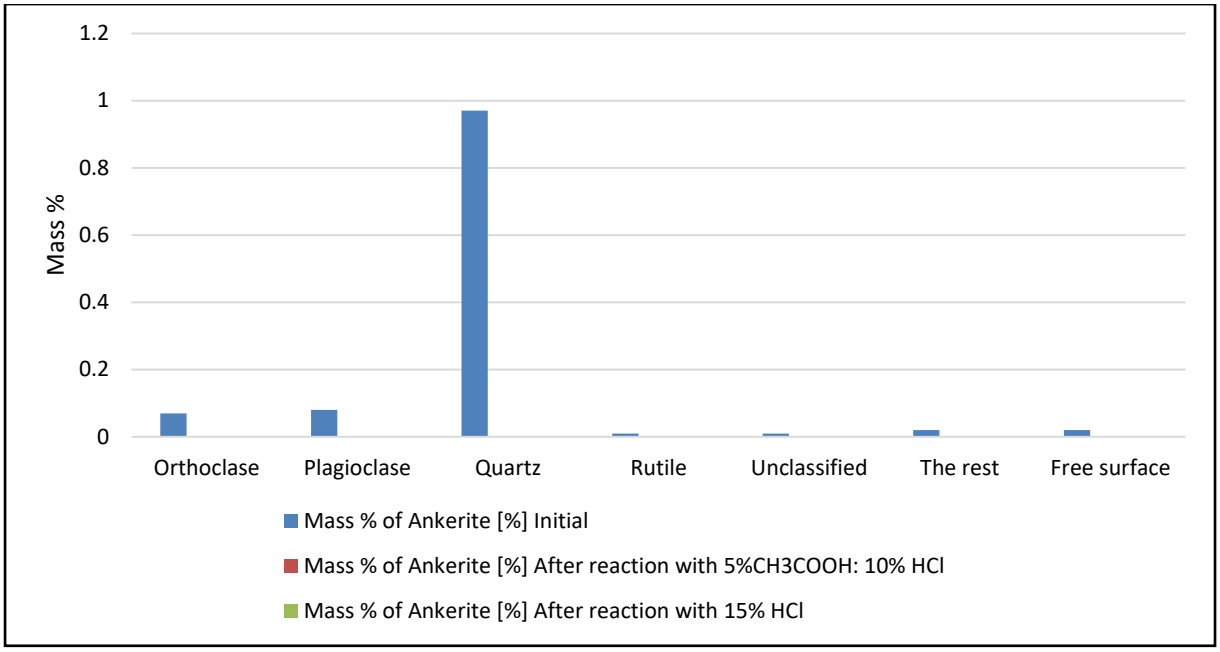

Figure 5.16. Ankerite Mineral Locking in Berea sandstone before and after Pre-flush

Rutile mineral was also soluble by the applied acids, that's why the locking of rutile with each mineral has been decreased or completely disappeared as shown in Figure 5.17.

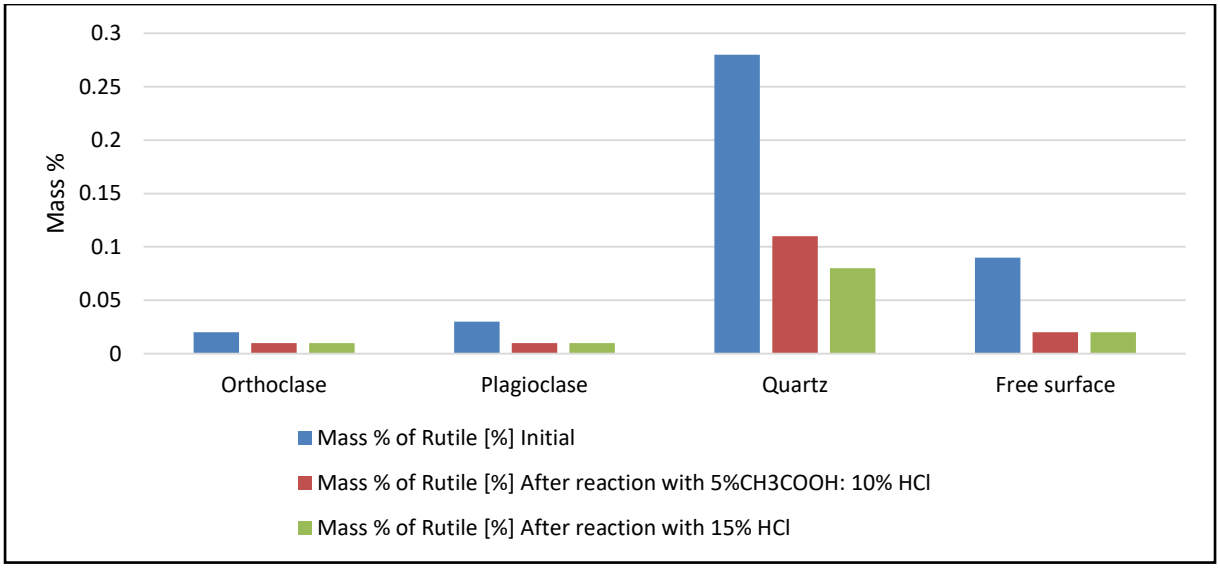

Figure 5.17. Rutile Mineral Locking in Berea sandstone before and after Pre-flush

From the elemental and mineral analysis, it can be concluded that 15% HCl was more effective in the dissolution of certain minerals and elements. These acids were not effective in dissolving quartz mineral as silicon is not soluble by any acid. Whereas, the minerals consist of iron, calcium, magnesium, manganese, and titanium were readily soluble in these acids. Rutile,

magnetite, and ankerite are the examples of such minerals. Therefore, if the reservoir consists of minerals such as above mentioned elements, these acids can be applied as an acidizing fluid to increase the permeability and productivity of the reservoir. The next section of analysis consists of grain, porosity and particle distribution through which elemental and mineral can be validated.

5.3.5 Grain Size distribution

The number of grains of different important minerals before and after acidizing was discussed from Figure 5.18 through Figure 5.23. Few points need to be considered to analyze grain size distribution:

1. The selected size range was different for different minerals; based on the size of each mineral present inside the core sample. For example, in Berea sandstone, the highest size was shown by quartz which indicates that big grains of quartz were present inside the core sample.
2. The change in the number of grains in particular size range showed the dissolving power of the acid towards that mineral.

The number of grains of ankerite, rutile, zircon and hematite/magnetite (Figure 5.18 through Figure 5.21 respectively) was changed significantly after the reaction. In fact, some of the minerals are completely wiped out as seen in Figures 5.18 and 5.21. It revealed that these minerals were dissolved effectively by the applied acids. On the other hand, the change in the grain size of orthoclase and quartz was not that effective (Figure 5.22 and Figure 5.23). This illustrates the less solubility of these minerals by the applied acids. These results can be validated by the mineral mass analysis presented in Table C8 (Appendix C). However, 15% HCl is more effective in the dissolution of orthoclase grains where almost 4500 grains has been dissolved compared to almost 2500 when 5%CH_3COOH: 10% HCl was applied.

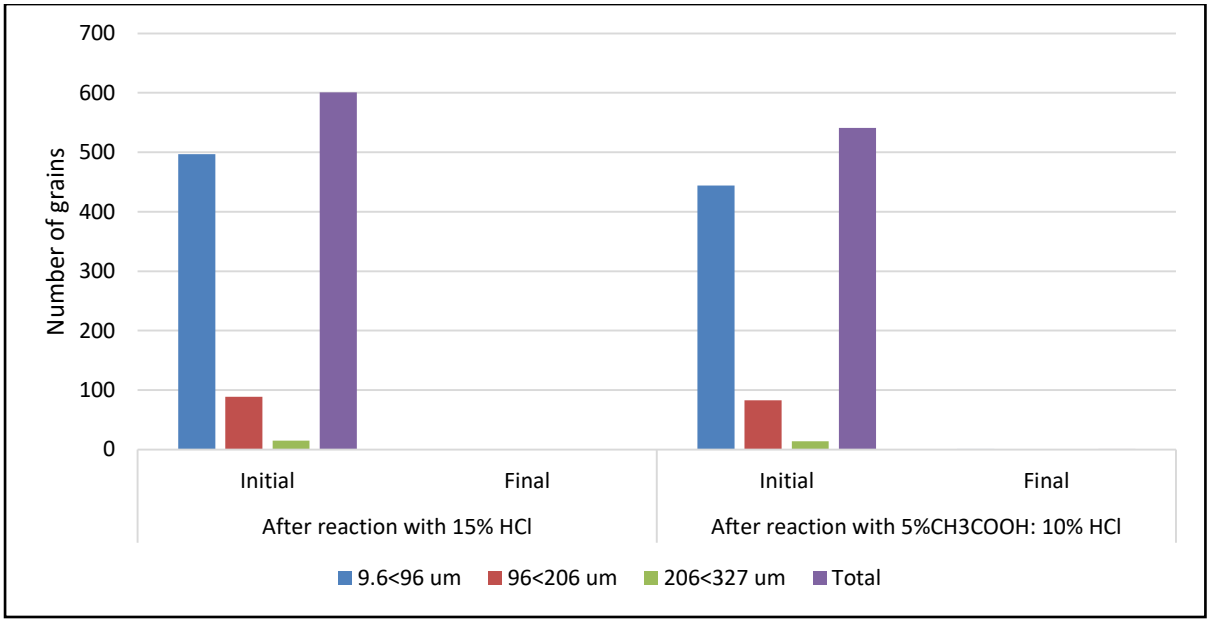

Figure 5.18. Grain size distribution of Ankerite in Berea sandstone before and after Pre-flush

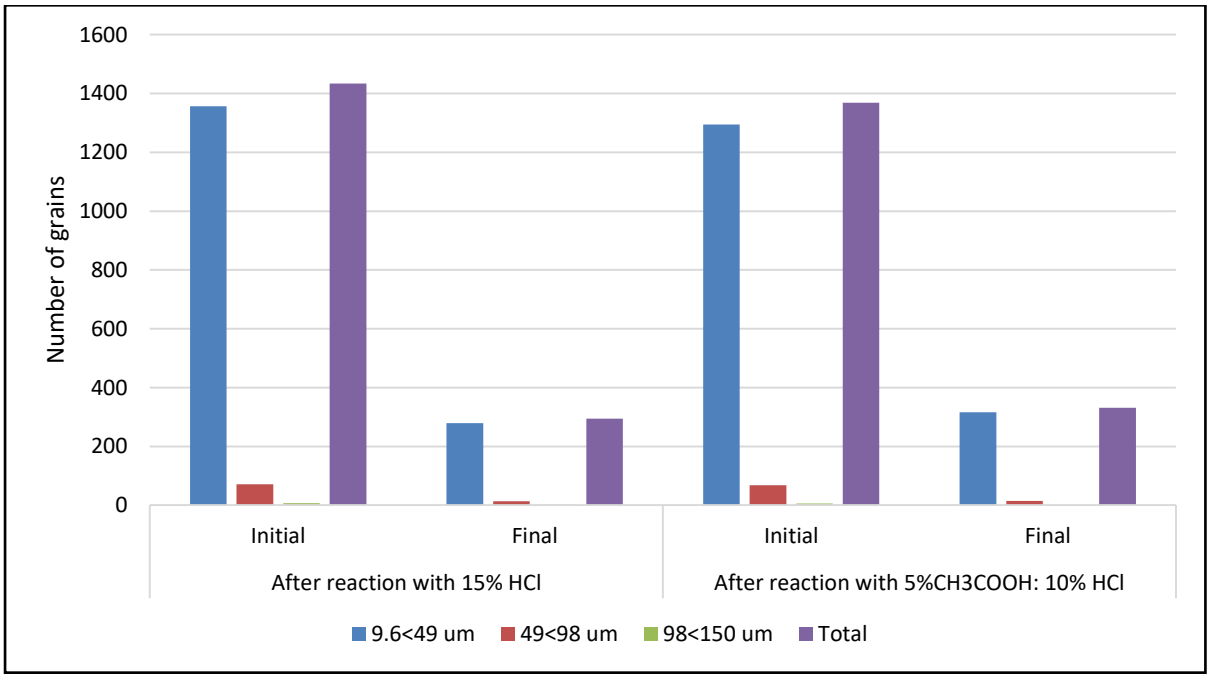

Figure 5.19. Grain size distribution of Rutile in Berea sandstone before and after Pre-flush

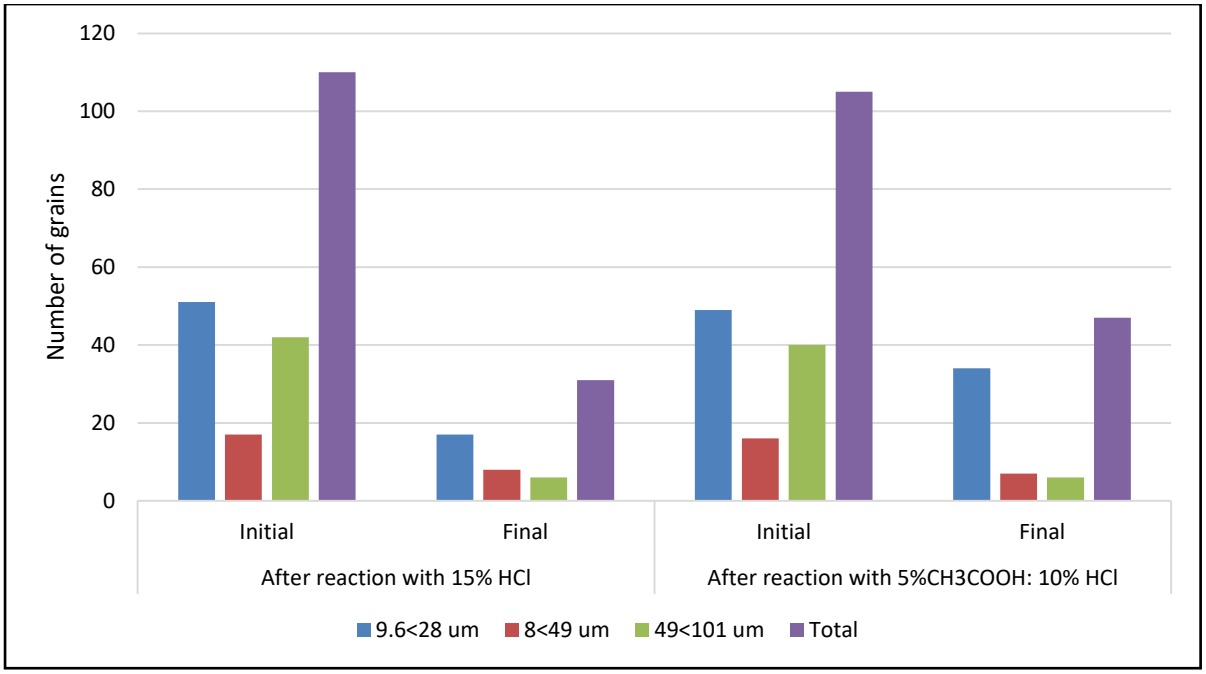

Figure 5.20. Grain size distribution of Zircon in Berea sandstone before and after Pre-flush

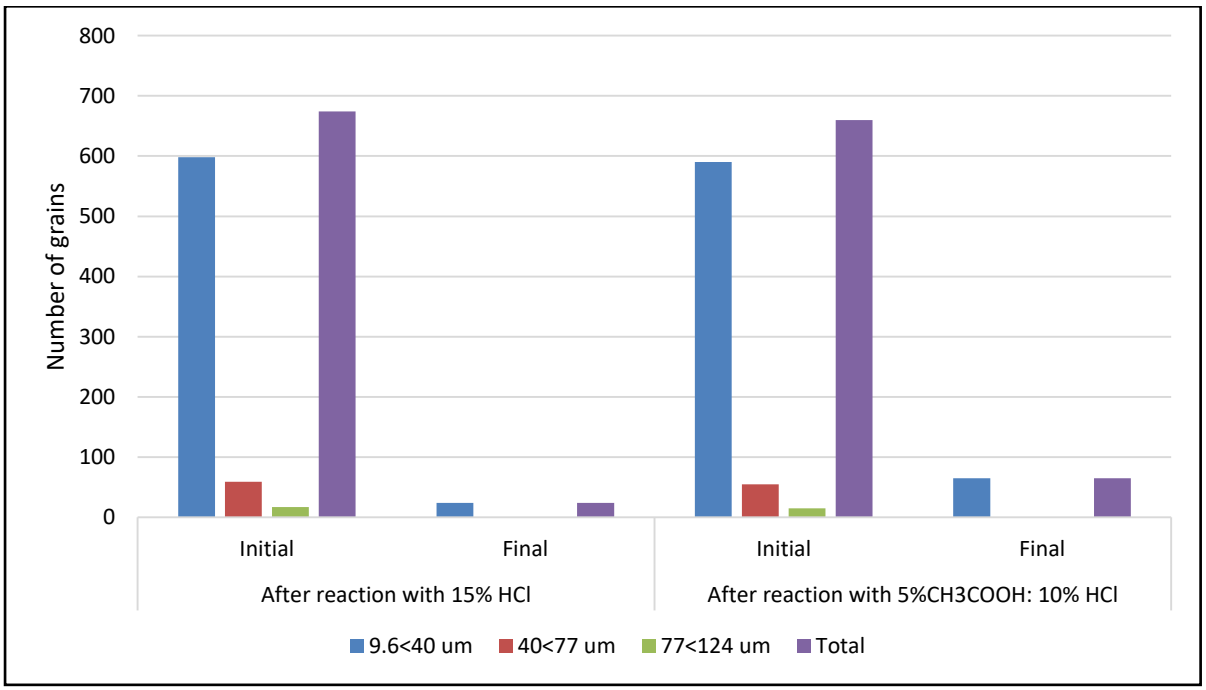

Figure 5.21. Grain size distribution of Magnetite in Berea sandstone before and after Pre-flush

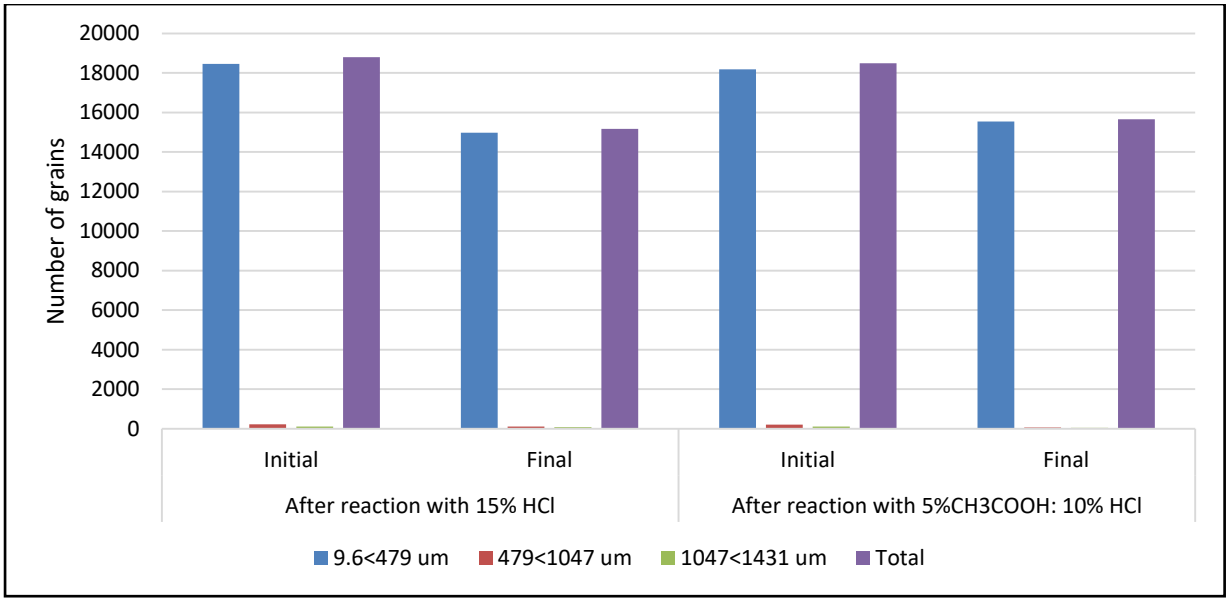

Figure 5.22. Grain size distribution of Quartz in Berea sandstone before and after Pre-flush

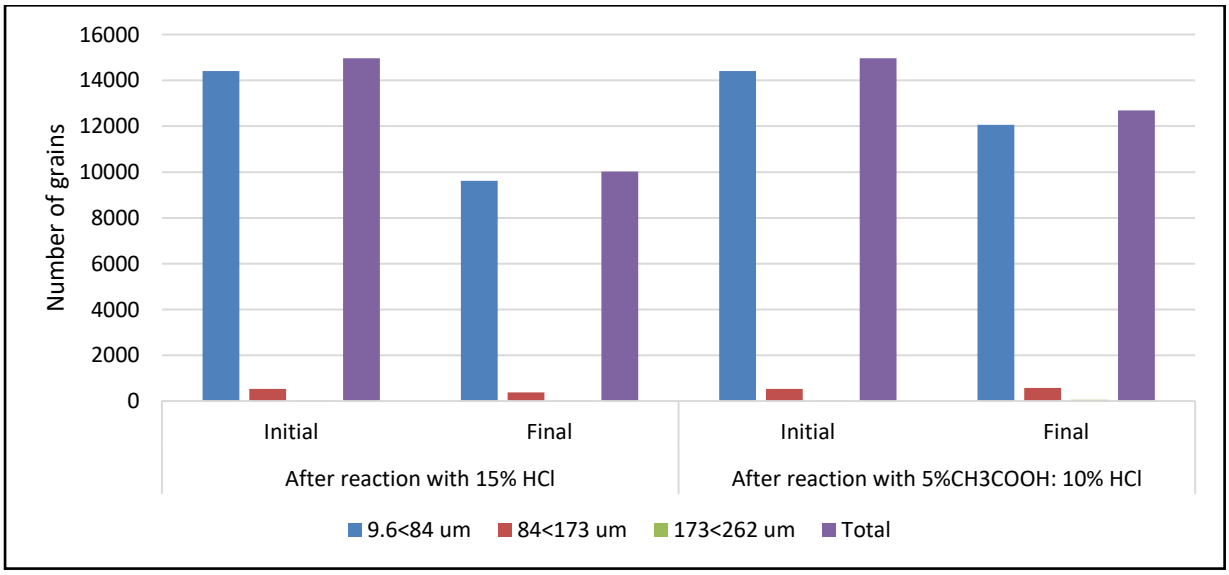

Figure 5.23. Grain size distribution of Orthoclase in Berea sandstone before and after Pre-flush

5.3.6 Panorama Images

Panorama analysis shows the high quality (Black Scattered Electron, BSE) image of the core surface. It shows the presence of matrix and different minerals on the surface of the core sample. The obtained images after the acidizing procedure can illustrate the dissolution of the matrix and minerals due to the creation of new pore spaces. In this project, the high-resolution images of unreacted and reacted samples have been used to identify the position of new pores

spaces created and prominent dissolution of minerals identified. Scanning Electron Microscope (SEM) instrument is usually used to get BSE images. BSE usually is a detector, which is used to get black scattered electrons in different directions. Scattered electrons are collected by the detectors which are placed above the sample and information collected as a function of the composition of the sample. While the information collected from the side detectors is a function of surface topography. Images obtained using BSE technique are instant depending on the scan rate. The magnification is based on the instrument and number of phases information can be collected very quickly. It can be used for spot analysis also by capturing the images on the film. BSE images are only limited to grayscale because they only record one variable, average Z (a combination of all the elements in a sample. All pictures are taken from a distance of 5mm.

5.3.6.1 Magnetite Dissolution

Figure 5.24 represents the dissolution of magnetite mineral after the core flooding experiments. Blue color spots on the left Figures 5.4 (a, c) represent the presence of magnetite mineral in initial samples. Clear dissolution of magnetite mineral after acidizing can be observed in Figures 5.4 (b, d). This showed that the effect of different acids on the pore topology of the Berea sandstone core sample. Magnetite was completely dissolved by both applied acids which validate the mineral mass analysis results (table C8).

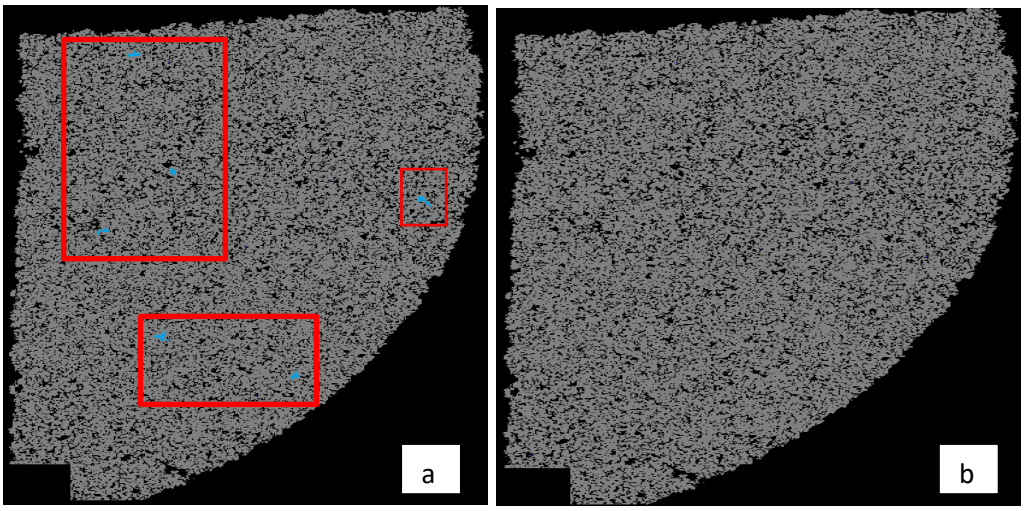

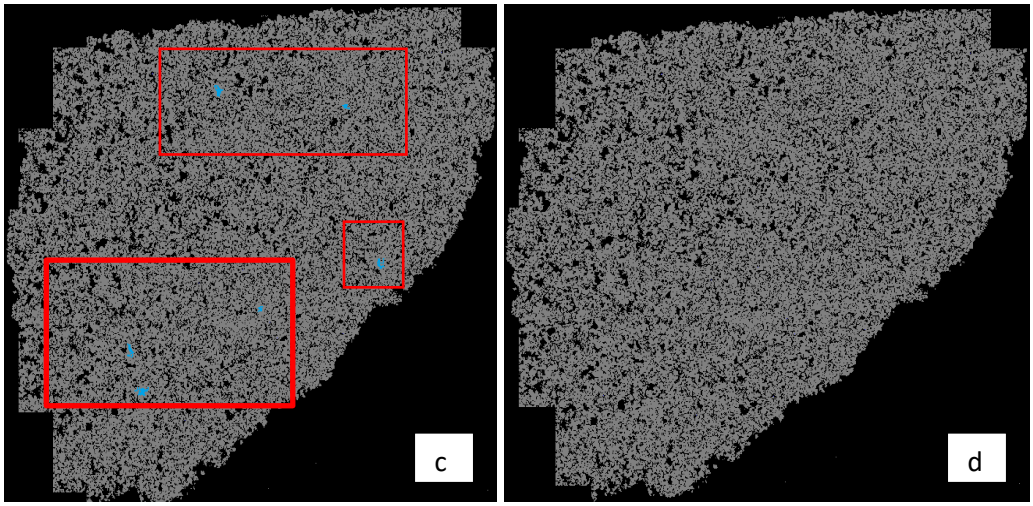

Figure 5.24. Panorama of magnetite before and after reaction; unreacted samples (left), reacted with 15% HCl (top right), reacted with 5%CH_3COOH: 10% HCl (bottom right).

5.3.6.2 Ankerite Dissolution

Figure 5.25 represents the presence of ankerite mineral in the initial and reacted core samples. As discussed in mineral mass analysis about the dissolution of ankerite by all these acids, the phase image also confirmed this ability of the acids. Ankerite mineral is shown in Figure 5.5 (a, c) was disappeared/dissolved by the applied acids as shown in Figure 5.5 (b, d), creating new pore spaces and increasing the permeability and porosity.

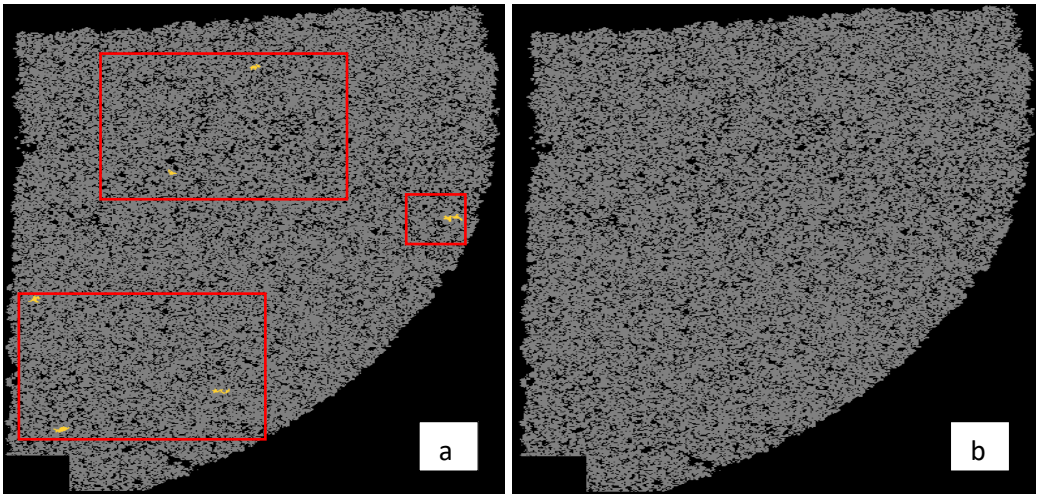

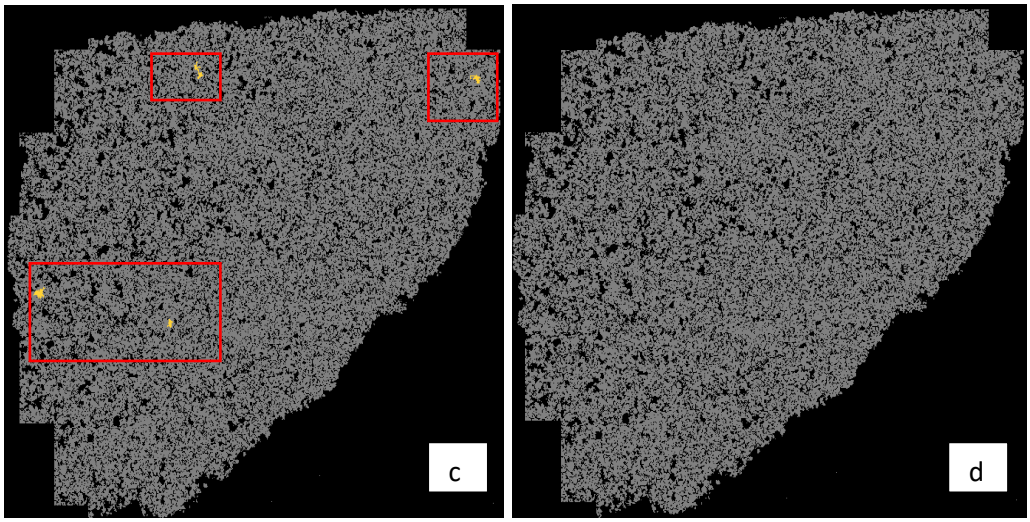

Figure 5.25. Panorama of ankerite before and after reaction; unreacted samples (left), reacted with 15% HCl (top right), reacted with 5%CH_3COOH: 10% HCl (bottom right).

5.3.6.3 Zircon dissolution

Figure 5.26 represents the change in the presence of heavy mineral Zircon after the core flooding experiments. Zircon mineral is a combination of heavy element zirconium and silicon with oxide. Zircon mineral was dissolved effectively by both acids as shown in Figure 5.26 (b, d). Few traces of zirconium were found in the reacted core sample with 5%CH_3COOH: 10% HCl, but no traces of this mineral has been found when reacted with 15% HCl; validated by the mineral mass analysis presented in Table C8 (appendix C). It showed the effectiveness of this acid in dissolving zirconium mineral. More dissolution of these ions and minerals can ensure better main acid stage of sandstone acidizing.

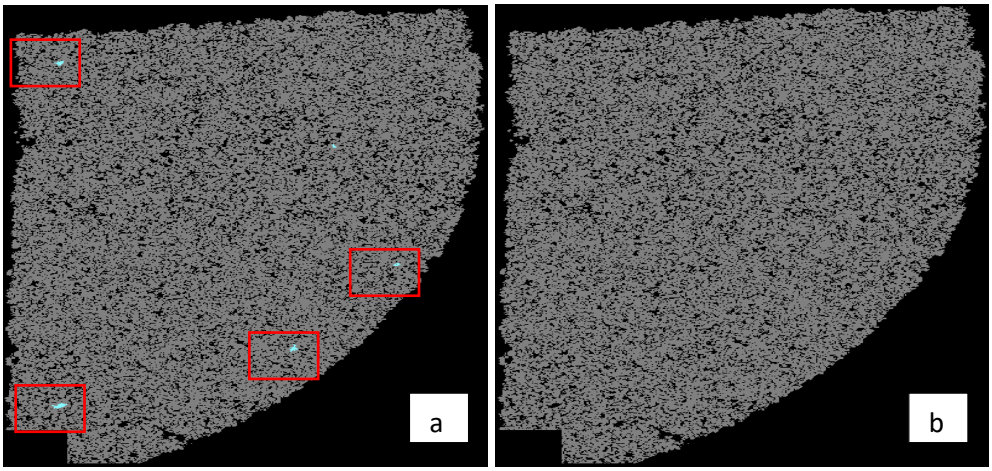

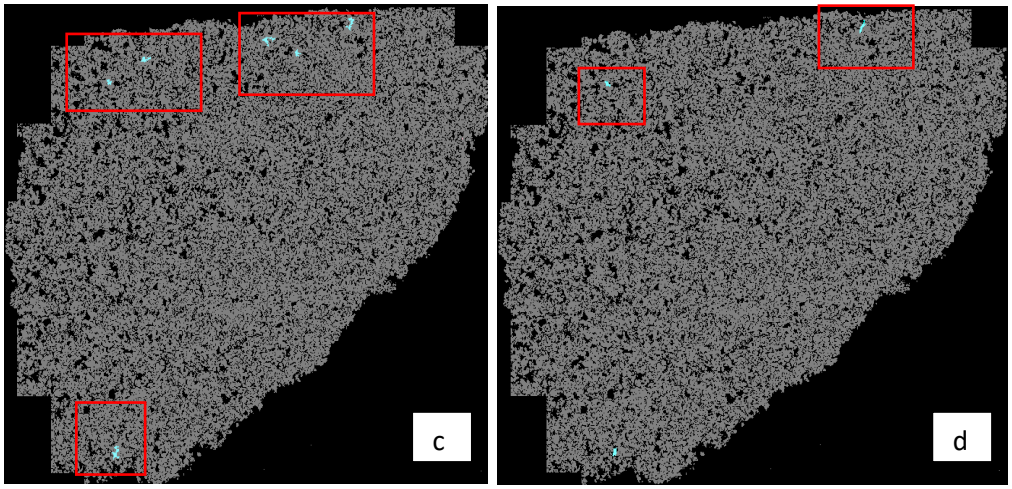

Figure 5.26. Panorama of zircon before and after reaction; unreacted samples (left), reacted with 15% HCl (top right), reacted with 5%CH_3COOH: 10% HCl (bottom right).

5.3.6.4 Rutile Dissolution

Figure 5.27 represents the dissolution of rutile mineral after the core flooding experiments. Rutile mineral is an oxide ore of heavy element titanium. Rutile mineral was readily soluble by both acids and an only small amount of mineral was left after the reaction that may be due to its locking with other minerals like orthoclase, plagioclase, and quartz as mentioned in Table C14 (Appendix C).

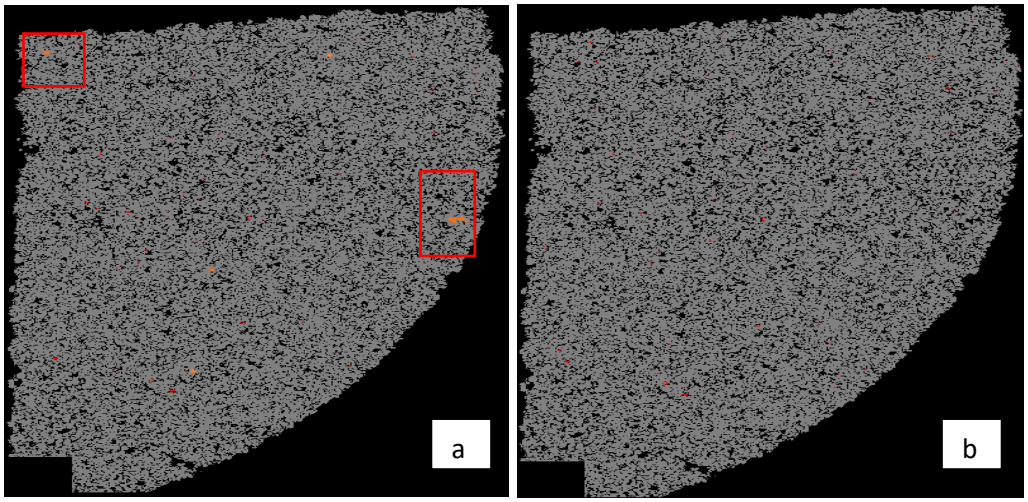

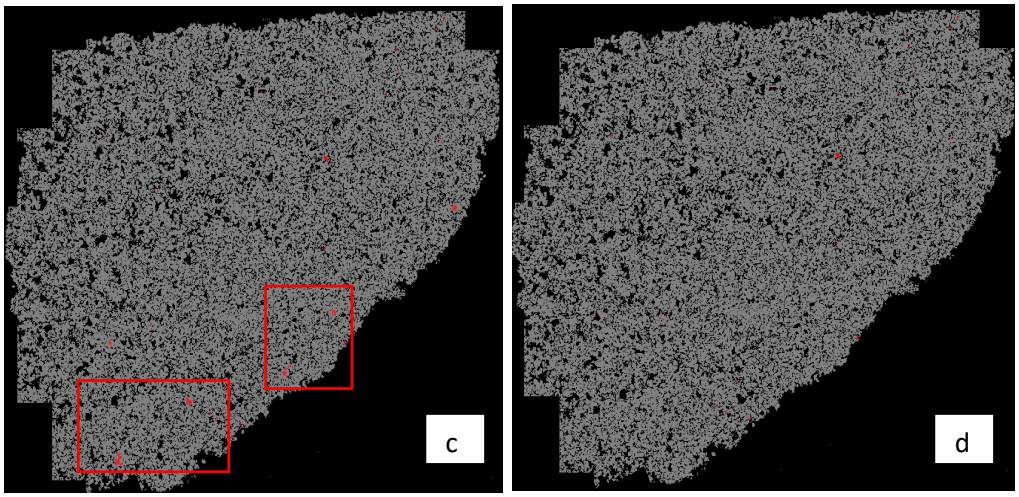

Figure 5.27. Panorama of rutile before and after reaction; unreacted samples (left), reacted with 15% HCl (top right), reacted with 5%CH_3COOH: 10% HCl (bottom right).

Dissolution of minerals which consist of potassium, sodium, and calcium was not efficient because of their complex mineral behavior. These complex minerals locked different elements together by strong bonding and cementing. Magnesium was dissolved because it exits in the form of ankerite only which was soluble in these acids. These results also validated the previous ICP analysis results discussed in chapter four where a high concentration of magnesium was dissolved. The high concentration of sodium, potassium and calcium ions observed in effluent samples during ICP analysis is mainly due to the dissolution of free ions present inside the core sample.

5.3.7 Porosity distribution

Table 5.1 shows the distribution of pore spaces present inside the core samples before and after acidizing application. This analysis was very important to understand the effect of acids in creating small or big size pore spaces. Small size pore spaces are not effective in creating mobile pores, but they can increase the reservoir porosity. The "size range" depends on the type of core sample. If the core sample has low permeability and porosity, the size range will be different compared to a high permeable and porous formation.

- 15% HCl created 8,073 number of pore spaces in size range of "9.6<63" microns compared to 6,110 number of pore spaces created by 5%CH_3COOH: 10% HCl.
- 15% HCl also created 117 new pore spaces within the size range of "63<133" microns compared to 25 number of new holes created by 5%CH_3COOH: 10% HCl.

- 15% HCl also created 7 new pore spaces within the size range of "133<193" microns compared to only 1 number of the new hole created by 5%CH_3COOH: 10% HCl.
- In total, 29.2% new pore spaces have been created by 15% HCl compared to 27.9% increment by 5%CH_3COOH: 10% HCl.

This shows the effectiveness of 15% HCl in creating new pore spaces. These results can be validated by the permeability and porosity results discussed in chapter 4 where more increase porosity and permeability is observed when 15% HCl was used for acidizing.

Table 5.1. Porosity Distribution in Berea sandstone before and after preflush

Size range	**Number of holes**			
	After reaction with 5%CH_3COOH: 10% HCl		**After reaction with 15% HCl**	
	Initial	**Final**	**Initial**	**Final**
9.6<63	21630	27740	27535	35608
63<133	370	395	545	662
133<193	9	10	8	15
Total	22009	28143	28088	36285

5.3.8 Particles size Distribution

Figures 5.28 (a, b) represents the number of small, medium and large size particles in Berea sandstone samples before and after acidizing with Pre-flush acids. It can be seen that both acid combinations managed to rescue the number of solid particles which showed their power to increase pore spaces and to remove different minerals.

- **15% HCl** managed to dissolve in total 11,340 particles (Table C21), 4,876 particles in the range of 9.6 < 11 um, 3,594 particles in the range of 13 < 29 um, 2,071 particles from 29 < 122 um, 640 from 122 < 434 and 159 particles from the range of 434 < 1547.
- **5%CH_3COOH: 10% HCl** managed to dissolve in total 7,891 particles (table C.21), 3,199 particles in the range of 9.6 < 11 um, 2,271 particles in the range of 13 < 29 um, 1,817 particles from 29 < 122 um, 484 from 122 < 434 and 120 particles from the range of 434 < 1547.

15% HCl proved to be more effective in the dissolution of different particles from sandstone core samples. It dissolved 32.8% particles compared to an initial number of particles present inside the sample while the dissolving power of 5%CH_3COOH: 10% HCl is 26.7%. These dissolved particles can be different minerals depending on the grain area covered by each mineral. Most of these dissolved particles consist of ankerite, magnetite, rutile, and quartz discussed in previous grain size distribution section.

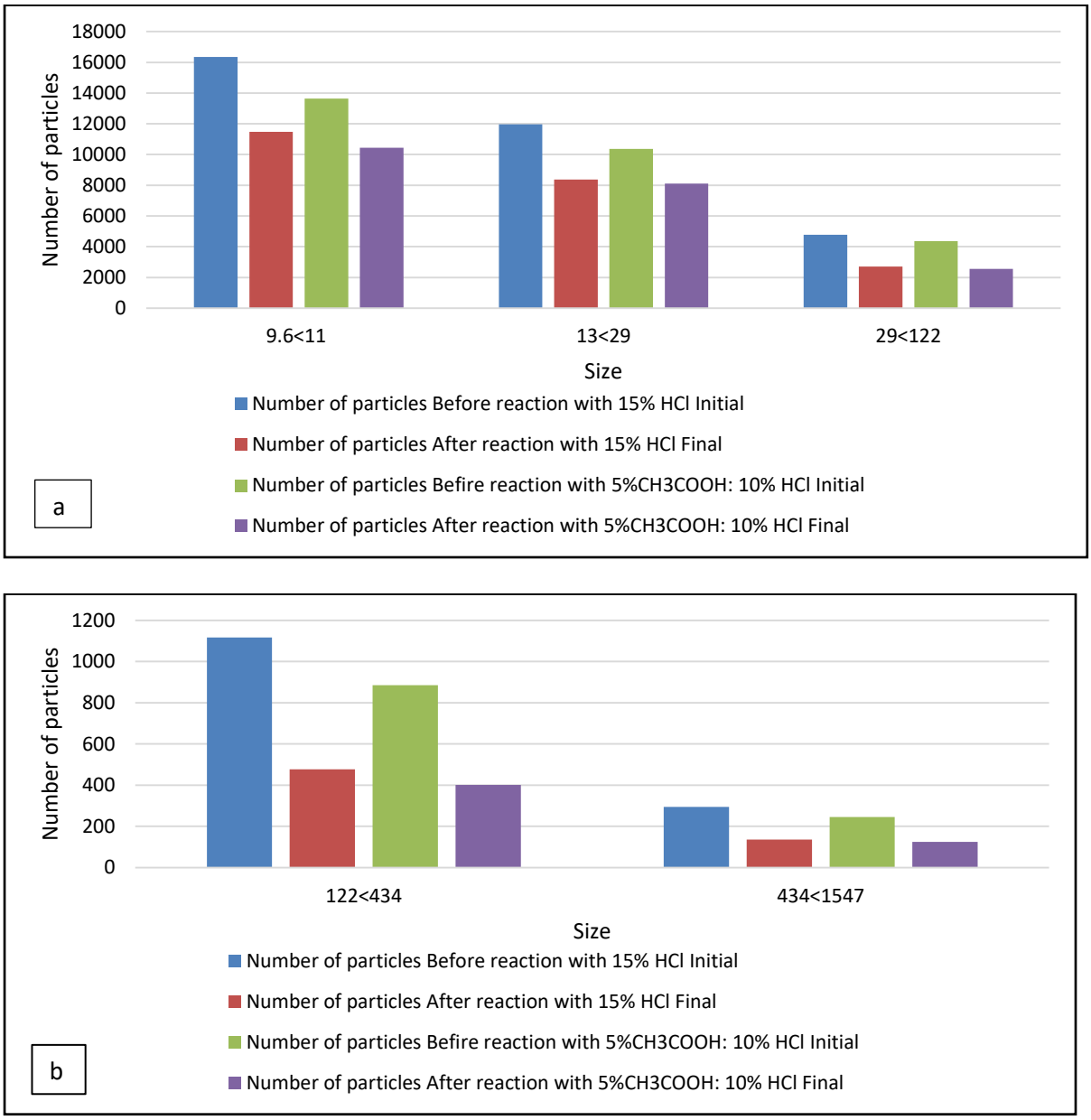

Figure 5.28. Particles distribution in Berea sandstone before and after Pre-flush

The difference between particles size distribution and grain size distribution can be explained as; the grain consists of single minerals like quartz or ankerite but a particle can be a

combination of different minerals embedded together as a single identity. That's why the total number of grains is higher than the total number of particles. But usually, minerals are present inside the sample as a single identity with few exceptions.

5.3.9 Density Distribution

Particles density distribution represents the number of particles in certain density range presented in Figures 5.29 (a, b, c). The sample acidized was Berea sandstone, while the density of sandstone was around 2.65 g/cm^3. Consequently, Figure 5.29a shows most number of particles in the range 2.6 < 2.7 g/cm^3. Some of the particles (quartz, orthoclase, plagioclase, ankerite, and kaolinite) representing different density minerals were shown in Figure 5.30. However, orthoclase having lowest density of 2.56 g/cm^3, on the other hand, the density of ankerite was highest (2.97 g/cm^3). The density of rutile was in the range of 4.2 < 4.4 g/cm^3, while zirconium density was higher than that. It can be seen that both acids dissolved rutile where a number of particles in density range "4.2 < 4.4 g/cm^3" was significantly decreased from 334 to 63 in case of 15% HCl and 321 to 53 in case of 5%CH_3COOH: 10% HCl. Heavy minerals with density range from "5.0 < 5.3" were dissolved effectively by these applied acids.

Figure 5.29a illustrated that some amount of sandstone particles has been dissolved during acidizing with these acids. For this reason, the number of particles was decreased in the range of 2.6 to 2.7 g/cm^3. To summarize, both of these applied acids dissolved a large number of particles in each density range. These results can be validated from the previous analysis, where these acids dissolved almost all types of minerals and reduced number of grains of each mineral and created fresh pore spaces of different micron sizes.

Every mineral shows different density value due to the presence of different elements inside. The particle with a higher density the XRD curve moves towards the right side and vice versa. The white color in Figure 5.30 represents the pore spaces while black dotes represent unidentified minerals.

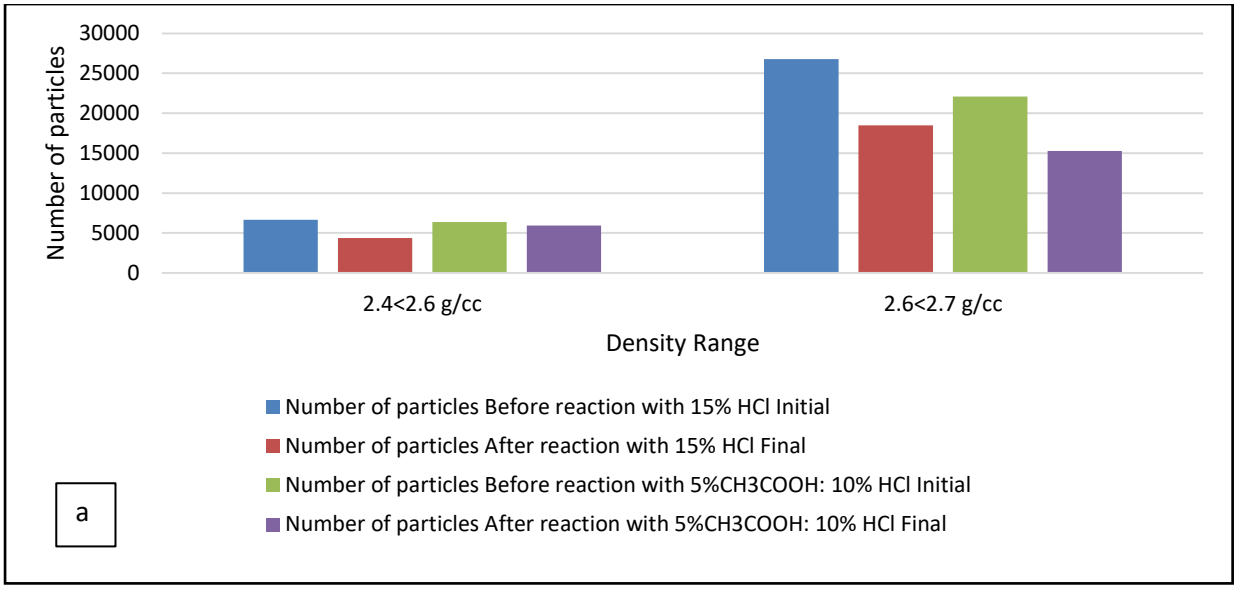

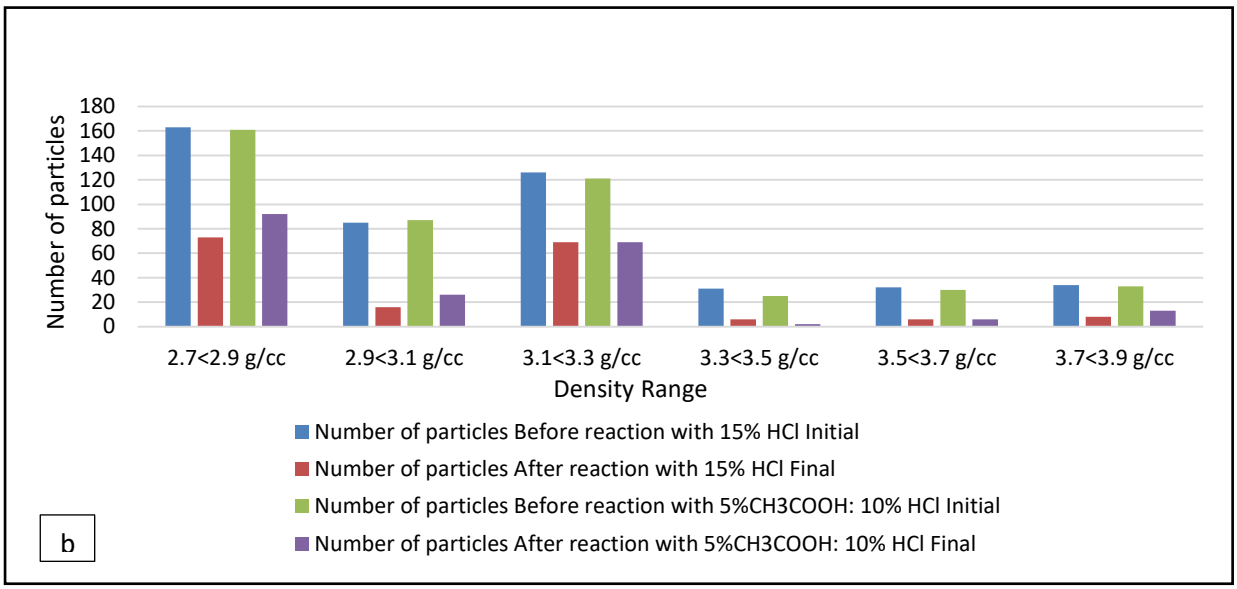

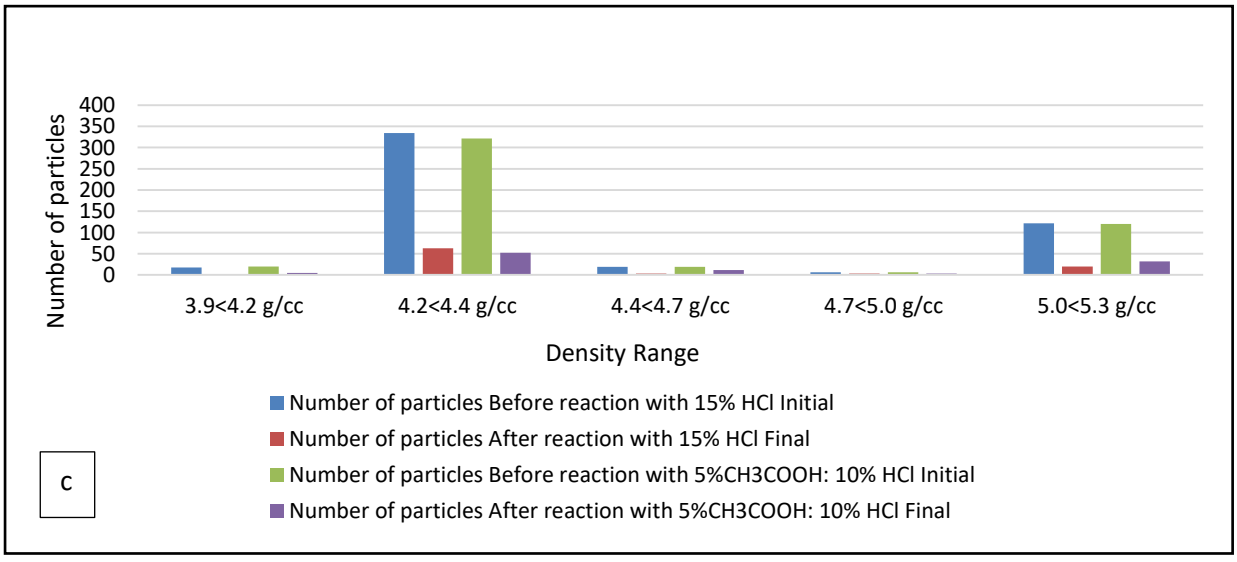

Figure 5.29. Particles Density distribution in Berea sandstone before and after Pre-flush

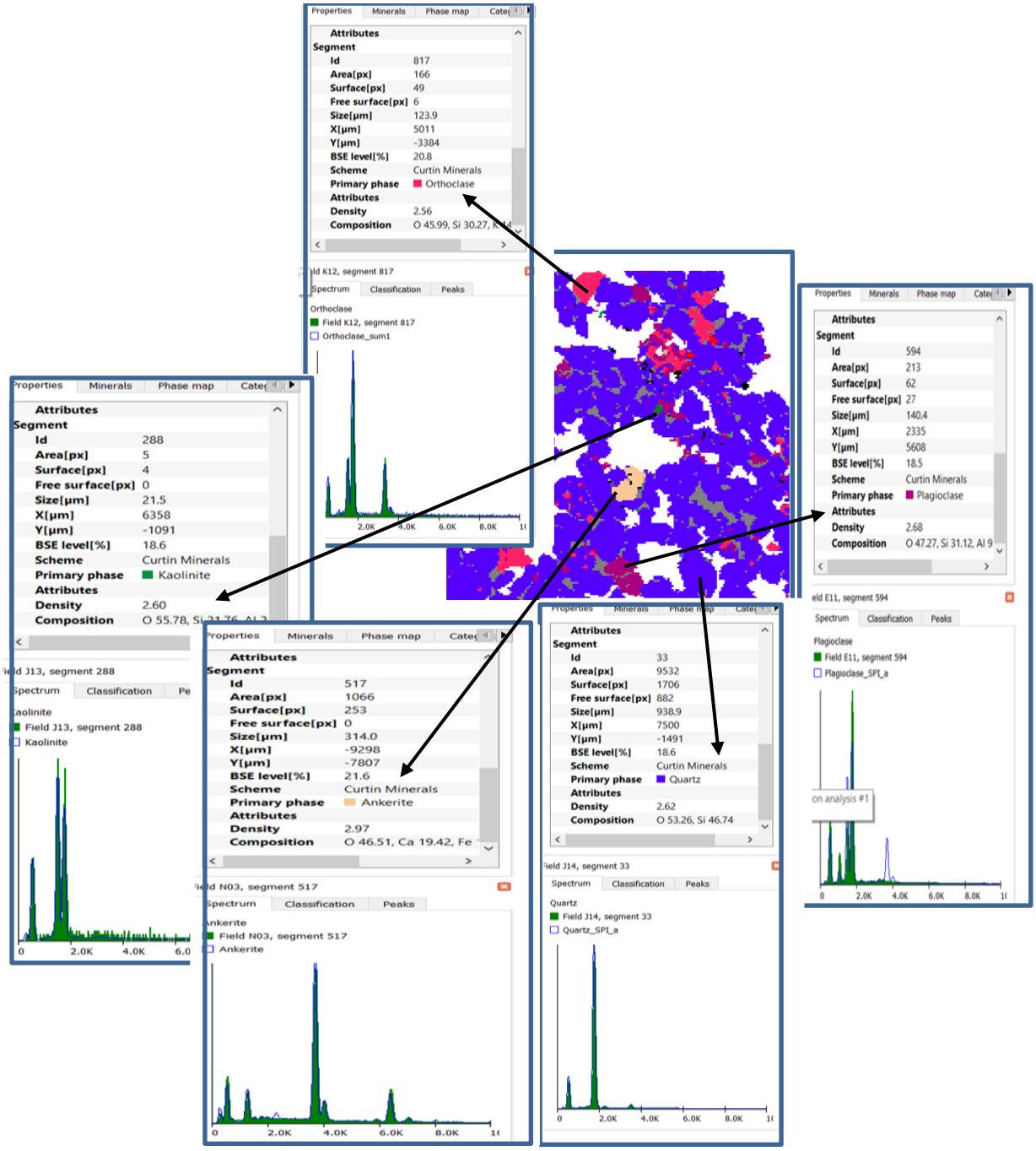

Figure 5.30. Density pattern of different particles present in Berea sandstone Core sample

5.4 Results of reaction with Chelates

Chelates are usually applied during the main acid stage of sandstone acidizing or they are applied as a single acid without applying preflush stage as these do not include the fluoride ions which may form a precipitate when reacted with different minerals. As discussed in chapter 3, in this project three different chelating agents (GLDA, EDTA, and HEDTA) were applied and their effects had been investigated on Berea sandstone, Colton sandstone, and Guelph dolomite core samples.

5.4.1 Reacted with Berea Sandstone

In this section effects of all three chelating agents on Berea sandstone, core samples had been discussed and analyzed. These chelating agents were applied on unreacted Berea sandstone core samples instead of pre-flushed samples in order to see their effects on all minerals present inside the core samples.

5.4.1.1 Elemental analysis

The sample is homogeneous in nature, therefore, the constant initial elemental composition was applied for elemental analysis of samples reacted with chelates. All three chelating agents showed good solubility towards magnesium, potassium, calcium, titanium, and iron mentioned in Figure 5.31. A small amount of aluminum was also dissolved by all three chelates.

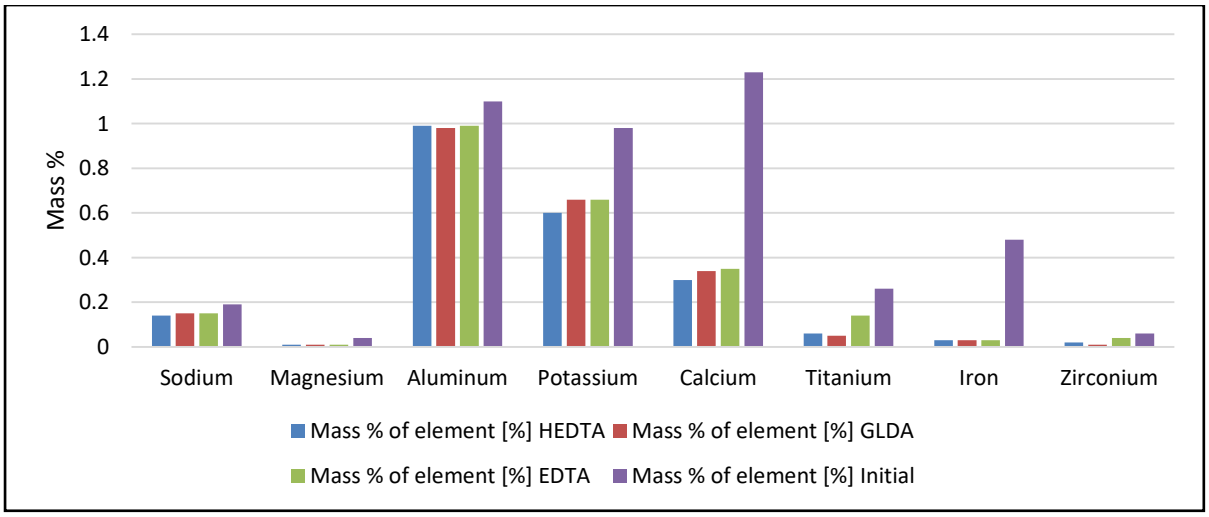

Figure 5.31. Elemental mass in Berea before and after reaction with chelating agents

Where,

- Mass % of the element [%] initial; represents the mass of element before reaction with chelating agents
- Mass % of the element [%] HEDTA represents sample reacted with HEDTA and similarly for EDTA and GLDA

5.4.1.2 Element Deportment

As discussed earlier, deportment shows the presence of an element of interest in certain minerals. Figure 5.32 shows the presence of calcium in albite, ankerite, and plagioclase. All chelates were effective in dissolving ankerite mineral, therefore, the concentration of calcium became less. On the contrary, an only a small amount of plagioclase and albite were dissolved by all chelates, which is due to the complex nature of these minerals. However, HEDTA being readily biodegradable and more reactive compared to EDTA and GLDA dissolved around 25% of plagioclase compared to the initial concentration.

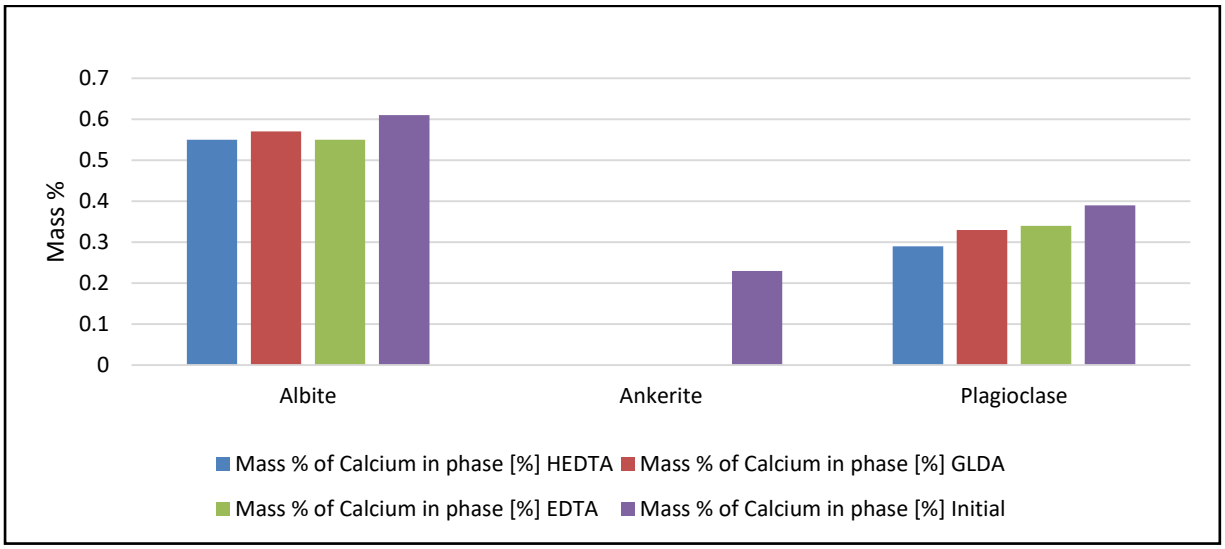

Figure 5.32. Calcium deportment in Berea Sandstone before and after reaction with chelating agents

Figure 5.33 shows the presence of iron in the form of ankerite, magnetite, and pyrite. After acidizing all three chelates showed the complete dissolution of the iron element in all form of minerals. It shows the effectiveness of these chelates in dissolving the minerals consist of iron, magnesium, calcium, and manganese. Berea sandstone is conventional sandstone formation where most of the matrix is consist of quartz mineral, while a small quantity of other minerals like albite, orthoclase, pyrite, magnetite, and ankerite were also present. These chelates do not dissolve silicon, therefore, the increase in porosity and permeability discussed earlier mostly is due to the dissolution of these minerals present in small quantities.

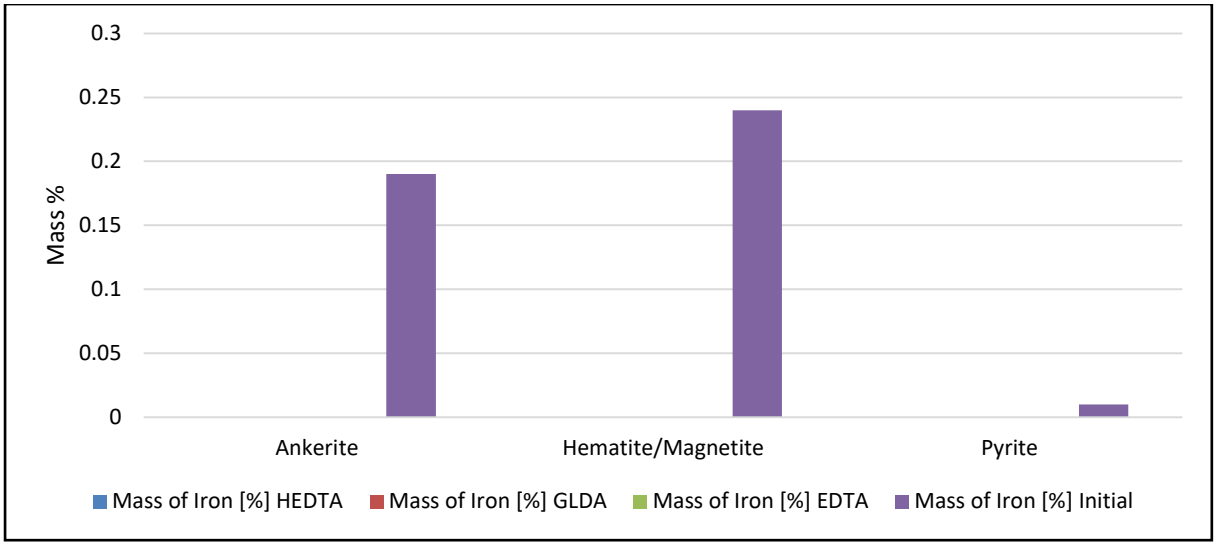

Figure 5.33. Iron deportment in Berea Sandstone before and after reaction with chelating agents

Potassium was found in the form of orthoclase and muscovite (Figure 5.34), both having a complex molecular formula where elements were bounded together. That's why the dissolution of these minerals was less because chelates couldn't form a bond around the element of interest.

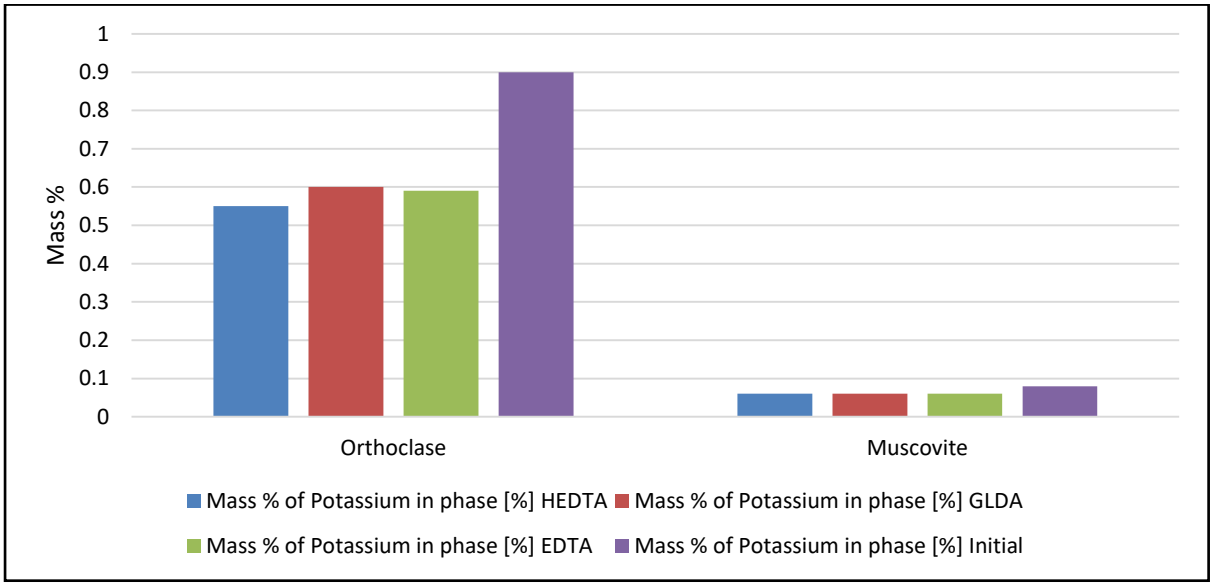

Figure 5.34. Potassium deportment in Berea Sandstone before and after reaction with chelating agents

Magnesium was present in the form of Magnesiogedrite ($Mg_3Fe_2Al_2(Si_6Al_2O_{22})(OH)_2$) in a trace amount and this complex mineral had been dissolved almost completely by all the chelates as shown in Figure 5.35. Because the mineral was present in trace amount that's why the dissolution of this mineral by applied chelates couldn't be discussed effectively.

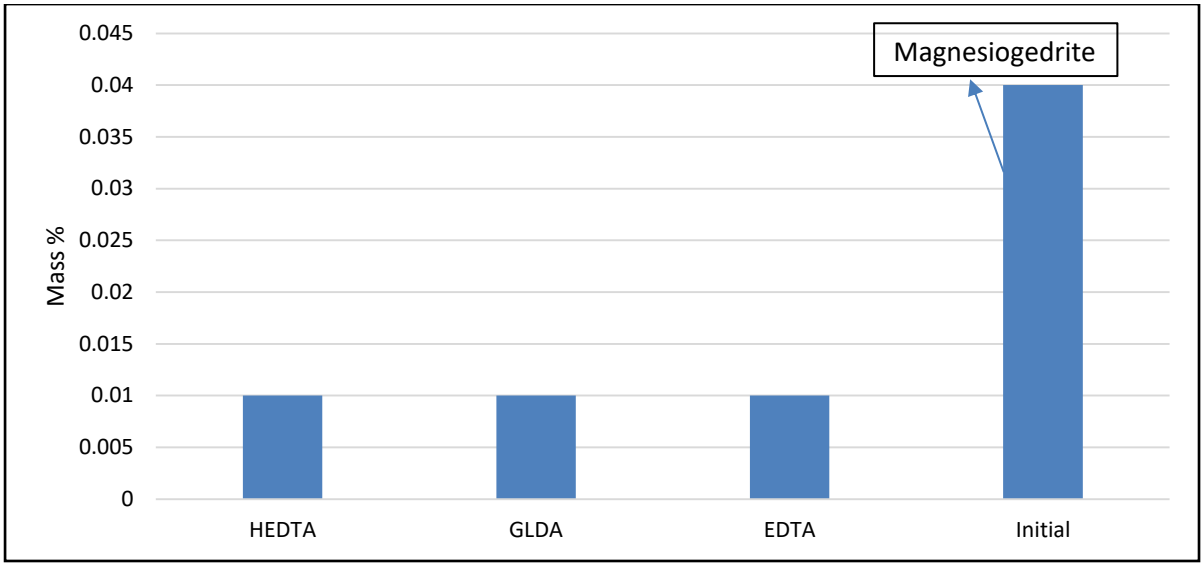

Figure 5.35. Magnesium deportment in Berea Sandstone before and after reaction with chelating agents

Sodium was found in the form of Albite and an only trace amount of albite had been dissolved by these chelates mentioned in Figure 5.36. This can be validated from the previously discussed element deportment of calcium (Figure 5.32) where the dissolution of albite is very less.

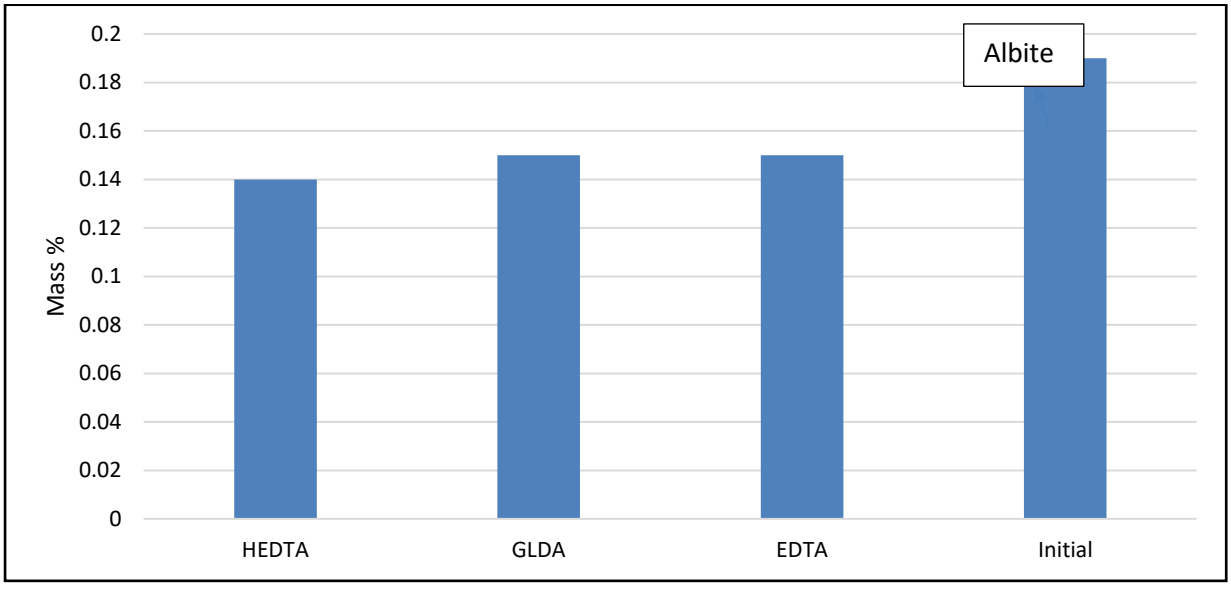

Figure 5.36. Sodium deportment in Berea Sandstone before and after reaction with chelating agents

Silicon was found in the form of various minerals as it is the major constituent of sandstone rock samples. Figure 5.37 showed the presence of silicon in various minerals like kaolinite, plagioclase, albite, and orthoclase. A small quantity of kaolinite, plagioclase, and orthoclase was dissolved by the applied chelates especially HEDTA. While the solubility of muscovite

and albite was very less in any chelate and only trace amount was dissolved. These results can be further validated by performing mineral mass analysis of the core samples.

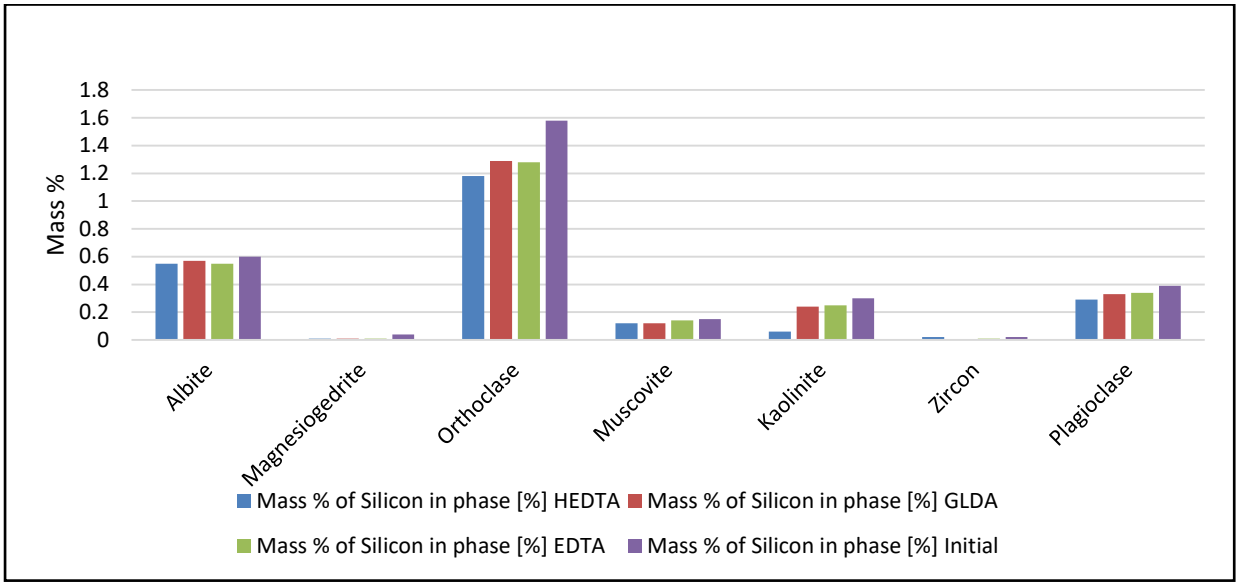

Figure 5.37. Silicon deportment in Berea Sandstone before and after reaction with chelating agents

5.4.1.3 Mineral Analysis

Mineral composition is very important to analyze the mineralogy after acidizing the core samples because it can explain the chelating power of the chelating agent. The relative mineral mass analysis describes the dissolution of different minerals present inside the sample. This analysis is effective to show that what type of mineral has been dissolved and is contributing towards the porosity and permeability increment.

Figure 5.38 represents the mineral mass change in Berea sandstone sample after reaction with all three chelates. Albite and kaolinite relative mineral mass had been increased after the reaction, which indicated that they were not dissolved by the chelates. Likewise, an increase in relative mass of quartz showed that it was not soluble by these chelates (Appendix D, Table D8). On the other hand, orthoclase relative mineral mass had been decreased indicting its solubility by these chelates. The maximum solubility of zircon and rutile had been seen when GLDA was applied. All three chelates showed chelating power towards orthoclase, zircon, ankerite, magnetite, pyrite, and Magnesiogedrite, while GLDA showed the maximum power in dissolving rutile and zircon.

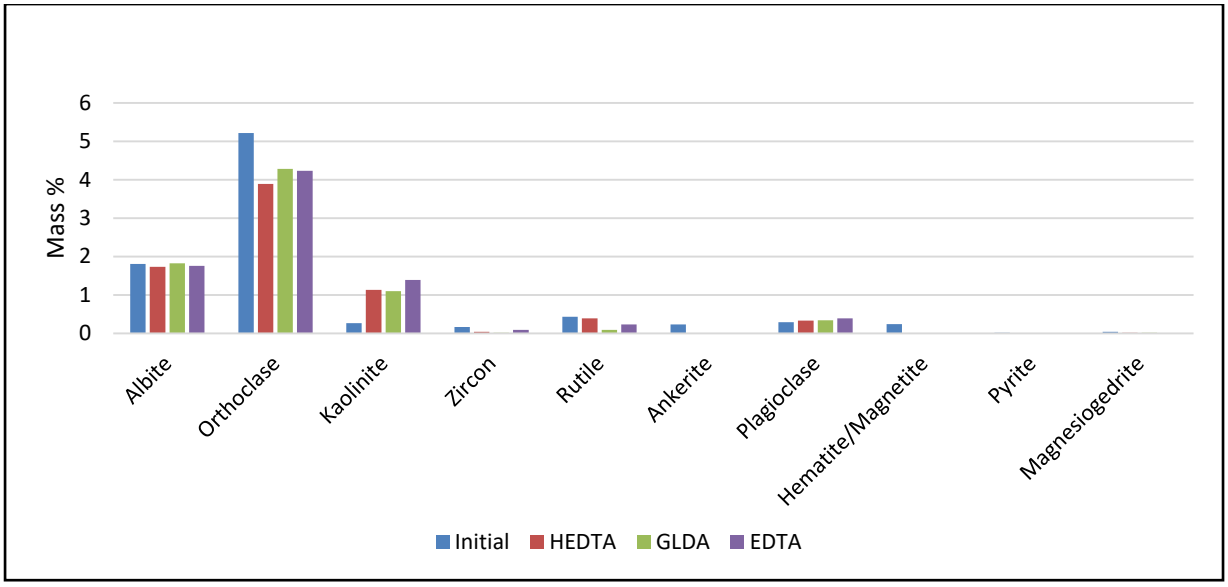

Figure 5.38. Mineral mass in Berea Sandstone before and after reaction with chelating agents

5.4.1.4 Mineral Locking

Quartz mineral was locked with almost all the minerals present inside the core sample, but most of it exists in the form of the free surface (Appendix D, Table D9). The maximum increase in the percentage of the free surface has been observed when the core sample was allowed to react with GLDA, where the percentage of free surface increased from 74.02% to 77.90%. GLDA was also very effective in decreasing the locking of kaolinite, zircon, and rutile with quartz as shown in Figure 5.39. Likewise, HEDTA was effective in decreasing the locking of orthoclase with quartz.

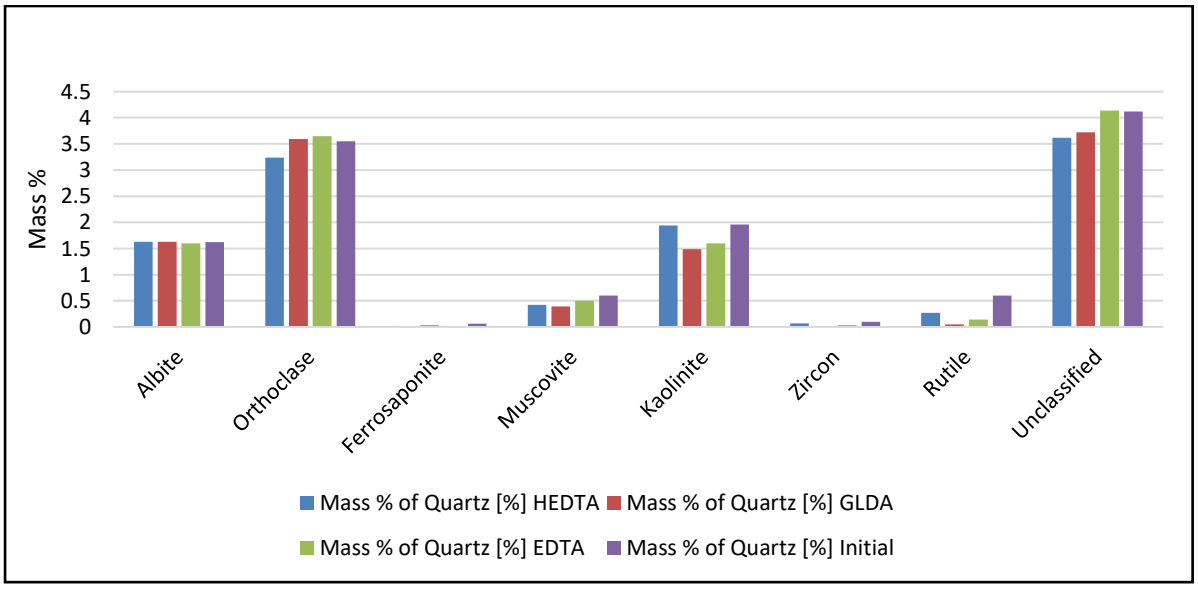

Figure 5.39. Quartz Mineral Locking in Berea Sandstone before and after reaction with chelating agents

The rutile mineral was locked with orthoclase, kaolinite, and quartz. After reaction with the chelates, the locking of rutile with orthoclase and kaolinite has been removed as presented in Figure 5.40. GLDA proved to be more effective because after reaction most of the mineral locking of rutile with quartz was diminished compared to other chelates.

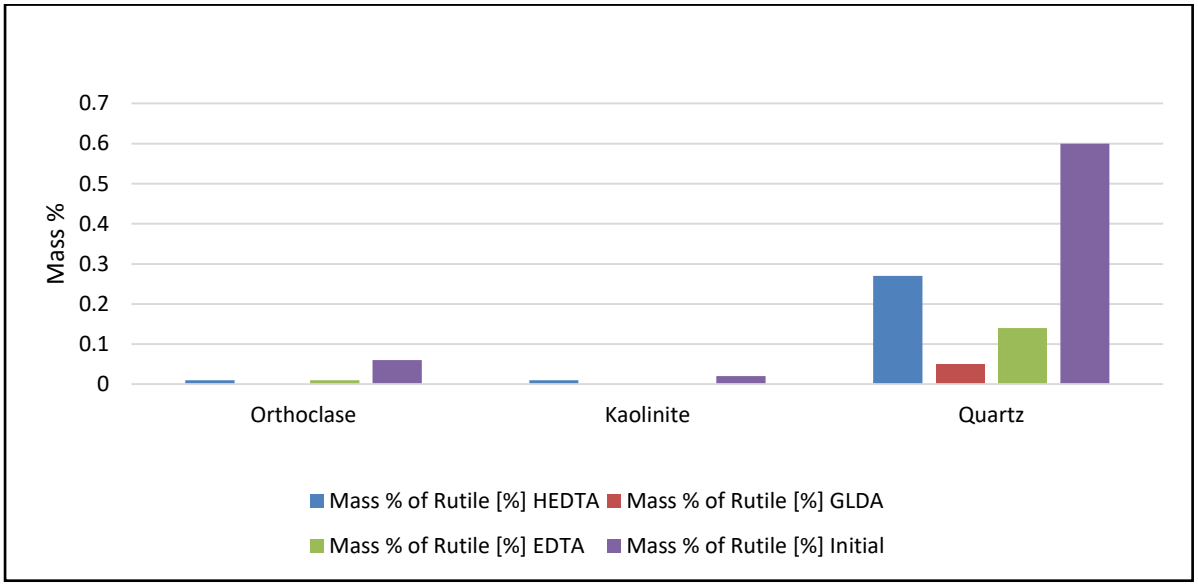

Figure 5.40. Rutile Mineral Locking in Berea Sandstone before and after reaction with chelating agents

Mineral locking of other minerals like albite, orthoclase, kaolinite, and plagioclase has not been changed significantly as these minerals were not dissolved effectively by these chelates, explained in the mineral mass analysis section. While the mineral locking of ankerite, magnetite, and pyrite has been diminished completely because of their solubility by these chelates.

5.4.1.5 Grain Size Distribution

The number of grains of different important minerals before and after acidizing was discussed from Figure 5.41 through Figure 5.46. The number of grains of ankerite, calcite, hematite/magnetite and rutile (Figure 5.41 through Figure 5.44 respectively) has been changed significantly after the reaction. It illustrated that these minerals have been dissolved by the chelates. Contrary to the change in the grain size of kaolinite and quartz was negligible (Figure 5.45 and Figure 5.46 respectively). This established the insolubility of these minerals by the applied chelates. HEDTA showed some dissolution power towards quartz and dissolved around 4000 grains while GLDA proved effective for kaolinite and dissolved around 1500 grains.

These results can be validated by the mineral mass analysis presented in Table D8 (Appendix D).

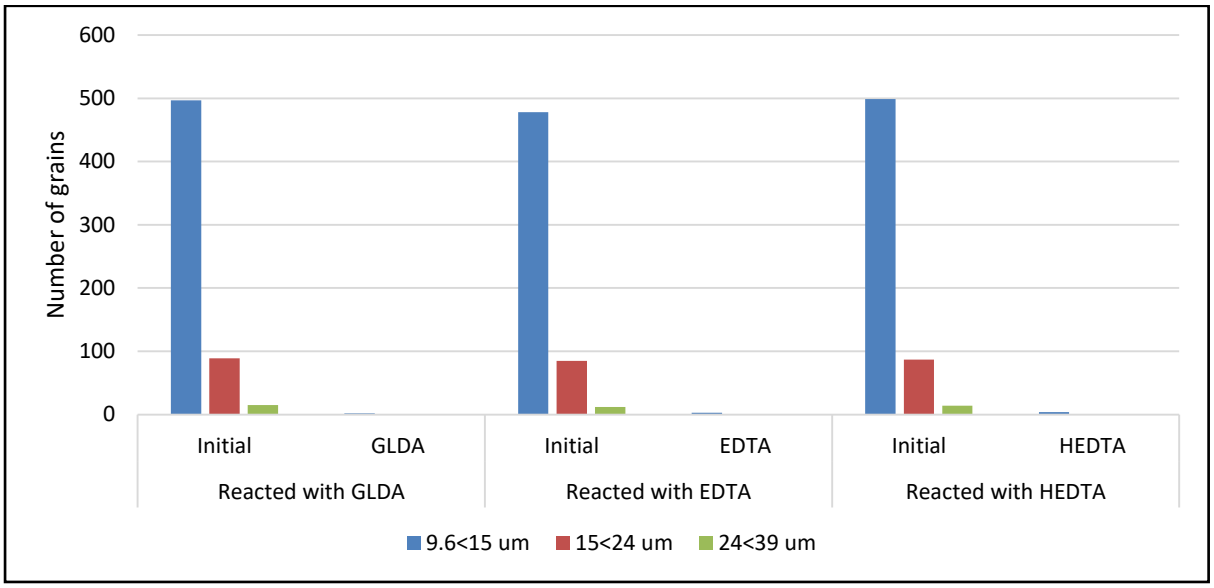

Figure 5.41. Grain size distribution of Ankerite in Berea Sandstone before and after reaction with chelating agents

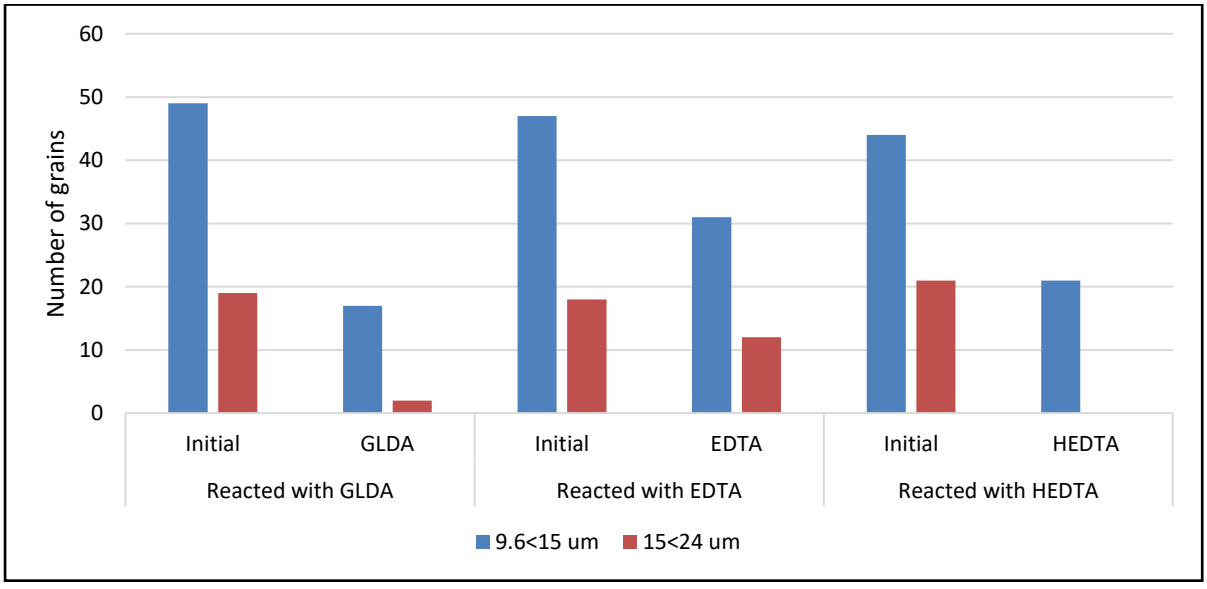

Figure 5.42. Grain size distribution of Calcite in Berea Sandstone before and after reaction with chelating agents

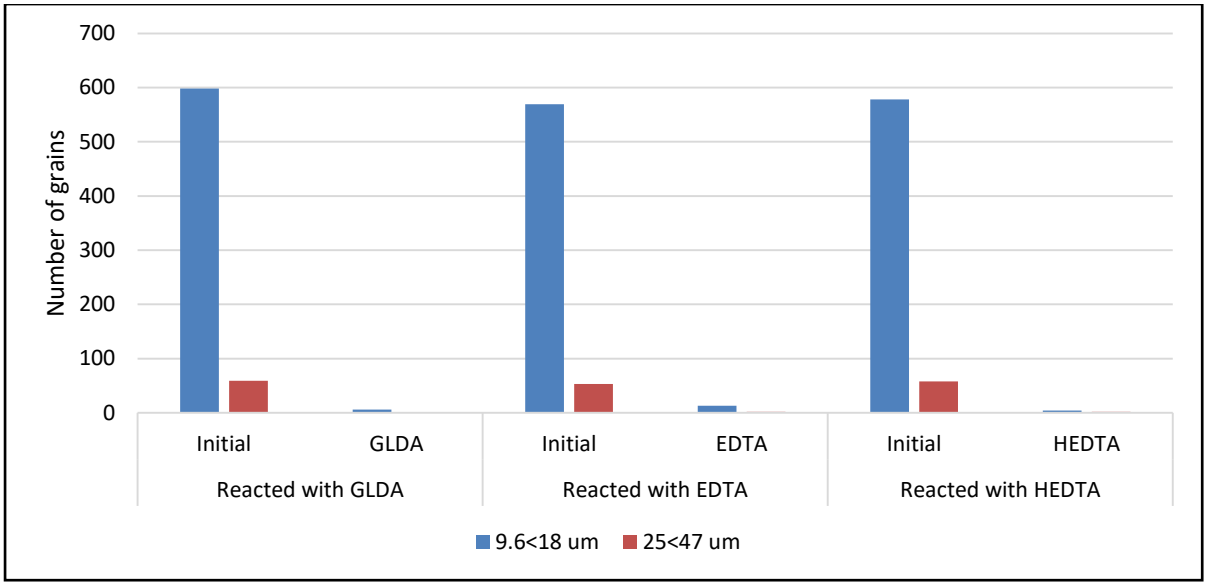

Figure 5.43. Grain size distribution of Magnetite in Berea Sandstone before and after reaction with chelating agents

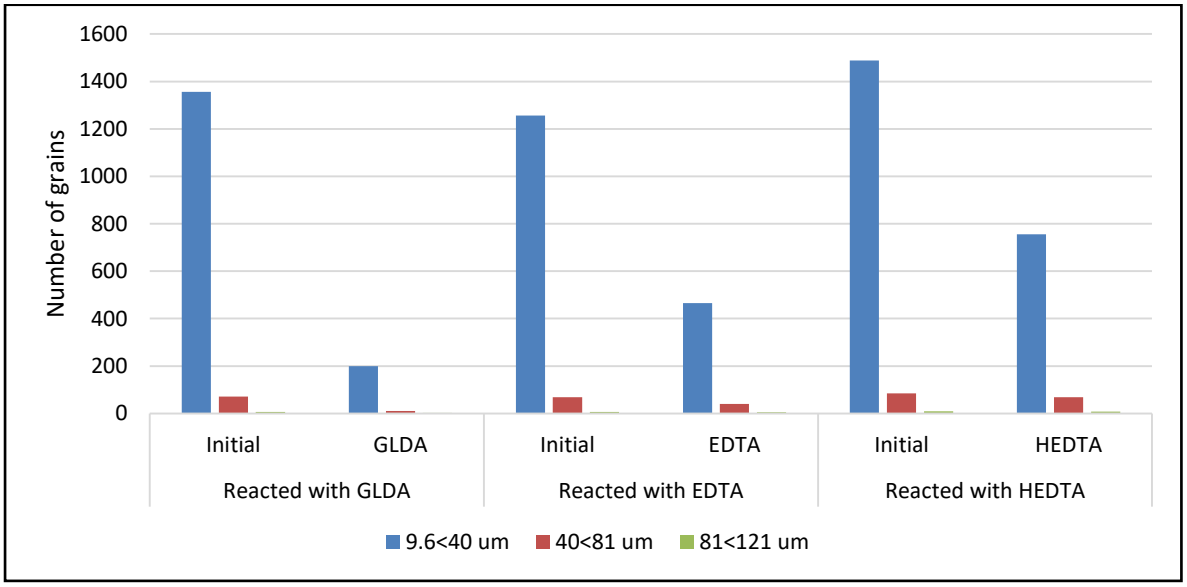

Figure 5.44. Grain size distribution of Rutile in Berea Sandstone before and after reaction with chelating agents

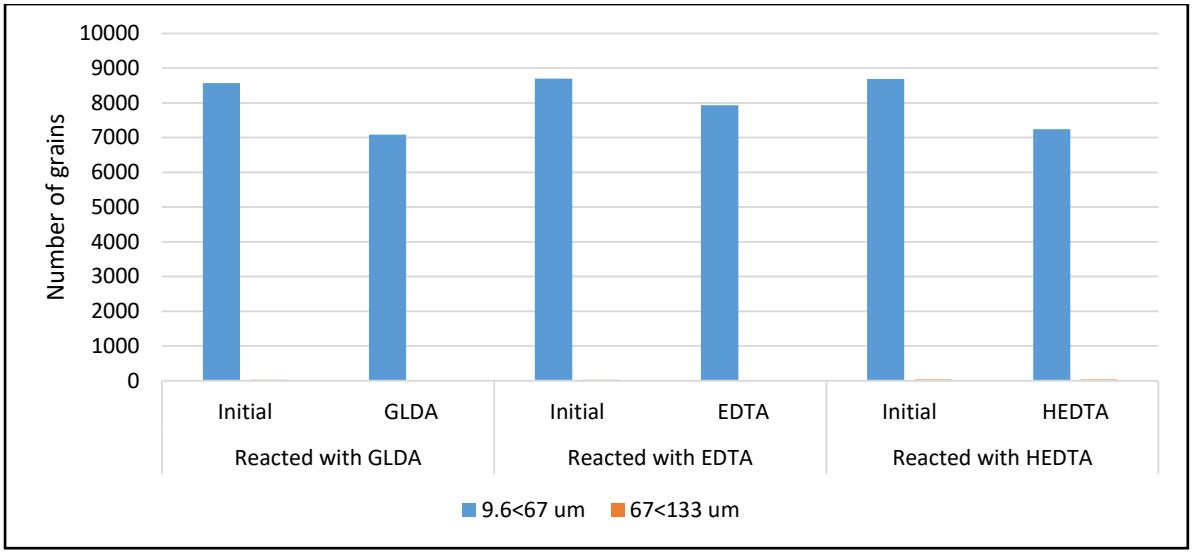

Figure 5.45. Grain size distribution of Kaolinite in Berea Sandstone before and after reaction with chelating agents

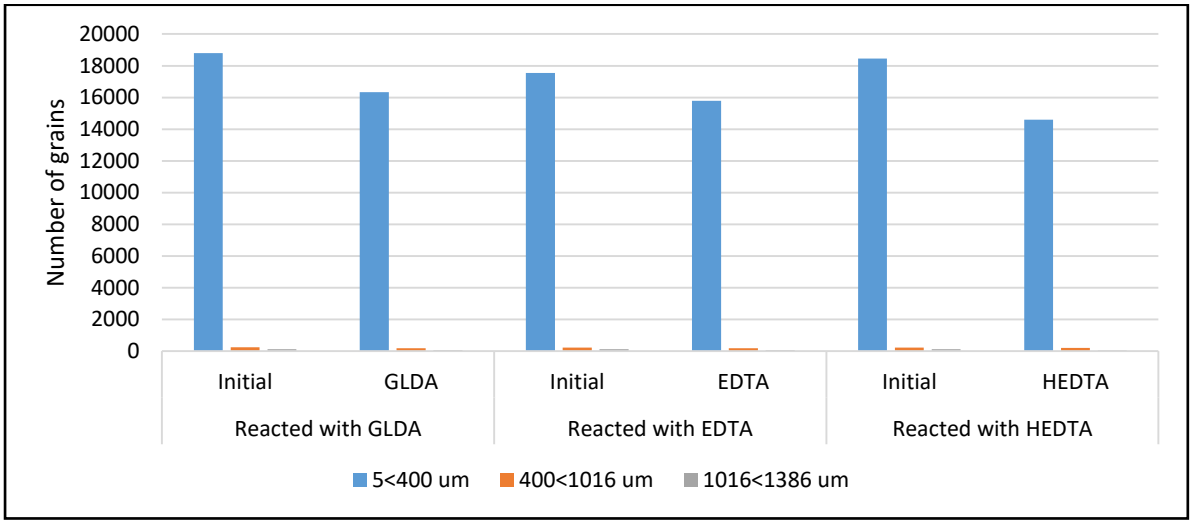

Figure 5.46. Grain size distribution of Quartz in Berea Sandstone before and after reaction with chelating agents

5.4.1.6 Panorama

Figures 5.47 to 5.52 represents the BSE images of the Berea sandstone core sample before and after the reaction with different chelating agents. Black dots represent the pore spaces present inside the sample while dark grey grains represents the matrix which was quartz in case of sandstone sample. The bright or light grey spots represented the presence of different minerals other than quartz. Figure 5.47 and Figure 5.48 illustrated the complete panorama and more focused images respectively of the core sample reacted with HEDTA. Both Figures signified the dissolution of minerals in the core sample when reacted with HEDTA.

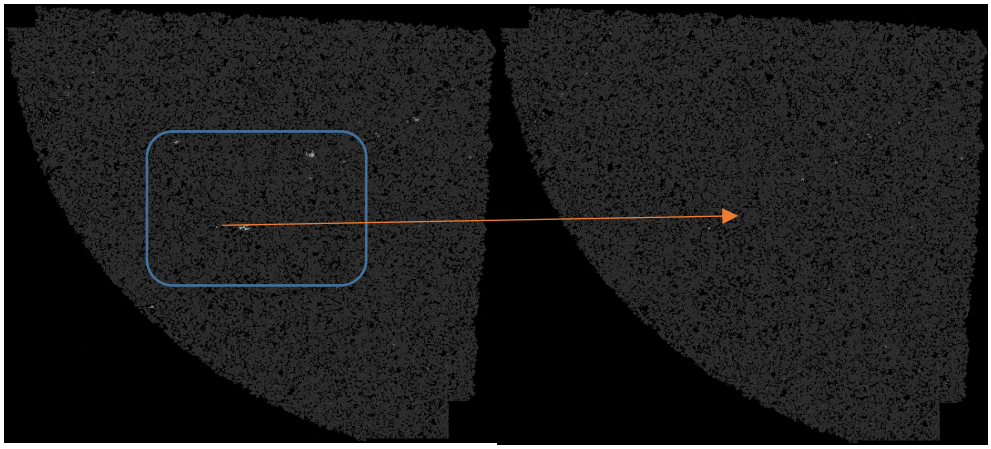

Figure 5.47. Dissolution of minerals when Berea sandstone reacted with HEDTA, unreacted (left), reacted (right)

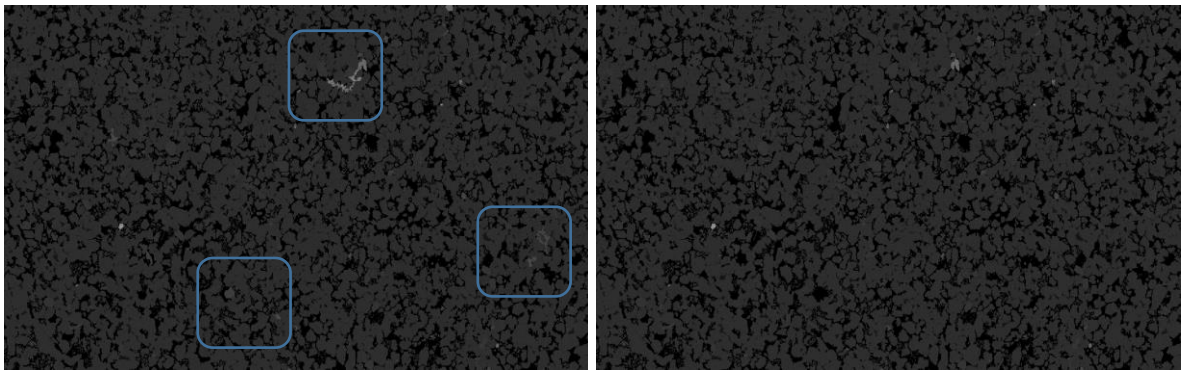

Figure 5.48. Pore spaces in Berea sandstone when reacted with HEDTA, unreacted (left), reacted (right)

Figure 5.49 and Figure 5.50 represent the complete panorama and more focused image respectively of core samples reacted with GLDA. Figure 5.50 showed the significant dissolution of minerals when reacted with GLDA.

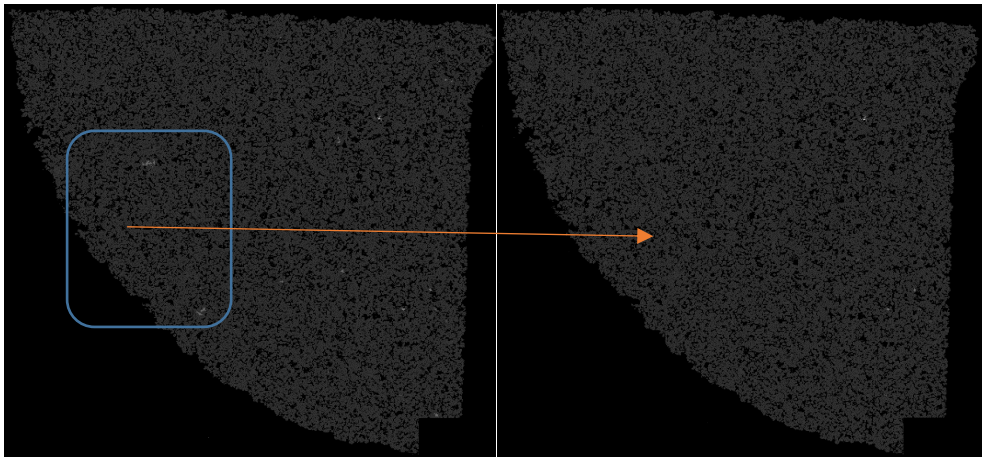

Figure 5.49. Dissolution of minerals when Berea sandstone reacted with GLDA, unreacted (left), reacted (right)

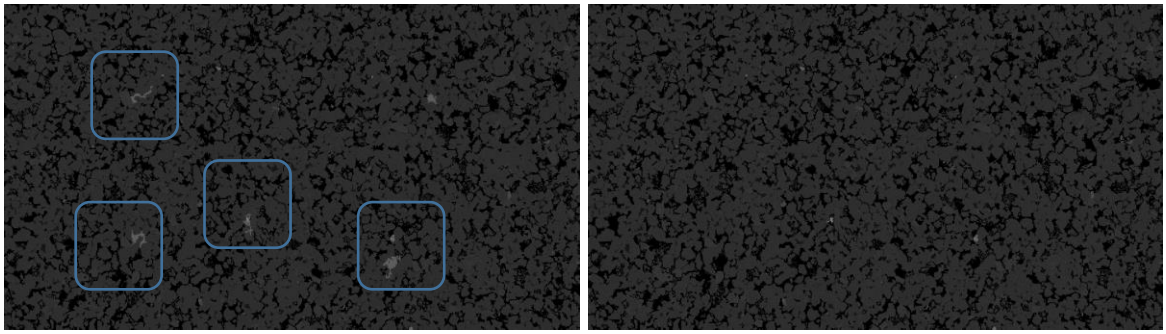

Figure 5.50. Pore spaces in Berea sandstone when reacted with GLDA, unreacted (left), reacted (right)

Figure 5.51 and Figure 5.52 represents the complete panorama and more focused image respectively of core samples reacted with EDTA. Clear dissolution of minerals can be observed in Figure 5.52. To summarize, if all the pictures considered, it seems reasonable to conclude that these chelating agents were effective in creating fresh pore spaces in the sandstone core sample.

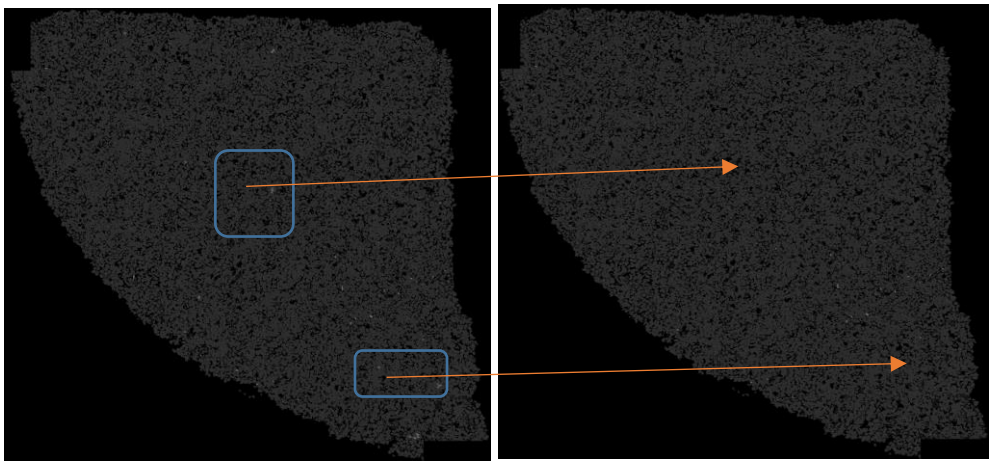

Figure 5.51. Dissolution of minerals when Berea sandstone reacted with EDTA, unreacted (left), reacted (right)

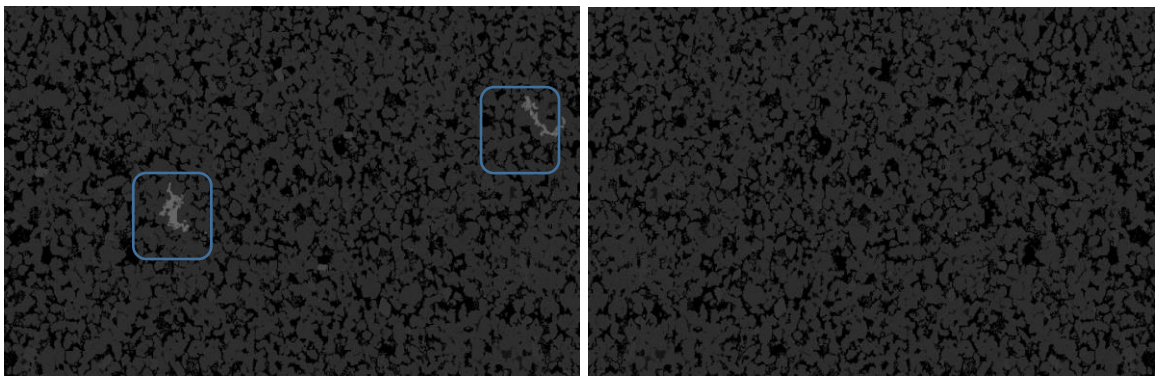

Figure 5.52. Pore spaces in Berea sandstone when reacted with EDTA, unreacted (left), reacted (right)

5.4.1.7 Pore Size Distribution

Table 5.2 represents the distribution of small, medium and large size holes in Berea sandstone samples reacted with different chelating agents. 3862, 3090 and 1443 new pore spaces have been created in Berea sandstone when reacted with EDTA, HEDTA, and GLDA respectively. Where GLDA is effective in creating medium size pore spaces and introduced 132 new pore spaces compared to 101 by HEDTA and 88 by EDTA. Large wormholes have been created too when core samples were reacted with all chelates while maximum change has been observed with HEDTA, where 5 new pores have been introduced by HEDTA compared to 2 by GLDA and 1 by EDTA. It can be concluded from this analysis that EDTA is effective in creating small pore spaces while GLDA in medium size and HEDTA in creating large size pore spaces. Most effective chelate on Berea sandstone formation from porosity distribution is EDTA.

Table 5.2. Porosity distribution in Berea sandstone before and after reaction with chelating agents

Size range	**Number of holes**					
	Reacted with HEDTA		**Reacted with GLDA**		**Reacted with EDTA**	
	Initial	HEDTA	Initial	GLDA	Initial	EDTA
9.6 – 50 µm	21,589	24,573	20,990	22,299	22,850	26,623
50 – 101 µm	450	551	389	521	550	638
101 – 180 µm	15	20	16	18	14	15
Total	22,054	25,144	21,395	22,838	23,414	27,276

5.4.1.8 Particle size distribution

Figures 5.53 (a, b) represents the number of small, medium and large size particles in Berea sandstone samples before and after acidizing with chelates. It can be seen that all chelates combinations managed to rescue some number of solid particles which showed their power to increase pore spaces and to remove different minerals

- **HEDTA** managed to dissolve in total 2,156 particles (table D.17), 591 particles in the range of 9.6 < 11 um, 988 particles in the range of 13 < 29 um, 388 particles from 29 < 121 um, 112 from 121 < 430 and 77 particles from the range of 430 < 1528.
- **GLDA** managed to dissolve in total 1,419 particles (table D.17), 254 particles in the range of 9.6 < 11 um, 811 particles in the range of 13 < 29 um, 233 particles from 29 < 121 um, 79 from 121 < 430 and 42 particles from the range of 430 < 1528.

- **EDTA** managed to dissolve in total 1,783 particles (table D.17), 329 particles in the range of 9.6 < 11 um, 1,013 particles in the range of 13 < 29 um, 294 particles from 29 < 121 um, 100 from 121 < 430 and 47 particles from the range of 430 < 1528.

Chelate (HEDTA) proved to be more effective in the dissolution of different particles from sandstone core samples. It dissolved 6.4% particles compared to an initial number of particles present inside the sample while the dissolving power of GLDA and EDTA is 4.6% and 5.5% respectively. These dissolved particles can be different minerals depending on the grain area covered by each mineral. Most of these dissolved particles consist of zircon, ankerite, magnetite, and quartz. The particles of rutile were the main difference between the results of chelates as it is dissolved by GLDA effectively as discussed in Figure 5.38 previously.

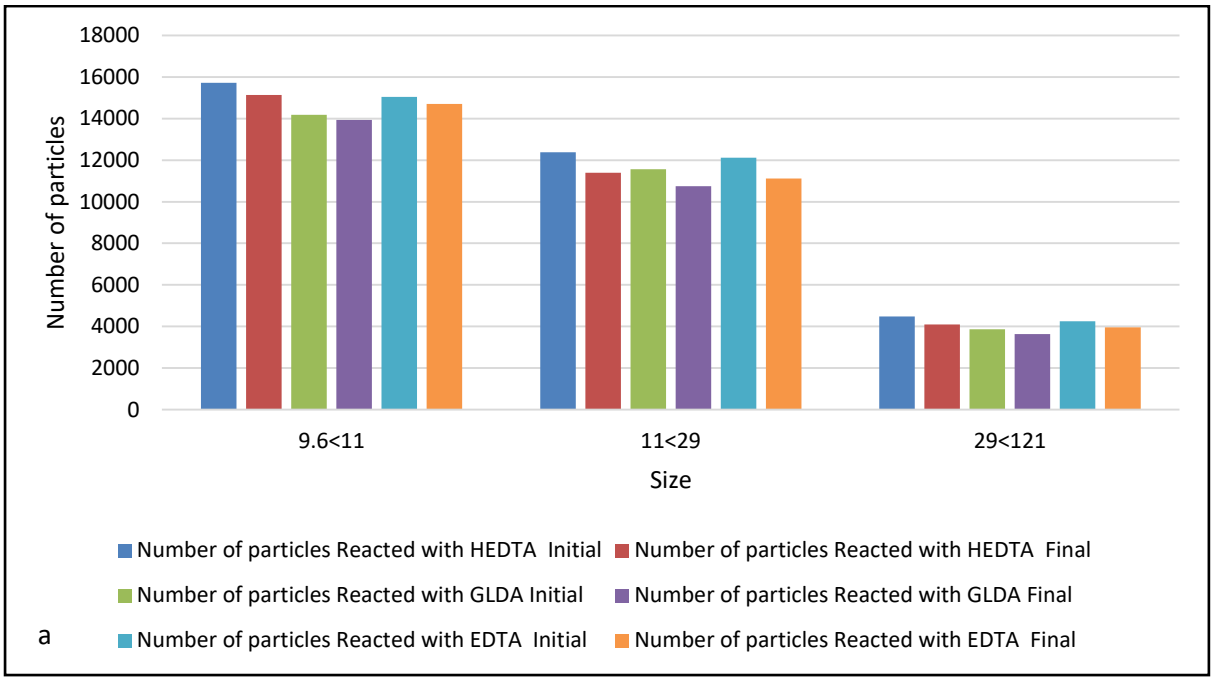

a

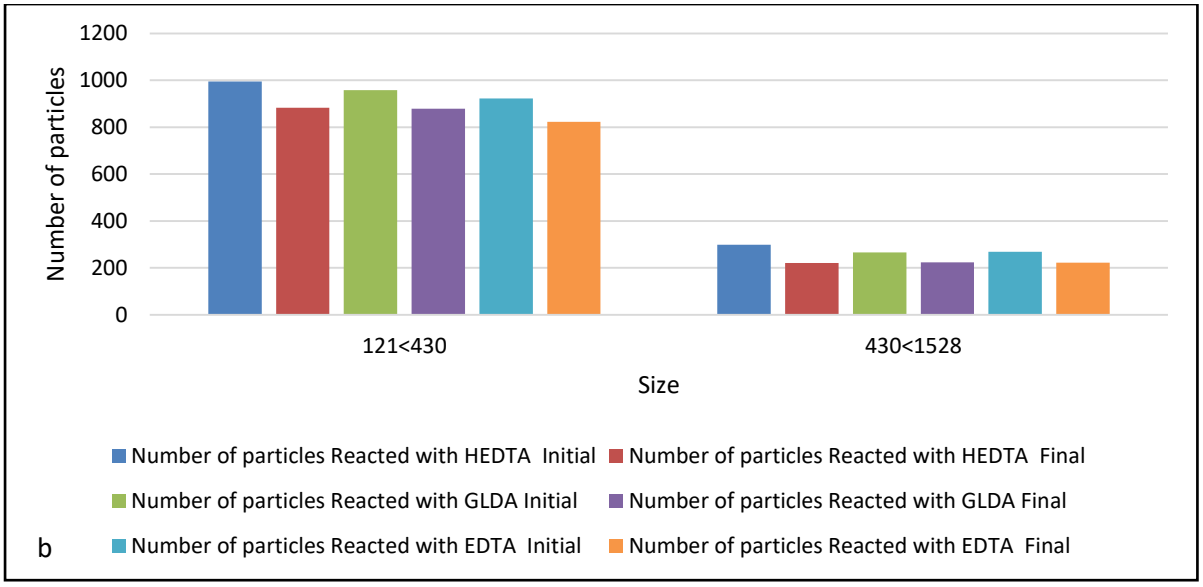

Figure 5.53. Number of particles in Berea Sandstone before and after reaction with chelating agents

5.4.1.9 Particle Density

Particles density distribution represents the number of particles in certain density range presented in Figures 5.54 (a, b, c). The sample acidized was Berea sandstone, while the density of sandstone was around 2.65 g/cm^3. That's why Figure 5.54b shows most number of particles in the range 2.5 < 2.8 g/cm^3. The power of these agents in dissolving light particles like orthoclase (density 2.56 g/cm^3) is not effective discussed earlier and confirmed/validated by Figure 5.54a where the change in number of light/less dense particles was less, while heavy particles like ankerite (2.97 g/cm^3) and rutile (4.2 g/cm^3) were dissolved effectively shown in Figure 5.54c.

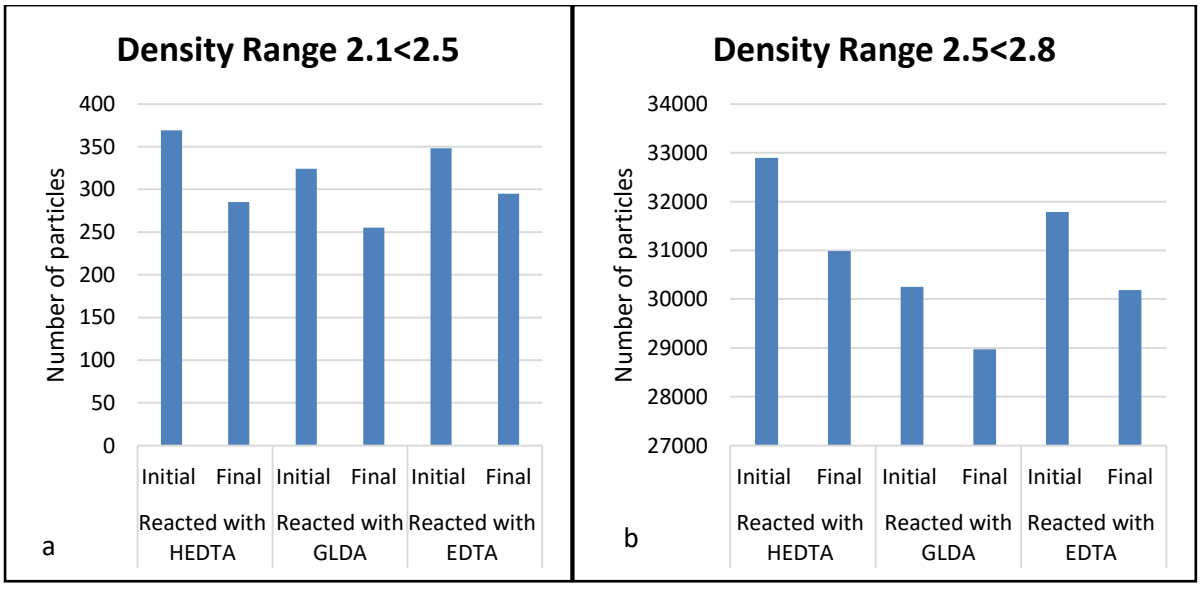

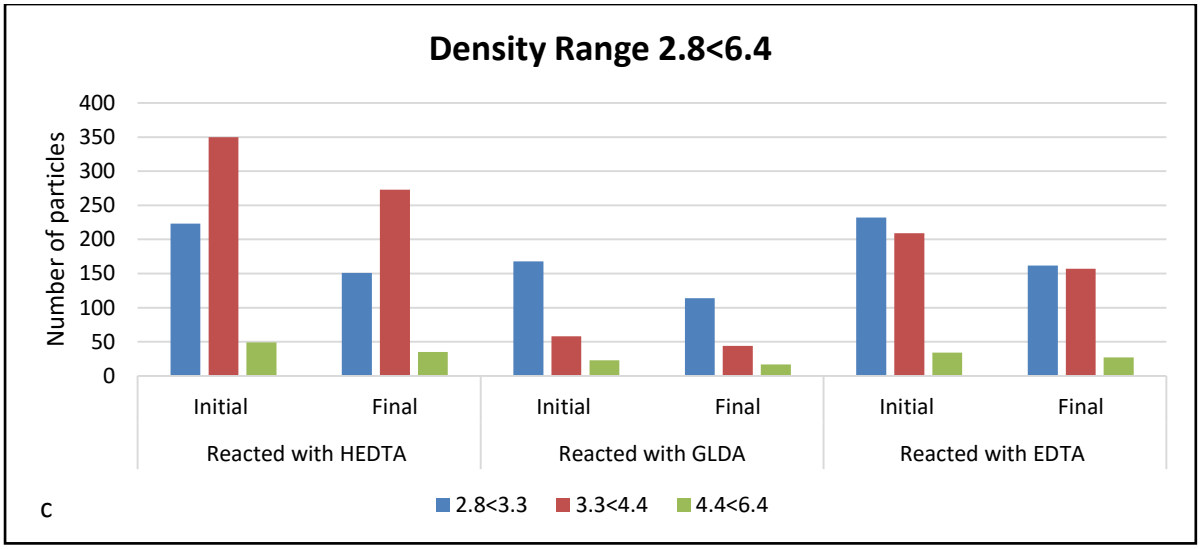

Figure 5.54. Particle Density distribution in Berea Sandstone before and after reaction with chelating agents

5.4.2 Reacted with Colton Sandstone

In this section, the effects of all three chelating agents on Colton sandstone core samples were discussed and analyzed. These acids were applied on unreacted Colton sandstone core samples instead of pre-flushed samples to see the effects of chelates on all minerals present inside the core samples.

5.4.2.1 Elemental analysis

The Colton sandstone is a tight sandstone, homogeneous in nature, and consists of different types of other minerals and less amount of quartz (dirty sandstone). As it is homogeneous, therefore, the initial elemental composition can be used for elemental analysis for all samples reacted with chelates. HEDTA chelate showed good dissolving power towards calcium and barium compared to other chelates applied, while EDTA showed dissolving power towards sodium and magnesium as seen in Figure 5.55. But overall dissolution in Colton sandstone was less as compared to the effects of these chelates on Berea sandstone, most probably due to the tight nature of the Colton sandstone. Due to this tight nature of the Colton sandstone, most of the pores are very small and do not allow chelates to enter because of the capillary nature of the pores. Therefore, as a result, the dissolution is less compared to the conventional sandstone.

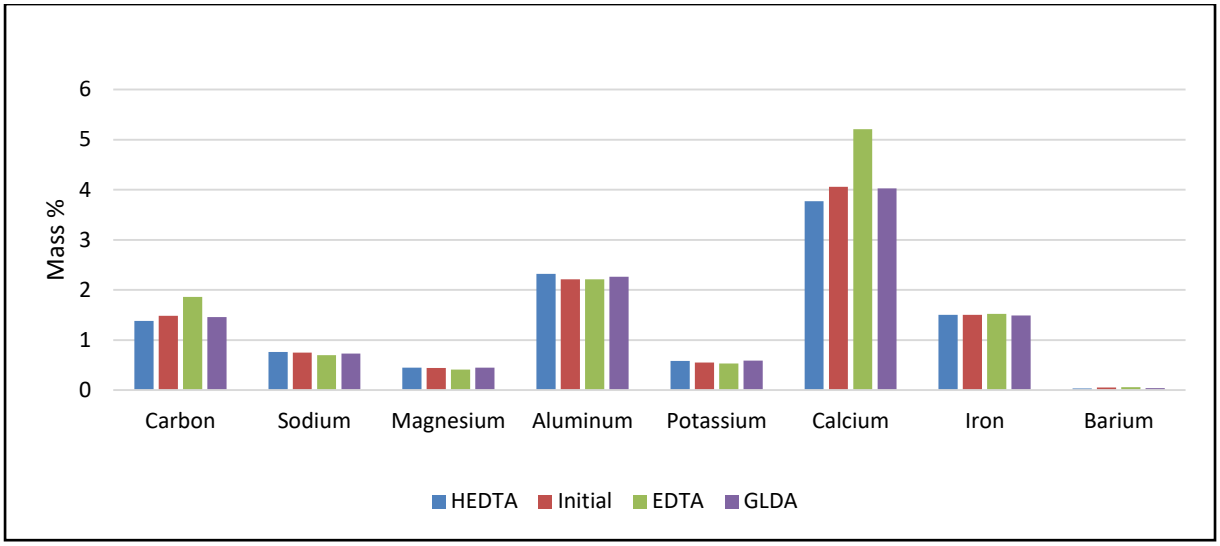

Figure 5.55. Elemental mass in Colton Sandstone before and after reaction with chelating agents

5.4.2.2 Element Deportment

Figure 5.56 represents the presence of silicon element in the form of different minerals. These were complex minerals of magnesium, calcium, manganese, and iron. Figure 5.56 clearly showed that albite and Magnesiogedrite minerals present in the Colton sandstone were dissolved by HEDTA chelate, while only trace amount of albite was dissolved by GLDA. Other minerals were insoluble by all the chelates applied, which resulted in less change in deportment of the elements present inside that mineral.

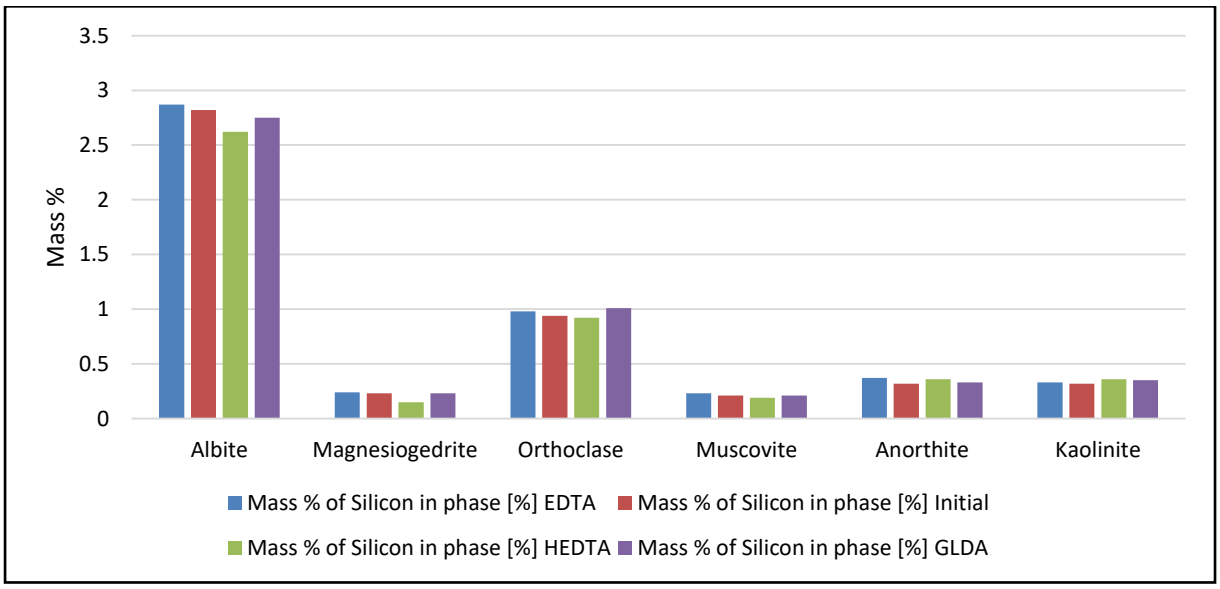

Figure 5.56. Silicon deportment in Colton Sandstone before and after reaction with chelating agents

Iron was found in the form of ankerite and magnetite in Colton sandstone. These minerals had been dissolved by the applied chelates in Berea sandstone. On the contrary, these chelates did not found to be effective in dissolving these minerals in the Colton sandstone; most probably due to its tight nature where minerals were bounded together. Figure 5.57 demonstrated that HEDTA chelate dissolved some concentration of all the minerals in which iron was present compared to other chelates which were not effective.

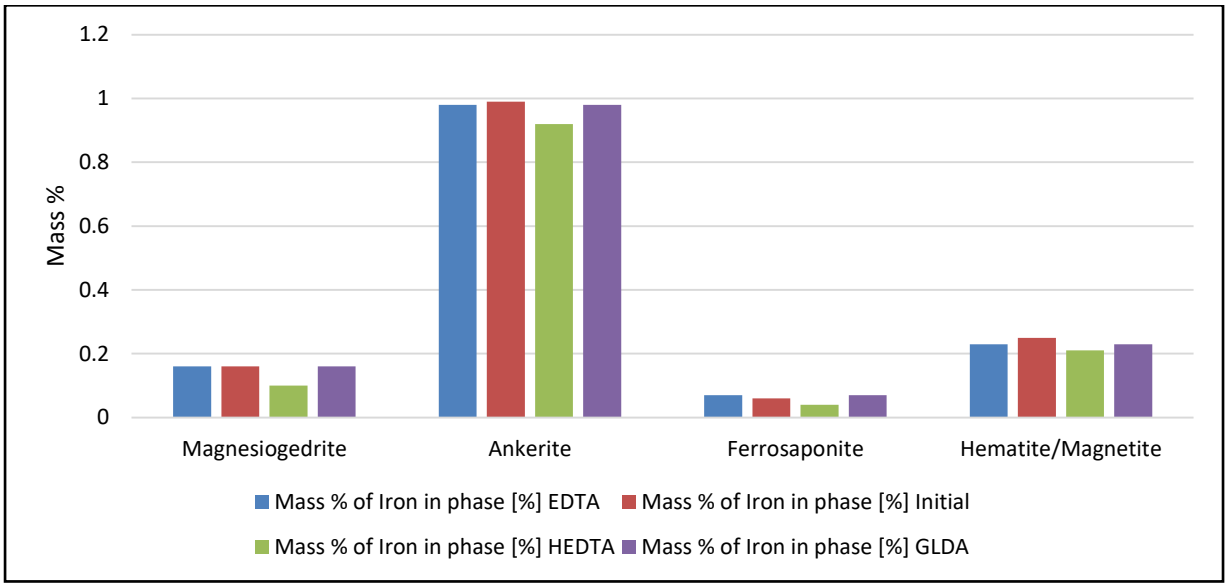

Figure 5.57. Iron deportment in Colton Sandstone before and after reaction with chelating agents

Figure 5.58 showed that calcium had been present in the form of calcite and was dissolved from Colton sandstone by HEDTA in small quantity, while other chelates remained ineffective. Other minerals like ankerite and albite were also present but their dissolution was very less, and an only trace amount of them had been dissolved by HEDTA and GLDA while EDTA remained ineffective. The ineffectiveness of EDTA is most probably due to its less biodegradability which resulted in less reactive nature of this chelate towards tight sandstone formation. In tight sandstone acidizing, the chelate should be readily biodegradable to ensure its maximum reach inside the capillary pores by reacting with the minerals present inside those pores.

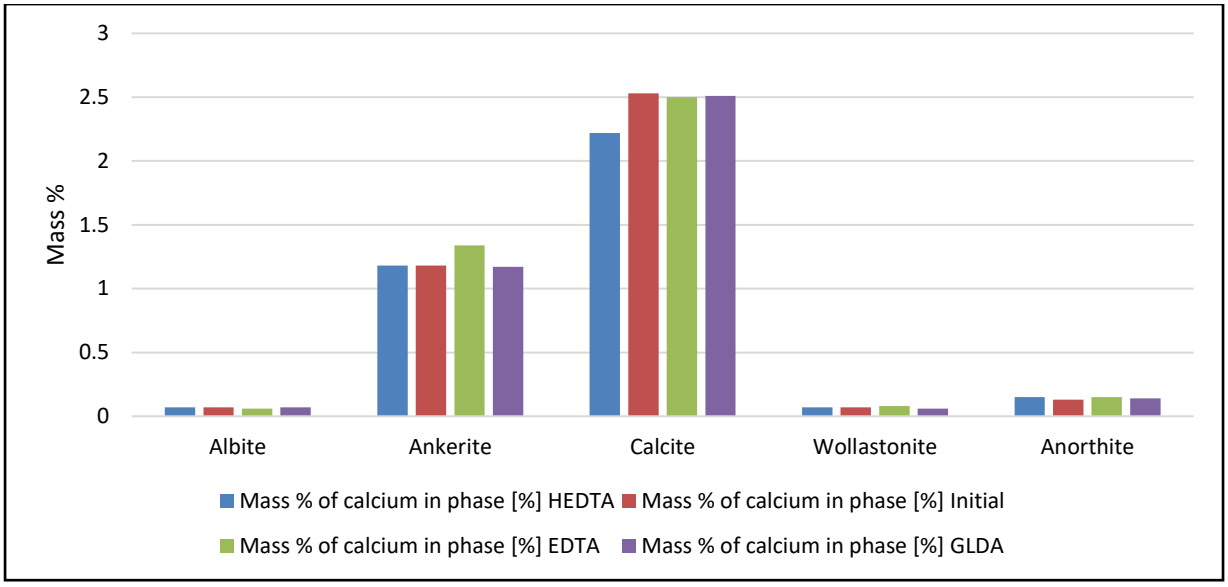

Figure 5.58. Calcium deportment in Colton Sandstone before and after reaction with chelating agents

Carbon was found in the form of ankerite and calcite mentioned in Figure 5.59. As discussed in Figure 5.58, calcite had been dissolved effectively by HEDTA, while other chelates remained ineffective. On the contrary, ankerite was not dissolved by any chelate as discussed earlier in Figure 5.57.

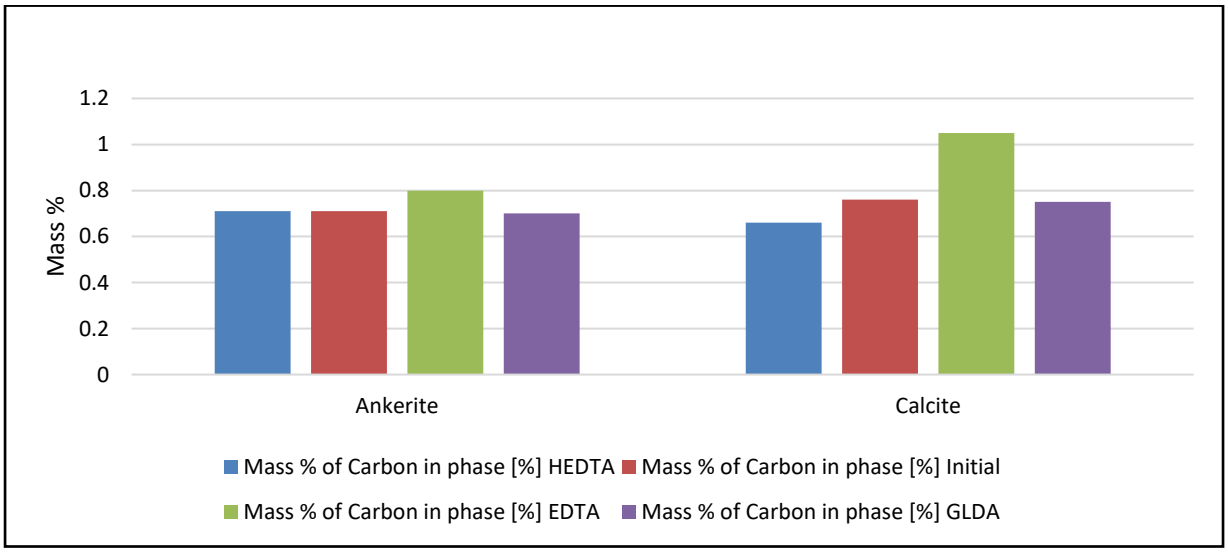

Figure 5.59. Carbon deportment in Colton Sandstone before and after reaction with chelating agents

5.4.2.3 Mineral Analysis

Mineral Analysis is applied to analyses the change in the mineralogy of the core samples before and after acidizing. Change in mineralogy describes the mineral composition of the core sample

which is very important in the analysis of acidizing experiments. It shows the relative decrease or increase of specific minerals and elements. Figure 5.60 represents the mineral mass change in Colton sandstone sample. It can be observed from the results that when HEDTA reacted with the Colton sandstone formation, there is an increase in relative weight of albite and orthoclase due to the decrease in the relative amount of calcite and quartz. While, when the core sample is reacted with EDTA, there is an increase in the relative amount of ankerite, calcite, and kaolinite because of the decrease in the relative weight of Magnesiogedrite, Muscovite and Dolomite. When core sample reacted with GLDA, there is an increase in relative weight of Garnet, orthoclase, and kaolinite because there is a decrease in relative weight of albite and dolomite.

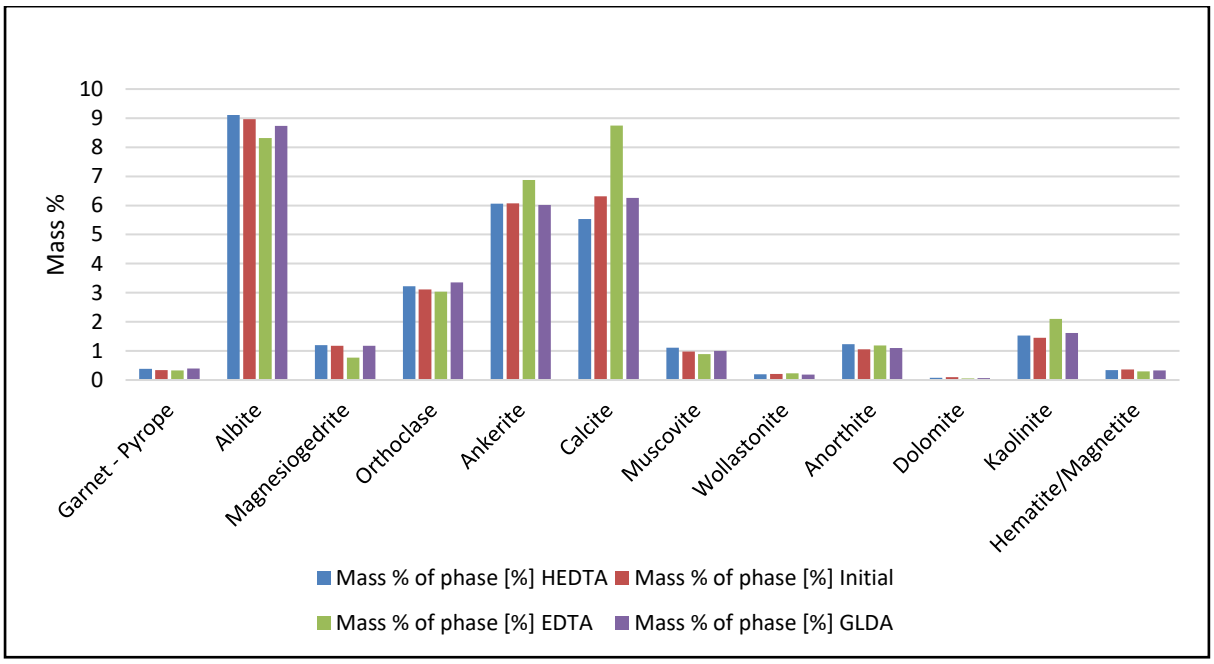

Figure 5.60. Mineral mass in Colton Sandstone before and after reaction with chelating agents

5.4.2.4 Mineral Locking

Figure 5.61 and Figure 5.62 demonstrate the locking of ankerite and calcite minerals respectively with different other minerals present in the Colton sandstone core sample. Mostly they were locked with quartz as seen in Figure 5.61 and 5.62, depicted that the boundary or perimeter of the grain was surrounded mostly by quartz mineral. As quartz was not soluble by these chelates, therefore, ankerite and calcite locked/surrounded with quartz were not dissolved by the applied chelates. That was the reason why ankerite and calcite were dissolved effectively by these chelates in Berea sandstone but not in the Colton sandstone. This locking prohibits the chelating agent to dissolve some minerals effectively as dissolved in Berea sandstone. Mineral

locking of ankerite with calcite has been decreased when reacted with HEDTA, which showed its ability to dissolve calcium element. On the contrary, locking of almost all the minerals with ankerite and calcite was increased when reacted with EDTA, which showed the ineffective chelating effect of this chelate on Colton sandstone formation. Figure 5.62 shows that quartz locking with calcite has been reduced when reacted with HEDTA which indicates that some amount of quartz was dissolved by HEDTA.

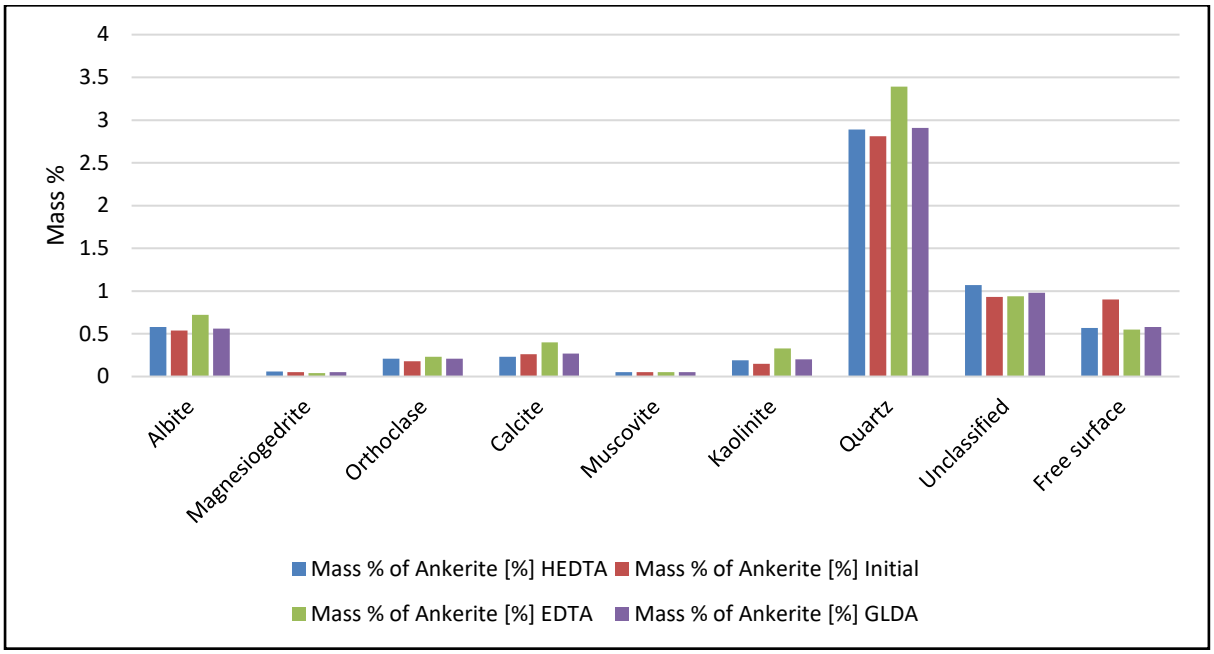

Figure 5.61. Ankerite mineral locking in Colton Sandstone before and after reaction with chelating agents

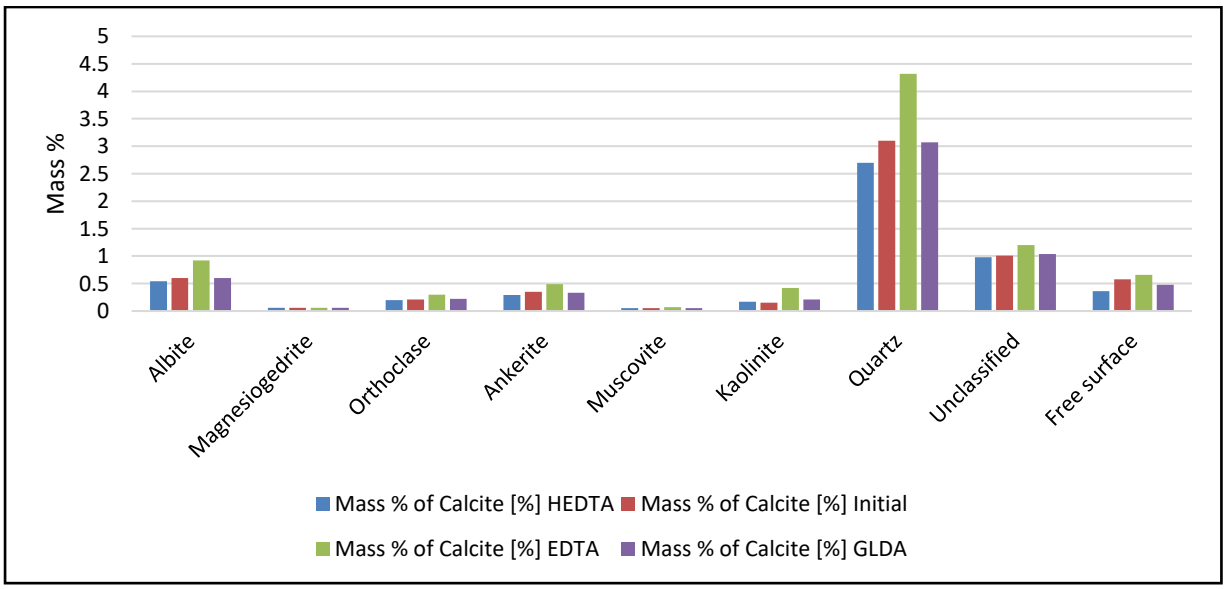

Figure 5.62. Calcite mineral locking in Colton Sandstone before and after reaction with chelating agents

Kaolinite was mainly locked with quartz and exists as a free surface as shown in Figure 5.63. After reaction with the chelates, the mineral locking of different minerals with quartz increased which showed that this mineral was not soluble by all these chelates. Mineral locking increased because the relative mineral mass of kaolinite mineral increased due to insolubility as discussed earlier in Figure 5.60. Due to the increase in the relative mineral mass, the overall mass % locking also increased.

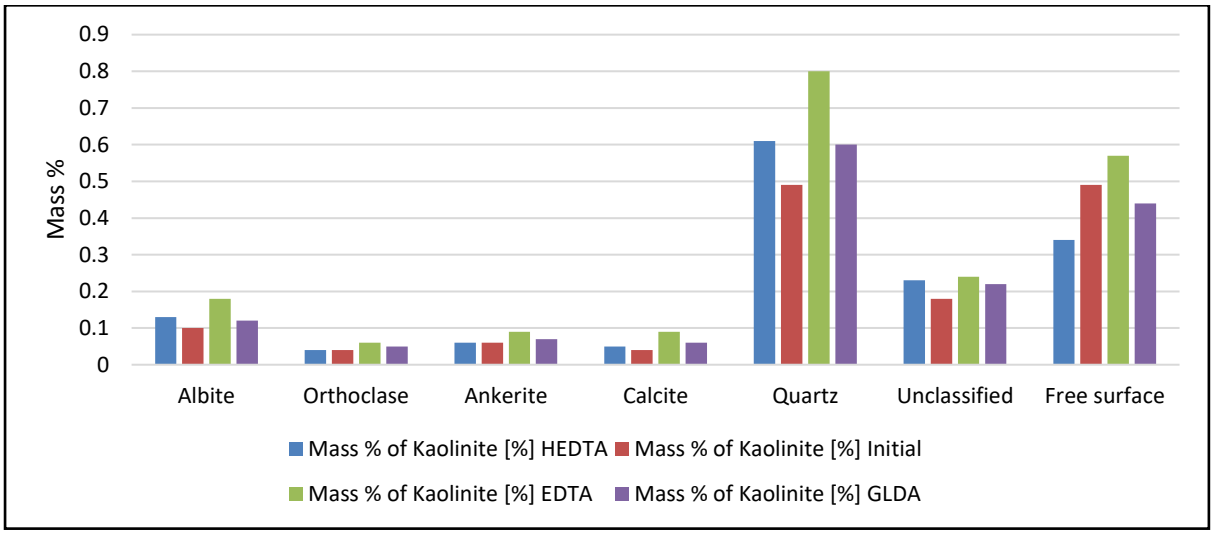

Figure 5.63. Kaolinite mineral locking in Colton Sandstone before and after reaction with chelating agents

Figure 5.64 shows the locking of magnesiogedrite mineral with different other minerals present in the Colton sandstone core sample. The maximum amount of magnesiogedrite was dissolved by EDTA, that's why it's locking with other minerals decreased consequently.

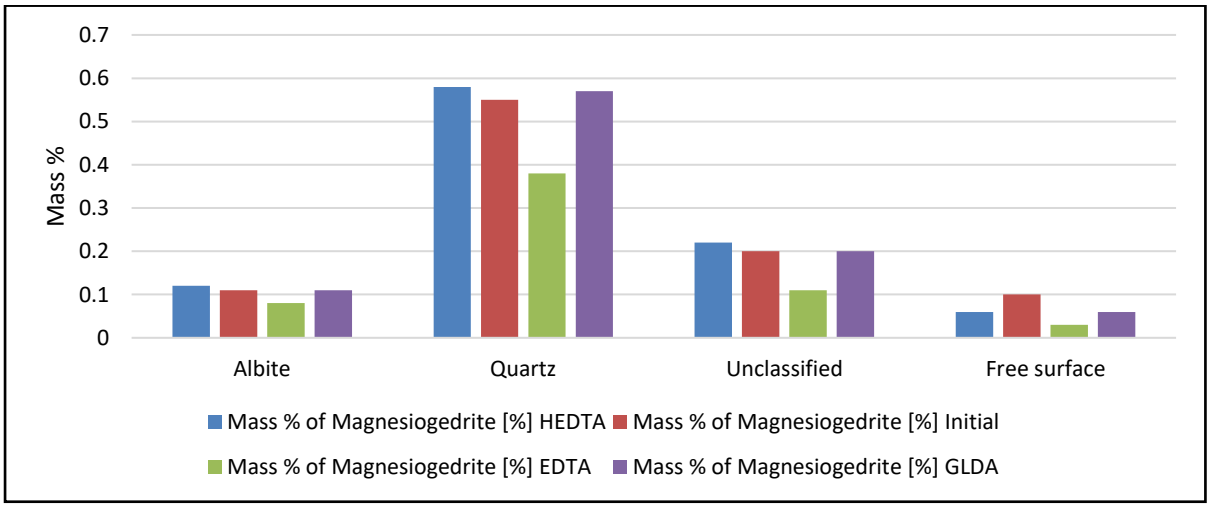

Figure 5.64. Magnesiogedrite mineral locking in Colton Sandstone before and after reaction with chelating agents

5.4.2.5 Grain Size Distribution

The number of grains of different important minerals before and after acidizing was discussed from Figure 5.65 through Figure 5.68. The number of grains of ankerite (Figure 5.65) and calcite (Figure 5.66) has been changed significantly after reacting with GLDA and HEDTA. It indicated that these minerals have been dissolved by the applied chelates. Conversely, the change in the number of grains of orthoclase was not significant (Figure 5.67), an only a small number of grains has been dissolved by EDTA and HEDTA. The number of grains of quartz has been reduced in small quantity also (Figure 5.68). Despite quartz being insoluble in these acids, the decrease in the number of grains showed the effective dissolution of free grains of quartz, mostly by HEDTA. This validates the results discussed earlier in mineral mass analysis.

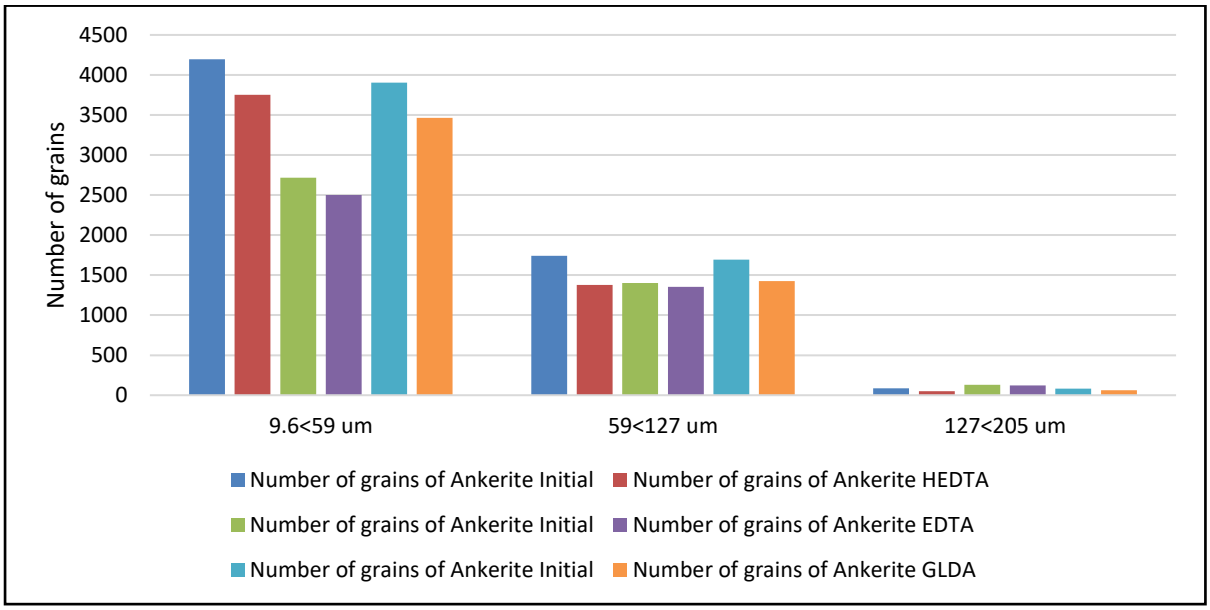

Figure 5.65. Grain size distribution of ankerite in Colton Sandstone before and after reaction with chelating agents

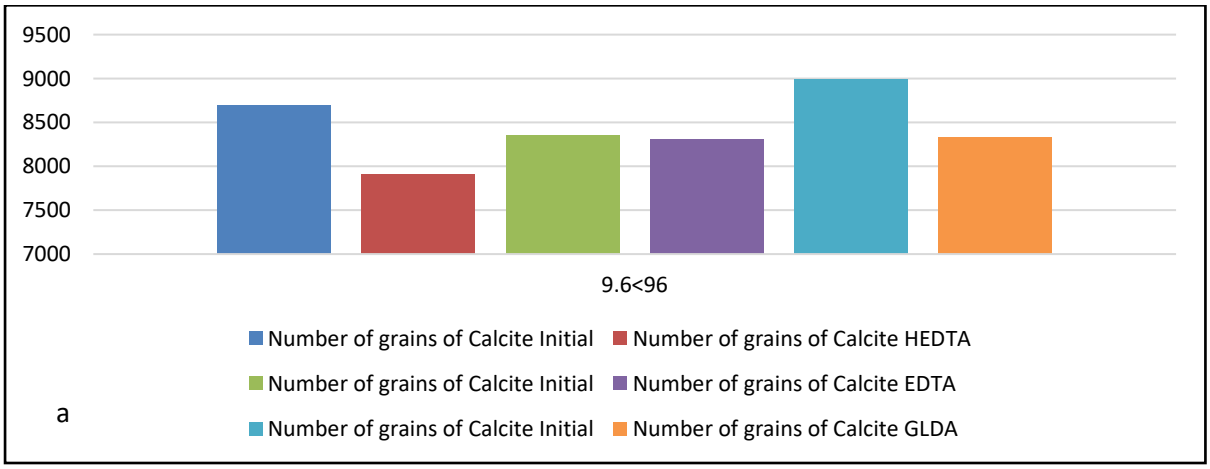

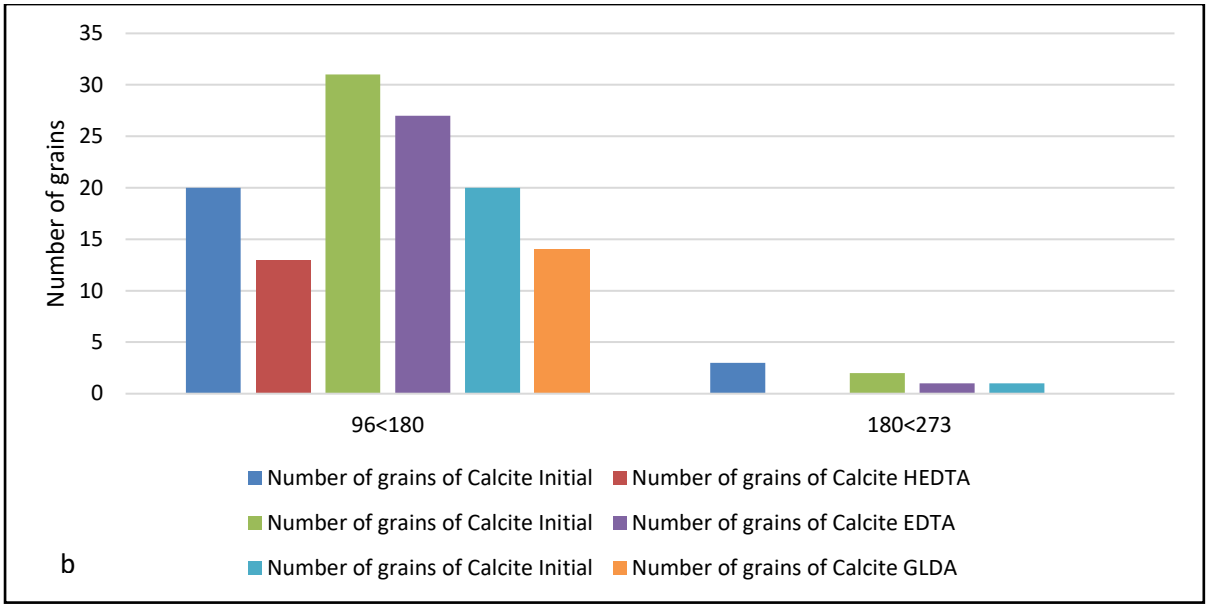

Figure 5.66. Grain size distribution of calcite in Colton Sandstone before and after reaction with chelating agents

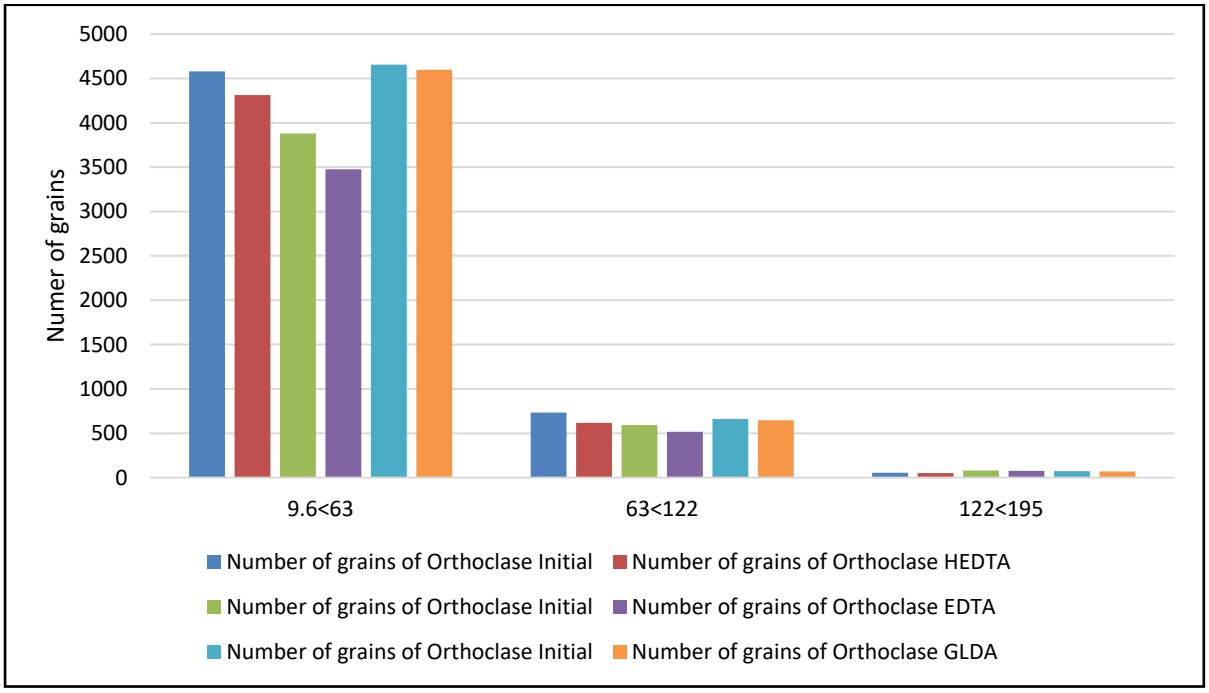

Figure 5.67. Grain size distribution of orthoclase in Colton Sandstone before and after reaction with chelating agents

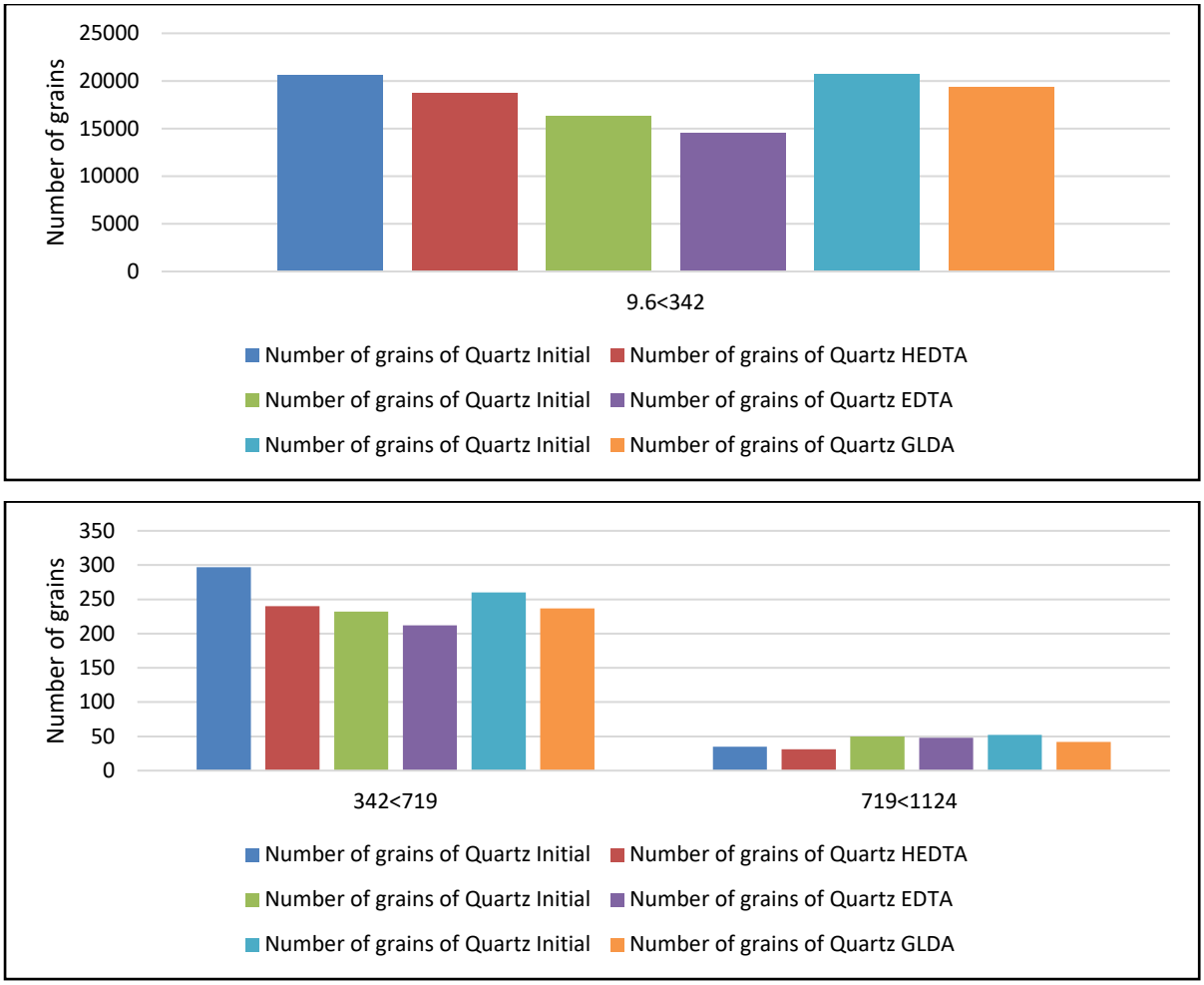

Figure 5.68. Grain size distribution of quartz in Colton Sandstone before and after reaction with chelating agents

5.4.2.6 Panorama

Figures 5.69 through Figure 5.74 represent the BSE images of the Colton sandstone core sample before and after the reaction with different chelating agents. Black dots represent the pore spaces present inside the sample while dark grey grains represent the matrix which was quartz in case of sandstone sample. The bright or light grey spots represent the presence of different minerals other than quartz. Figure 5.69 and Figure 5.70 represents the complete panorama and more focused images respectively of the core sample reacted with GLDA. Both Figures signified the dissolution of minerals in the core sample when reacted with GLDA.

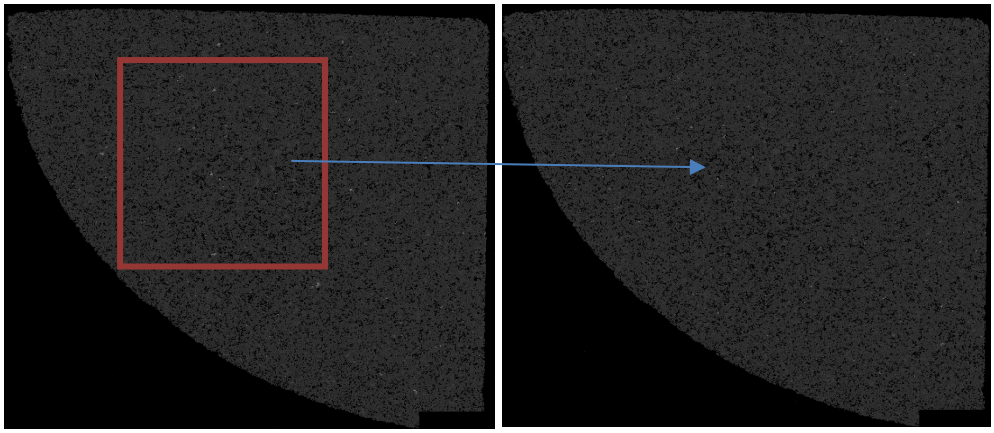

Figure 5.69. Dissolution of minerals when Berea sandstone reacted with GLDA unreacted sample (left), reacted (right)

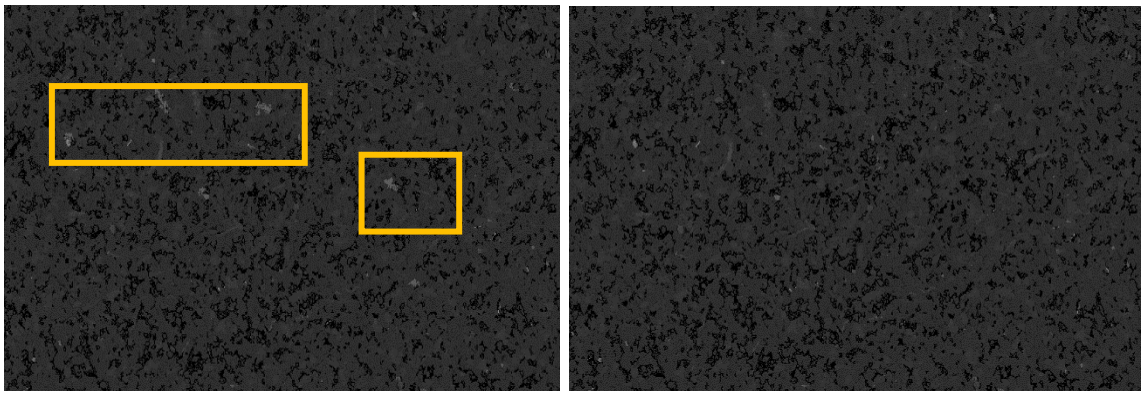

Figure 5.70. Pore spaces in sandstone when sample reacted with GLDA, unreacted sample (left), reacted (right)

Figure 5.71 and Figure 5.72 represent the complete panorama and more focused images respectively of the core sample reacted with EDTA. Both Figures signified the dissolution of minerals in the core sample when reacted with EDTA. Figure 5.71 was not clear and dissolution cannot be seen clearly but more focused image clearly demonstrated the dissolution of different minerals.

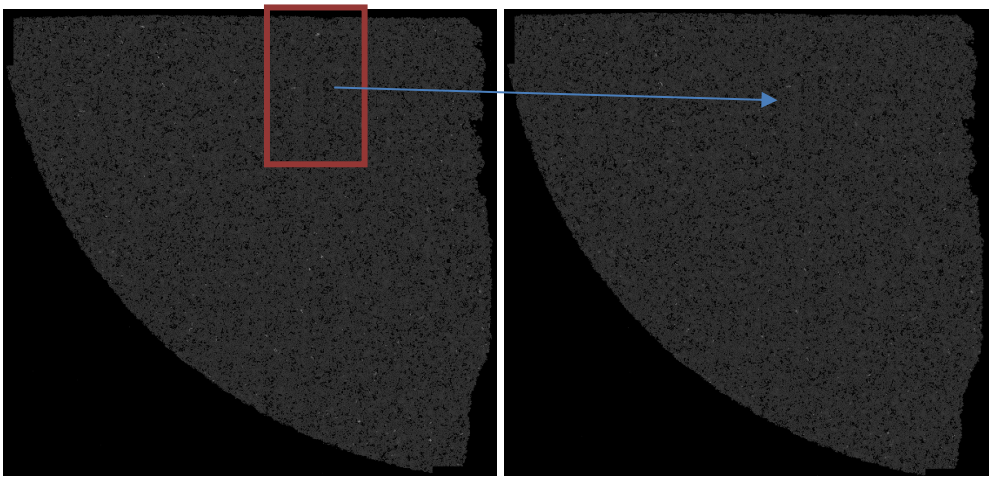

Figure 5.71. Dissolution of minerals when Berea sandstone reacted with EDTA unreacted sample (left), reacted (right)

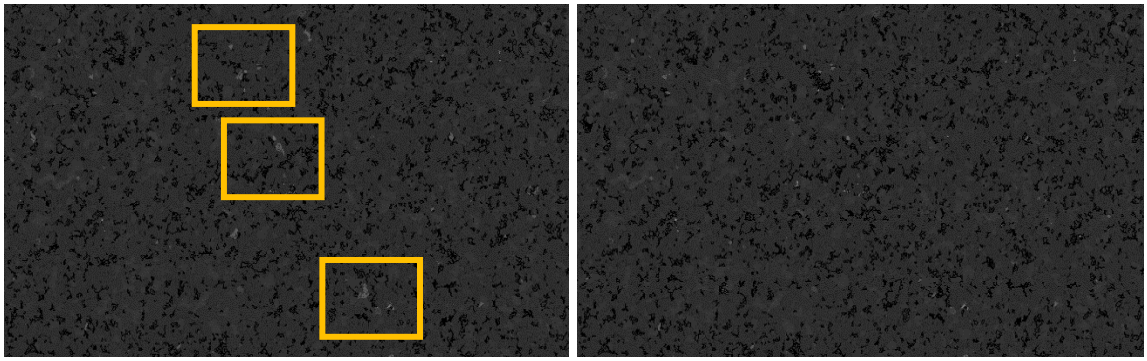

Figure 5.72. Pore spaces in sandstone when sample reacted with EDTA, reacted sample (left), unreacted (right)

Figure 5.73 and Figure 5.74 represent the complete panorama and more focused images respectively of the core samples reacted with HEDTA. Both Figures signified the dissolution of minerals in the core sample when reacted with HEDTA. To summarize, if all the pictures considered, it seems reasonable to conclude that these chelating agents were effective in creating fresh pore spaces in the sandstone core sample.

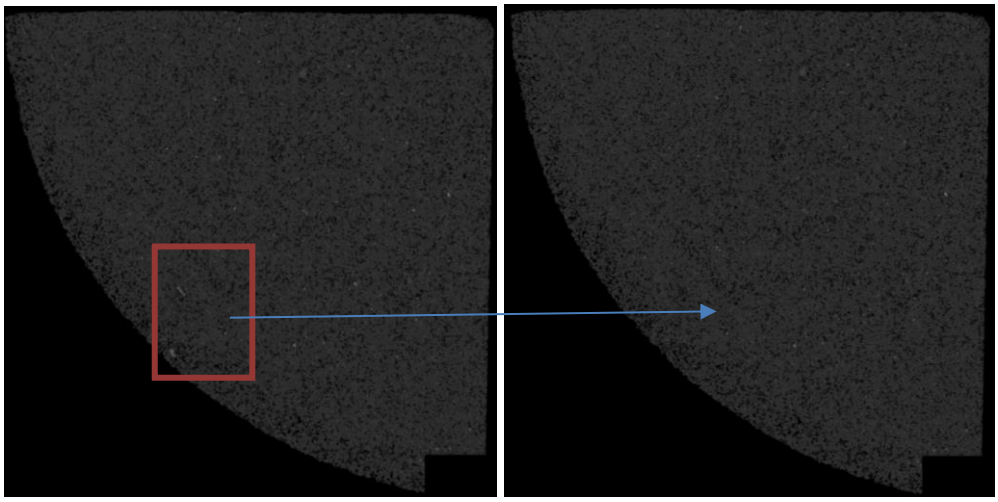

Figure 5.73. Dissolution of minerals when Berea sandstone reacted with HEDTA unreacted sample (left), reacted (right)

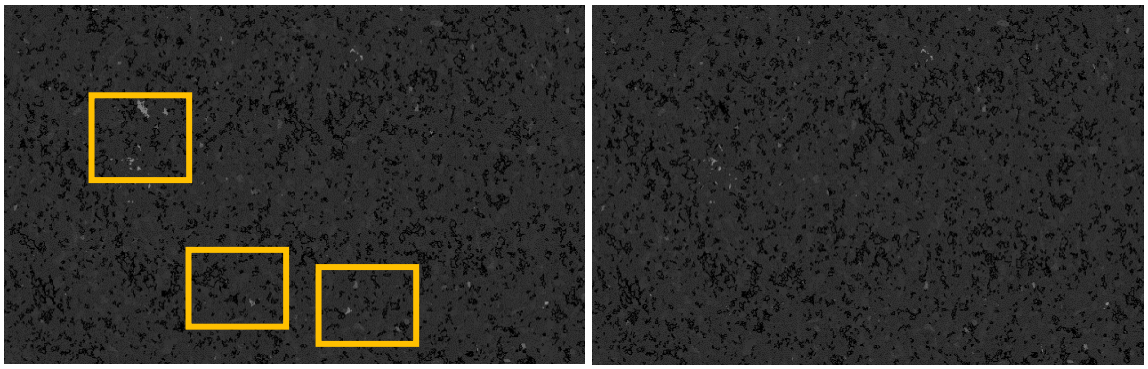

Figure 5.74. Pore spaces in sandstone when sample reacted with HEDTA, reacted sample (left), unreacted (right)

5.4.2.7 Porosity Distribution

Porosity distribution represents the concentration of different size of pores in the core sample. It can be evaluated to determine the creation of new pores before and after acidizing of core samples. Table 5.3 represents the distribution of small, medium and large pore holes in sandstone samples reacted with different chelating agents. Note that the initial concentration of small holes is very high as the sample is tight sandstone. The increase in small holes can be observed when the sample is reacted with chelate with the highest number of small pores increment in case of HEDTA.

New small pores; 4627, 1651 and 2843, were created in the core sample when reacted with HEDTA, EDTA, and GLDA respectively. It shows the effective action of HEDTA on Colton sandstone samples. The increment of medium and large size pore spaces is negligible by all chelates. The change in porosity is mainly due to the creation of small new pore spaces after

the reaction. The less increment of pore spaces by EDTA may be attributed to the precipitation of minerals inside the pore spaces.

Table 5.3. Initial and final pore size distribution of Colton sandstone

Size range / Number of holes	**Reacted with HEDTA**		**Reacted with GLDA**		**Reacted with EDTA**	
	Initial	HEDTA	Initial	GLDA	Initial	EDTA
9.6 – 33 µm	52,590	57,217	53,780	55,431	46,252	49,095
33 – 68 µm	862	871	1,371	1,373	1,390	1,393
68 – 98 µm	5	7	16	16	17	17
Total	53,457	58,095	55,167	56,820	47,659	50,505

5.4.2.8 Particle Size distribution

Figures 5.75 (a, b, c) represent the change in the number of different size of particles before and after the acidizing in a sandstone formation. HEDTA dissolved a large number of small grain particles, where 15,202 particles were dissolved while EDTA dissolved 13,131 and GLDA dissolved around 11,581 particles. If these results are compared with the mineral analysis mentioned in Figure 5.60; HEDTA was good in the dissolution of quartz and calcite compared to EDTA and GLDA mentioned in table E.15 (Appendix E). Size of calcite grain was small and thus a lot of small particles were dissolved as HEDTA was good in chelating calcite and also dissolved small quantities of ankerite. The ankerite particles were usually large in size, which represents the dissolution of large size particles by HEDTA.

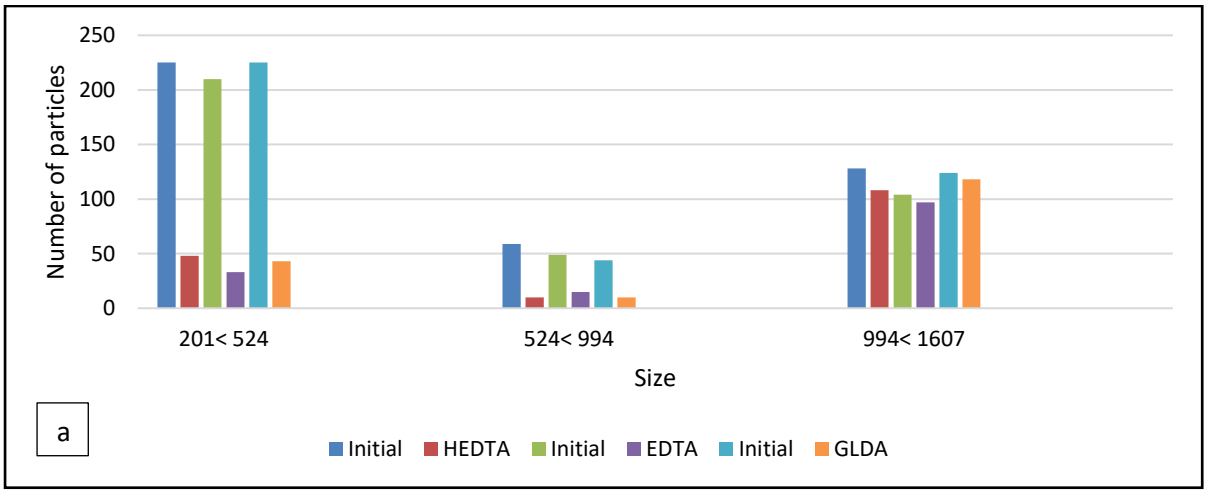

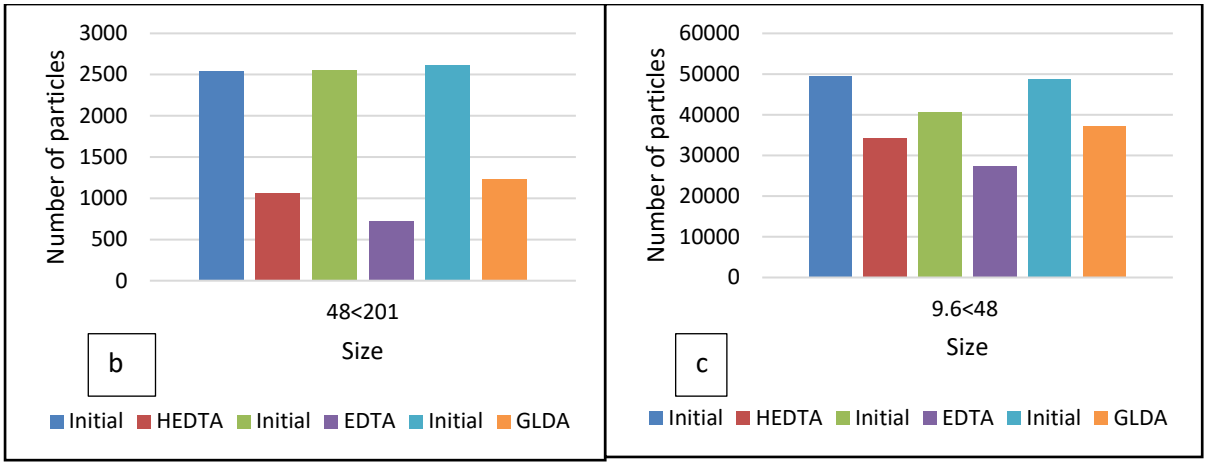

Figure 5.75. Number of Particles in Colton Sandstone before and after reaction with chelating agents

5.4.2.9 Density Distribution

Particles density distribution represents the number of particles in certain density range presented in Figures 5.76 (a, b, c). The sample acidized was Colton sandstone, while the density of sandstone was around 2.65 g/cm^3. Consequently, Figure 5.76b showed most number of particles in the range 2.4 < 2.8 g/cm^3. The power of these agents in dissolving light particles like orthoclase was not effective discussed earlier and confirmed/validated by Figure 5.76a, where the change in number of light/less dense particles was less. On the other hand, a heavy particle like ankerite (2.97 g/cm^3) was dissolved effectively shown in Figure 5.76c.

Figures 5.76a illustrated that some amount of heavy particles ranged from 3.7 < 10 g/cm^3 have been dissolved during acidizing with these chelates especially when reacted with HEDTA. Likewise, Figure 5.76c depicted that minerals in the range of 2.8 < 3.7 g/cm^3 have been dissolved effectively by all chelates. To summarize, all of these applied chelates dissolved a large number of particles in each density range. Figure 5.77 showed minerals with different density values. These results can be validated from the previous analysis, where these acids dissolved minerals of interest, reduced number of grains of different minerals and created fresh pore spaces of different micron sizes.

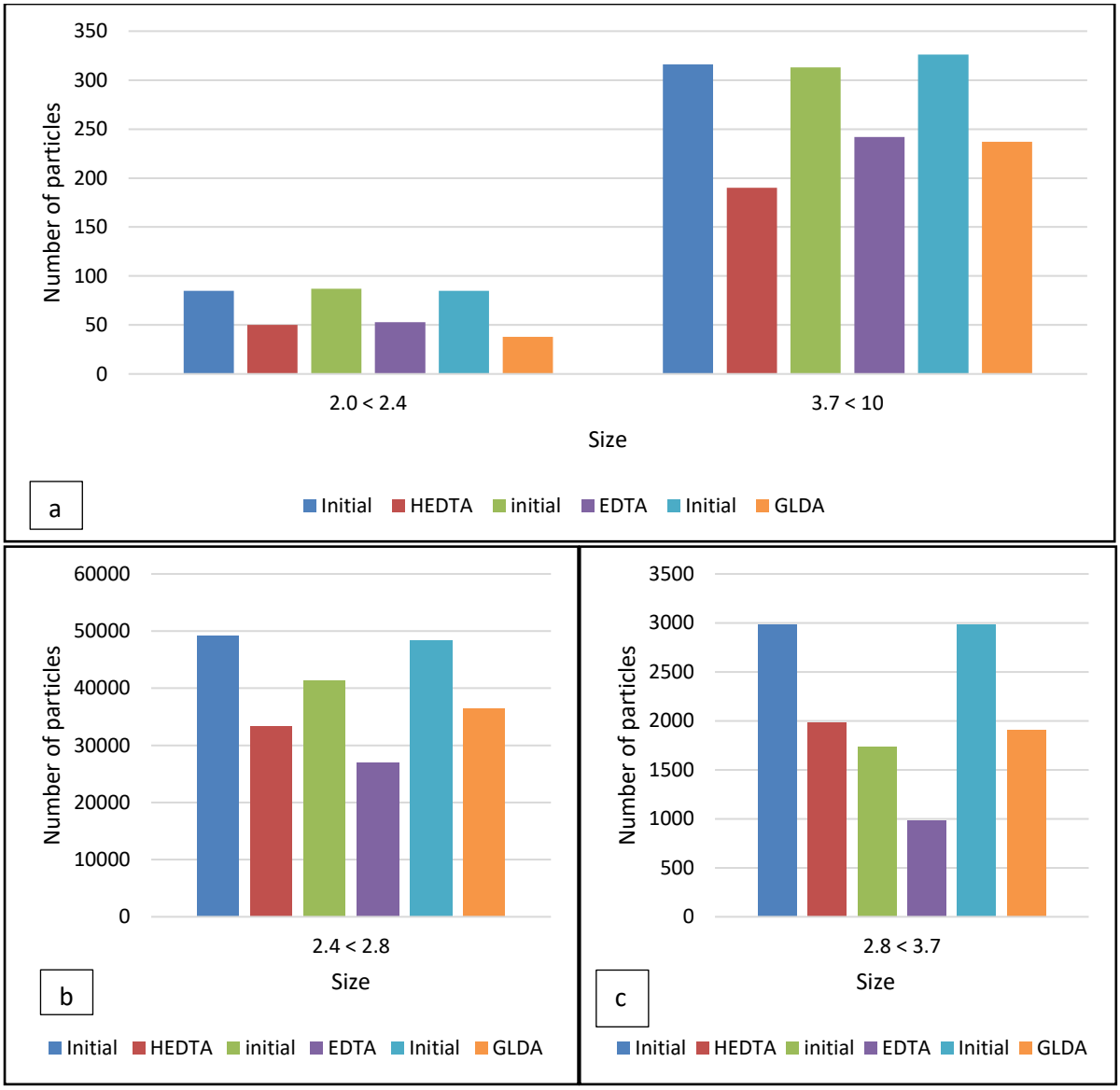

Figure 5.76. Particles density distribution in Colton Sandstone before and after reaction with chelating agents

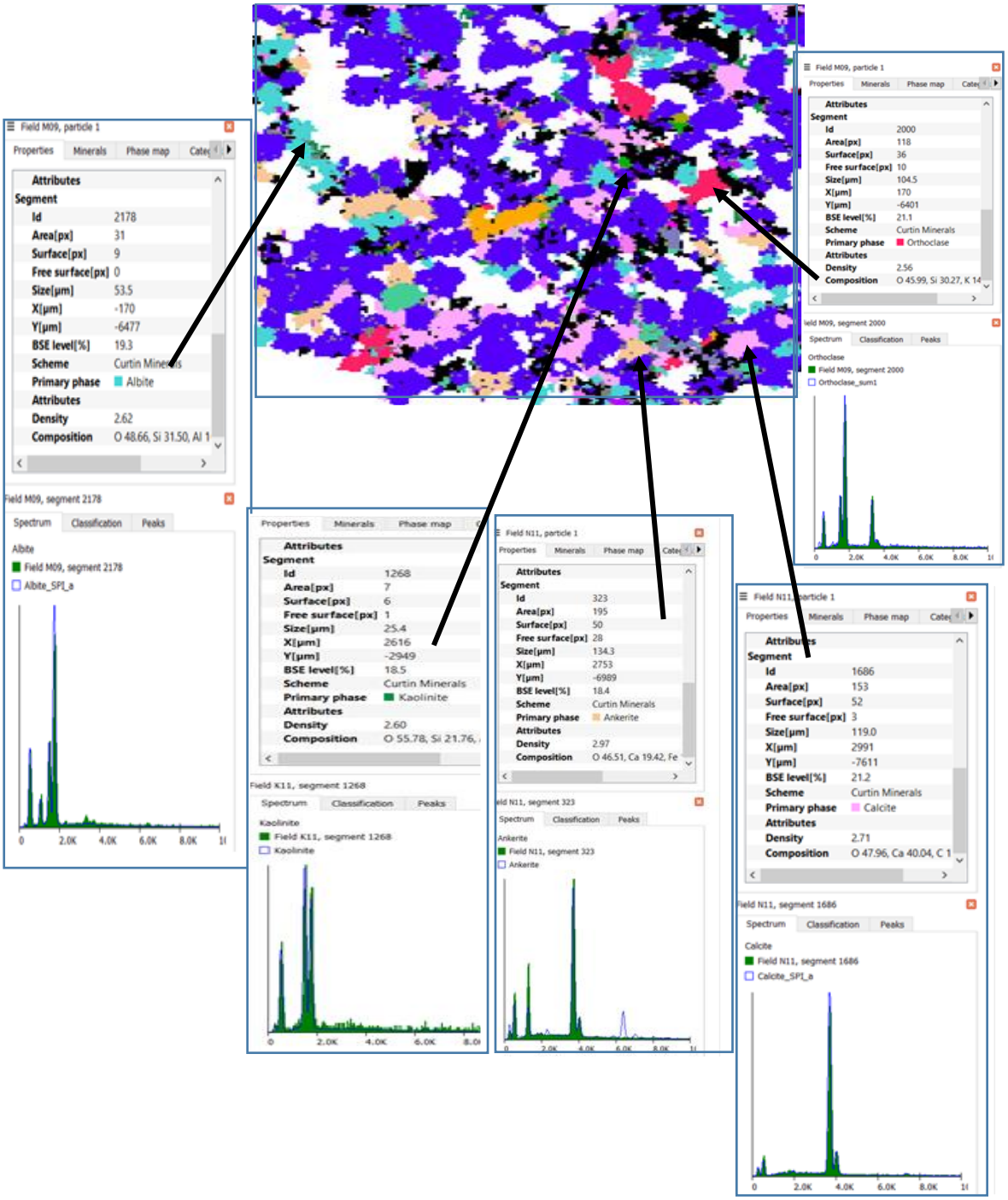

Figure 5.77. Density pattern of different particles present in Colton sandstone Core sample

5.4.3 Reacted with Guelph Dolomite

In this section effects of all three chelating agents on Guelph dolomite core samples had been discussed and analyzed. These acids were applied on unreacted Guelph dolomite core samples instead of pre-flushed samples to see the effects of chelates on all minerals present inside the core samples.

5.4.3.1 Elemental analysis

The Guelph dolomite is a type of carbonate mostly consist of ankerite, heterogeneous in terms of permeability and porosity, and consists of small amount of other minerals like calcite and dolomite. As it is homogeneous in terms of mineralogy, therefore, the same initial elemental composition can be used for elemental analysis of all samples reacted with chelates. Elemental composition (Figure 5.78) did not signify any changes after acidizing. The most probable reason behind this can be attributed to the high concentration of ankerite mineral, which is a matrix (insoluble) in case of Guelph dolomite sample. On the other hand, ankerite mineral was dissolved by these chelates effectively when reacted with sandstone formation. Despite this not good elemental analysis, rest of the analysis was performed to further clarify the reaction mechanism of these chelates with dolomite formation.

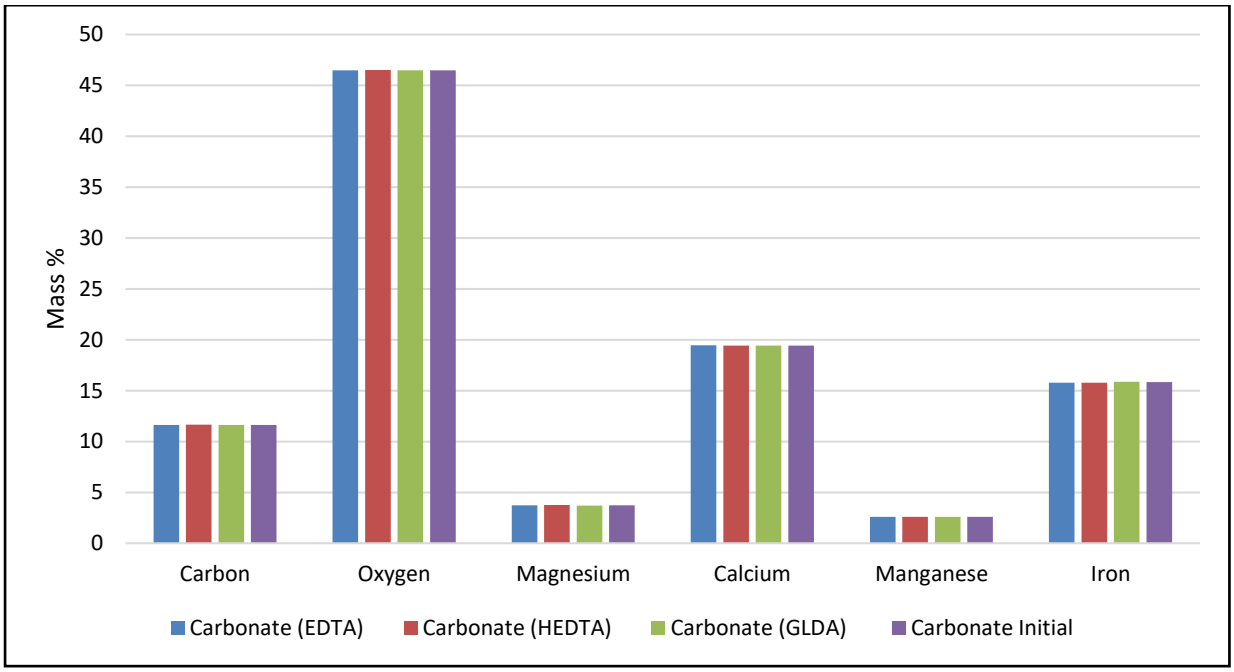

Figure 5.78. Elemental mass of Guelph dolomite before and after reaction with chelating agents

5.4.3.2 Deportment

As discussed earlier, deportment shows the presence of an element of interest in certain minerals. Figure 5.79 shows the presence of calcium in dolomite and calcite present inside the Guelph dolomite core sample. The Figure elaborated that calcium was dissolved by GLDA from both minerals to some extent compared to other chelates. These results did not satisfy elemental analysis, which showed no dissolution of elements. This can be explained by the fact that elemental analysis is relative analysis, means if one element dissolved and the second element remained undissolved then the percentage of second element increases. Consequently, if both elements are dissolved in equal percentage then relative mass remains the same for both of them.

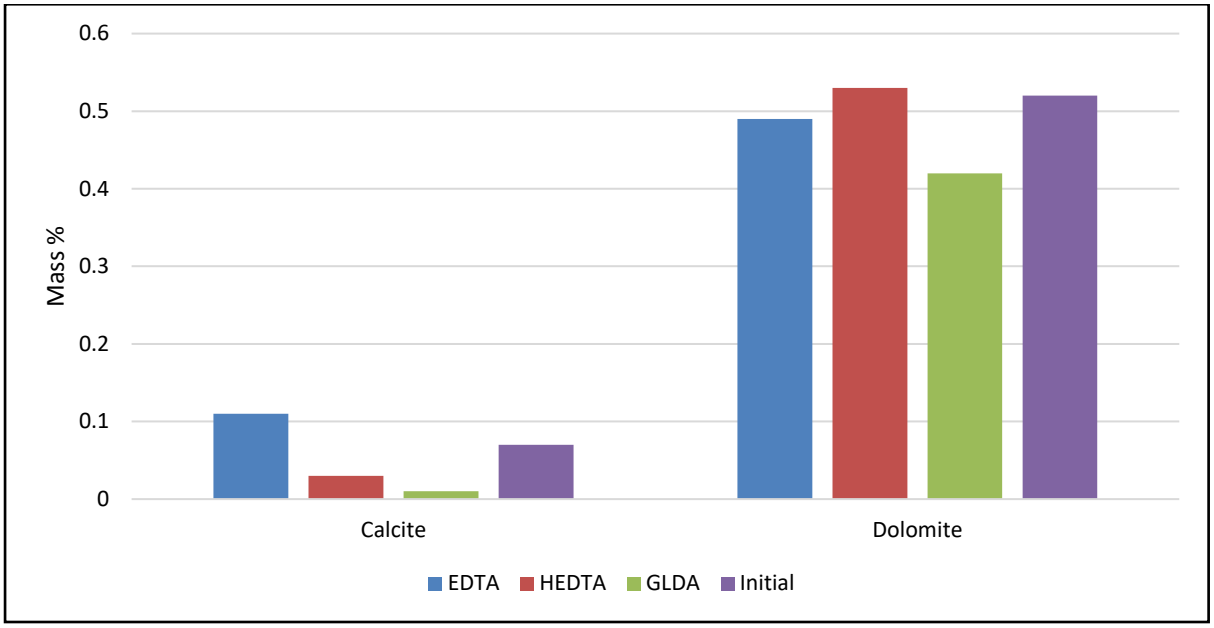

Figure 5.79. Calcium deportment in Guelph dolomite before and after reaction with chelating agents

Magnesium is present in the form of ankerite and dolomite. Ankerite was not dissolved by any of these chelates as explained before, while on the other hand, a small amount of dolomite was dissolved by GLDA as mentioned in Figure 5.79 and Figure 5.80.

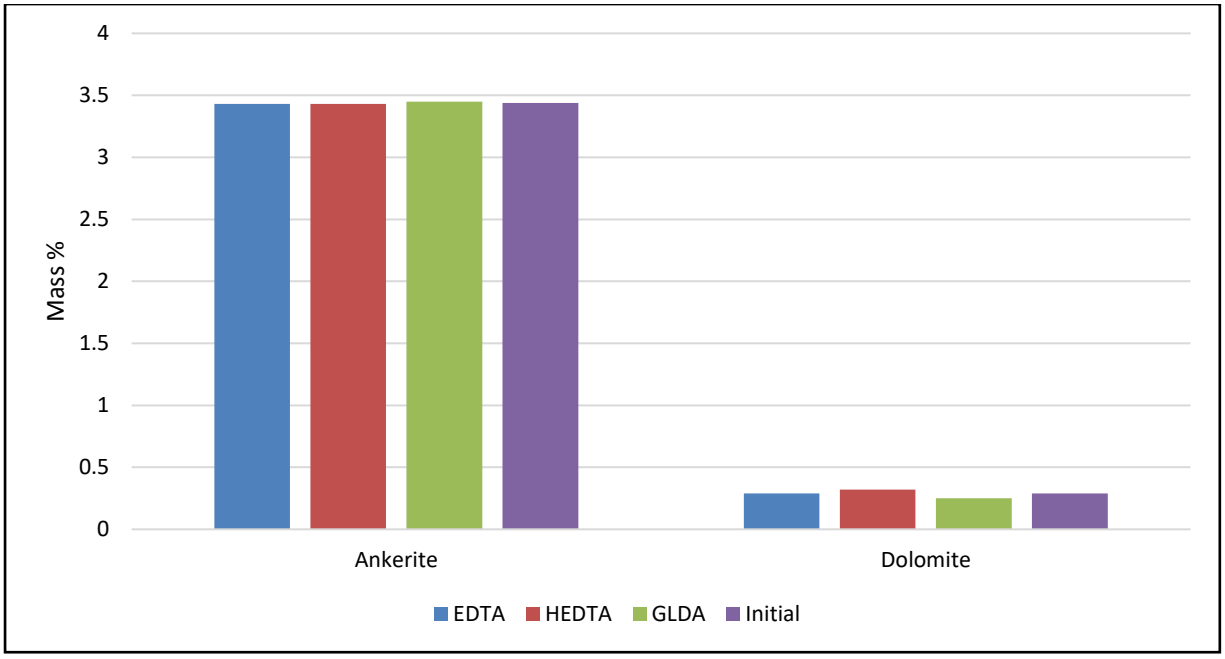

Figure 5.80. Magnesium deportment in Guelph dolomite before and after reaction with chelating agents

5.4.3.3 Mineral Analysis

Figure 5.81 represents the mineral mass change in dolomite sample after reaction with all three chelates. There was an increase in relative weight of dolomite, which is the indication of dissolution of other minerals (Appendix F, Table F4). HEDTA and GLDA were effective in dissolving calcite ion. A small amount of ankerite had been dissolved by EDTA and HEDTA. The relative weight of quartz has been increased representing no dissolution of this mineral.

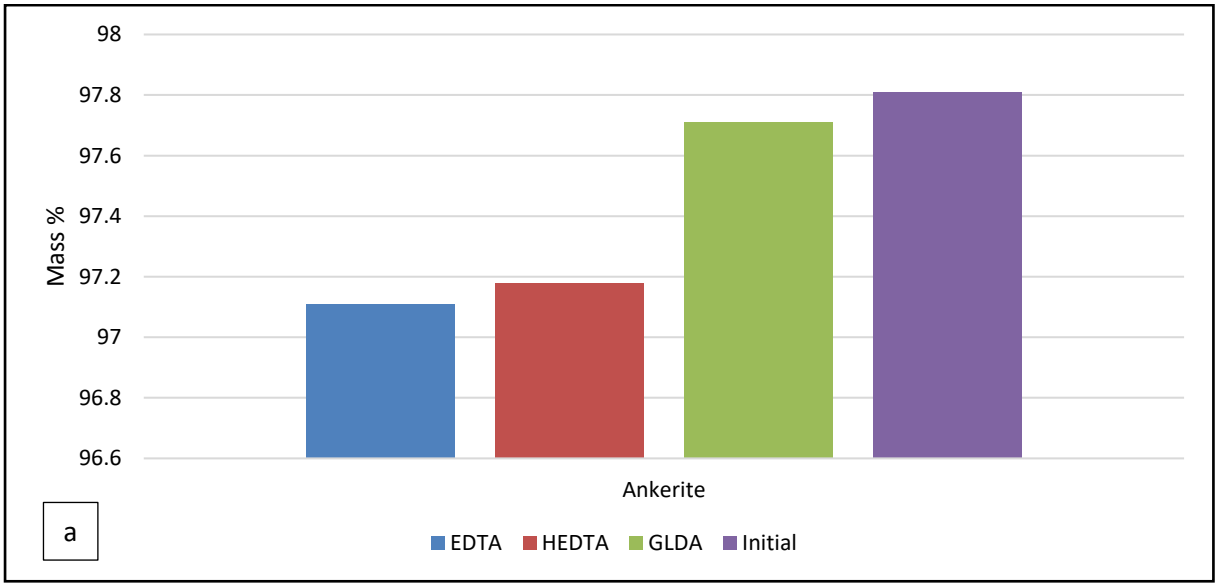

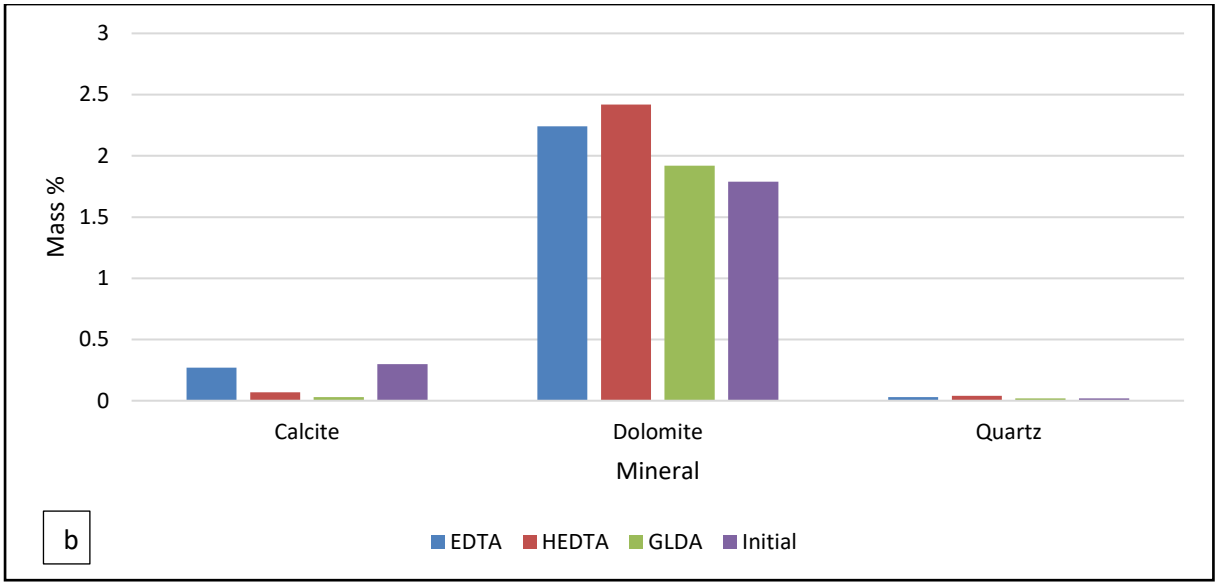

Figure 5.81. Mineral mass in Guelph dolomite before and after reaction with chelating agents

5.4.3.4 Mineral Locking

Calcite mineral was locked with ankerite and dolomite present inside the core sample as mentioned in Figure 5.82. Most of the mineral locking of calcite with ankerite and dolomite has been removed efficiently when reacted with GLDA and HEDTA, while the effect of EDTA was negligible. This illustrated that the usage of HEDTA and GLDA can be effective in dolomite acidizing.

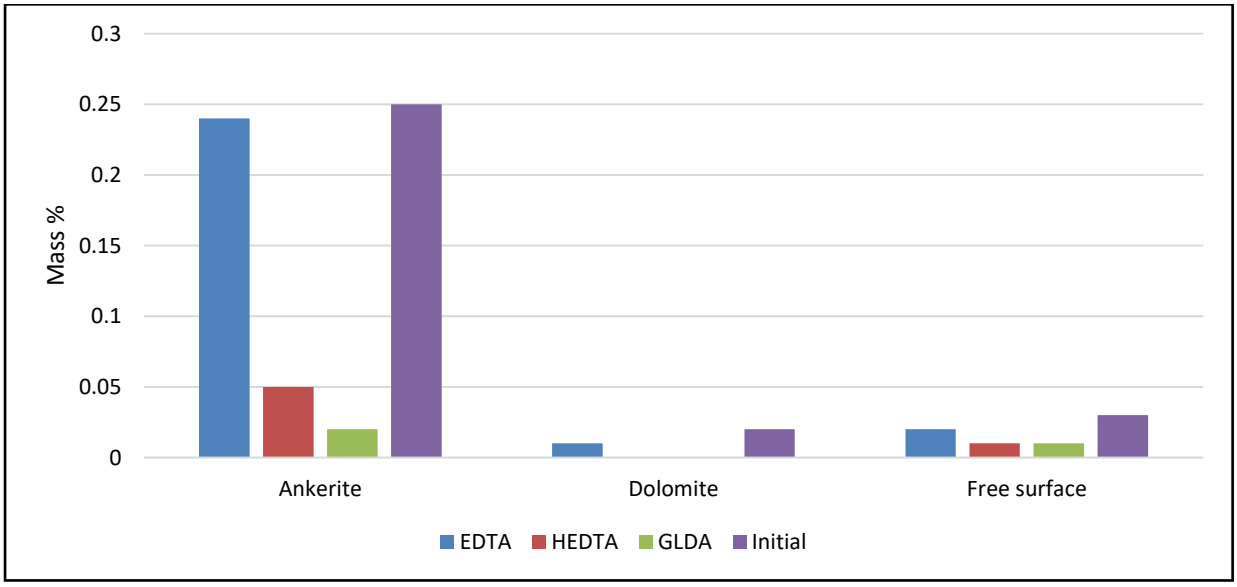

Figure 5.82. Calcite Mineral Locking in Guelph dolomite before and after reaction with chelating agents

Dolomite mineral was locked with ankerite only and exist as a free surface as shown in Figure

5.81. As dolomite mineral was insoluble by all three chelates, consequently the relative mineral mass increased as a result of the dissolution of other minerals especially calcite as discussed in Figure 5.82. This dissolution of calcite was also responsible for the increase in the free surface area of the dolomite.

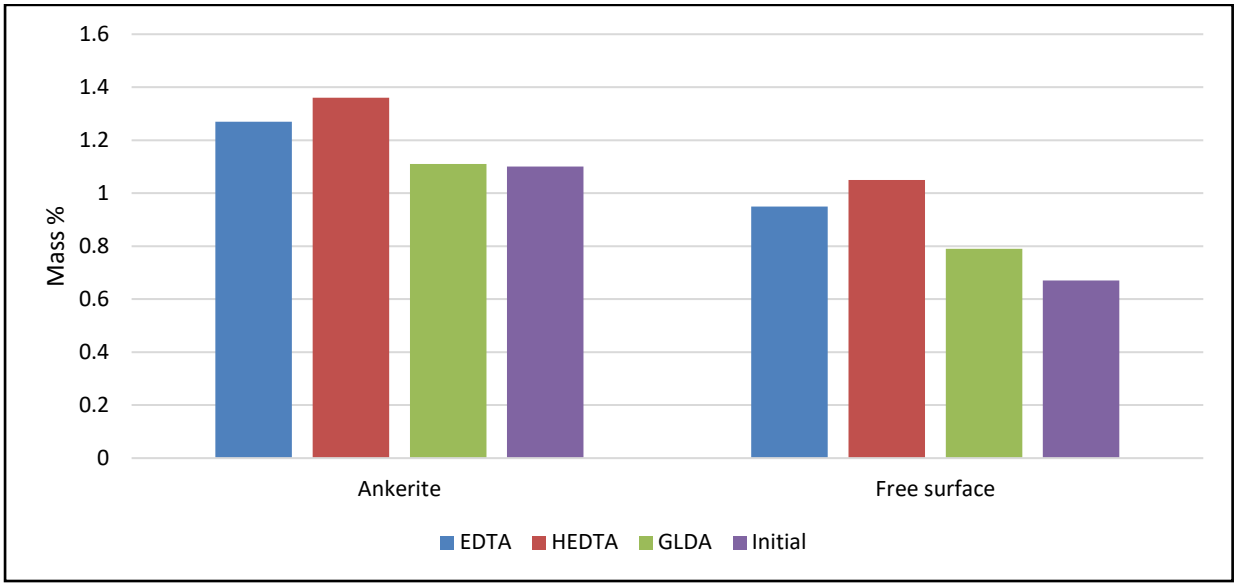

Figure 5.83. Dolomite Mineral Locking in Guelph dolomite before and after reaction with chelating agents

Ankerite mineral was locked with calcite, dolomite, and quartz as shown in table F.7. There was no significant change observed in the locking of ankerite with other minerals because of its insolubility in the applied chelates mentioned in Figure 5.84.

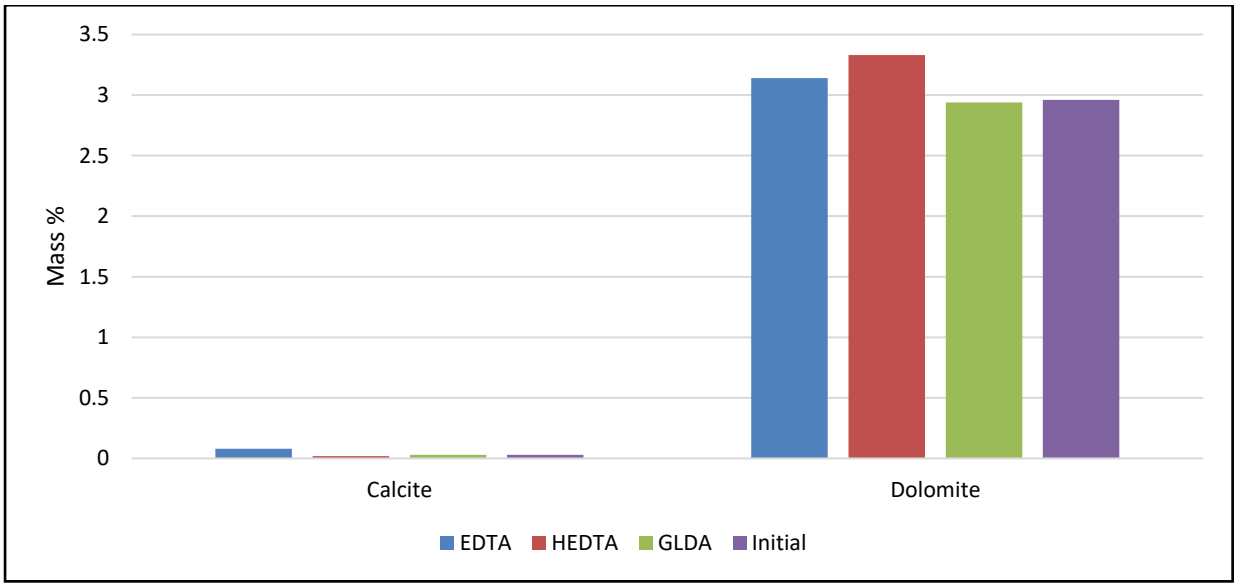

Figure 5.84. Ankerite Mineral Locking in Guelph dolomite before and after reaction with chelating agents

5.4.3.5 Grain Size Distribution

The number of grains of different important minerals before and after acidizing was discussed from Figure 5.85 through Figure 5.87. The selected size range was different for different minerals; based on the size of each mineral present inside the core sample. The highest size was shown by ankerite which depicted that big grains of ankerite were present inside the core sample. As discussed earlier, the change in the number of grains in particular size range showed the dissolving power of the chelate towards that mineral. There was no change observed in the number of grains of ankerite as shown in Figure 5.86 which established no dissolution of the matrix. Contrary, the number of grains of calcite (Figure 5.86) has been changed significantly after the reaction. It demonstrated that calcite has been dissolved by the chelates, especially by GLDA and HEDTA. However, the change in the number of grains of dolomite was also negligible (Figure 5.87).

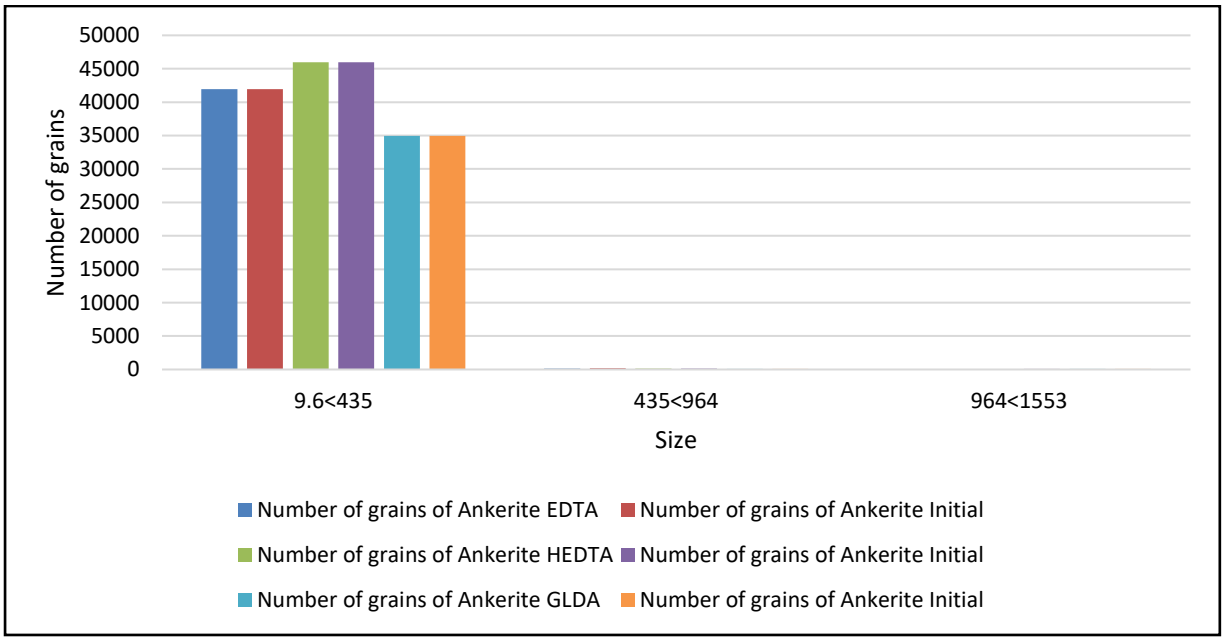

Figure 5.85. Grain size distribution of ankerite in Guelph dolomite before and after reaction with chelating agents

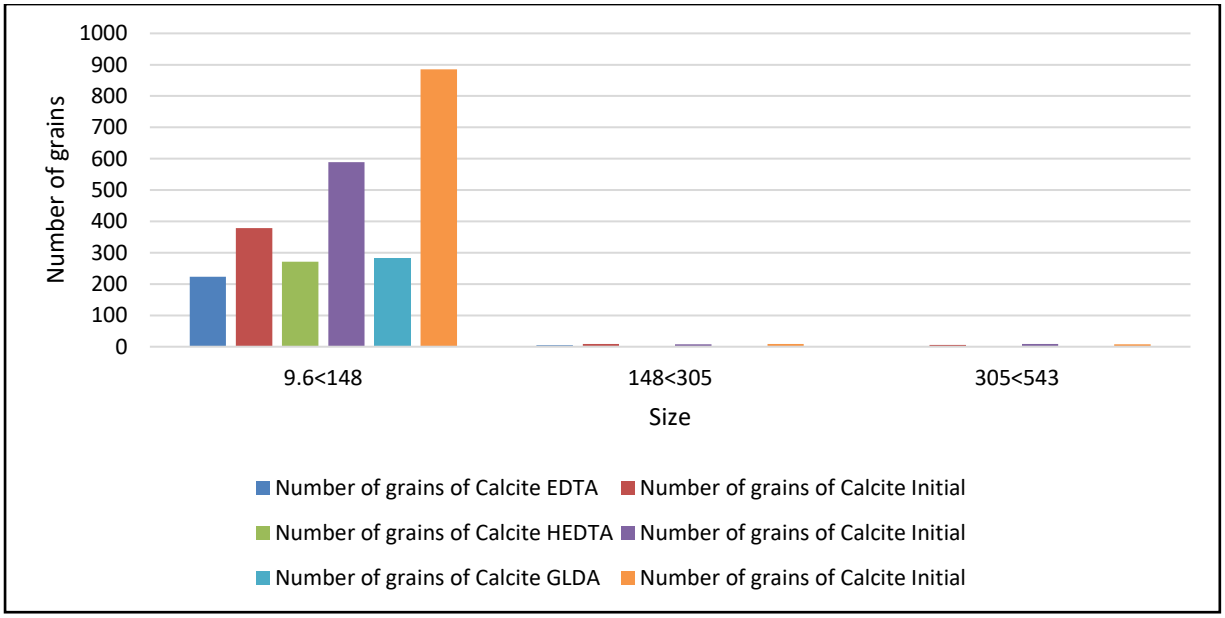

Figure 5.86. Grain size distribution of calcite in Guelph dolomite before and after reaction with chelating agents

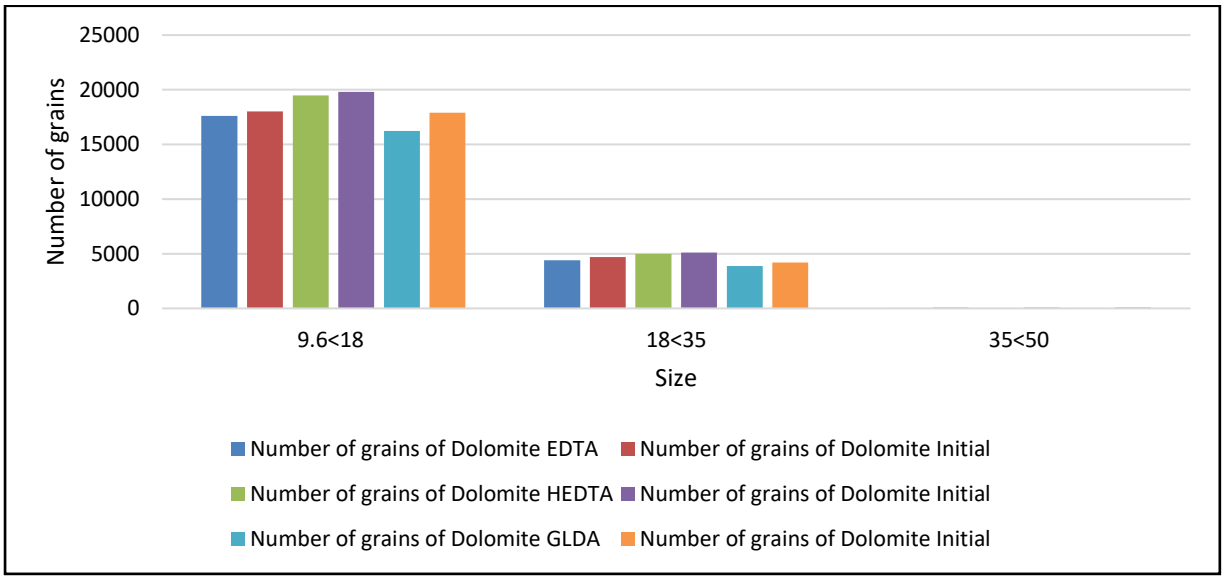

Figure 5.87. Grain size distribution of dolomite in Guelph dolomite before and after reaction with chelating agents

5.4.3.6 Panorama

Figures 5.88 to 5.93 represent the dissolution and pore spaces generation in dolomite samples where orange color represents the ankerite matrix while the pink color was the indication of the presence of calcite. It has been observed that new pores spaces and dissolution of the matrix was observed in all acidized samples. Figure 5.88 and Figure 5.89 represent the complete panorama and more focused images respectively of the core sample reacted with EDTA.

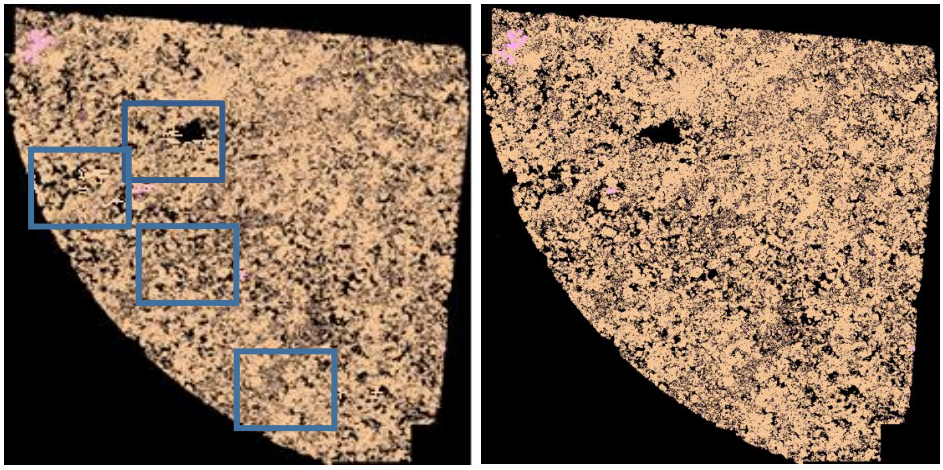

Figure 5.88. Dissolution of calcite and ankerite when sample reacted with EDTA, unreacted (left), reacted (right)

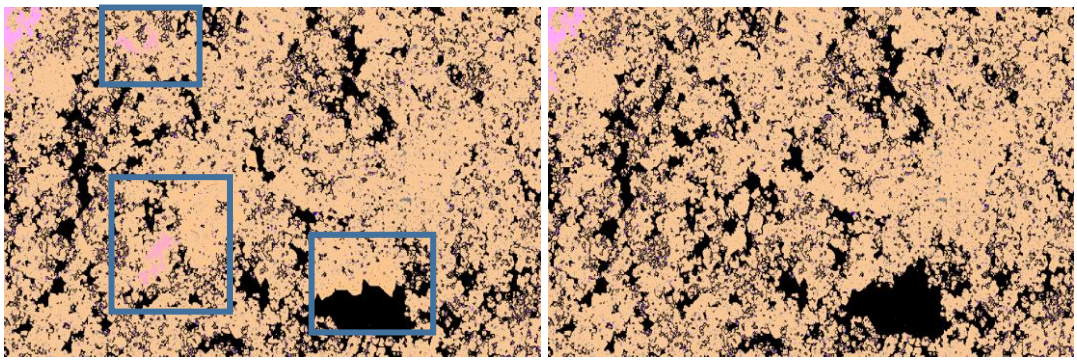

Figure 5.89. Dissolution of calcite and ankerite when sample reacted with EDTA, unreacted (left), reacted (right)

Figure 5.90 and Figure 5.91 represent the complete panorama and more focused images respectively of the core sample reacted with HEDTA.

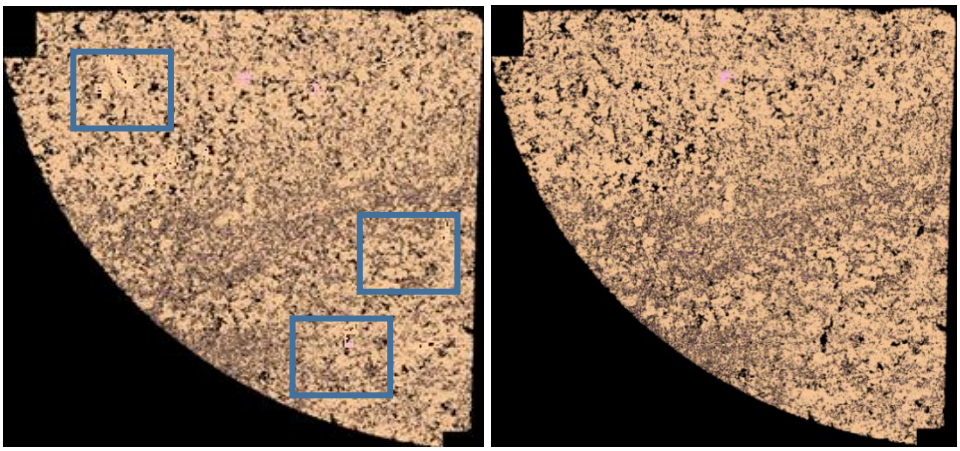

Figure 5.90. Dissolution of calcite and ankerite when sample reacted with HEDTA, unreacted (left), reacted (right)

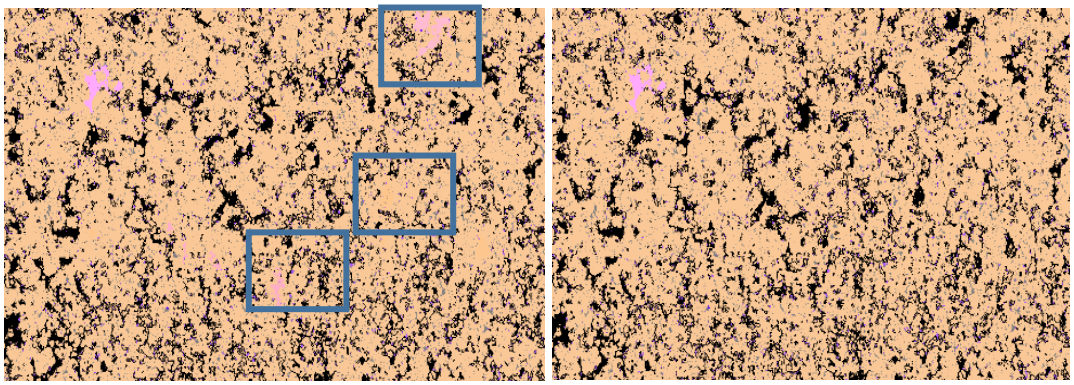

Figure 5.91. Dissolution of calcite and ankerite when sample reacted with HEDTA, unreacted (left), reacted (right)

Figure 5.92 and Figure 5.93 represent the complete panorama and more focused images respectively of the core sample reacted with GLDA. To summarize, if all the pictures considered, it seems reasonable to conclude that these chelating agents were effective in creating fresh pore spaces in the dolomite core sample.

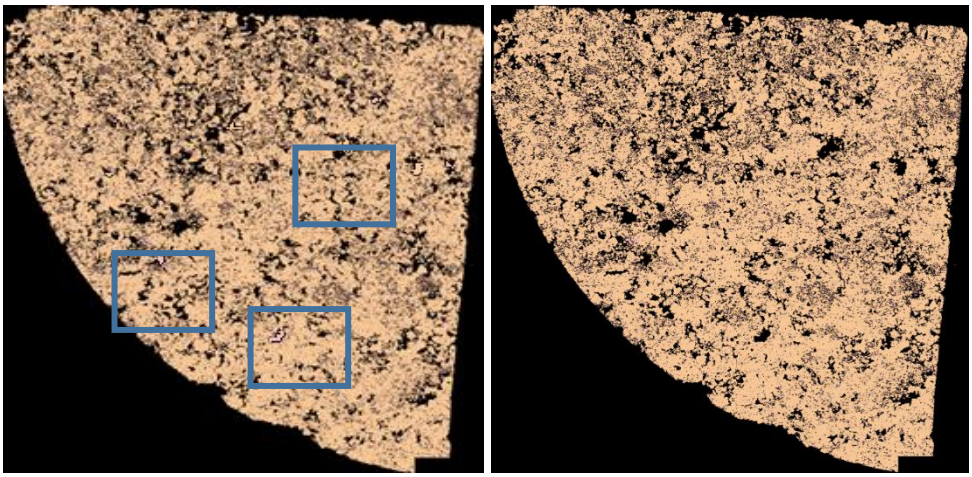

Figure 5.92. Dissolution of calcite and ankerite when sample reacted with GLDA, unreacted (left), reacted (right)

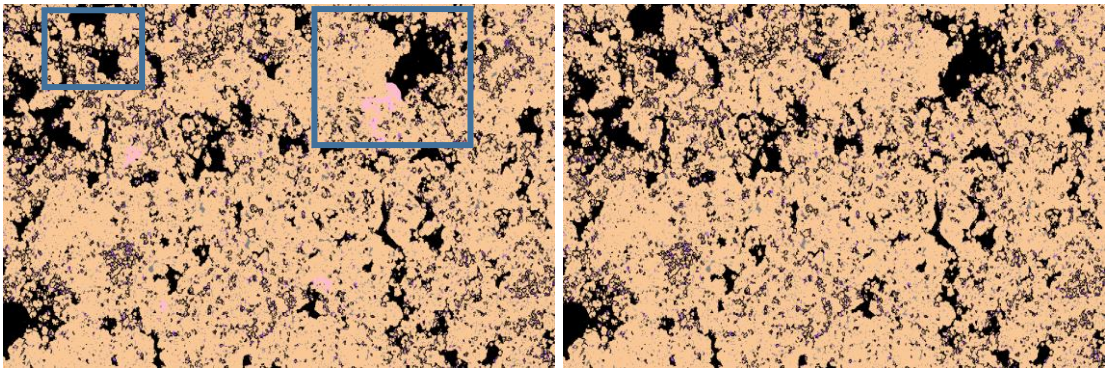

Figure 5.93. Dissolution of calcite and ankerite when sample reacted with GLDA, unreacted (left), reacted (right)

5.4.3.7 Porosity distribution

Table 5.4 represents the distribution of small, medium and large size pore spaces inside the dolomite core sample before and after reaction with different chelates. HEDTA managed to increase the total pore spaces by 3046 where GLDA only introduced 2117 new holes and EDTA even less than that, only 545 new pore spaces have created.

Now if concentrated on a number of small pore spaces; HEDTA introduced 2743 new pore spaces while GLDA managed to introduce 1952 new pore spaces. HEDTA is also effective in creating medium size pore spaces while GLDA managed to introduce more number of large size spaces compare to HEDTA where 11 new large pores have been created by GLDA while HEDTA managed to create only 2 large pore spaces. Most effective chelate on dolomite formation was found to be HEDTA which introduced in cumulative 3046 new pore spaces.

Table 5.4. Initial and final pore size distribution of Dolomite formation

Size range	**Number of holes**					
	Reacted with EDTA		**Reacted with HEDTA**		**Reacted with GLDA**	
	Initial	**EDTA**	**Initial**	**HEDTA**	**Initial**	**GLDA**
9.6<30	46558	47031	46013	48756	49089	51041
30<67	458	527	417	718	502	656
67<146	16	19	16	18	25	36
Total	47032	47577	46446	49492	49616	51733

5.4.3.8 Particle size distribution

Figure 5.94 (a, b, c) represents the number of small, medium and large size particles in Guelph dolomite samples before and after acidizing. It can be seen that all chelating agents managed to rescue the number of solid particles which shows their power to increase pore spaces and to remove different minerals.

Chelate (EDTA) managed to dissolve 3879 small size particles, 235 particles in the range of 47 – 199 um, 137 in the range from 199 – 520 um. While from 520 – 1590, it managed to dissolve 84 particles. These dissolved particles can be different minerals depends on the grain area covered by each mineral. In the case of dolomite, these particles were mostly ankerite and

calcite. GLDA dissolved 4010 small size particles which are more than dissolution power of HEDTA which dissolves 3879 particles. Also, table 6 showed that more number of medium and large size particles are dissolved by GLDA compared to HEDTA and EDTA. Therefore, it can be concluded that GLDA is more efficient in acidizing of clean dolomite formation.

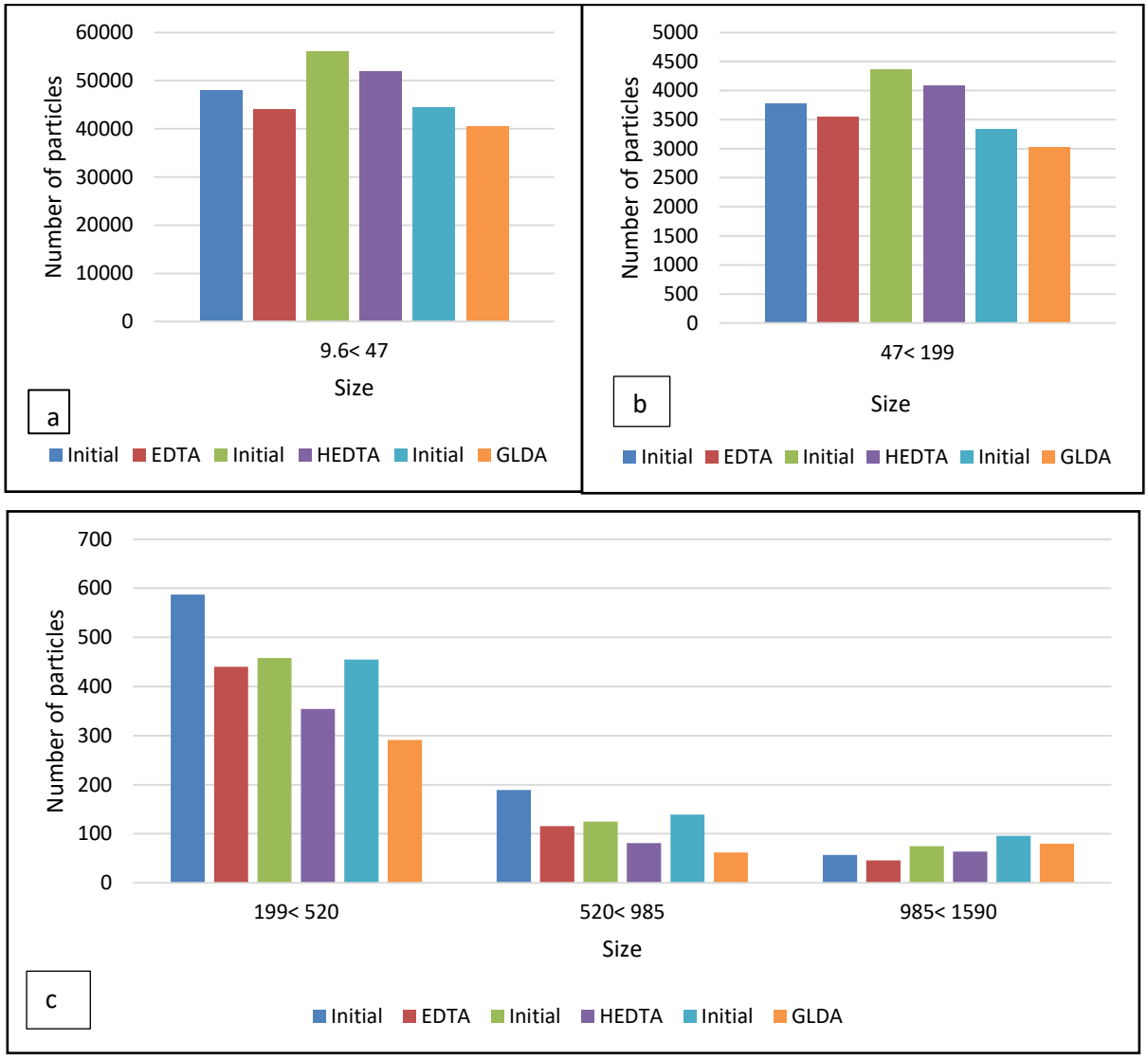

Figure 5.94. Number of Particles in Guelph dolomite Sample before and after reaction with chelating agents

5.4.3.9 Particle density distribution

Particles density distribution represents the number of particles in certain density range presented in Figures 5.95 (a, b, c). The sample was Guelph dolomite and mostly consist of ankerite mineral where the density of ankerite is almost 2.97 g/cm^3. Consequently, Figure 5.95c showed a maximum number of particles in the range 2.8 < 3.0 g/cm^3 and solubility of this mineral was very less. Therefore, the change in a number of particles was also very less. On

the other hand, the power of these chelating agents in dissolving calcite (density 2.71 g/cm^3) was very high, discussed earlier and confirmed by Figure 5.95b where the change in the number of particles was significant, while heavy particles in the range of 3.0 < 6.7 g/cm^3 were not dissolved effectively shown in Figure 5.95a. Figure 5.96 showed minerals with different density values.

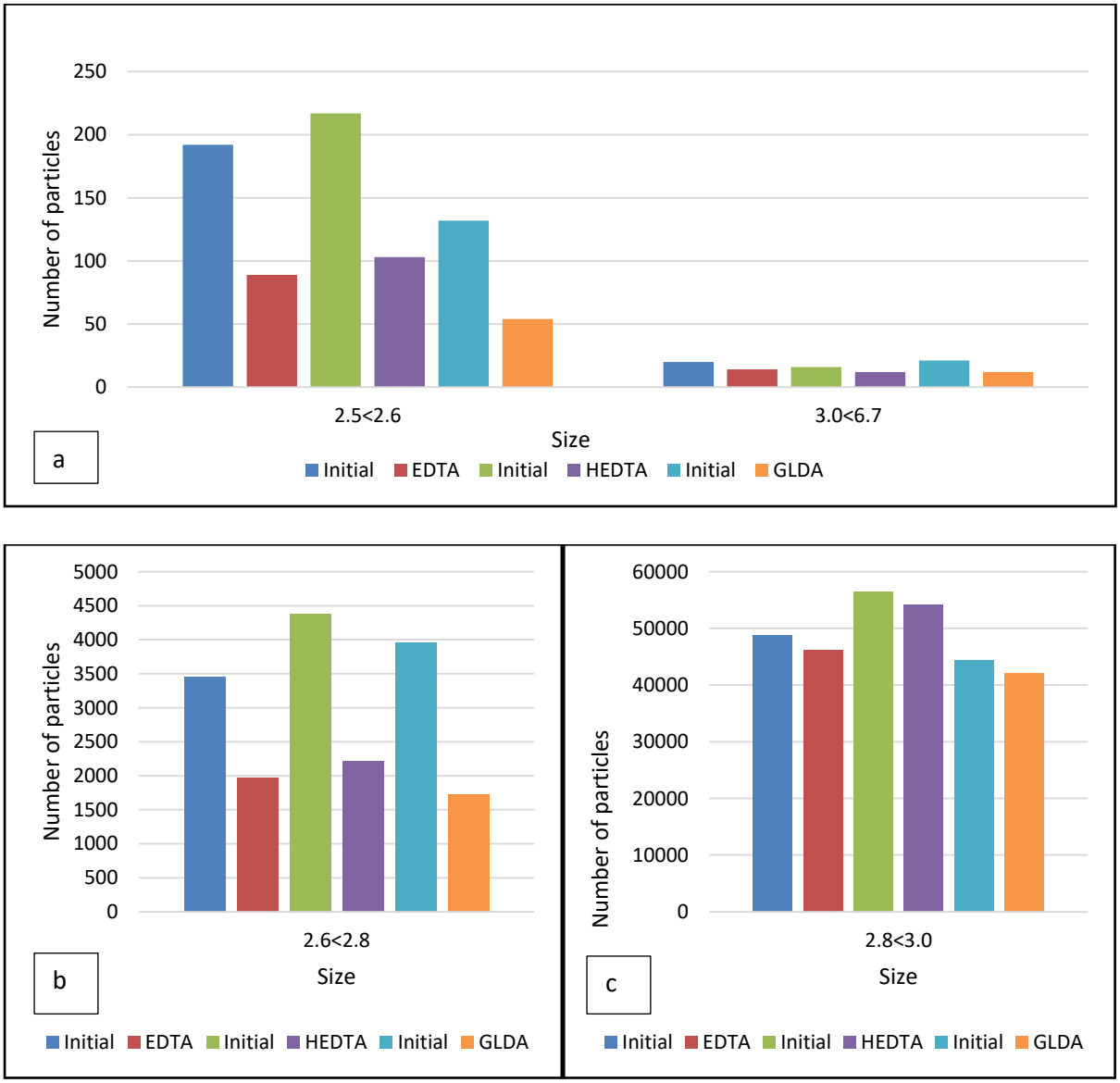

Figure 5.95. Particles density distribution in Guelph dolomite before and after reaction with chelating agents

Figure 5.96. Density pattern of different particles present in Guelph Dolomite Core sample

Chapter 6

Conclusions, Limitations, and Recommendations

6.1 Benefits of chelates

The use of conventional acids during acidizing especially high-temperature wells pose major problems including uncontrolled reaction rates and well tabular corrosion. Therefore, due to the shortcomings offered by the conventional acids, chelating agents were applied and usually showed good dissolving power towards the ions like sodium, potassium, calcium, magnesium, and iron. They are a good iron controlling agents, low corrosion and low sludging tendencies. These chelating agents also reduced Health Safety and Environment issues (HSE) because:

1. These agents are less toxic to mammals and other aquatic living organisms compared to other acids like HCl, HF or HCOOH.
2. Most of the fluids that are coming out to the surface after reaction is at pH values from 5 to 7. Hence neutralization is not required and can be added to well production fluids usually.
3. Because these are less corrosive, therefore, fewer concentrations of Nickel (Ni) and Chromium (Cr) will be encountered in well returns compared to other acids.

6.2 Performance Criteria

Generally, the increment in permeability, the porosity of core samples and dissolution of minerals is considered as a technical success. On the other hand, economic success is referred to the net production rate and oil price. The success of this thesis is measured or justified based on technical results and not the economic analysis. The technical success of this project is based on permeability, porosity distribution, mineralogy, and wettability difference after the acidizing operation. To compare the effectiveness of the acid or chelate treatment on the formations with different properties like permeability or porosity, similar mineralogical conditions should be valid. It is already established that there is no comparison between the carbonate and sandstone acidizing. The carbonate matrix acid stimulation treatments can be compared with the carbonate acidizing while the sandstone matrix acid stimulation treatments can be compared with the sandstone acidizing. The main reason behind this is the heterogeneity in the carbonate reservoirs and different matrix minerals. A clear understanding of the carbonate reservoir and the sandstone reservoirs is necessary to improve the oil and gas production from them.

6.3 Relationship of Acidizing with CO_2

Geological sequestration of CO_2 is one of the important to reduce greenhouse gases emission in the atmosphere. Usually, there are three types of techniques for CO_2 storage i.e., pore-level trapping, dissolution into brine and precipitation of dissolved CO_2 in the form of the mineral. The acidizing operation makes reservoir water (brine) a low pH solution. This principle is the main driver in the dissociation of dissolved CO_2. Low brine water consequently reacts with a lot of minerals inside the reservoir. A most important example is the dissolution of carbonate cement. Other reactions may include the weathering, where acid can extracts cations from certain aluminosilicates (clays and feldspar etc.). These cations may form an insoluble precipitate of carbonates. These reactions can determine the additional storage of CO_2 by mineralization. These reactions are known as geochemical reactions (dissolution and mineral precipitation) are usually very slow. The most important source of CO_2 storage in mineralization is calcite. Source of calcium is required to produce a calcite precipitate which can be produced by any mineral dissolution consist of calcium which can act as a precursor for calcite precipitation. More calcium precipitation will occur if we inject CO_2 in calcium-rich aquifer. Dissolution of calcium carbonate, anorthite and other calcium-containing minerals releases free calcium ions which can be used for CO_2 storage. Therefore, the chelate which was good in the dissolution of calcium carbonate or minerals related to calcium can prove to be effective for CO_2 storage.

6.4 Conclusions

Matrix acidizing of sandstone or carbonate reservoirs is an essential step to ensure high production by the removal of damage or by introducing new pathways or wormholes around the wellbore. Many studies have been performed so far highlights the importance of acidizing treatment in different formations. Many researchers developed different acid combinations and applied different chelating agents to get the best results related to the permeability, porosity, and precipitation but still, there are some limitations like fast spending of the acid, precipitation reactions, less penetration of acids and corrosion of pipelines. New acid combinations are required for future sandstone acidizing aspect and further study is needed on current technology because of the limitations of present acid combinations at high-temperature wells and limited study of these combinations on different sandstone formations. New combinations proposed or used at high temperatures are expensive and not regularly applied at field operations due to their limitations. Some combinations are not developed completely as their mechanisms are

not yet known and poorly understood. All the developed guidelines are representative of mud acid only, whereas no guidelines have been established or proposed for other acids used during sandstone acidizing. Therefore, comprehensive knowledge is required for the relevant reactants and their chemistry and also extensive research is required using these combinations. In the future, acid combinations should be developed which can be applied economically at high-temperature operations and to mitigate the precipitation reaction issue at elevated temperatures. In future, pore scale imaging will be very beneficial to find the change in topology, morphology, and wettability of the rock sample due to acidizing. The objective of this work is to give the reader a better understanding of chelating agents in oil field applications.

This work found that HEDTA significantly affected the permeability and porosity of the tight sandstone and dolomite formations where permeability increment doubled compared to the original permeability. In addition, HEDTA proved to be efficient in dissolving ions like calcium, magnesium, sodium, and potassium whereas GLDA introduced more number of big holes in case of dolomite acidizing, leading to a greater increase in permeability. It also summarizes the results obtained through a variety of tests which includes dissolution, Inductively Coupled Plasma (ICP), pore size and particle size distribution, which helped in understanding the interactions of the chelating agent with formation rock. Generally, this work conceded the applications of chelating agents in the field of stimulation sector, including the latest developments in the field of chelating agents. The research can be helpful for further investigation of applications of chelating agents in the oil and gas industry. Some of the major points concluded from the analysis of chelating agents and pre-flush acid stage are presented below:

- The porosity of Colton sandstone, Guelph dolomite, and Berea sandstone is greatly affected by the application of HEDTA chelate as compared to other chelates where it increases 10.10%, 6.3% and 6.8% porosity.
- The permeability of Colton sandstone and Guelph dolomite is greatly affected by the application of HEDTA chelate as compared to other chelates where it increases permeability by 100%.
- Chelate (HEDTA) chelate is also effective in dissolving positive ions (sodium, magnesium, potassium, calcium) in tight sandstone formation, where it dissolves 4290 ppm, 1370 ppm, 313 ppm, and 4600 ppm respectively.

- Chelate (HEDTA) chelate is also effective in dissolving positive ions (sodium, magnesium, potassium, calcium) in dolomite formations, where it dissolves 4440 ppm, 2570 ppm, 2310 ppm, and 4320 ppm respectively.
- Chelate (GLDA) is very effective in the dissolution of potassium and calcium from Berea sandstone, 9160 ppm, and 8220 ppm respectively.
- Chelate (GLDA) is very effective in the dissolution of potassium and calcium from dolomite formation, 2610 ppm and 2010 ppm respectively.
- Berea contains a high amount of iron ions, which are effectively removed by all the chelates.
- A quite significant change in number pores has been observed by applying the chelates especially HEDTA on sandstone and dolomite formations, 4627 and 3862 new pores respectively.
- Chelate (EDTA) proved to be effective in creating new pore spaces in Berea formation, 3773 new pore spaces.
- Chelate (GLDA) proved to be effective in the creation of more medium and large size new pore spaces in case of dolomite formation, 11 new large pore spaces compared to 2 by HEDTA and 3 by EDTA.
- Chelate (HEDTA) has a very good ability to dissolve Calcium (Ca) ions and was able to form wormholes at 1.85 pH value.
- Moreover, NMR analysis concluded that fresh large pore spaces have been created using the chelates especially HEDTA, results were quite significant for all type of core samples used (Berea, Colton, and dolomite).
- Acid combination (5%CH_3COOH: 10% HCl) had a significant effect on the porosity of the core sample and removed positive ions efficiently. It can prove to be a promising aspect in future preflush sandstone acidizing operations. The application of this acid caused more dissolution of carbonates, calcium, magnesium, and sodium ions which ultimately resulted in more increment of the porosity of the core sample as compared to the conventional acid.
- 15% HCl cause more increment in permeability of the sandstone formation and this acid also proved to be effective in creating more new pore spaces (2,063) and dissolving more number of particles (3,441) compared to 5%CH_3COOH: 10% HCl.
- Chelate (HEDTA) can be recommended for tight sandstone and carbonate acidizing, while GLDA can be good and effective for Berea and dolomite formations.

- The pore size distribution showed an overall increase in the number of pores for all the three core samples. The increase described the dissolution of minerals from the core samples when reacted with the chelating agents and acids. The increase in the large size pores has tremendously contributed to the overall porosity increment.
- The mineral mass percentage changes showed the dissolution of different minerals present inside the core samples. Power to dissolve different minerals of each acid or chelating agent is different from each other.
- Panorama analysis showed that there is an increment of pores and dissolution of minerals when chelating agents and acids applied to all the core samples.
- Particle density distribution illustrates the power of chelating agents and acids to dissolve minerals of specific density range.
- Mineral locking analysis was very important to analyze in order to determine the dissolution of minerals as some minerals can be dissolved by particular chelate or acid but their solubility decreases due to locking with other minerals.
- Chelate (HEDTA) is more soluble in water compared to EDTA, that's why the pH value of HEDTA solution less compared to EDTA solution. This showed that only HEDTA can be prepared as a formulation with <5 pH value due to its higher solubility compared to EDTA.

6.5 Limitations

- Pre-flush acids were applied to one type of formation only i.e., sandstone formation. Because there is no need for the pre-flush stage during dolomite acidizing.
- TIMA analysis was conducted on two core samples reacted with 15% HCl and 5%CH_3COOH: 10% HCl (15% HCl is the representative of conventional acid while 5%CH_3COOH: 10% HCl representative of hydrochloric and acetic acid combination).
- The temperature range was set at 80^oC and confining pressure was set at 1,000 psi due to safety and hazardous conditions.
- CT scan analysis was conducted on two samples only i.e., dolomite formation reaction with HEDTA and Berea formation reacted with HEDTA. These core samples were selected based on the performance of chelates on these formations.

6.6 Future Recommendations

- Application of chelating agents on Berea sandstone, Colton sandstone and limestone formations at very high-temperature ranges of more than 200^{o}C followed by TIMA, ICP, NMR, and CT scan analysis.
- F^{0}NMR analysis should be conducted also along with ICP analysis to determine the speed of reaction and reaction co-efficient.
- This work was performed at a constant flow rate of 1cm^{3}/sec, in future different flow rates were suggested to determine the effect of flow rate on mineral and face dissolution.
- Although there is the minimal effect of pressure on the acidizing results still high pressure acidizing is suggested to determine its effect on mineral dissolution and speed of reaction.

References

Abdelmoneim, S. S. and H. A. Nasr-El-Din (2015). Determining the Optimum HF Concentration for Stimulation of High Temperature Sandstone Formations, Society of Petroleum Engineers, SPE-174203-MS, https://doi.org/10.2118/174203-MS

Adachi, J., Siebrits, E., Peirce, A., & Desroches, J. (2007). "Computer simulation of hydraulic fractures." International Journal Of Rock Mechanics And Mining Sciences **44**(5): 739 - 757.

Adler, P.M., Jacquin, C.G., and Quiblier, J.A., 1990, Flow in simulated porous media: International Journal of Multi phase Flow, v. 16, p. 691–712, doi: 10.1016/ 0301-9322(90)90025-E.

Adler, P.M., Jacquin, C.G., and Thovert, J.F., 1992, The formation factor of reconstructed porous media: Water Resources Research, v. 28, p. 1571–1576, doi: 10.1029/ 92WR00059.

Allan, C.C., Tsapin, A.I., Kuebler, K., Haskin, L., and Wang, A., 2002, Analysis inside the box- studying rock and soil in biological quarantine: Lunar Planet. Science XXXIII, abstract 1222.

Alotaibi, M., Nasralla, R., & Nasr-El-Din, H, 2011. Wettability Studies Using Low-Salinity Water in Sandstone Reservoirs. SPE Reservoir Evaluation & Engineering, 14(06), 713-725. http://dx.doi.org/10.2118/149942-pa

Al-Harthy, S. (2009). "Options for High-Temperature Well Stimulation." Oil Field Review **20**(4).

Al-Anazi, H. A., H. A. Nasr-El-Din and S. K. Mohamed (1998). Stimulation of Tight Carbonate Reservoirs Using Acid-in-Diesel Emulsions: Field Application, Society of Petroleum Engineers, SPE-39418-MS, https://doi.org/10.2118/39418-MS

Al-Dahlan, M. N., H. A. Nasr-El-Din and A. A. Al-Qahtani (2001). Evaluation of Retarded HF Acid Systems, SPE-65032-MS, https://doi.org/10.2118/65032-MS

Al-Harbi, B. G., M. H. Al-Khaldi and K. A. AlDossary (2011). Interactions of Organic-HF Systems with Aluminosilicates: Lab Testing and Field Recommendations, Society of Petroleum Engineers, SPE-144100-MS, https://doi.org/10.2118/144100-MS

Al-Harbi, B. G., M. N. Al Dahlan and M. H. Khaldi (2012). Aluminum and Iron Precipitation During Sandstone Acidizing Using Organic-HF Acids, Society of Petroleum Engineers, SPE-151781-MS, https://doi.org/10.2118/151781-MS

Al-Harthy, S. (2008/2009). "Options for High-Temperature Well Stimulation." Oil Field Review **20**(4).

Al-Mutairi, S. H., A. D. Hill and H. A. Nasr-El-Din (2008). "Effect of Droplet Size, Emulsifier Concentration, and Acid Volume Fraction on the Rheological Properties and Stability of Emulsified Acids" SPE-107741-MS, https://doi.org/10.2118/107741-MS

Al-Mutairi, S. H., H. A. Nasr-El-Din, A. D. Hill and A. Al-Aamri (2009). "Effect of Droplet Size on the Reaction Kinetics of Emulsified Acid With Calcite", SPE-112454-MS, https://doi.org/10.2118/112454-PA

Ali, A. H. A., W. W. Frenier, Z. Xiao and M. Ziauddin (2002). Chelating Agent-Based Fluids for Optimal Stimulation of High-Temperature Wells, Society of Petroleum Engineers, SPE-77366-MS, https://doi.org/10.2118/77366-MS

Ali, S. A., E. Ermel, J. Clarke, M. J. Fuller, Z. Xiao and B. Malone (2008). "Stimulation of High-Temperature Sandstone Formations From West Africa With Chelating Agent-Based Fluids", SPE-93805-PA, https://doi.org/10.2118/93805-PA

Almubarak, T., J. H. Ng and H. Nasr-El-Din (2017). Oilfield Scale Removal by Chelating Agents: An Aminopolycarboxylic Acids Review, Society of Petroleum Engineers, SPE-185636-MS, https://doi.org/10.2118/185636-MS

Anderson, W. G. (1987). "Wettability Literature Survey- Part 1: Rock/Oil/Brine Interactions and the Effects of Core Handling on Wettability."

Anderegg, G., Arnaud-Neu, f., Delgado, R. et al. 2005. Critical Evaluation Of Stability Constants of Metal Complexes of Complxenos for Biomedical and environmental Applications. Pure and Applied Chemistry, 77 (8); 1445-1495.

Barker, K. M., J. V. Breitigam, R. Brotherton, L. L. Goff, K. J. Hake and R. D. Schofield (2007). Crude Oils of Kentucky and Tennessee: Characteristics, Problems, and Solutions, Society of Petroleum Engineers, SPE-111142-MS, https://doi.org/10.2118/111142-MS

Bartko, K. M., C. T. Montgomery, C. L. Boney and V. L. Ward (1996). Development of a Stimulation Treatment Integrated Model, Society of Petroleum Engineers, SPE-35991-MS, https://doi.org/10.2118/35991-MS

Begum, Z. A., Rahman, I. M., Sawai, H. et al. 2012a. Stability Constants of FE(III) and Cr(III) Complexes with DL-2-(2-Carboxymethyl) nitrilotraiacetic acid (GLDA) and 3 Hydroxy-2,2-iminodisuccinic acid (HIDS) in Aqueous Solution. J. Chem. Eng. Data 57 (10): 2723-2732.

Begum, Z. A., Rahman, I. M., Tate, Y. et al. 2012b. Formation and Stability of Binary Complexes of Divalent Ecotoxic Ions (Ni, Cu, Zn, Cd, Pb) with Biodegradable Aminoploycarboxylate Chelants DL-2-(2-Carboxymethyl) nitrilotraiacetic acid, GLDA, and 3 Hydroxy-2,2-iminodisuccinic acid (HIDS) in Aqueous Solution. Journal of Solution Chemistry. 41 (10): 1161-1170.

Bernadiner, M. G., K. E. Thompson and H. S. Fogler (1992). "Effect of Foams Used During Carbonate Acidizing", SPE-21035-PA, https://doi.org/10.2118/21035-PA

Bernard, G. G. and L. W. Holm (1964). "Effect of Foam on Permeability of Porous Media to Gas", SPE-983-PA, https://doi.org/10.2118/983-PA

Bernard, G. G. and W. L. Jacobs (1965). "Effect of Foam on Trapped Gas Saturation and on Permeability of Porous Media to Water", SPE-1204-PA, https://doi.org/10.2118/1204-PA

Blackburn, C. R., J. C. Abel and R. Day (1990). "An Expert System To Design and Evaluate Matrix Acidizing", SPE-20337-PA, https://doi.org/10.2118/20337-PA

Blake R.E., a. W., L.M. (1999). "Kinetics of Feldspar and Quartz Dissolution at 70-80 and Near-Neutral pH : Effects of Organic Acid and NaCl." Geochim **63**(Cosmochim, Acta): 2043-2059.

Boyer, R. C. and C.-H. Wu (1983). The Role of Reservoir Lithology in Design of an Acidization Program: Kuparuk River Formation, North Slope, Alaska, Society of Petroleum Engineers, SPE-11722-MS, https://doi.org/10.2118/11722-MS

Buijse, M. A. (1997). Mechanisms of Wormholing in Carbonate Acidizing, Society of Petroleum Engineers, SPE-37283-MS, https://doi.org/10.2118/37283-MS

Buijse, M. A. and M. S. van Domelen (1998). Novel Application of Emulsified Acids to Matrix Stimulation of Heterogeneous Formations, Society of Petroleum Engineers, SPE-39583-MS, https://doi.org/10.2118/39583-MS

Buijse, M., P. de Boer, B. Breukel, and M. Klos (2003). Organic Acids in Carbonate Acidizing, Society of Petroleum Engineers, SPE-82211-MS, https://doi.org/10.2118/82211-PA

Byrne M, P. I. (2004). Core sample preparation—an insight into new procedures. International symposium of the society of core analysts, Abu Dhabi, UAE.

Cairns, A. J., G. A. Al-Muntasheri, M. Sayed, L. Fu and E. P. Giannelis (2016). Targeting Enhanced Production through Deep Carbonate Stimulation: Stabilized Acid Emulsions, Society of Petroleum Engineers, SPE-178967-MS, https://doi.org/10.2118/178967-MS

Cannan, W. L., A. R. Jennings, S. Huseini, T. P. Bordelon and S. Sardjono (1992). Increasing Arun Well Deliverability Through Effective Acid Fracturing, Society of Petroleum Engineers, SPE-22397-MS, https://doi.org/10.2118/22397-MS

Carlson, W., 2006, Three-dimensional imaging of earth and planetary materials: Earth and Planetary Science Letters, v. 249, p. 133–147, doi: 10.1016/j.epsl.2006 .06.020.

Carpenter, C. (2015). "Use of Weak-Acid and Nonacid Alternatives in Acidizing Horizontal Wells." SPE-0615-0097-JPT, https://doi.org/10.2118/0615-0097-JPT

Chen Q, Kinzelbach W, Ye C, Yue Y (2002) Variations of permeability and pore size distribution of porous media with pressure. J Environ Qual 31:500–505

Chen J, H. G., Flaum M (2006). "NMR wettability indices. Effect of OBM on wettability and NMR responses." J Pet Sci Eng **52**: 161-171.

Chiu, T.-J., E. A. Caudell and F.-L. Wu (1993). "Development of an Expert System To Assist With Complex Fluid Design", SPE-24416-MS, https://doi.org/10.2118/24416-PA

Clennell B, Raven M, Borysenko A, Sedev R, Dewhurst D (2006) Shale petrophysics: electrical, dielectric and nuclear magnetic resonance studies of mudrocks and clays.

SPWLA 47th annual logging symposium, Society of Petrophysicists and Well Log Analysts, Veracruz, Mexico

Coates G R., Marschall, D M Mardon, M, 1998, A New Characterization of Bulk-Volume Irreducible Using Magnetic Resonance, The Log Analyst, 39 (1): 51

Collier, R. (2013). Fracking's more dangerous bedflow: acidizing. The Next Generation.

Conway, M. W., M. Asadi, G. S. Penny and F. Chang (1999). A Comparative Study of Straight/Gelled/Emulsified Hydrochloric Acid Diffusivity Coefficient Using Diaphragm Cell and Rotating Disk, Society of Petroleum Engineers, SPE-56532-MS, https://doi.org/10.2118/56532-MS

Coulter, G. R. and A. R. Jennings, Jr. (1999). "A Contemporary Approach to Matrix Acidizing", SPE-56279-MS, https://doi.org/10.2118/56279-PA

Craft B C., Hawkins M and Ronald E. Terry, Applied Petroleum Reservoir Engineering, 2nd Edition, Prentice Hall PTR, Englewood Cliffs,

Crowe, C. W. and B. D. Miller (1974). New, Low-Viscosity Acid-In-Oil Emulsions Provide High Degree Of Retardation At High Temperature, Society of Petroleum Engineers., SPE-4937-MS, https://doi.org/10.2118/4937-MS

Crowe C, M. J., Touboul E and Thomas R (1992). "Trends in Matrix Acidizing." Oilfield Review **4**(4): 24 - 40

Cruz-Maya, J., Rosas-Flores, J., Godoy-Alcantar, M., Jan-Roblero, J., & Sanchez Silva, F. (2011). "A real-time virtual monitoring system of the skin factor for matrix acidizing treatments." Flow Measurement And Instrumentation **22**(5): 413-420.

Da Motta, E. P. and J. A. C.M. Dos Santos (1999). New Fluosilicic Acid System Removes Deep Clay Damage. SPE-73194-PA, https://doi.org/10.2118/73194-PA

Daccord, G., E. Touboul and R. Lenormand (1989). "Carbonate Acidizing: Toward a Quantitative Model of the Wormholing Phenomenon", SPE-16887-PA, https://doi.org/10.2118/16887-PA

de Rozieres, J. (1994). Measuring Diffusion Coefficients in Acid Fracturing Fluids and Their Application to Gelled and Emulsified Acids, Society of Petroleum Engineers, SPE-28552-MS, https://doi.org/10.2118/28552-MS

Economides, M. J., A. D. Hill, C. Ehlig-Economides, and D. Zhu (2013), Petroleum Production Systems, 2nd ed. Prentice Hall, Upper Saddle River, NJ.

Ettinger, R. A. and C. J. Radke (1992). "Influence of Texture on Steady Foam Flow in Berea Sandstone", SPE-19688-PA, https://doi.org/10.2118/19688-PA

Farley J T, M. B. M., Schoettle V (1970). "Design Criteria for Matrix Stimulation with Hydrofluoric - Hydrochloric Acid." JPT: 433-440.

Fattah, W. A. and H. A. Nasr-El-Din (2010). "Acid Emulsified in Xylene: A Cost-Effective Treatment To Remove Asphalting Deposition and Enhance Well Productivity." SPE-117251-PA, https://doi.org/10.2118/117251-PA

Fleury M, D. F. (2003). "Quantitative evaluation of porous media wettability using NMR relaxometry." Magn Reson Imaging **21**: 385–387.

Fourie, S., 1974, The cranial morphology of Thrinaxondon liohinus Seeley: Annals of the South African Museum, v. 65, p. 337–400.

Fredd, C. N., R. Tjia and H. S. Fogler (1997a). The Existence of an Optimum Damkohler Number for Matrix Stimulation of Carbonate Formations, Society of Petroleum Engineers, SPE-38167-MS, https://doi.org/10.2118/38167-MS

Fredd, C. N. and H. S. Fogler (1997b). Chelating Agents as Effective Matrix Stimulation Fluids for Carbonate Formations, Society of Petroleum Engineers, SPE-37212-MS, https://doi.org/10.2118/37212-MS

Fredd, C. N. and H. S. Fogler (1998a). "Alternative Stimulation Fluids and Their Impact on Carbonate Acidizing", SPE-31074-MS, https://doi.org/10.2118/31074-PA

Fredd, C. N., Fogler H. s. (1998b). "The Influence of Chelating Agents on the Kinetics of Calcite Dissolution." J Colloid Interface Sci **204**(1): 187-197.

Fredd, C. N. and H. S. Fogler (1999). "Optimum Conditions for Wormhole Formation in Carbonate Porous Media: Influence of Transport and Reaction." SPE-56995-PA, https://doi.org/10.2118/56995-PA

Frenier, W. W. (1986). Solvent for removing iron oxide deposits., US06697615, Dowell Schlumberger Inc.

Frenier, W. W., D. Wilson, D. Crump and L. Jones (2000). Use of Highly Acid-Soluble Chelating Agents in Well Stimulation Services, Society of Petroleum Engineers, SPE-63242-MS, https://doi.org/10.2118/63242-MS

Frenier, W. W. (2001). Novel Scale Removers Are Developed for Dissolving Alkaline Earth Deposits, Society of Petroleum Engineers, SPE-65027-MS, https://doi.org/10.2118/65027-MS

Frenier, W. W. and D. G. Hill (2002). Effect of Acidizing Additives on Formation Permeability During Matrix Treatments, Society of Petroleum Engineers, SPE-73705-MS, https://doi.org/10.2118/73705-MS

Frenier, W. W., M. Rainey, D. Wilson, D. Crump and L. Jones (2003). A Biodegradable Chelating Agent is Developed for Stimulation of Oil and Gas Formations, Society of Petroleum Engineers, SPE-80597-MS, https://doi.org/10.2118/80597-MS

Frenier, W., M. Brady, S. Al-Harthy, R. Arangath, K. S. Chan, N. Flamant and M. Samuel (2004). Hot Oil And Gas Wells Can Be Stimulated Without Acids, Society of Petroleum Engineers, SPE-86522-PA, https://doi.org/10.2118/86522-PA

Furui, K., D. Zhu and A. D. Hill (2008). "A New Skin-Factor Model for Perforated Horizontal Wells." SPE Drilling & Completion, SPE-77363-PA, https://doi.org/10.2118/77363-PA

Gdanski, R. (1998a). "Kinetics of Tertiary Reactions of Hydrofluoric Acid on Aluminosilicates", SPE-31076-PA, https://doi.org/10.2118/31076-PA

Gdanski, R. D. and C. E. Shuchart (1998b). "Advanced Sandstone-Acidizing Designs With Improved Radial Models", SPE-52397-PA, https://doi.org/10.2118/52397-PA

Ghommem, M., W. Zhao, S. Dyer, X. Qiu and D. Brady (2015). "Carbonate acidizing: Modeling, analysis, and characterization of wormhole formation and propagation." Journal of Petroleum Science and Engineering **131**(Supplement C): 18-33.

Gidley, J. L. (1971). "Stimulation of Sandstone Formations with The Acid-Mutual Solvent Method", SPE-3007-PA, https://doi.org/10.2118/3007-PA

Gidley, J. L. (1985). "Acidizing Sandstone Formations: A Detailed Examination of Recent Experience." SPE-14164-MS, https://doi.org/10.2118/14164-MS

Gilchrist, J. M. and O. M. N. Lietard (1994). Use of High-Angle, Acid-Fractured Wells on the Machar Field Development, Society of Petroleum Engineers, SPE-28917-MS, https://doi.org/10.2118/28917-MS

Gluyas J, S. R. (2004). Petroleum geoscience., Oxford.

Gomaa, A. M., J. Cutler, Q. Qu, J. Boles and X. Wang (2013). An Effective Single-Stage Acid System for Sandstone Formations, Society of Petroleum Engineers, SPE-165147-MS, https://doi.org/10.2118/165147-MS

Haberlah, D., Williams, M. A. J., Halverson, G., McTainsh, G. H., Hill, S. M., Hrstka, T., Jaime, P., Butcher, A. R., & Glasby, P., (2010), Loess and floods: high-resolution multi-proxy data of Last Glacial Maximum (LGM) slackwater deposition in the Flinders Ranges, semi-arid South Australia. Quaternary Science Reviews, , 29(19–20), 2673–2693

Hartman, R. L., B. Lecerf, W. Frenier, M. Ziauddin and H. S. Fogler (2003). Acid Sensitive Aluminosilicates: Dissolution Kinetics and Fluid Selection for Matrix Stimulation Treatments, SPE-82267-PA, https://doi.org/10.2118/82267-PA

Hashem, M. K., Nasr-El-Din, H. A. and Hopkins, J. A. (1999). An Experience in Acidizing Sandstone Reservoirs: A Scientific Approach, Society of Petroleum Engineers, SPE-56528-MS, https://doi.org/10.2118/56528-MS

Hassan, A. M. and H. S. Al-Hashim (2017). Evaluation of Carbonate Rocks Integrity After Sequential Flooding of Chelating Agent Solutions, Society of Petroleum Engineers, SPE-183760-MS, https://doi.org/10.2118/183760-MS

Hazlett, R.D., 1997, Statistical characterization and stochastic modelling of pore networks in relation to fl uid flow: Journal of Mathematical Geology, v. 29, p. 801–822, doi: 10.1007/BF02768903.

Heus, M., Lammers, H., and Volmer, A., (2008). Process to prepare amino acid-n, n-diacetic acid compounds, CA2671022, Akzo Nobel Chemicals International BV

Hill, A. D., K. Sepehrnoori and P. Y. Wu (1994). "Design of the HCl Preflush in Sandstone Acidizing." SPE-21720-PA, https://doi.org/10.2118/21720-PA

Hoefner, M. L. (1987). Matrix Acidizing in Carbonates Using Microemulsions: The Study of Flow, Dissolution and Channeling in Porous Media, U. of Michigan.

Holm, L. W. (1968). "The Mechanism of Gas and Liquid Flow Through Porous Media in the Presence of Foam", SPE-1848-PA, https://doi.org/10.2118/1848-PA

Ituen, E., Akaranta, O., & James, A., (2017). "Electrochemical and anticorrosion properties of 5-hydroxytryptophan on mild steel in a simulated well-acidizing fluid." Journal Of Taibah University For Science **11**(5): 788 - 800.

Ji, Q., L. Zhou and H. A. Nasr-El-Din (2014). Acidizing Sandstone Reservoirs Using Fines Control Acid, SPE-169395-MS, https://doi.org/10.2118/169395-MS

Johnson, L. M., S. D. Shepherd, G. D. Rothrock, A. J. Cairns and G. A. Al-Muntasheri (2016). Core/Shell Systems for Delayed Delivery of Concentrated Mineral Acid, SPE-173734-PA, https://doi.org/10.2118/173734-PA

Joshi, M., 1974, A class of stochastic models for porous media [Ph.D. thesis]: Lawrence, University of Kansas.

Jones, A. T. and D. R. Davies (1998). "Quantifying Acid Placement: The Key to Understanding Damage Removal in Horizontal Wells", SPE-31146-MS, https://doi.org/10.2118/31146-MS

Jones, A. T. and M. Dovle (1996). "Improving the Efficiency of Matrix Acidizing With a Succinoglycan Viscosifier", SPE-30122-PA, https://doi.org/10.2118/30122-PA

Kalfayan, L. J. and A. S. Metcalf (2000). Successful Sandstone Acid Design Case Histories: Exceptions to Conventional Wisdom, Society of Petroleum Engineers, SPE-63178-MS, https://doi.org/10.2118/63178-MS

Kalfayan, L. J. (2001). Production Enhancement with Acid Stimulation. Tulsa, Oklahoma, Penn Well Corporation.

Kankaria, S., H. A. Nasr-El-Din and S. Rimassa (2017). Matrix Acidizing of Carbonate Rocks Using New Mixtures of HCl/Methanesulfonic Acid, Society of Petroleum Engineers, SPE-184528-MS, https://doi.org/10.2118/184528-MS

Kasza, P., M. Dziadkiewicz and M. Czupski (2006). From Laboratory Research to Successful Practice: A Case Study of Carbonate Formation Emulsified Acid Treatments, Society of Petroleum Engineers, SPE-98261-MS, https://doi.org/10.2118/98261-MS

Khishvand M, A. M., Piri M (2013). "Trapped non-wetting phase clusters: an experimental investigation of dynamic effects at the pore scale using a micro-CT scanner." SCA **24**.

Khishvand M, A. M., Piri M (2016). "Micro-scale experimental investigation of the effect of flow rate on trapping in sandstone and carbonate rock samples." Adv Water Resour **94**: 379-399.

King, G. E. (1986). "Acidizing Concepts - Matrix vs. Fracture Acidizing." JPT, SPE-15279-PA, https://doi.org/10.2118/15279-PA

Krebs, M., B. Lungwitz, A. Souza, A. Pepin, S. Montoya, P. Schlicht, A. Boyd, E. Vidoto, R. Polli and T. Bonagamba (2014). The First Visualization of Acid Treatments on Carbonates With 3D Nuclear Magnetic Resonance Imaging (NMRI), Society of Petroleum Engineers.

Kumar, A., M. Noh, G. A. Pope, K. Sepehrnoori, S. Bryant and L. W. Lake (2004). Reservoir Simulation of CO2 Storage in Deep Saline Aquifers, Society of Petroleum Engineers, SPE-89343-PA, https://doi.org/10.2118/89343-PA

Leet LD, J. S. (1971). Physical geology. Prentice-Hall. New Jersey.

LePage, J. N., C. De Wolf, J. Bemelaar and H. A. Nasr-El-Din (2009). An Environmentally Friendly Stimulation Fluid for High-Temperature Applications, Society of Petroleum Engineers, SPE-121709-PA, https://doi.org/10.2118/121709-PA

Liu, Y., Gupta, R., Sharma, A., Wall, T., Butcher, A., Miller, G., Gottlieb, P., & French, D. (2005), Mineral matter–organic matter association characterisation by QEMSCAN and applications in coal utilisation. Fuel, 84(10), 1259–1267.

Lund, K., Fogler, H.S., and McCune (1973). "Acidizing - I, The Dissolution of Dolomite in Hydrochloric Acid." Chem. Eng. Sci **28**: 691-700.

Maheshwari, P. and V. Balakotaiah (2013). 3D Simulation of Carbonate Acidization with HCl: Comparison with Experiments, Society of Petroleum Engineers, SPE-164517-MS, https://doi.org/10.2118/164517-MS

Maheshwari, P., J. Maxey and V. Balakotaiah (2016). "Reactive-Dissolution Modeling and Experimental Comparison of Wormhole Formation in Carbonates with Gelled and Emulsified Acids", SPE-171731-PA, https://doi.org/10.2118/171731-PA

Mahmoud, M. A. and K. Z. Abdelgawad (2015). "Chelating-Agent Enhanced Oil Recovery for Sandstone and Carbonate Reservoirs." SPE-172183-PA, https://doi.org/10.2118/172183-PA

Mahmoud, M. A., H. A. Nasr-El-Din, C. De Wolf and A. Alex (2011a). Sandstone Acidizing Using A New Class of Chelating Agents, Society of Petroleum Engineers, SPE-139815-MS, https://doi.org/10.2118/139815-MS

Mahmoud, M. A., H. A. Nasr-El-Din, C. De Wolf, J. LePage and J. Bemelaar (2011b). "Evaluation of a New Environmentally Friendly Chelating Agent for High-Temperature Applications." SPE-127923-PA, https://doi.org/10.2118/127923-PA

Martell, A. E., and Calvin, M. (1952). Chemistry of the Metal chelate Compounds E. Cliffs. New Jersey: Prentice Hall, Chemistry Series, Prentice Hall**:** 471-513.

Martell, A. E.; Smith, R.M.; Moekaitis, R. J. NIST Standard Reference Datbase 46: NIST critically selected Stability Constants of Metal Complexes Database (Version 8.0 for Windows). Texas A&M University: College Station, TX, 2004

Martin, A. N. (2004). Stimulating Sandstone Formations with non-HF Treatment Systems, Society of Petroleum Engineers.

Marschall, D. M. 2000, HBVI: An NMR Method to Determine BVI as a Function of Reservoir Capillarity, SPWLA 41st Annu. Logging Symp., Dallas, 4–7 June. SPWLA-2000-KK.

McLeod, H. O., Jr., L. B. Ledlow and M. V. Till (1983). The Planning, Execution, and Evaluation of Acid Treatments in Sandstone Formations, Society of Petroleum Engineers, SPE-11931-MS, https://doi.org/10.2118/11931-MS

McLeod, H. O. and W. D. Norman (2000). Sandstone Acidizing, In Reservoir Stimulation. Chichester, UK, John wiley and Sons

Mohammadi, H., Delshad, M., & Pope, G. (2009). Mechanistic Modeling of Alkaline/Surfactant/Polymer Floods. SPE Reservoir Evaluation & Engineering, 12(04), 518-527. http://dx.doi.org/10.2118/110212-pa

Morgenthaler, L. (2013). "Technology Focus: Matrix Stimulation (June 2014)." Journal Of Petroleum Technology, **68**(6).

Muecke, T. W. (1982). Principles of Acid Stimulation, Society of Petroleum Engineers, SPE-10038-MS, https://doi.org/10.2118/10038-MS

Mungan, N. (1966). "Certain Wettability Effects In Laboratory Waterfloods." SPE-1203-PA, https://doi.org/10.2118/1203-PA

Nasr-El-Din, H. A., H. A. Al-Anazi and S. K. Mohamed (2000). "Stimulation of Water-Disposal Wells Using Acid-in-Diesel Emulsions: Case Histories." SPE-65069-PA, https://doi.org/10.2118/65069-PA

Nasr-El-Din, H. A. and A. Y. Al-Humaidan (2001). Iron Sulfide Scale: Formation, Removal and Prevention, SPE-68315-MS, https://doi.org/10.2118/68315-MS

Nasr-El-Din, H. A., S. H. Al-Mutairi, M. Al-Jari, A. S. Metcalf and W. Walters (2002). Stimulation of a Deep Sour Gas Reservoir Using Gelled Acid, Society of Petroleum Engineers, SPE-75501-MS, https://doi.org/10.2118/75501-MS

Nasr-El-Din, H. A., M. M. Samuel and S. K. Kelkar (2007). Investigation of a New Single-stage Sandstone Acidizing Fluid for High Temperature Formations, Society of Petroleum Engineers, SPE-107636-MS, https://doi.org/10.2118/107636-MS

Navarrete, R. C., B. A. Holms, S. B. McConnell and D. E. Linton (1998). Emulsified Acid Enhances Well Production in High-Temperature Carbonate Formations, Society of Petroleum Engineers, SPE-50612-MS, https://doi.org/10.2118/50612-MS

Nitters, G., L. Roodhart, H. Jongma, V. Yeager, M. Buijse, D. Fulton, J. Dahl and E. Jantz (2000). Structured Approach to Advanced Candidate Selection and Treatment Design of Stimulation Treatments, Society of Petroleum Engineers, SPE-63179-MS, https://doi.org/10.2118/63179-MS

Nwoke, L., C. Uchendu, J. Arukhe, P. Essel, F. Ndinemenu, A. Vecchio and S. Fatusin (2004). Phosphonic Acid Complex for Stimulating HF-Sensitive Reservoirs - A Revolutionary Response, Society of Petroleum Engineers, SPE-89415-MS, https://doi.org/10.2118/89415-MS

Organization of Petroleum Exporting Countries, (2016). OPEC world oil outlook, October 2017, available from: http://www.opec.org

Øren, P.-E., and Bakke, S., 2002, Process based reconstruction of sandstones and prediction of transport properties: Transport in Porous Media, v. 46, p. 311–343, doi:\ 10.1023/A:1015031122338.

Owete, O. S. and W. E. Brigham (1987). "Flow Behavior of Foam: A Porous Micromodel Study." SPE-11349-MS, https://doi.org/10.2118/11349-PA

Pandya, N. and S. Wadekar (2013). A Novel Emulsified Acid System for Stimulation of Very High-Temperature Carbonate Reservoirs, International Petroleum Technology Conference. IPTC-16452-MS, https://doi.org/10.2523/IPTC-16452-MS

Pereira, A. Z. I., M. Germino, L. C. Paixao, T. J. L. De Oliveira and P. D. Fernandes (2012). Used Approaches for Carbonates Acidizing Offshore Brazil, Society of Petroleum Engineers, SPE-151797-MS, https://doi.org/10.2118/151797-MS

Persoff, P., C. J. Radke, K. Pruess, S. M. Benson and P. A. Witherspoon (1991). "A Laboratory Investigation of Foam Flow in Sandstone at Elevated Pressure.", SPE-18781-PA, https://doi.org/10.2118/18781-PA

Peters, F. W. and A. Saxon (1989). Nitrified Emulsion Provides Dramatic Improvements in Live Acid Penetration, Society of Petroleum Engineers, SPE-19496-MS, https://doi.org/10.2118/SPE-19496-MS

Pirrie, D., Butcher, A. R., Power, M. R., Gottlie, P., & Miller, G. L., (2004), Rapid quantitative mineral and phase analysis using automated scanning electron microscopy (QemSCAN); potential applications in forensic geosciences. In: Pye, K. & croft, D. (Eds), forensic geoscience. Geological Society, London, Special Publications, 232, 123–136

Plummer, L. N., Wigley, T.M.L., and Parkhurst, D.L., (1978). "The Kinetics of Calcite Dissolution in CO2-water system at 5o to 60o and 0.0 atm to 1.0 atm CO2." A. J. Sci **278**: 179-216.

Ponce da Motta, E., B. Plavnik and R. S. Schechter (1992). "Optimizing Sandstone Acidization", SPE-19426-PA, https://doi.org/10.2118/19426-PA

Qiu, X. W., W. Zhao, S. J. Dyer, A. Al Dossary, S. Khan and A. S. Sultan (2011). Revisiting Reaction Kinetics and Wormholing Phenomena During Carbonate Acidizing, International

Petroleum Technology Conference, IPTC-17285-MS, https://doi.org/10.2523/IPTC-17285-MS

Rae, P. and G. Di Lullo (2002). Achieving 100 Percent Success In Acid Stimulation Of Sandstone Reservoirs, SPE-77808-MS, https://doi.org/10.2118/77808-MS

Rae, P. J. and G. Lullo (2007). Single Step Matrix Acidising with HF - Eliminating Preflushes Simplifies the Process, Improves the Results, Society of Petroleum Engineers, SPE_107296-MS, https://doi.org/10.2118/107296-MS

Saneifar, M., Fahes, M., Lewis-Hosein, R., Hassna, B., & HIll, D. (2010). The Effect of Spent Acid on Carbonate Rock Wettability. Trinidad And Tobago Energy Resources Conference. http://dx.doi.org/10.2118/133166-ms

Saneifar, M., Nasr-El-Din, H., Nasralla, R., Fahes, M., & HIll, D. (2011). Effect of Spent Acids on the Wettability of Sandstones and Carbonates at High Temperature and Pressure. SPE European Formation Damage Conference. http://dx.doi.org/10.2118/144132-ms

Santoro, L., Rollinson, G. K., Boni, M., & Mondillo, N. (2015). Automated scanning electron microscopy (Qemscan ®)-based mineral identification and quantification of the Jabali Zn-Pb-ag nonsulfide deposit (Yemen). Economic Geology, 110(4), 1083–1099.

Shafiq, M. U. and M. T. Shuker (2013). Finding Suitable Acid for Acidizing of Low Permeable Sandstone Formation: A Research, Society of Petroleum Engineers, SPE-169641-MS, https://doi.org/10.2118/169641-MS

Shafiq, M. U; M. T. S. a. A. K. (2014). "Performance Comparison of New Combinations od Acids with Mud Acid in Sandstone Acidizing." RJASET **7**(2): 323-328.

Shafiq, M. U., Ben Mahmud, H. K., Hamid, M. A., (2015). Comparison of Buffer Effect of Different Acids During Sandstone Acidizing. CUTSE 2014. I. C. S. M. S. a. Engineering, IOP Publishing. **78**.

Shafiq, M. U., Ben Mahmud, H. K. (2016). An Effective Acid Combination for Enhanced Properties and Corrosion Control of Acidizing Sandstone Formation. CUTSE 2015. I. C. S. M. S. a. Engineering. Miri, Sarawak, IOP Publishing. **121**.

Shafiq, Mian Umer, Ben Mahmud, H.K., 2017. Sandstone matrix acidizing knowledge and future development. J Petrol Explor Prod Technol 1–12, Vol 7, 4, pp 1205-1216

Shafiq, M.U., Ben Mahmud, H.K., Rezaee, R., Testamanti, N., 2017. Investigation of changing pore topology and porosity during matrix acidizing using different chelating agents. In: IOP Conf. Series: Materials Science and Engineering, 217, 012023 (2017).

Shafiq M,U., Ben Mahmud, H, K., Arif, M., 2018. Mineralogy and Pore topology Analysis during Matrix Acidizing of Tight Sandstone and dolomite formations using Chelating agents", Journal of Petroleum Science and Engineering, 167, 869–876

Shaughnessy, C. M. and K. R. Kunze (1981). "Understanding Sandstone Acidizing Leads to Improved Field Practices." SPE-9388-PA, https://doi.org/10.2118/9388-PA

Shaughnessy, C. M. and W. E. Kline (1983). "EDTA Removes Formation Damage at Prudhoe Bay." SPE-11188-PA, https://doi.org/10.2118/11188-PA

Shuchart, C. E. (1997). Chemical Study of Organic-HF Blends Leads to Improved Fluids, Society of Petroleum Engineers, SPE-37281-MS, https://doi.org/10.2118/37281-MS

Shuler, P. J., Wang, K. S., Dunn, K. et al.Effects of Scale Dissolvers on Barium Sulphate Deposit: A Macrosccopic and Microscopic Study. Presented at CORROSION 2002, Denver, Colorado, 7-11 April.

Simon, D. E. and M. S. Anderson (1990). Stability of Clay Minerals in Acid, Society of Petroleum Engineers, SPE-19422-MS, https://doi.org/10.2118/19422-MS

Sidaoui, Z. and A. S. Sultan (2016). Formulating a Stable Emulsified Acid at High Temperatures: Stability and Rheology Study, International Petroleum Technology Conference, SPE-19012-MS, https://doi.org/10.2523/IPTC-19012-MS

Simon, D. E. and M. S. Anderson (1990). Stability of Clay Minerals in Acid, Society of Petroleum Engineers, SPE-19422-MS, https://doi.org/10.2118/19422-MS

Smith, C. F. and A. R. Hendrickson (1965). "Hydrofluoric Acid Stimulation of Sandstone Reservoirs", SPE-980-PA, https://doi.org/10.2118/980-PA

Sopngwi, J.-J. S., A. Gauthreaux, D. E. Kiburz, T. Kashib, E. A. Reyes, A. Beuterbaugh, A. L. Smith and S. K. Smith (2014). Successful Application of a Differentiated Chelant-Based Hydrofluoric Acid for the Removal of Aluminosilicates, Fines, and Scale in Offshore Reservoirs of the Gulf of Mexico, Society of Petroleum Engineers, SPE-168171-MS, https://doi.org/10.2118/168171-MS

Starkey, J., and Samantaray, A.K., 1994, A microcomputerbased system for quantitative petrographic analysis: Computers & Geosciences, v. 20, no. 9, p. 1285–1296, doi: 10.1016/0098-3004(94)90055-8.

Sutherland, D. N., & Gottlieb, P. (1991). Application of automated quantitative mineralogy in mineral processing. Minerals Engineering, 4(7–11), 753–762.

Sutton, G. D. and R. M. Lasater (1972). Aspects of Acid Additive Selection in Sandstone Acidizing, Society of Petroleum Engineers, SPE-4114-MS, https://doi.org/10.2118/4114-MS

Taron J, E. D. (2009). "Thermal-hydrologic-mechanical-chemical processes in the evolution of engineered geothermal reservoirs." Int J Rock Mech Min Sci **46**(5): 855-864.

Thomas, R. L., H. A. Nasr-El-Din, J. D. Lynn, S. Mehta and S. R. Zaidi (2001). Precipitation During the Acidizing of a HT/HP Illitic Sandstone Reservoir in Eastern Saudi Arabia: A Laboratory Study, SPE-71690-MS, https://doi.org/10.2118/71690-MS

Thomas, R. L., Nasr-El-Din H. A., Mehta, S., Hilab, V. and Lynn J. D. (2002). The Impact of HCl to HF Ratio on Hydrated Silica Formation During the Acidizing of a High Temperature

Sandstone Gas Reservoir in Saudi Arabia, Society of Petroleum Engineers, SPE-77370-MS, https://doi.org/10.2118/77370-MS

Timur A 1969 Effective Porosity and Permeability of Sandstones Investigated Through Nuclear Magnetic Principles, The Log Analyst, 10 (1): 3.

Uchendu, C. V., L. A. Nwoke, O. Akinlade and J. Arukhe (2006). A New Approach to Matrix Sandstone Acidizing Using a Single Step HF System: A Niger Delta Case Study, Society of Petroleum Engineers, SPE-103041-MS, https://doi.org/10.2118/103041-MS

Urraca, M. and F. Udvari (2009). Novel Chelating Based Technology Application on Complex and Heterogeneous Injector Wells in the Algyo Field - Hungary, Society of Petroleum Engineers, SPE-120468-MS, https://doi.org/10.2118/120468-MS

Van Domelen, M. S., W. G. F. Ford and T. J. Chiu (1992). An Expert System for Matrix Acidizing Treatment Design, SPE-24779-MS, https://doi.org/10.2118/24779-MS

Veatch, R. W., Jr. and Z. A. Moschovidis (1986). An Overview of Recent Advances in Hydraulic Fracturing Technology, SPE-14085-MS, https://doi.org/10.2118/14085-MS

Ward, I., Merigot, K. & McInnes, B.I.A. (2017), "Application of Quantitative Mineralogical Analysis in Archaeological Micromorphology: a Case Study from Barrow Is., Western Australia", J Archaeol Method Theory, https://doi.org/10.1007/s10816-017-9330-6

Wellington, S.L., and Vinegar, H.J., 1987, X-ray computerized tomography: Journal of Petroleum Technology, v. 39, p. 885–898, doi: 10.2118/16983-PA.

Wendell, D. J., W. G. Anderson and J. D. Meyers (1987). "Restored-State Core Analysis for the Hutton Reservoir." SPE-14298-PA, https://doi.org/10.2118/14298-PA

Wildenschild D, S. A. (2013). "X-ray imaging and analysis techniques for quantifying pore-scale structure and processes in subsurface porous medium systems." Adv Water Resour **51**: 217-246.

Wilson, A. (2016). "Sandstone-Acidizing System Eliminates Need for Preflush and Post-Flush Stages." SPE-0616-0059-JPT, https://doi.org/10.2118/0616-0059-JPT

Xiong, C. (2010). Application and Study of Acid Techniques Using Novel Selective Emulsified Acid System. CPS, SPE International Oil and Gas Conference and Exhibition. China, Beijing, SPE-131216-MS, https://doi.org/10.2118/131216-MS

Xiong, H. and S. A. Holditch (1995). "An Investigation Into the Application of Fuzzy Logic to Well Stimulation Treatment Design." SPE-27672-PA, https://doi.org/10.2118/27672-PA

Xu, W., Ayirala, S., & Rao, D. 2008. Measurement of Surfactant-Induced Interfacial Interactions at Reservoir Conditions. SPE Reservoir Evaluation & Engineering, 11(01), 83-94. http://dx.doi.org/10.2118/96021-pa

Yang, F., H. A. Nasr-El-Din and B. A. Harbi (2012). Acidizing Sandstone Reservoirs Using HF and Organic Acids, SPE-157250-MS, https://doi.org/10.2118/157250-MS

Yeong, C.L.Y., and Torquato, S., 1998a, Reconstructing random media: Physical Review E: Statistical Physics, Plasmas, Fluids, and Related Interdisciplinary Topics, v. 57, p. 495–506.

Yeong, C.L.Y., and Torquato, S., 1998b, Reconstructing random media. II. Three-dimensional media from two-dimensional cuts: Physical Review E: Statistical Physics, Plasmas, Fluids, and Related Interdisciplinary Topics, v. 58, p. 224–233.

Yildiz, T. (2006). "Assessment of Total Skin Factor in Perforated Wells." SPE Reservoir Evaluation & Engineering, SPE-82249-PA, https://doi.org/10.2118/82249-PA

Ying-Hsiao, L., J. D. Fambrough and C. T. Montgomery (1998). Mathematical Modeling of Secondary Precipitation from Sandstone Acidizing, Society of Petroleum Engineers, SPE-53001-MS, https://doi.org/10.2118/53001-PA

Zerhboub, M., E. Touboul, K. Ben-Naceur and R. L. Thomas (1994). "Matrix Acidizing: A Novel Approach to Foam Diversion." SPE Production & Facilities, SPE-22854-PA, https://doi.org/10.2118/22854-PA

Zhou, L. and H. A. Nasr-El-Din (2013). Acidizing Sandstone Formations Using a Sandstone Acid System For High Temperatures, Society of Petroleum Engineers, SPE-165084-MS, https://doi.org/10.2118/165084-MS

Zhou, L. and H. A. Nasr-El-Din (2016). "Phosphonic-Based Hydrofluoric Acid: Interactions With Clay Minerals and Flow in Sandstone Cores." Society of Petroleum Engineers, SPE-164472-PA, https://doi.org/10.2118/164472-PA

Appendix A

Table A1. Permeability results before and after pre-flush

Sample Name	Initial Permeability (md)	Final Permeability (md)	% change
15% HCl	122.76	152.16	23.94
2.5% CH_3COOH: 15% HCl	166.32	179.99	8.21
5% CH_3COOH: 10% HCl	113.16	123.23	8.89
3% CH_3COOH: 12%HCl	124.53	137.49	11.99

Table A2. Porosity results before and after pre-flush

Sample Name	Initial Porosity (%)	Final Porosity (%)	% change
15% HCl	19.56	20.61	5.34
2.5% CH_3COOH: 15% HCl	19.65	20.65	5.05
5% CH_3COOH: 10% HCl	19.52	20.74	6.24
3% CH_3COOH: 12%HCl	19.03	19.92	4.65

Table A3. Porosity Analysis before and after chelating agent acidizing

Chelate	Colton Sandstone		Guelph Dolomite		Berea Sandstone	
	Initial Porosity	Final Porosity	Initial Porosity	Final Porosity	Initial Porosity	Final Porosity
HEDTA	11.49	12.65	14.19	15.09	19.70	21.04
EDTA	10.56	11.66	16.80	16.82	19.04	20.01
GLDA	12.13	13.01	21.20	21.63	18.98	20.09

Table A4. Permeability Analysis before and after chelating agent acidizing

Chelate	Colton Sandstone		Guelph Dolomite		Berea Sandstone	
	Initial Permeability	Final Permeability	Initial Permeability	Final Permeability	Initial Permeability	Final Permeability
HEDTA	0.4633	0.9542	9.80	18.11	165.12	166.34
EDTA	0.7120	0.8380	104.27	113.20	124.53	127.35
GLDA	0.8069	0.9025	405.55	435.22	80.41	84.93

Table A5. pH value before and after reaction (Preflush stage)

Acid Combination	Initial pH	Maximum pH value	% change
15% HCl	0.06	0.23	283
2.5% CH_3COOH: 15% HCl	0.055	0.38	590
5% CH_3COOH: 10% HCl	0.09	0.41	355
3% CH_3COOH: 12%HCl	0.067	0.15	123

Table A6. pH value before and after reaction (chelating agents)

Chelate		Initial pH	Maximum value pH	% change
Colton	EDTA	2.7	7.06	161
	GLDA	1.25	5.7	356
	HEDTA	1.85	5.53	198
Guelph	EDTA	2.7	6.6	144
	GLDA	1.25	5.27	321
	HEDTA	1.85	5.6	202
Berea	EDTA	2.7	4.66	72
	GLDA	1.25	3.02	141
	HEDTA	1.85	3.28	77

Table A7. Concentration of ions dissolved (ICP analysis) during acidizing (pre-flush stage)

Element	5% CH_3COOH: 10% HCl (ppm)	15% HCl (ppm)
Sodium	3520	2790
Magnesium	1740	1250
Aluminium	151	97.6
Silicon	144	94.8
Phosphorous	195	152
Sulfur	43.8	48
Potassium	6550	6190
Calcium	6210	4340
Titanium	<1.2	<1.2
Chromium	18.1	8.05
Manganese	246	157
Iron	4420	2690
Cobalt	2.66	1.4
Nickel	17.2	7.12
Copper	7.19	3.2
Zinc	6.79	3.1
Strontium	5.15	5.03
Barium	3.04	2.45
Lead	6.12	4.84

Table A8. Concentration of ions dissolved (ICP analysis) during acidizing of Colton sandstone with chelates

(ICP Analysis), Concentrations in ppm Colton Sandstone									
	HEDTA			**EDTA**			**GLDA**		
Pore Volume	5	10	15	5	10	15	5	10	15
Minerals									
Sodium	3221	4109	4290	3000	3650	3710	2410	2790	2870
Magnesium	1029	1307	1370	492	598	614	545	850	900
Aluminium	50	120	136			0.43			0.96
Sulphur	30	50	67	65	95	105	20	25	27
Potassium	150	300	313	350	780	869	100	120	130
Calcium	3300	4400	4600	500	989	1090	2100	2500	2640
Iron	4	180	207			0.29			3.28
Silicon	55	89	97			4.47			0.10
Strontium	42	69	77	32	48	55	39	55	65

Table A9. Concentration of ions dissolved (ICP analysis) during acidizing of Guelph Dolomite with chelates

(ICP Analysis), Concentrations in ppm Guelph dolomite									
	HEDTA			**EDTA**			**GLDA**		
Pore Volume	5	10	15	5	10	15	5	10	15
Minerals									
Sodium	3200	4000	4440	3210	4500	4930	3300	4700	5440
Magnesium	1540	2300	2570	110	160	198	1000	1450	1570
Aluminium			6.65			2.27			0.96
Sulphur	100	125	133	85	105	111	15	25	26.60
Potassium	1500	2140	2310	1240	1790	1970	620	990	1130
Calcium	3120	4000	4320	105	155	178	1250	2300	2640
Iron	20	48	54.90			7.81			3.28
Silicon			0.68			0.95			0.96
Strontium	20	28	30.50	12	17.50	19.20	14	18.5	20.10

Table A10. Concentration of ions dissolved (ICP analysis) during acidizing of Berea sandstone with chelates

(ICP Analysis), Concentrations in ppm Berea Sandstone									
	HEDTA			**EDTA**			**GLDA**		
Pore Volume	5	10	15	5	10	15	5	10	15
Minerals									
Sodium	4500	5900	6200	4400	5700	5990	4150	5450	5610
Magnesium	1020	1780	1938	980	1698	1843	1560	2545	2702

Aluminum	185	345	377	100	145	156	125	178	190
Sulfur	30	50	55	30	52	58	30	55	61
Potassium	4520	6125	6612	4450	6120	6629	4600	7890	9160
Calcium	4250	5890	6364	4150	5950	6262	4780	7580	8220
Iron	3685	4589	4782	3520	4150	4467	3480	4050	4565
Strontium			5.49			5.36			15.45
Silicon	124	210	235	89	138	157	125	168	186

Table A11. NMR parameters used during the NMR measurements

Parameter	**Value**	**Abbreviation**
TE in experiment (μs)	100	TE
No of echoes acquire	50000	NECH
No of scans	256	NS
Time between expts.	30	RD
90 degree pulse (μs)	27.6	P90
180 degree pulse (μs)	55.2	P180

Appendix B

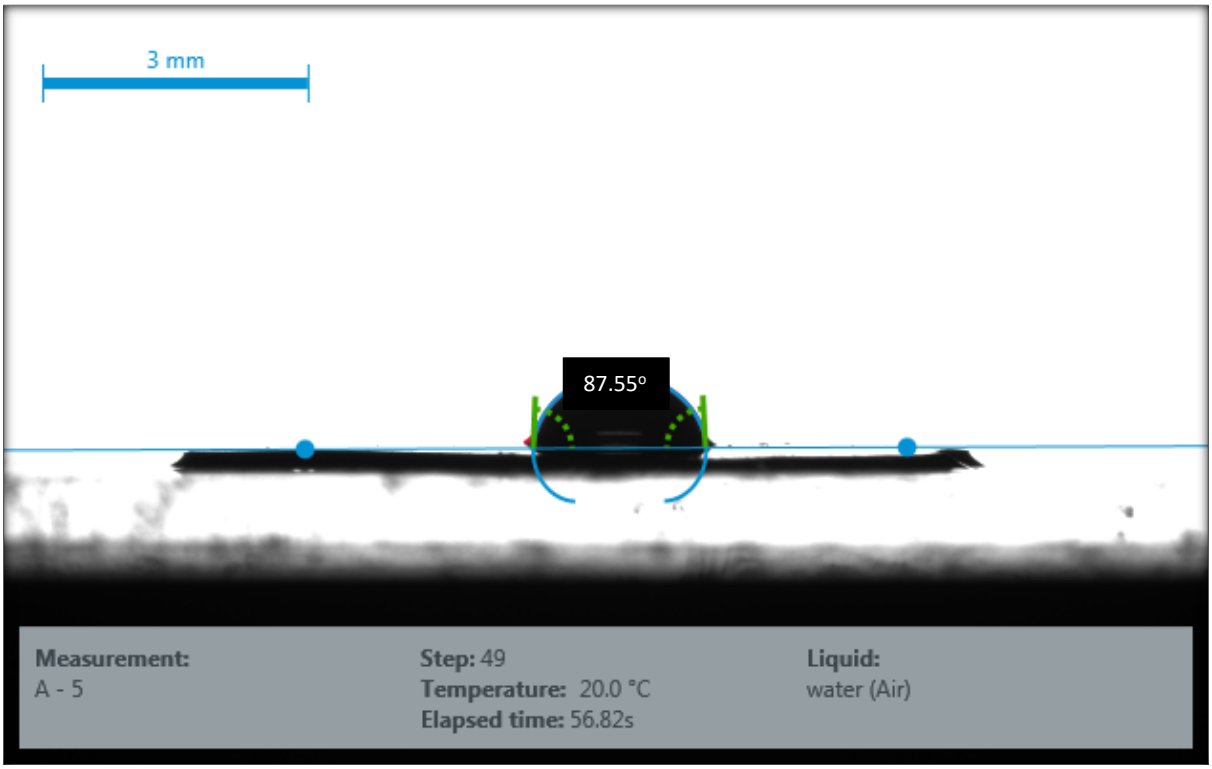

Figure B1. Contact angle measurement of Dolomite core sample reacted with EDTA

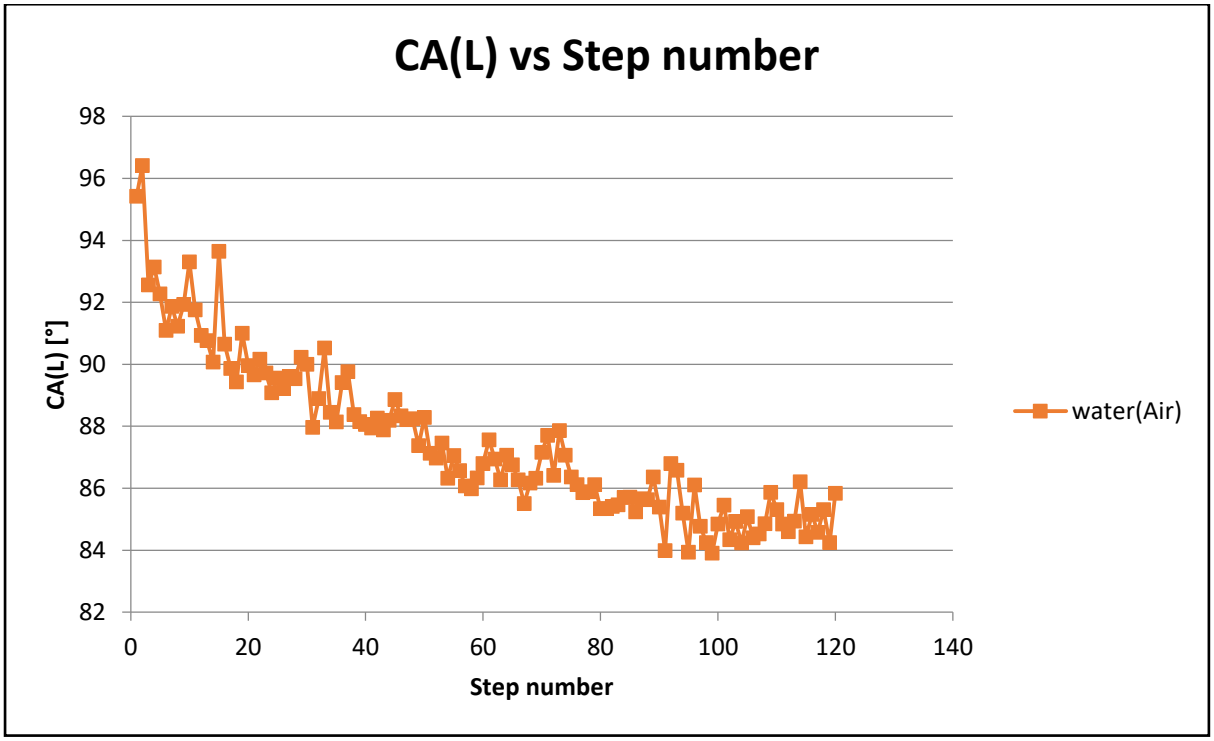

Figure B2. Number of steps vs Calibration for wettability measurement of Dolomite core sample reacted with EDTA

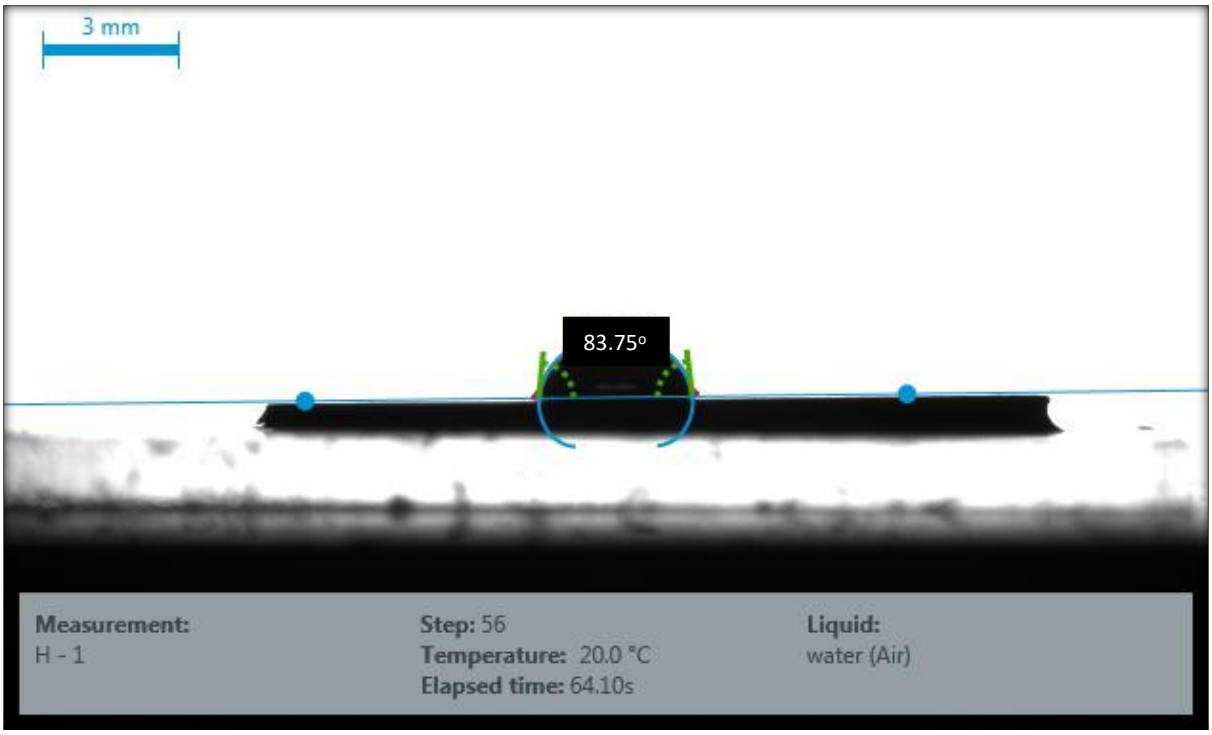

Figure B3. Contact angle measurement of Dolomite core sample reacted with GLDA

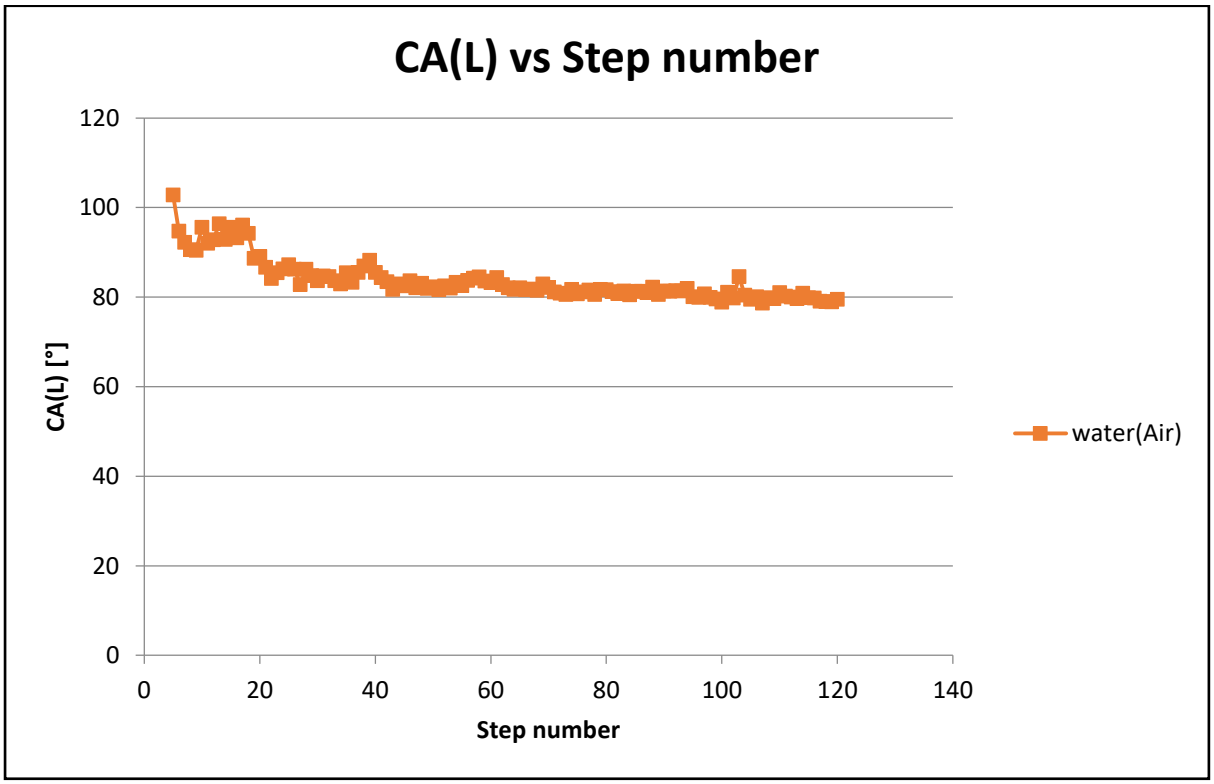

Figure B4. Number of steps vs Calibration for wettability measurement of Dolomite core sample reacted with GLDA

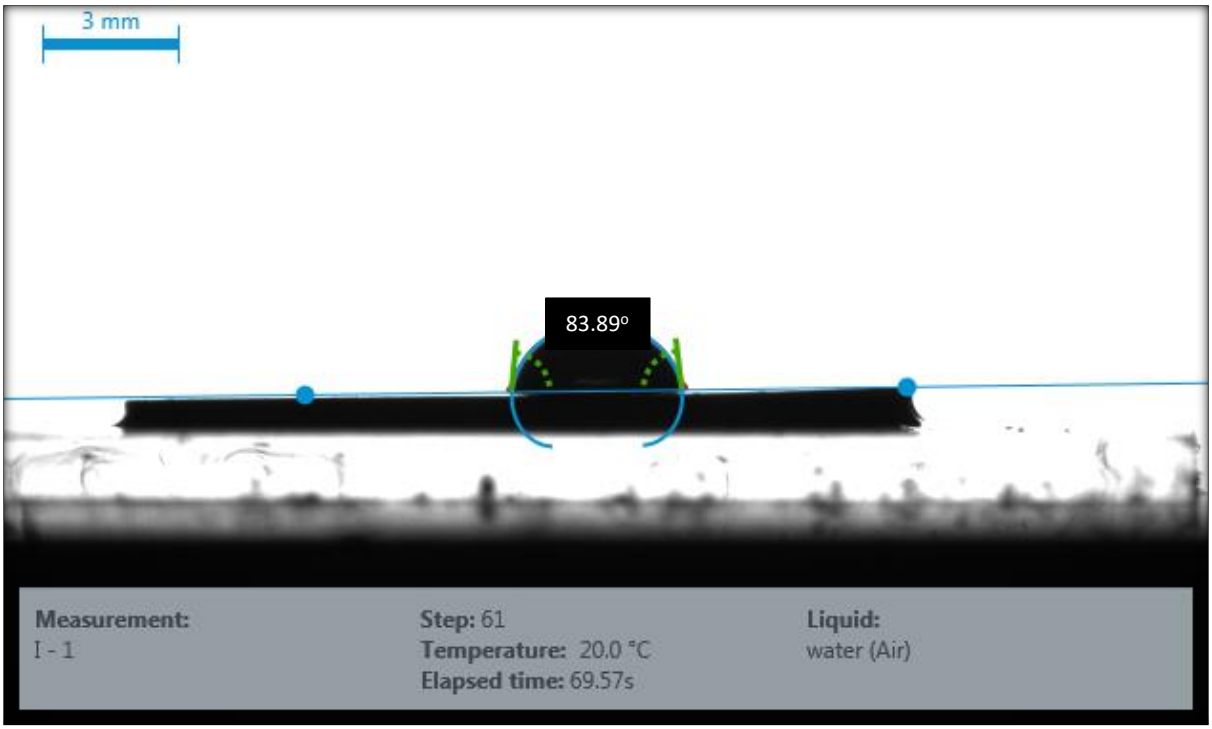

Figure B5. Contact angle measurement of Dolomite core sample reacted with HEDTA

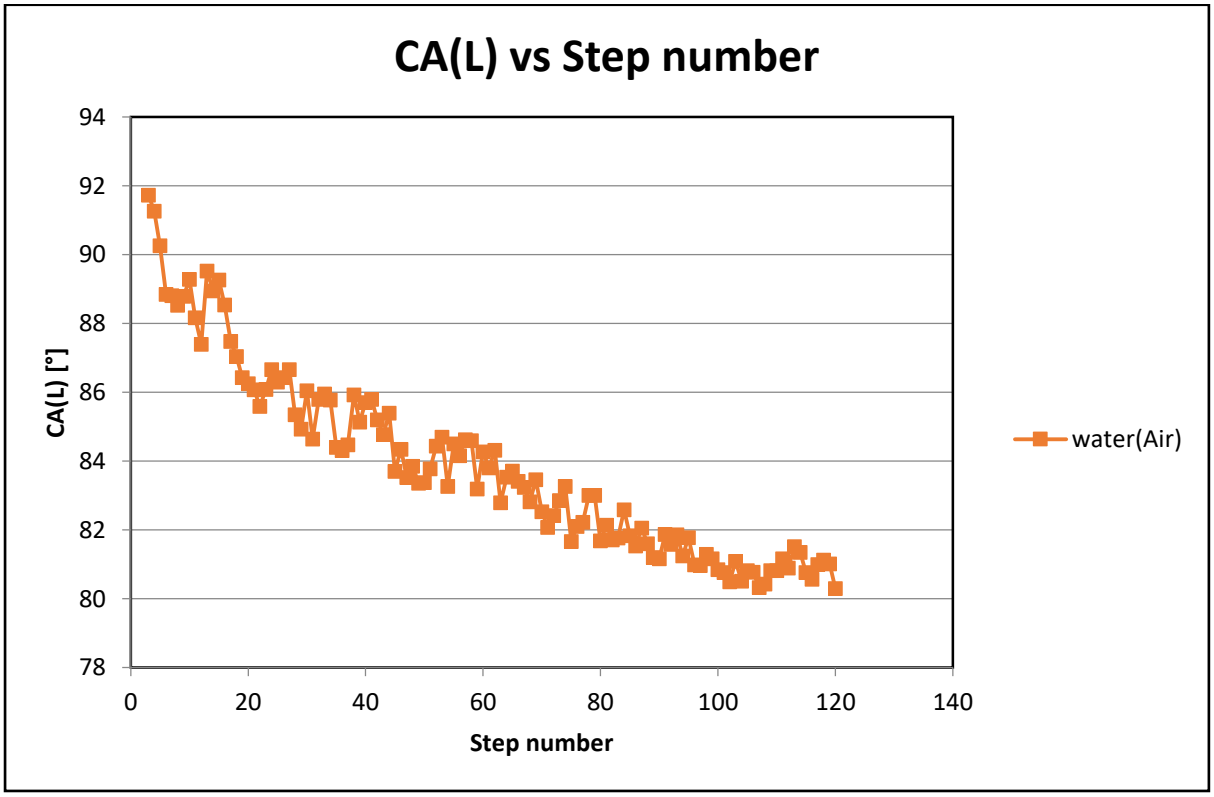

Figure B6. Number of steps vs Calibration for wettability measurement of Dolomite core sample reacted with HEDTA

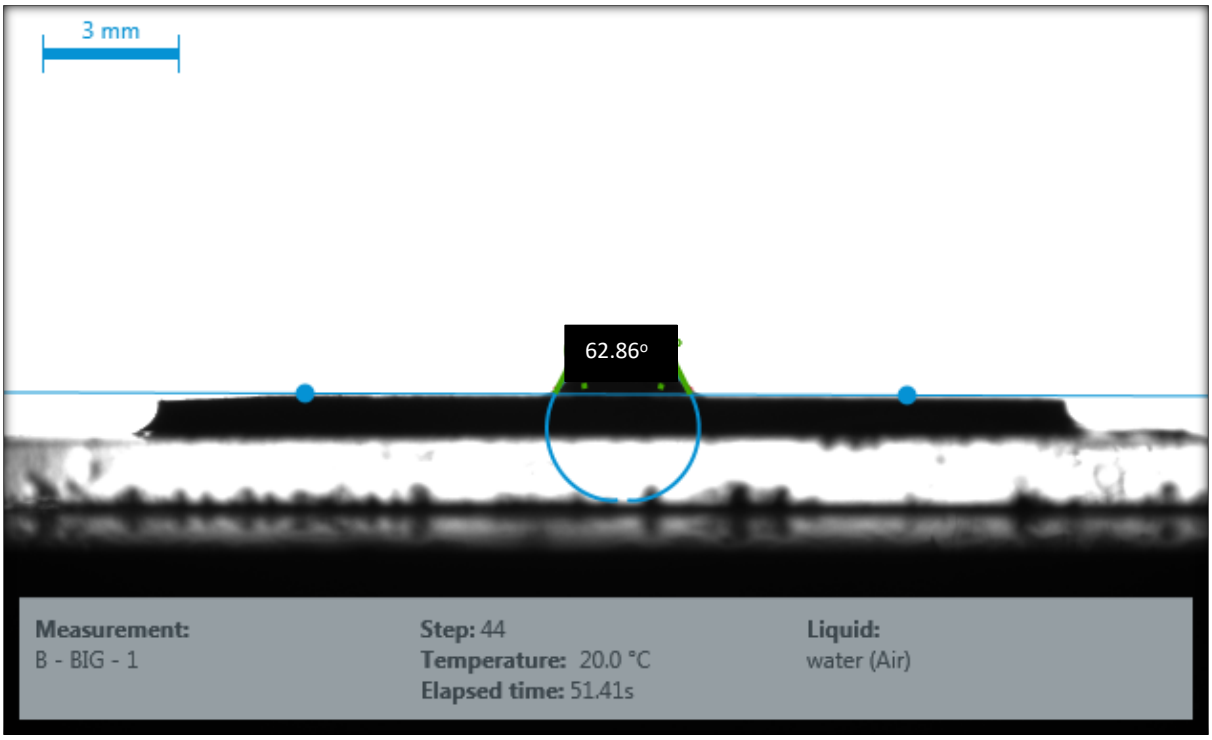

Figure B7. Contact angle measurement of Berea core sample reacted with HEDTA

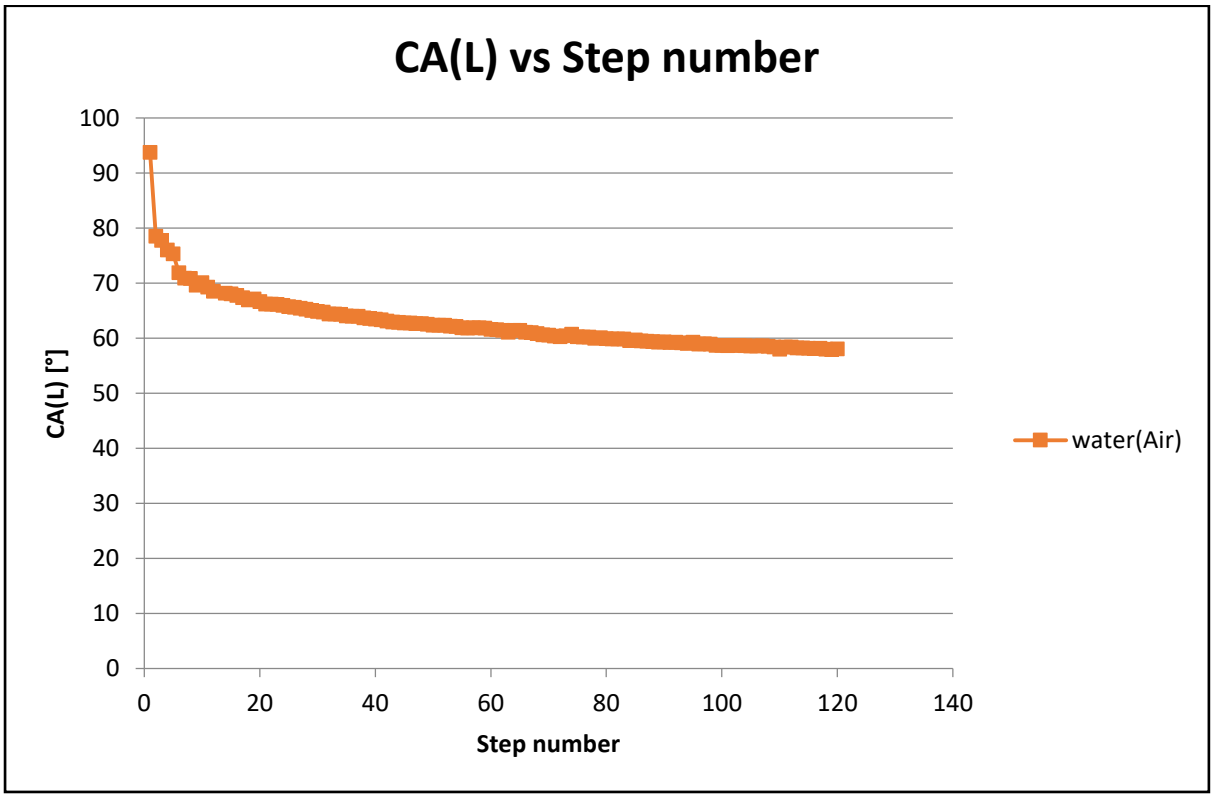

Figure B8. Number of steps vs Calibration for wettability measurement of Berea sample reacted with HEDTA

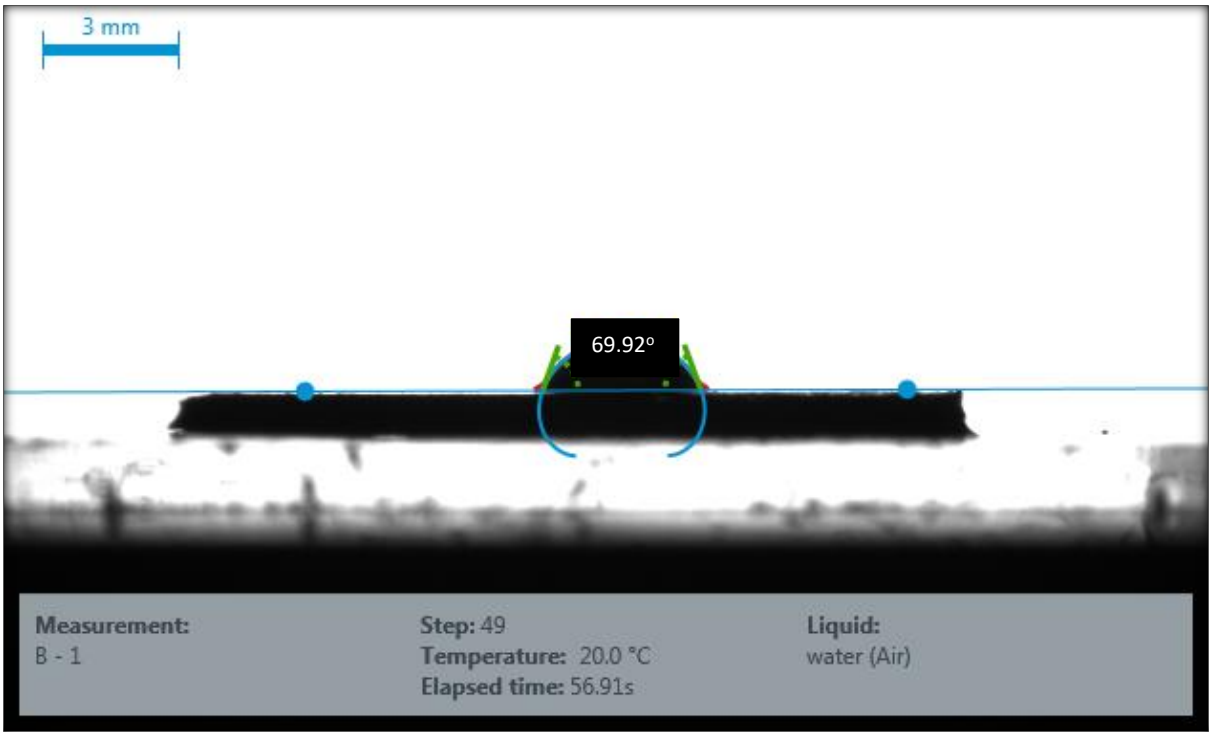

Figure B9. Contact angle measurement of Berea core sample reacted with EDTA

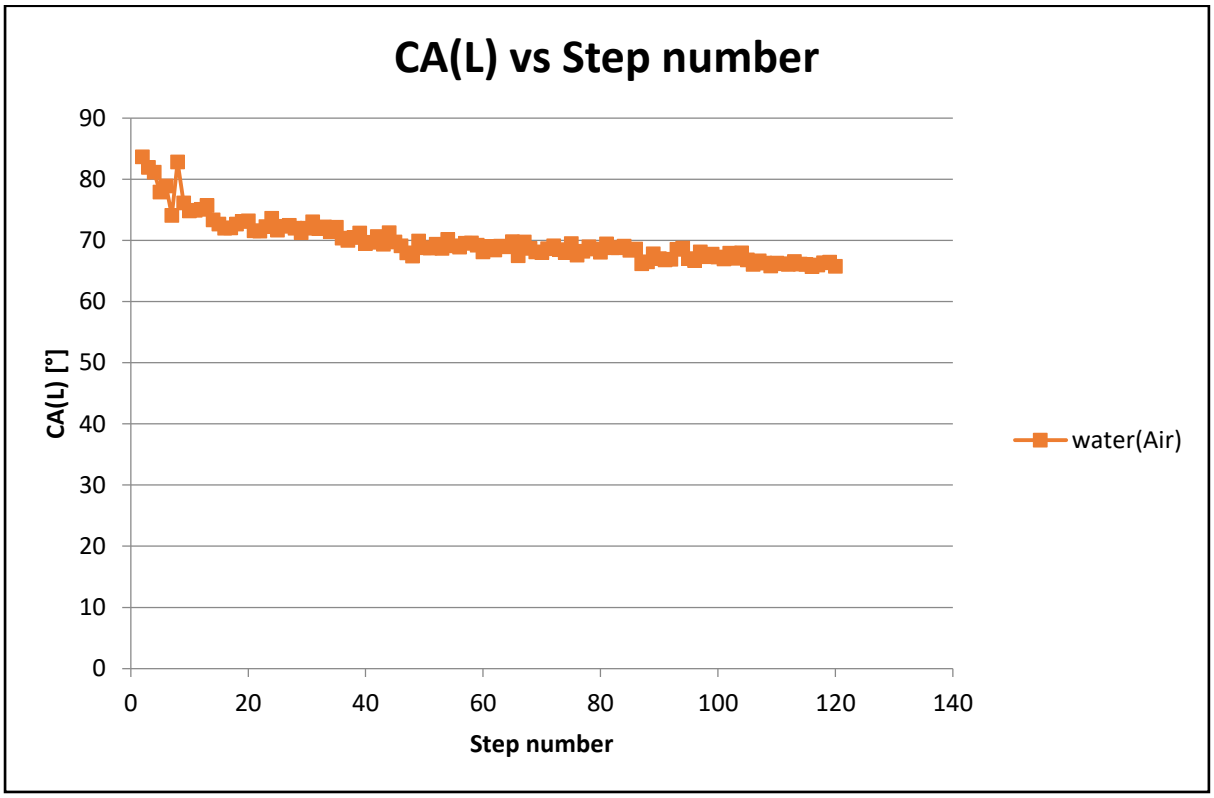

Figure B10. Number of steps vs Calibration for wettability measurement of Berea sample reacted with EDTA

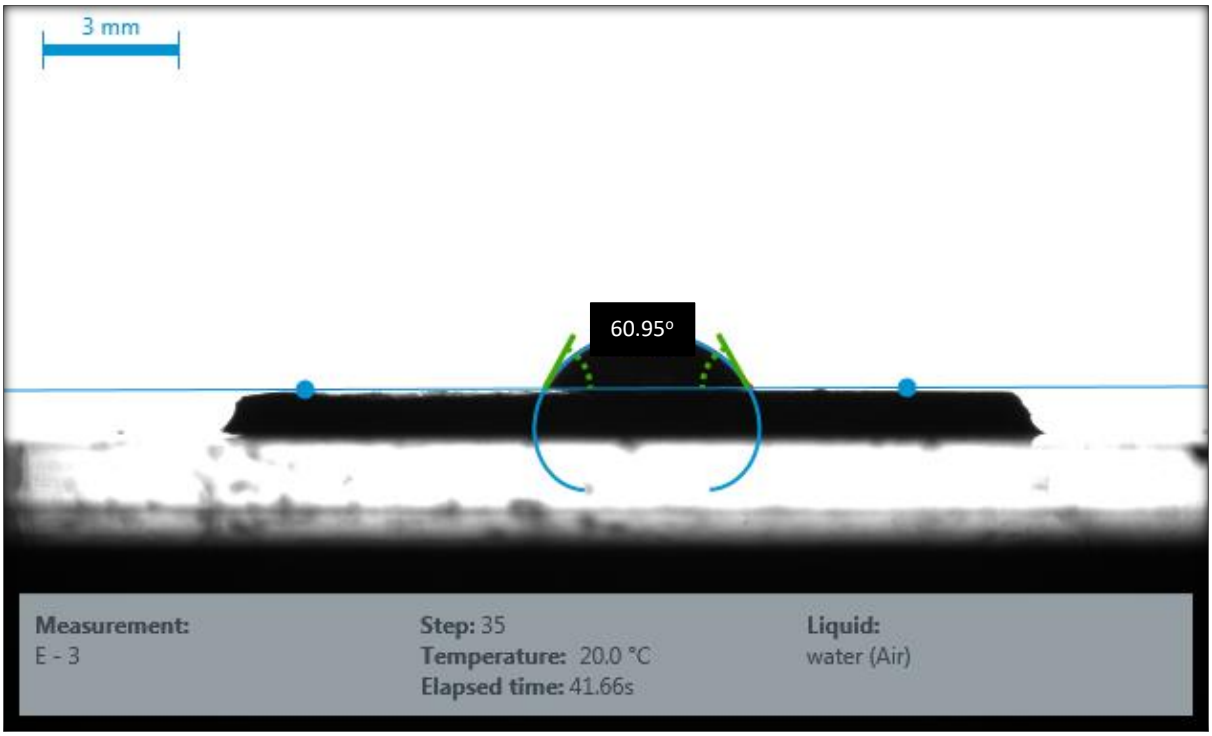

Figure B11. Contact angle measurement of Berea core sample reacted with GLDA

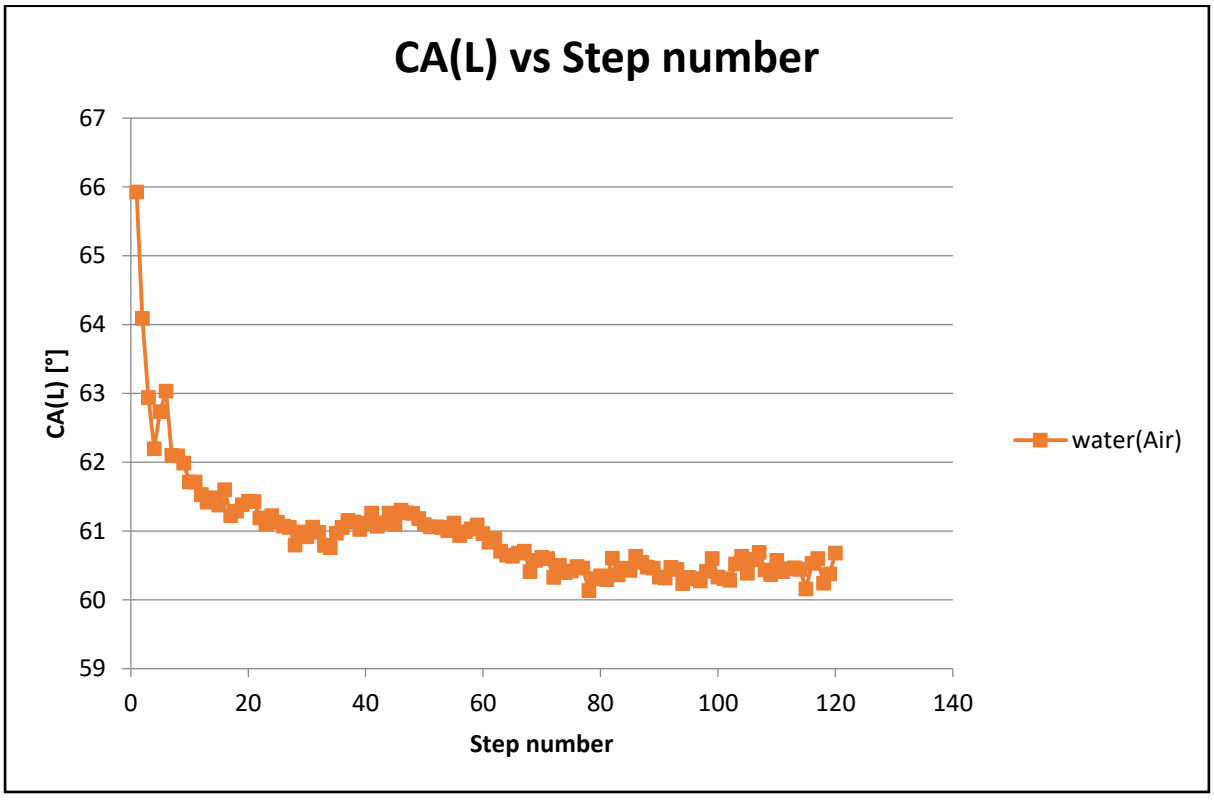

Figure B12. Number of steps vs Calibration for wettability measurement of Berea sample reacted with GLDA

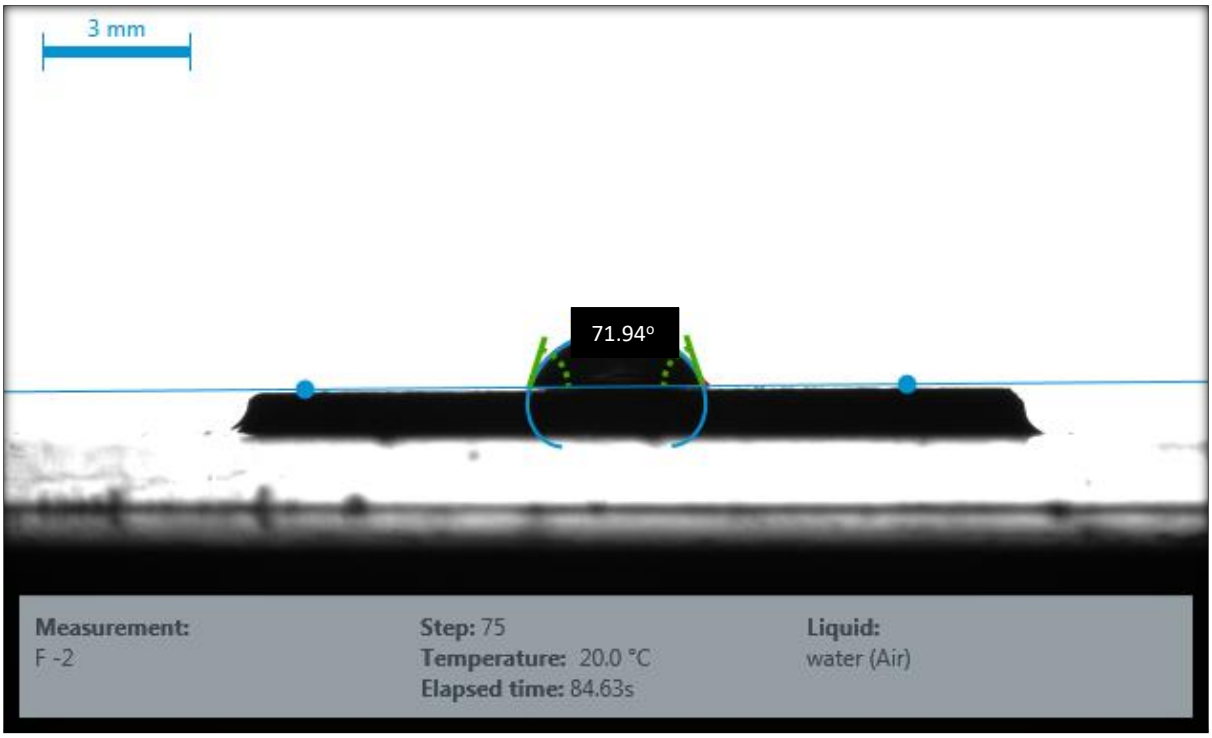

Figure B13. Contact angle measurement of Initial Berea core sample

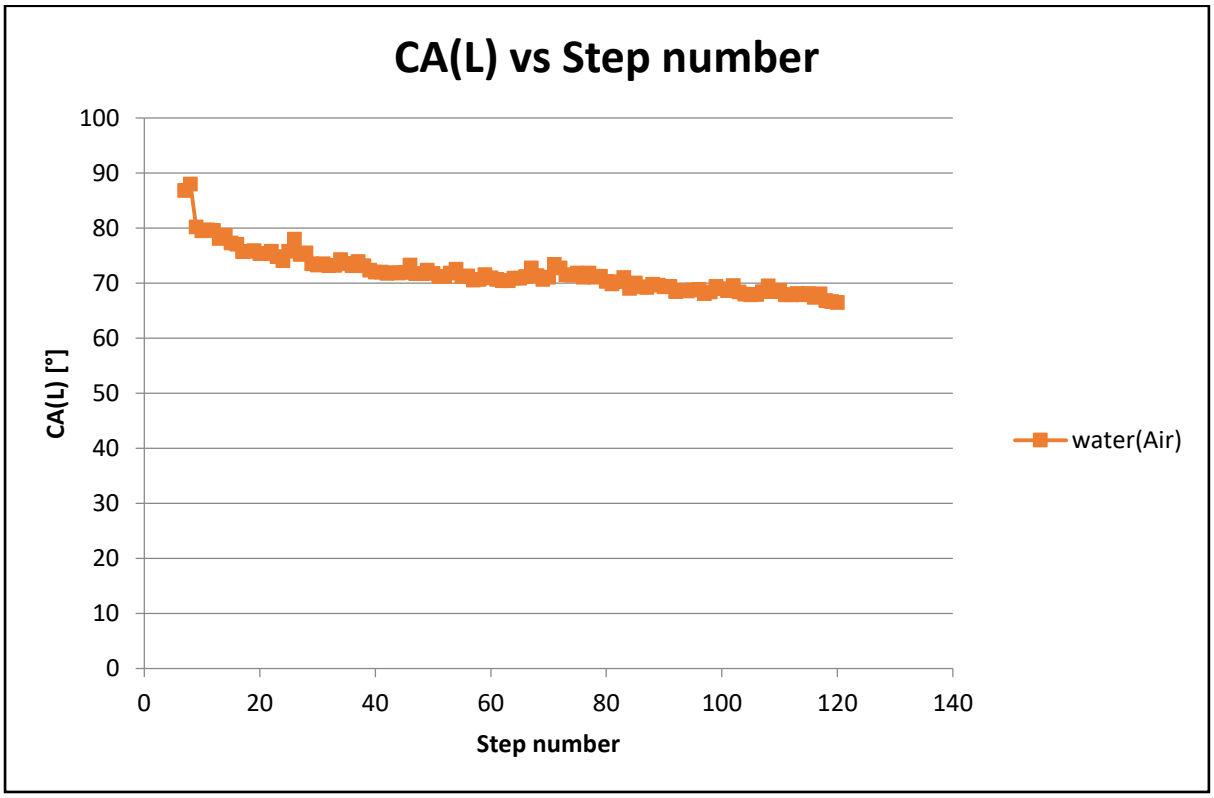

Figure B14. Number of steps vs Calibration for wettability measurement of initial Berea sample

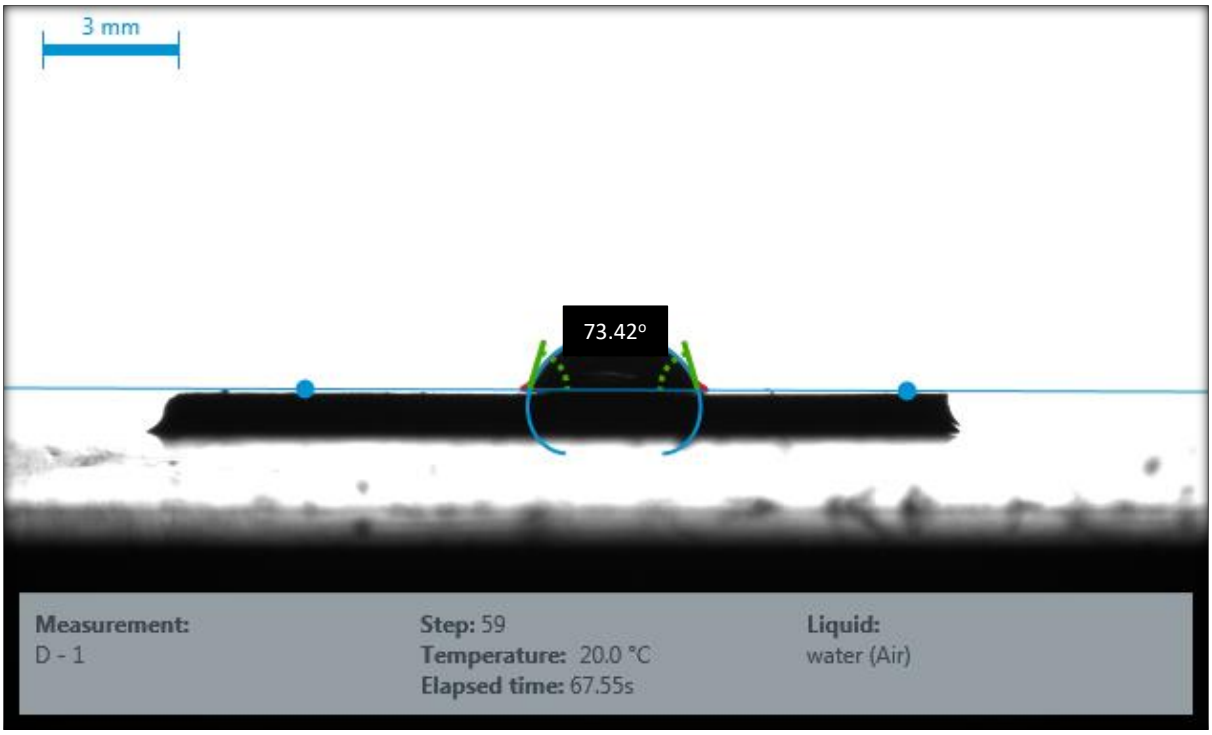

Figure B15. Contact angle measurement of Colton core sample reacted with GLDA

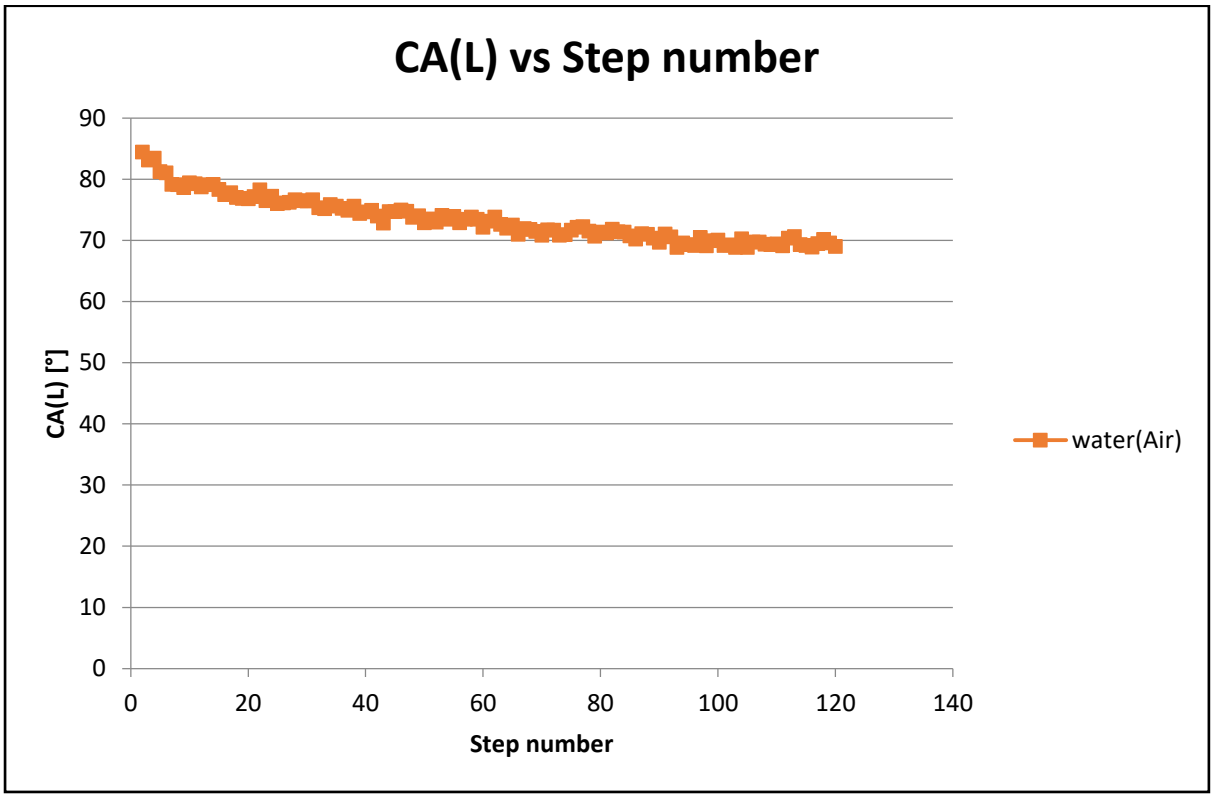

Figure B16. Number of steps vs Calibration for wettability measurement of Colton sample reacted with GLDA

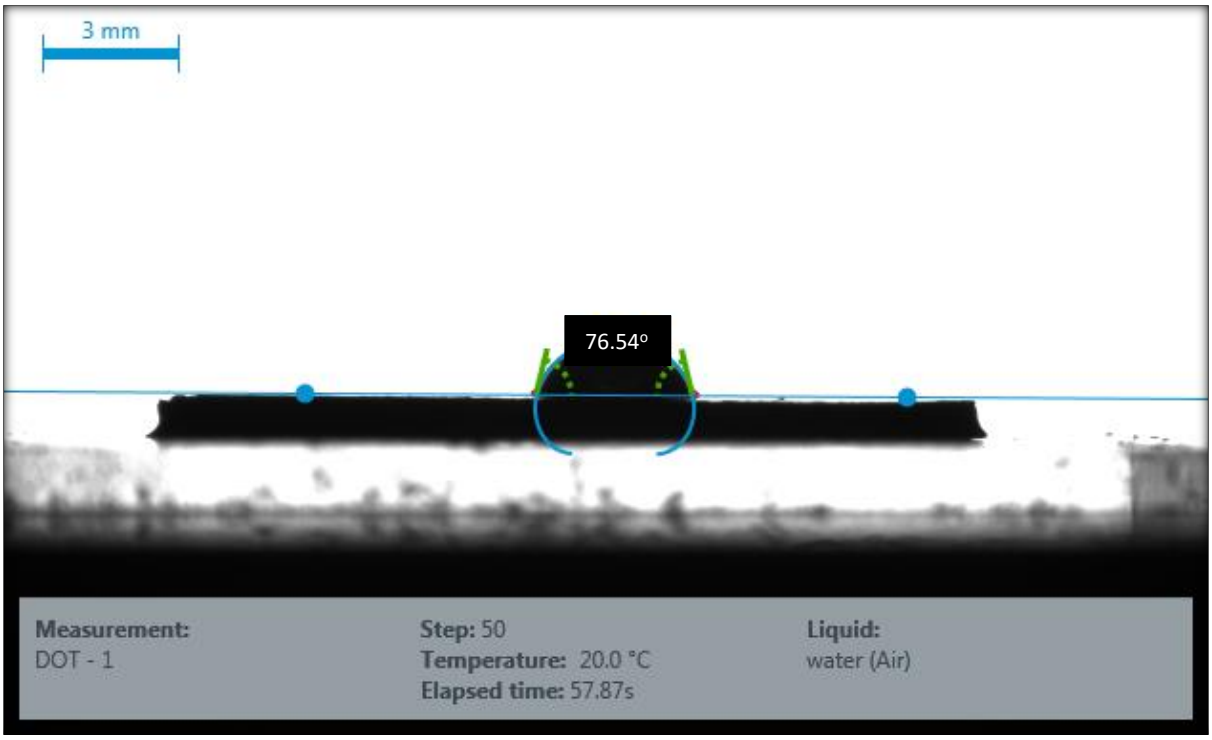

Figure B17. Contact angle measurement of Colton core sample reacted with EDTA

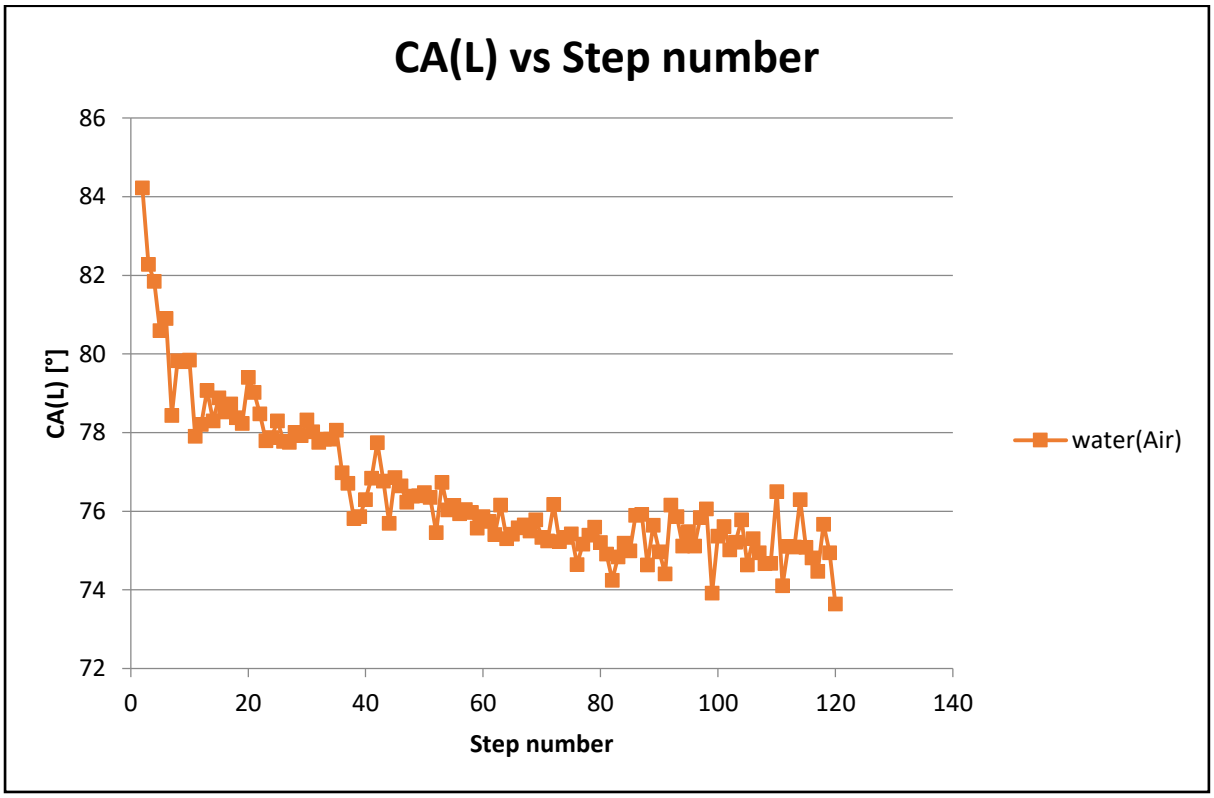

Figure B18. Number of steps vs Calibration for wettability measurement of Colton sample reacted with EDTA

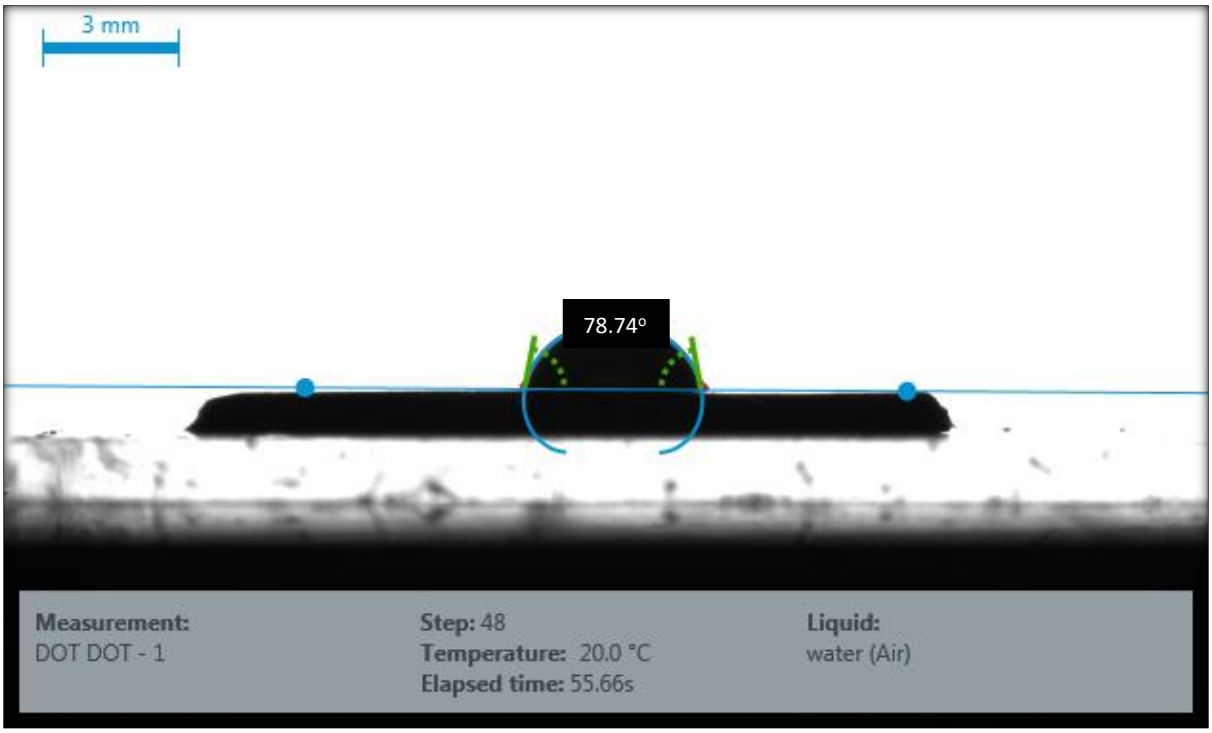

Figure B19. Contact angle measurement of Initial Colton core sample

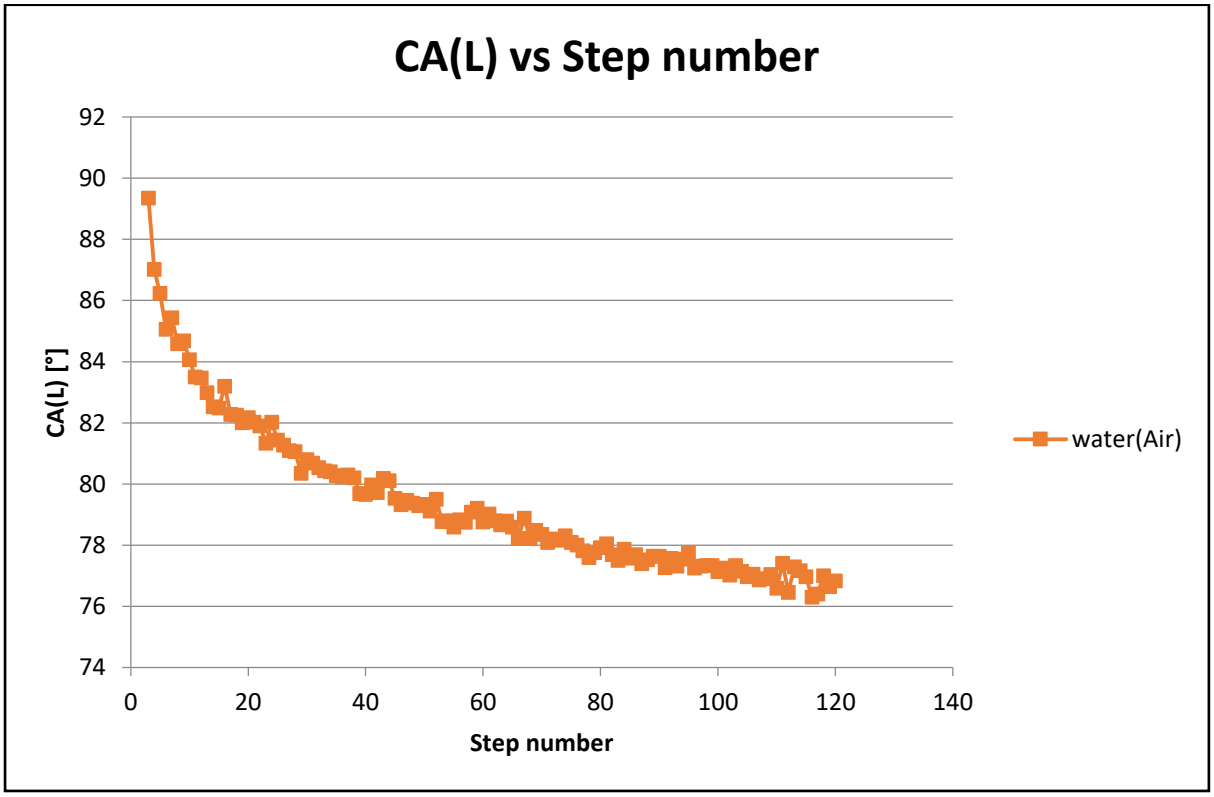

Figure B20. Number of steps vs Calibration for wettability measurement of Initial Colton core sample

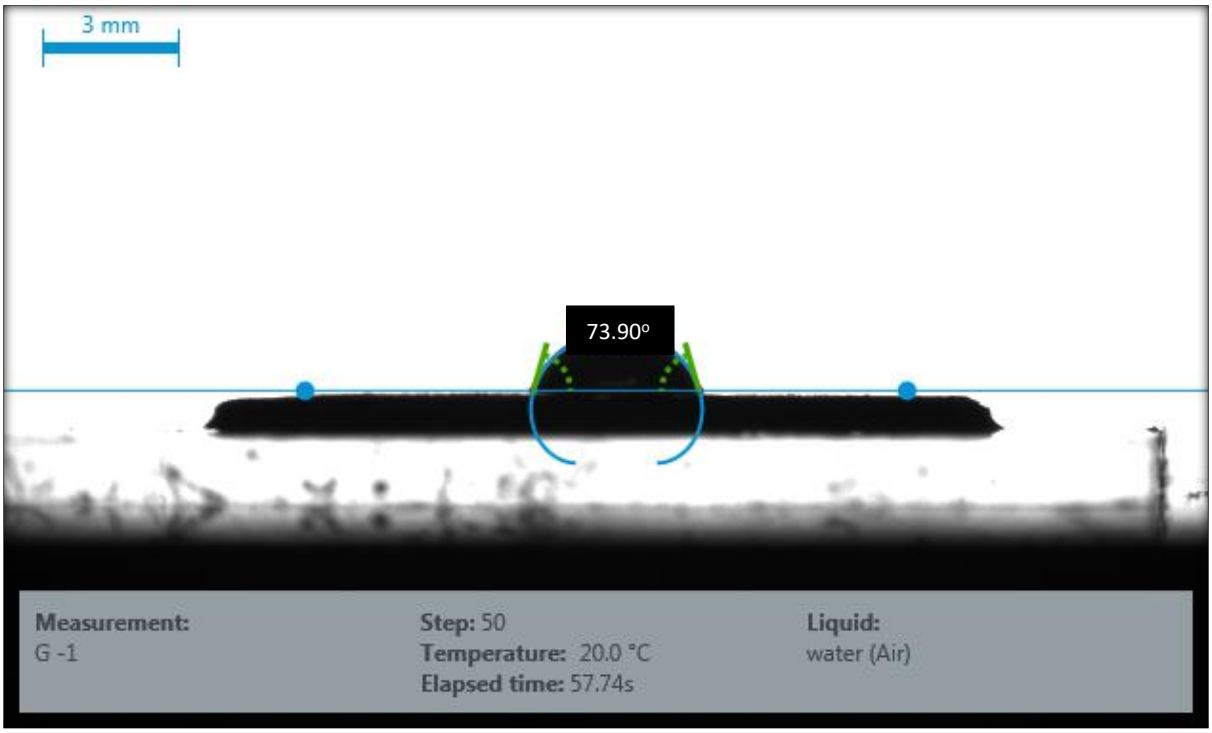

Figure B21. Contact angle measurement of Colton core sample reacted with HEDTA

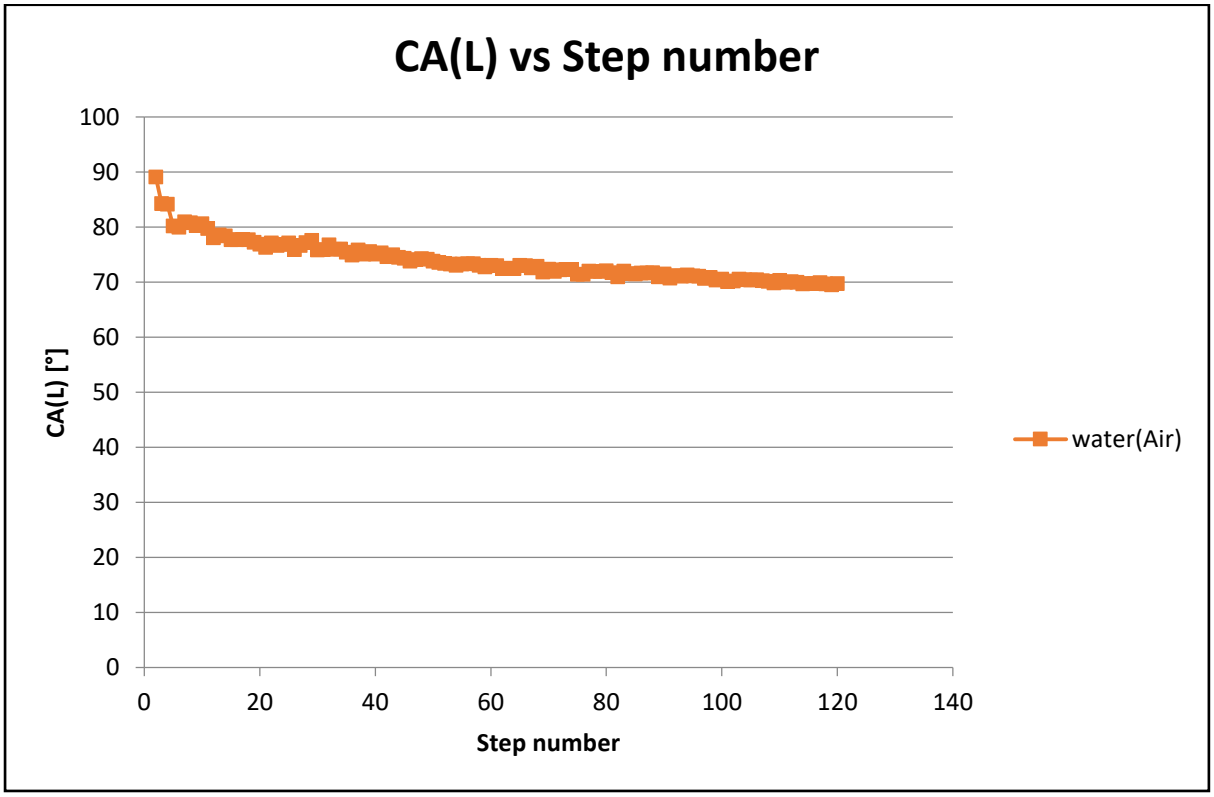

Figure B22. Number of steps vs Calibration for wettability measurement of Colton core sample reacted with HEDTA

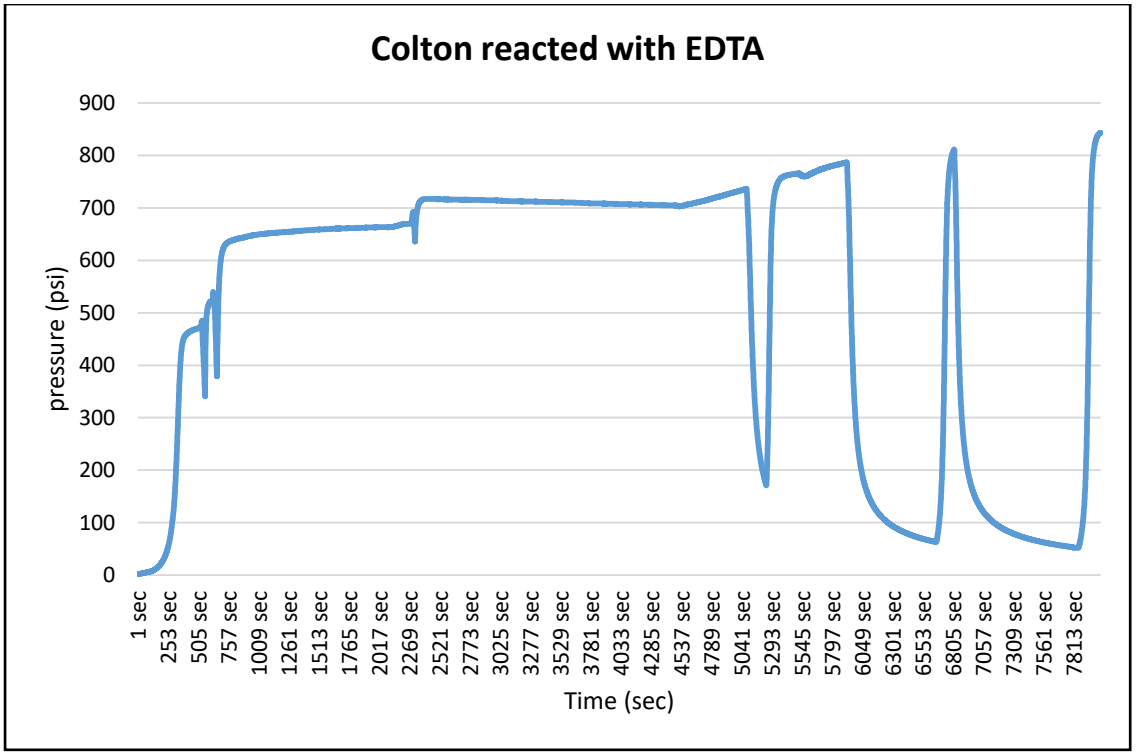

Figure B23. Pressure response vs time during core flooding of Colton sandstone with EDTA

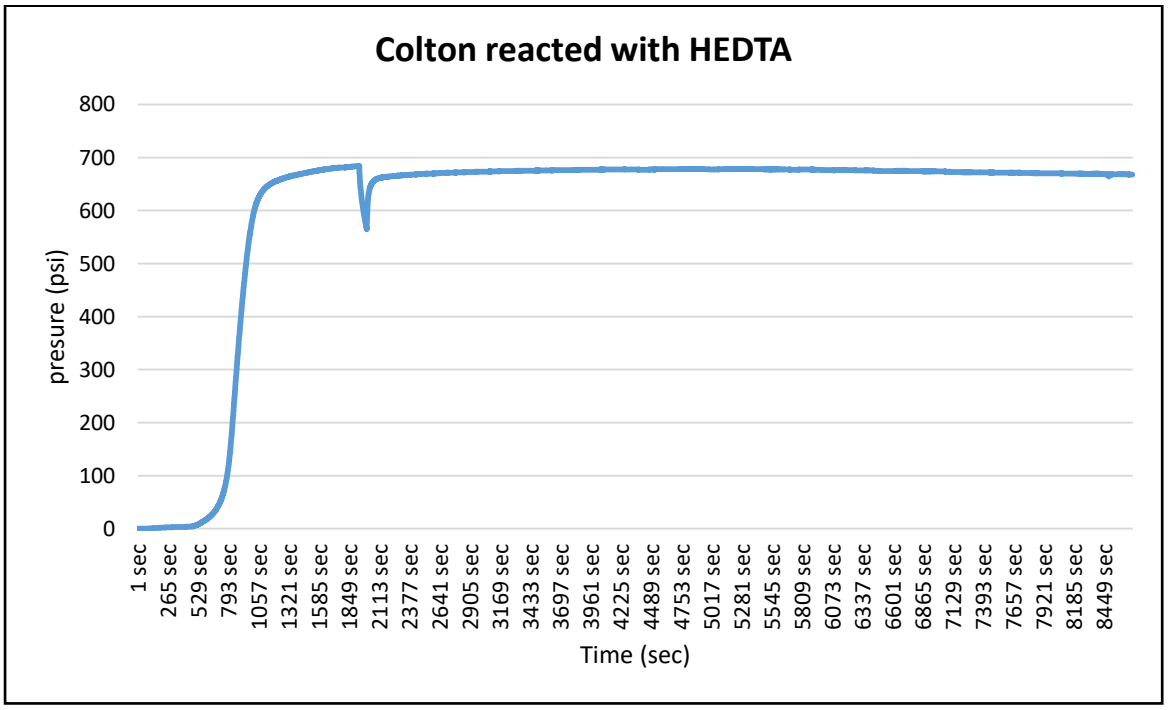

Figure B24. Pressure response vs time during core flooding of Colton sandstone with HEDTA

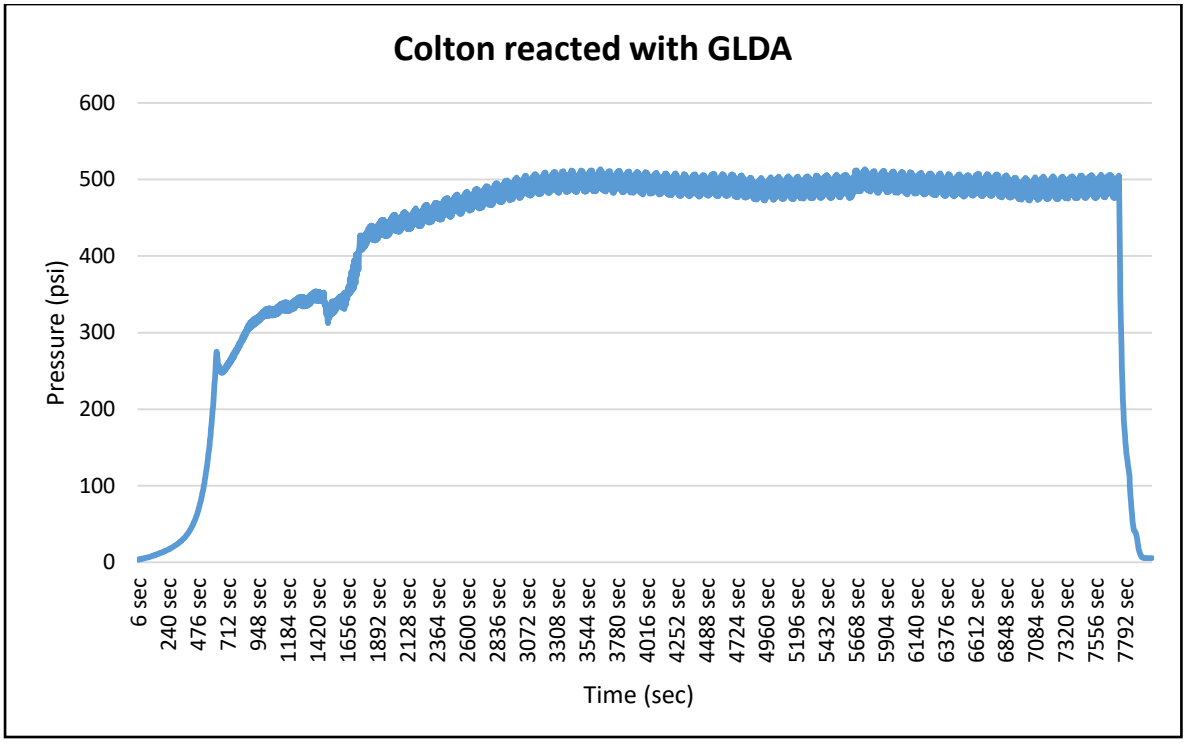

Figure B25. Pressure response vs time during core flooding of Colton sandstone with GLDA

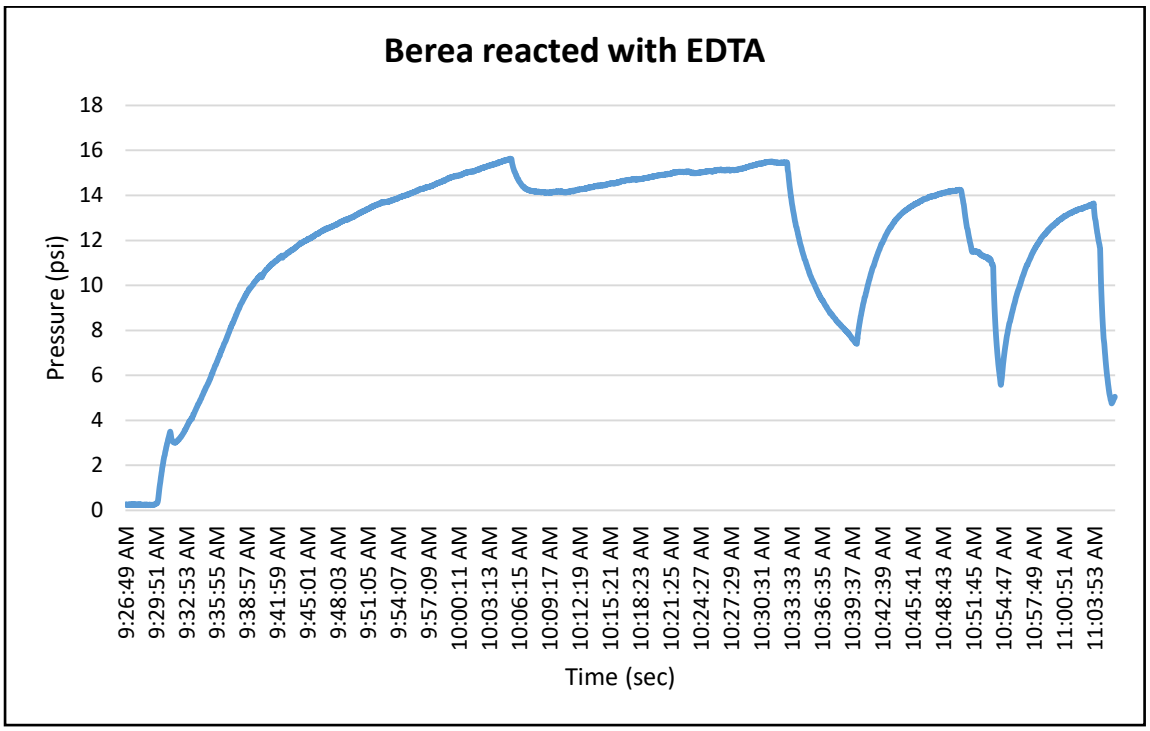

Figure B26. Pressure response vs time during core flooding of Berea sandstone with EDTA

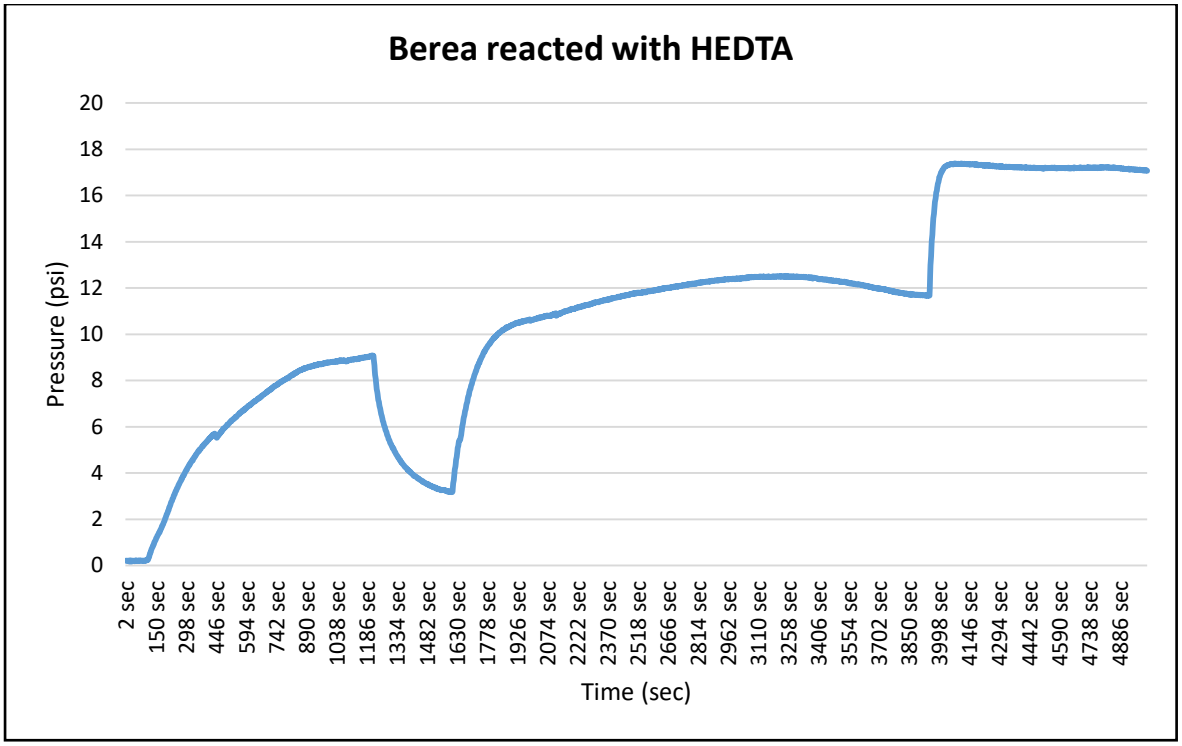

Figure B27. Pressure response vs time during core flooding of Berea sandstone with HEDTA

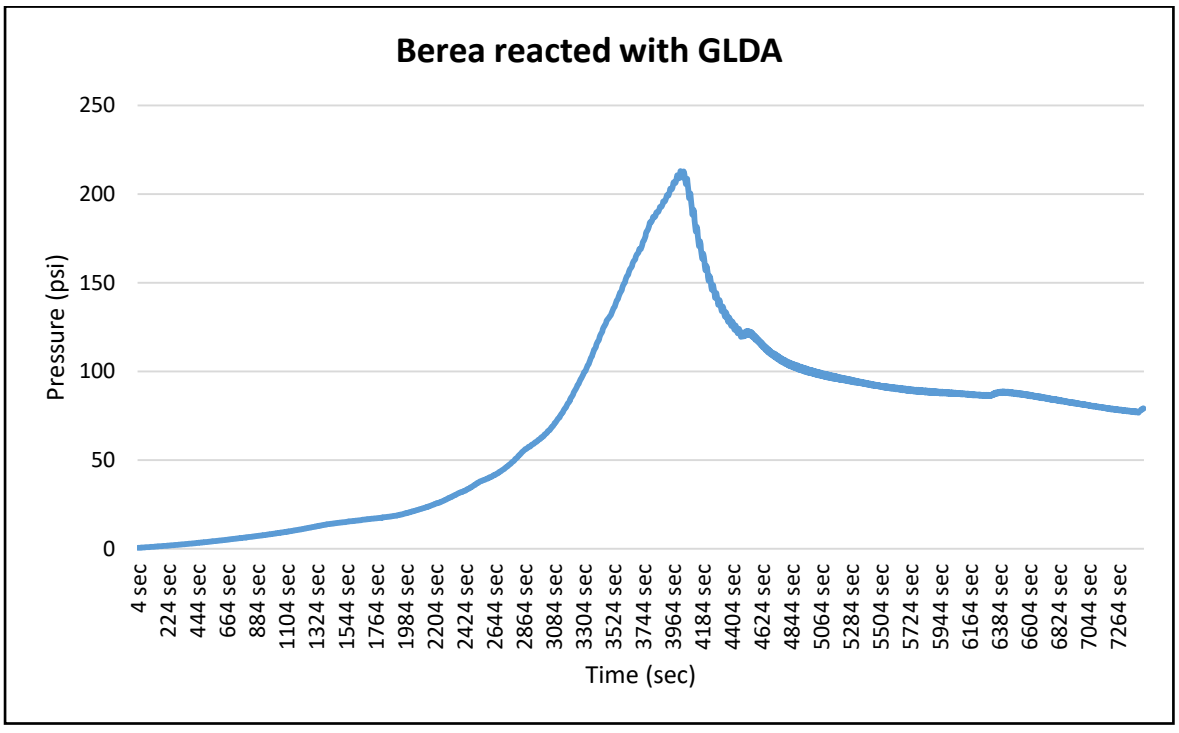

Figure B28. Pressure response vs time during core flooding of Berea sandstone with GLDA

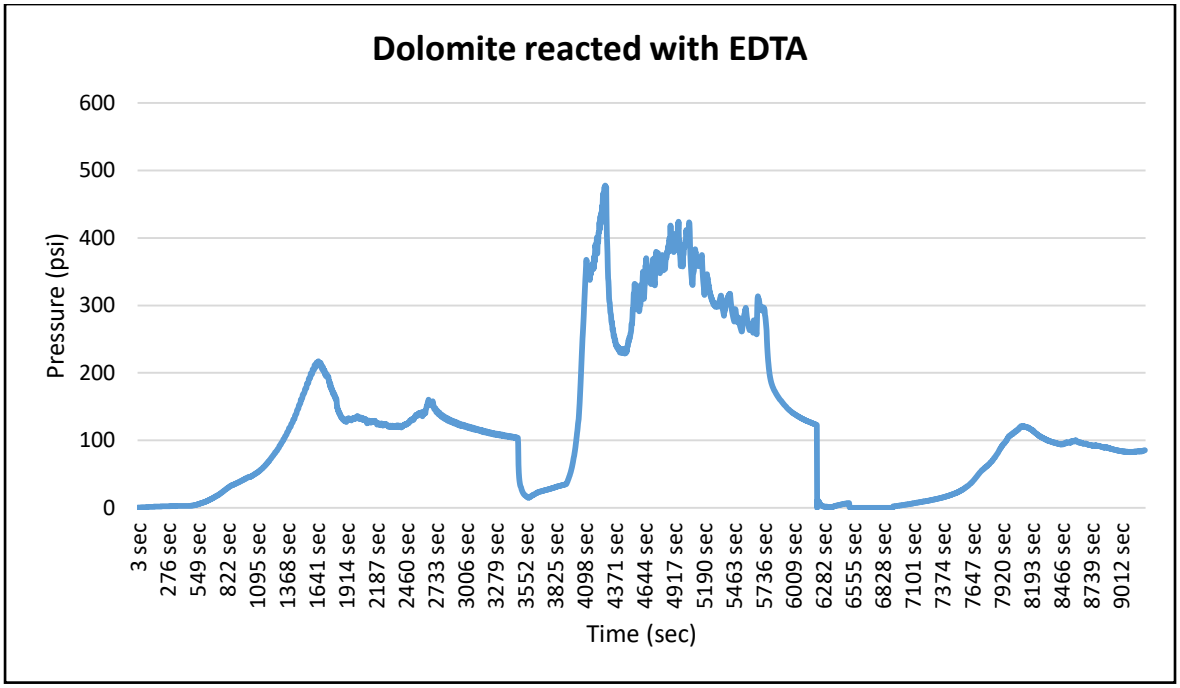

Figure B29. Pressure response vs time during core flooding of Guelph Dolomite with EDTA

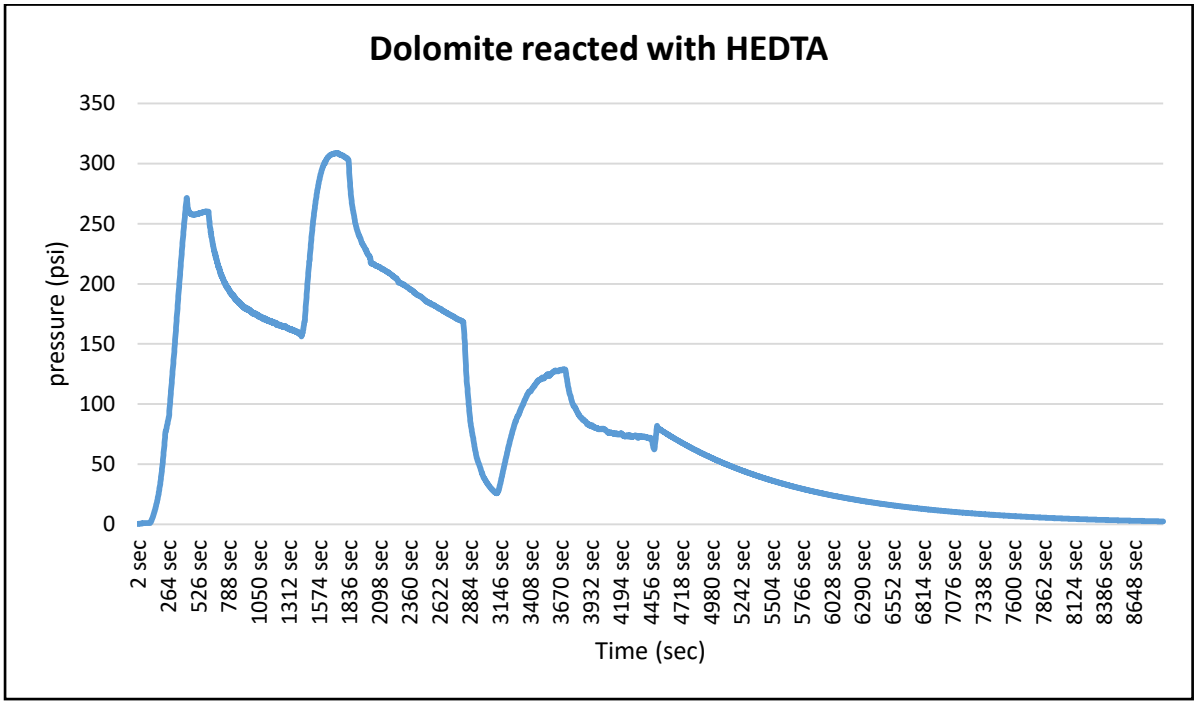

Figure B30. Pressure response vs time during core flooding of Guelph dolomite with HEDTA

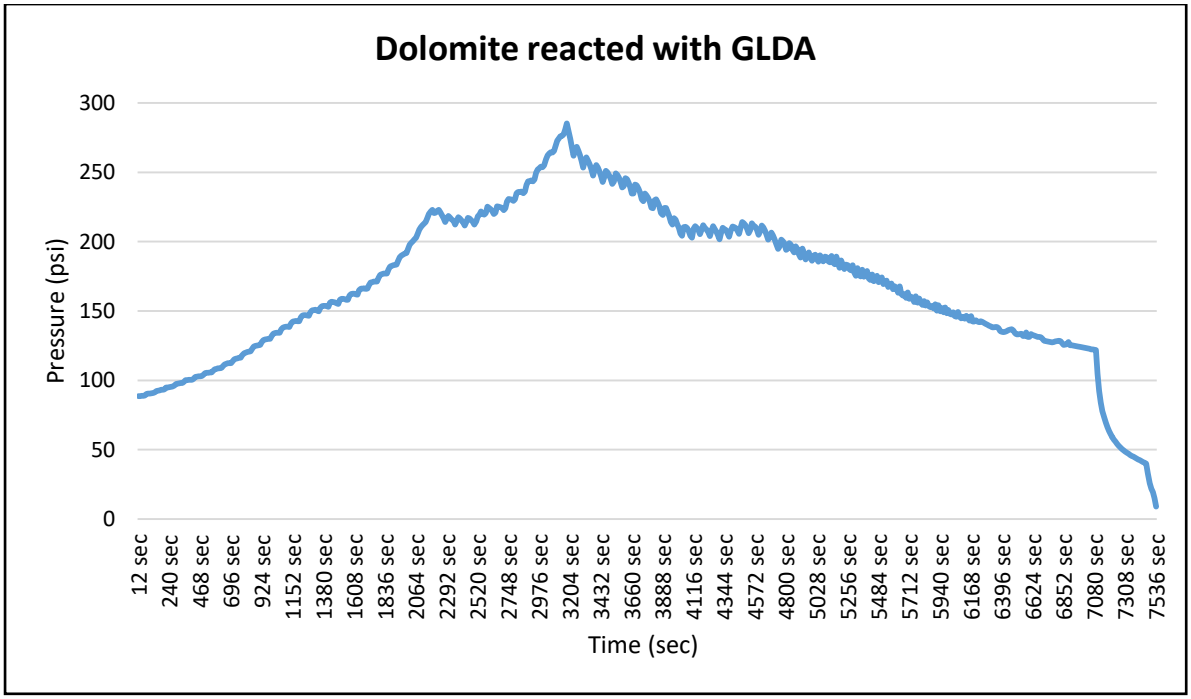

Figure B31. Pressure response vs time during core flooding of Guelph dolomite with GLDA

Table B1. Breakthrough time and volume injected

Sample	Breakthrough	Time	PV injected (15 PV) (ml)
Berea	Sample A	16 mins	213.975
	Sample B	18 mins	251.40
	Sample C	17 mins	250.50
	Sample D	15 mins	244.80
Colton	Sample A	28 mins	133.59
	Sample B	40 mins	144.90
	Sample C	30 mins	150.00
dolomite	Sample A	15 mins	212.32
	Sample B	9 mins	181.51
	Sample C	13 mins	270.855
Berea (Group 2)	Sample A	17 mins	263.89
	Sample B	16 mins	256.23
	Sample C	17 mins	244.20

Appendix C

Table C1: Elemental mass of Berea Sandstone before and after Pre flush stage

Element	Mass [%]		
	Initial	After reaction with 5%CH_3COOH: 10% HCl	After reaction with 15% HCl
Oxygen	52.30	52.48	52.49
Silicon	43.95	44.74	44.80
Aluminum	1.10	1.18	1.15
Potassium	0.92	0.81	0.74
Calcium	0.61	0.39	0.40
Sodium	0.25	0.22	0.19
Iron	0.48	0.03	0.02
Titanium	0.26	0.09	0.07
Carbon	0.14	0.00	0.00
Zirconium	0.06	0.02	0.01
Magnesium	0.05	0.01	0.01
Manganese	0.03	0.00	0.00
Total	99.90	99.98	99.99

Table C2: Iron deportment in Berea Sandstone before and after Pre flush

Minerals	Mass of Iron [%]		
	Initial	After reaction with 5%CH_3COOH: 10% HCl	After reaction with 15% HCl
Ankerite	0.19	0	0
Hematite/Magnetite	0.24	0.01	0.01
Pyrite	0.01	0.01	0
Total	0.48	0.03	0.02

Table C3: Potassium deportment in Berea Sandstone before and after Pre flush

Primary phases	Mass % of Potassium in phase [%]		
	Initial	After reaction with 5%CH_3COOH: 10% HCl	After reaction with 15% HCl
Orthoclase	0.90	0.80	0.73
Muscovite	0.01	0.01	0.01
Total	0.92	0.81	0.74

Table C4: Silicon deportment in Berea Sandstone before and after Pre flush

Primary phases	Mass % of Silicon in phase [%]		
	Initial	After reaction with 5%CH_3COOH: 10% HCl	After reaction with 15% HCl
Orthoclase	1.94	1.72	1.58
Plagioclase	1.62	1.45	1.37
Kaolinite	0.06	0.05	0.04
Zircon	0.02	0.01	0.01
Quartz	41.20	41.12	40.49
Total	44.61	44.58	43.69

Table C5: Titanium deportment in Berea Sandstone before and after Pre flush

Primary phases	Mass % of Titanium in phase [%]		
	Initial	After reaction with 5%CH_3COOH: 10% HCl	After reaction with 15% HCl
Rutile	0.26	0.09	0.07
Total	0.26	0.09	0.07

Table C6: Calcium deportment in Berea Sandstone before and after Pre flush

Primary phases	Mass % of Calcium in phase [%]		
	Initial	After reaction with 5%CH_3COOH: 10% HCl	After reaction with 15% HCl
Ankerite	0.23	0	0
Plagioclase	0.39	0.33	0.34
Total	0.33	0.39	0.61

Table C7: Magnesium deportment in Berea Sandstone before and after Pre flush

Primary phases	Mass % of Magnesium in phase [%]		
	Initial	After reaction with 5%CH_3COOH: 10% HCl	After reaction with 15% HCl
Ankerite	0.04	0	0
Total	0.04	0.01	0.01

Table C8: Mineral mass in Berea Sandstone before and after Pre flush

Minerals	Mass [%]		
	Initial	After reaction with 5%CH_3COOH: 10% HCl	After reaction with 15% HCl
Quartz	86.63	88.29	88.54
Orthoclase	5.26	5.71	6.45
Plagioclase	4.68	5.24	4.43
Ankerite	1.18	0.00	0.00
Kaolinite	0.26	0.25	0.19
Rutile	0.44	0.15	0.11
Muscovite	0.18	0.18	0.14
Hematite/Magnetite	0.34	0.01	0.01
Zircon	0.14	0.04	0.02
Schorl	0.09	0.05	0.03
Total	99.2	100	100

Table C9: Magnetite Mineral Locking in Berea Sandstone before and after Pre flush

Locking phase	Mass of Hematite/Magnetite [%]		
	Initial	After reaction with 5%CH_3COOH: 10% HCl	After reaction with 15% HCl
Quartz	0.26	0	0
Plagioclase	0.02	0	0
Orthoclase	0.02	0	0
Free surface	0.04	0.01	0.01
Total	0.34	0.01	0.01

Table C10: Quartz Mineral Locking in Berea Sandstone before and after Pre flush

Locking phase	Mass of Quartz [%]		
	Initial	After reaction with 5%CH_3COOH: 10% HCl	After reaction with 15% HCl
Orthoclase	5.71	5.62	5.11
Ankerite	0.41	0	0
Muscovite	0.14	0.12	0.13
Plagioclase	6.19	5.09	5.53
Kaolinite	0.38	0.36	0.28
Zircon	0.07	0.02	0.01
Hematite/Magnetite	0.19	0	0.01
Rutile	0.31	0.11	0.06
Free surface	73.50	74.97	76.25
Total	88.55	87.97	86.63

Table C11: Orthoclase Mineral Locking in Berea Sandstone before and after Pre flush

Locking phase	Mass of Orthoclase [%]		
	Initial	After reaction with 5%CH_3COOH: 10% HCl	After reaction with 15% HCl
Plagioclase	0.38	0.35	0.32
Free surface	1.19	1.42	2.02

Table C12: Plagioclase Mineral Locking in Berea Sandstone before and after Pre flush

Locking phase	Mass of Plagioclase [%]		
	Initial	After reaction with 5%CH_3COOH: 10% HCl	After reaction with 15% HCl
Orthoclase	0.38	0.35	0.32

Ankerite	0.02	0	0
Free surface	1.22	1.22	1.28

Table C13: Ankerite Mineral Locking in Berea Sandstone before and after Pre flush

Locking phase	**Mass of Ankerite [%]**		
	Initial	**After reaction with 5%CH_3COOH: 10% HCl**	**After reaction with 15% HCl**
Orthoclase	0.07	0	0
Plagioclase	0.08	0	0
Quartz	0.97	0	0
Rutile	0.01	0	0
Unclassified	0.01	0	0
The rest	0.02	0	0
Free surface	0.02	0	0
Total	1.17	0	0

Table C14: Rutile Mineral Locking in Berea Sandstone before and after Pre flush

Locking phase	**Mass of Rutile [%]**		
	Initial	**After reaction with 5%CH_3COOH: 10% HCl**	**After reaction with 15% HCl**
Orthoclase	0.02	0.01	0.01
Plagioclase	0.03	0.01	0.01
Quartz	0.28	0.11	0.08
Free surface	0.09	0.02	0.02
Total	0.43	0.15	0.11

Table C15: Grain size distribution of Ankerite in Berea Sandstone before and after Pre flush

Size range (µm)	**Number of grains of Ankerite**			
	After reaction with 15% HCl		**After reaction with 5%CH3COOH: 10% HCl**	
	Initial	**Final**	**Initial**	**Final**
9.6<96	497	0	444	1

96<206	89	0	83	0
206<327	15	0	14	0
Total	601	0	541	1

Table C16: Grain size distribution of Rutile in Berea Sandstone before and after Pre flush

Size range (µm)	**Number of grains of Rutile**			
	After reaction with 15% HCl		**After reaction with 5%CH3COOH: 10% HCl**	
	Initial	**Final**	**Initial**	**Final**
9.6<49	1356	279	1294	316
49<98	71	14	68	15
98<150	7	1	6	0
Total	1434	294	1368	331

Table C17: Grain size distribution of Zircon in Berea Sandstone before and after Pre flush

Size range (µm)	**Number of grains of Zircon**			
	After reaction with 15% HCl		**After reaction with 5%CH3COOH: 10% HCl**	
	Initial	**Final**	**Initial**	**Final**
9.6<28	51	17	49	34
8<49	17	8	16	7
49<101	42	6	40	6
Total	110	31	105	47

Table C18: Grain size distribution of Magnetite in Berea Sandstone before and after Pre flush

Size range (µm)	**Number of grains of Hematite/Magnetite**			
	After reaction with 15% HCl		**After reaction with 5%CH3COOH: 10% HCl**	
	Initial	**Final**	**Initial**	**Final**
9.6<40	598	24	590	65
40<77	59	0	55	0
77<124	17	0	15	0
Total	674	24	660	65

Table C19: Grain size distribution of Quartz in Berea Sandstone before and after Pre flush

Size range (µm)	Number of grains of Quartz			
	After reaction with 15% HCl		After reaction with 5%CH3COOH: 10% HCl	
	Initial	Final	Initial	Final
9.6<479	18459	14978	18183	15547
479<1047	221	118	205	61
1047<1431	109	75	106	51
Total	18789	15171	18494	15659

Table C20: Grain size distribution of Orthoclase in Berea Sandstone before and after Pre flush

Size range (µm)	Number of grains of Orthoclase			
	After reaction with 15% HCl		After reaction with 5%CH3COOH: 10% HCl	
	Initial	Final	Initial	Final
9.6<84	14403	9621	14403	12058
84<173	536	376	536	578
173<262	25	24	25	56
Total	14964	10021	14964	12692

Table C21: Number of particles in Berea Sandstone before and after Pre flush

Size range (µm)	Number of particles			
	After reaction with 15% HCl		After reaction with 5%CH3COOH: 10% HCl	
	Initial	Final	Initial	Final
9.6<11	16355	11479	13638	10439
13<29	11971	8377	10373	8102
29<122	4775	2704	4372	2555

122<434	1117	477	885	401
434<1547	295	136	245	125
Total	34513	23173	29513	21622

Table C22: Particles Density distribution in Berea Sandstone before and after Pre flush

Density range (g/cm^3)	**Number of particles**			
	After reaction with 15% HCl		**After reaction with 5%CH3COOH: 10% HCl**	
	Initial	**Final**	**Initial**	**Final**
2.2<2.3	12	10	10	8
2.3<2.4	107	44	105	91
2.4<2.6	6664	4384	6362	5924
2.6<2.7	26760	18465	22093	15287
2.7<2.9	163	73	161	92
2.9<3.1	85	16	87	26
3.1<3.3	126	69	121	69
3.3<3.5	31	6	25	2
3.5<3.7	32	6	30	6
3.7<3.9	34	8	33	13
3.9<4.2	18	0	20	5
4.2<4.4	334	63	321	52
4.4<5.0	25	6	25	15
5.0<5.3	122	20	120	32
Total	34513	23170	29513	21622

Appendix D

Table D1: Elemental mass in Berea Sandstone before and after reaction with chelating agents

Element	Mass of element [%]			
	HEDTA	GLDA	EDTA	Initial
Oxygen	50.98	50.97	50.77	50.99
Sodium	0.14	0.15	0.15	0.19
Magnesium	0.01	0.01	0.01	0.04
Aluminum	0.99	0.98	0.99	1.10
Silicon	43.47	43.6	43.35	44.39
Potassium	0.60	0.66	0.66	0.98
Calcium	0.30	0.34	0.35	1.23
Titanium	0.06	0.05	0.14	0.26
Iron	0.03	0.03	0.03	0.48
Zirconium	0.02	0.01	0.04	0.06
Total	96.55	96.53	96.21	99.10

Table D2: Calcium deportment in Berea Sandstone before and after reaction with chelating agents

Primary phases	Mass % of Calcium in phase [%]			
	HEDTA	GLDA	EDTA	Initial
Albite	0.55	0.57	0.55	0.61
Ankerite	0	0	0	0.23
Plagioclase	0.29	0.33	0.34	0.39
Total	0.30	0.34	0.35	1.23

Table D3: Iron deportment in Berea Sandstone before and after reaction with chelating agents

Minerals	Mass of Iron [%]			
	HEDTA	GLDA	EDTA	Initial
Ankerite	0	0	0	0.19
Hematite/Magnetite	0	0	0	0.24
Pyrite	0	0	0	0.01
Total	0	0	0	0.48

Table D4: Potassium deportment in Berea Sandstone before and after reaction with chelating agents

Primary phases	Mass % of Potassium in phase [%]			
	HEDTA	GLDA	EDTA	Initial
Orthoclase	0.55	0.6	0.59	0.9
Muscovite	0.06	0.06	0.06	0.08
Total	0.6	0.66	0.66	0.98

Table D5: Magnesium deportment in Berea Sandstone before and after reaction with chelating agents

Primary phases	Mass % of Magnesium in phase [%]			
	HEDTA	GLDA	EDTA	Initial
Magnesiogedrite	0.01	0.01	0.01	0.04
Total	0.01	0.01	0.01	0.04

Table D6: Sodium deportment in Berea Sandstone before and after reaction with chelating agents

Primary phases	Mass % of Sodium in phase [%]			
	HEDTA	GLDA	EDTA	Initial
Albite	0.14	0.15	0.15	0.19
Total	0.14	0.15	0.15	0.19

Table D7: Silicon deportment in Berea Sandstone before and after reaction with chelating agents

Primary phases	Mass % of Silicon in phase [%]			
	HEDTA	GLDA	EDTA	Initial
Albite	0.55	0.57	0.55	0.60
Magnesiogedrite	0.01	0.01	0.01	0.04
Orthoclase	1.18	1.29	1.28	1.58
Muscovite	0.12	0.12	0.14	0.15
Kaolinite	0.06	0.24	0.25	0.30
Zircon	0.02	0	0.01	0.02

Quartz	41.27	41.33	41.08	40.49
Plagioclase	0.29	0.33	0.34	0.39
Total	43.47	43.6	43.35	44.39

Table D8: Mineral mass in Berea Sandstone before and after reaction with chelating agents

Minerals	**Mass of phase [%]**			
	HEDTA	**GLDA**	**EDTA**	**Initial**
Albite	1.73	1.82	1.76	1.81
Orthoclase	3.89	4.28	4.23	5.22
Kaolinite	1.13	1.10	1.39	0.26
Zircon	0.04	0.01	0.09	0.16
Quartz	86.63	88.43	87.9	88.3
Rutile	0.39	0.09	0.23	0.43
Ankerite	0	0	0	0.23
Plagioclase	0.33	0.34	0.39	0.29
Hematite/Magnetite	0	0	0	0.24
Pyrite	0	0	0	0.01
Magnesiogedrite	0.01	0.01	0.00	0.04

Table D9: Quartz Mineral Locking in Berea Sandstone before and after reaction with chelating agents

Locking phase	**Mass % of Quartz [%]**			
	HEDTA	**GLDA**	**EDTA**	**Initial**
Albite	1.63	1.63	1.60	1.62
Orthoclase	3.24	3.59	3.65	3.55
Ferrosaponite	0.02	0.03	0.02	0.06
Muscovite	0.42	0.39	0.5	0.6
Kaolinite	1.94	1.49	1.6	1.96
Zircon	0.07	0	0.04	0.10
Rutile	0.27	0.05	0.14	0.60
Unclassified	3.62	3.72	4.14	4.12
Free surface	76.97	77.39	76.07	74.02
Total	88.3	88.43	87.9	86.63

Table D10: Rutile Mineral Locking in Berea Sandstone before and after reaction with chelating agents

Locking phase	Mass % of Rutile [%]			
	HEDTA	GLDA	EDTA	Initial
Orthoclase	0.01	0	0.01	0.06
Kaolinite	0.01	0	0	0.02
Quartz	0.27	0.05	0.14	0.60
Total	0.39	0.09	0.23	0.43

Table D11: Grain size distribution of Ankerite in Berea Sandstone before and after reaction with chelating agents

Size range (µm)	Number of grains of Ankerite					
	Reacted with GLDA		Reacted with EDTA		Reacted with HEDTA	
	Initial	GLDA	Initial	EDTA	Initial	HEDTA
9.6<15	497	2	478	3	499	4
15<24	89	0	85	0	87	0
24<39	15	1	12	1	14	0
Total	601	3	575	4	600	4

Table D12: Grain size distribution of Calcite in Berea Sandstone before and after reaction with chelating agents

Size range (µm)	Number of grains of Calcite					
	Reacted with GLDA		Reacted with EDTA		Reacted with HEDTA	
	Initial	GLDA	Initial	EDTA	Initial	HEDTA
9.6<15	49	17	47	31	44	21
15<24	19	2	18	12	21	0
Total	68	19	65	43	65	21

Table D13: Grain size distribution of Magnetite in Berea Sandstone before and after reaction with chelating agents

Size range (µm)	Number of grains of Hematite/Magnetite					
	Reacted with GLDA		Reacted with EDTA		Reacted with HEDTA	
	Initial	GLDA	Initial	EDTA	Initial	HEDTA
9.6<18	598	6	569	13	578	4
25<47	59	0	53	2	58	2
Total	657	6	622	15	636	7

Table D14: Grain size distribution of Rutile in Berea Sandstone before and after reaction with chelating agents

Size range (µm)	Number of grains of Rutile					
	Reacted with GLDA		Reacted with EDTA		Reacted with HEDTA	
	Initial	GLDA	Initial	EDTA	Initial	HEDTA
9.6<40	1356	199	1257	465	1489	756
40<81	71	11	69	40	85	69
81<121	7	3	6	5	9	8
Total	1434	213	1332	510	1583	833

Table D15: Grain size distribution of Kaolinite in Berea Sandstone before and after reaction with chelating agents

Size range (µm)	Number of grains of Kaolinite					
	Reacted with GLDA		Reacted with EDTA		Reacted with HEDTA	
	Initial	GLDA	Initial	EDTA	Initial	HEDTA
9.6<67	8569	7084	8699	7937	8685	7246

67<133	31	19	29	16	38	35
133<217	6	2	3	1	3	2
Total	8606	7105	8731	7954	8726	7283

Table D16: Grain size distribution of Quartz in Berea Sandstone before and after reaction with chelating agents

Size range (µm)	**Number of grains of Quartz**					
	Reacted with GLDA		**Reacted with EDTA**		**Reacted with HEDTA**	
	Initial	**GLDA**	**Initial**	**EDTA**	**Initial**	**HEDTA**
5<400	18789	16341	17554	15781	18459	14604
400<1016	228	175	226	181	221	188
1016<1386	116	51	111	50	109	42
Total	19133	16567	17891	16012	18789	14834

Table D17: Number of particles in Berea Sandstone before and after reaction with chelating agents

Size range (µm)	**Number of particles**					
	Reacted with HEDTA		**Reacted with GLDA**		**Reacted with EDTA**	
	Initial	**Final**	**Initial**	**Final**	**Initial**	**Final**
9.6<11	15724	15133	14182	13928	15040	14711
11<29	12385	11397	11559	10748	12125	11112
29<121	4485	4097	3859	3626	4256	3962
121<430	995	883	958	879	923	823
430<1528	298	221	265	223	269	222

Total	33887	31731	30823	29404	32613	30830

Table D18: Particle Density distribution in Berea Sandstone before and after reaction with chelating agents

Density range (g/cm^3)	**Number of particles**					
	Reacted with HEDTA		**Reacted with GLDA**		**Reacted with EDTA**	
	Initial	Final	Initial	Final	Initial	Final
2.1<2.5	369	285	324	255	348	295
2.5<2.8	32896	30987	30250	28974	31790	30189
2.8<3.3	223	151	168	114	232	162
3.3<4.4	350	273	58	44	209	157
4.4<6.4	49	35	23	17	34	27
Total	33887	31731	30823	29404	32613	30830

Appendix E

Table E1: Elemental mass in Colton Sandstone before and after reaction with chelating agents

Element	Mass % of element [%]			
	EDTA	Initial	HEDTA	GLDA
Carbon	1.38	1.48	1.86	1.46
Oxygen	43.74	44.29	45.42	44.2
Sodium	0.76	0.75	0.70	0.73
Magnesium	0.45	0.44	0.41	0.45
Aluminum	2.32	2.21	2.21	2.26
Silicon	30.82	31.08	30.77	30.98
Potassium	0.58	0.55	0.53	0.59
Calcium	3.77	4.06	5.21	4.03
Iron	1.5	1.5	1.52	1.49
Barium	0.03	0.05	0.06	0.04
Total	85.68	86.72	89.03	86.53

Table E2: Silicon deportment in Colton Sandstone before and after reaction with chelating agents

Primary phases	Mass % of Silicon in phase [%]			
	EDTA	Initial	HEDTA	GLDA
Garnet - Pyrope	0.08	0.07	0.07	0.08
Albite	2.87	2.82	2.62	2.75
Magnesiogedrite	0.24	0.23	0.15	0.23
Orthoclase	0.98	0.94	0.92	1.01
Muscovite	0.23	0.21	0.19	0.21
Wollastonite	0.05	0.05	0.06	0.05
Anorthite	0.37	0.32	0.36	0.33
Kaolinite	0.33	0.32	0.36	0.35
Quartz	25.53	25.98	25.84	25.81
Total	30.82	31.08	30.77	30.98

Table E3: Iron deportment in Colton Sandstone before and after reaction with chelating agents

Primary phases	Mass % of Iron in phase [%]			
	EDTA	Initial	HEDTA	GLDA
Magnesiogedrite	0.16	0.16	0.10	0.16
Ankerite	0.98	0.99	0.92	0.98
Ferrosaponite	0.07	0.06	0.04	0.07
Hematite/Magnetite	0.23	0.25	0.21	0.23
Total	1.5	1.5	1.52	1.49

Table E4: Calcium deportment in Colton Sandstone before and after reaction with chelating agents

Primary phases	Mass % of calcium in phase [%]			
	EDTA	Initial	HEDTA	GLDA
Albite	0.07	0.07	0.06	0.07
Ankerite	1.34	1.18	1.18	1.17
Calcite	2.50	2.53	2.22	2.51
Wollastonite	0.07	0.07	0.08	0.06
Anorthite	0.15	0.13	0.15	0.14
Total	3.77	4.06	5.21	4.03

Table E5: Carbon deportment in Colton Sandstone before and after reaction with chelating agents

Primary phases	Mass % of Carbon in phase [%]			
	EDTA	Initial	HEDTA	GLDA
Ankerite	0.80	0.71	0.71	0.70
Calcite	1.05	0.76	0.66	0.75
Total	1.86	1.48	1.38	1.46

Table E6: Mineral mass in Colton Sandstone before and after reaction with chelating agents

Primary phases	Mass % of phase [%]			
	HEDTA	Initial	EDTA	GLDA

Garnet - Pyrope	0.38	0.34	0.33	0.39
Albite	9.11	8.96	8.32	8.73
Magnesiogedrite	1.20	1.18	0.77	1.18
Orthoclase	3.22	3.11	3.03	3.35
Ankerite	6.06	6.07	6.88	6.02
Calcite	5.53	6.31	8.74	6.26
Muscovite	1.11	0.98	0.89	1.0
Wollastonite	0.20	0.21	0.23	0.19
Anorthite	1.23	1.06	1.19	1.10
Guelph dolomite	0.08	0.10	0.05	0.07
Kaolinite	1.53	1.45	2.10	1.62
Hematite/Magnetite	0.34	0.36	0.30	0.33
Quartz	54.62	55.59	55.28	55.22
Unclassified	14.32	13.28	10.97	13.47
Total	98.93	99	99.08	98.93

Table E7: Ankerite mineral locking in Colton Sandstone before and after reaction with chelating agents

Locking phase	**Mass % of Ankerite [%]**			
	HEDTA	**Initial**	**EDTA**	**GLDA**
Albite	0.58	0.54	0.72	0.56
Magnesiogedrite	0.06	0.05	0.04	0.05
Orthoclase	0.21	0.18	0.23	0.21
Calcite	0.23	0.26	0.40	0.27
Muscovite	0.05	0.05	0.05	0.05
Kaolinite	0.19	0.15	0.33	0.2
Hematite/Magnetite	0.01	0.01	0.01	0.01
Quartz	2.89	2.81	3.39	2.91
Unclassified	1.07	0.93	0.94	0.98
Free surface	0.57	0.9	0.55	0.58
Total	6.06	6.07	6.88	6.02

Table E8: Calcite mineral locking in Colton Sandstone before and after reaction with chelating agents

Locking phase	Mass % of Calcite [%]			
	HEDTA	Initial	EDTA	GLDA
Albite	0.54	0.6	0.92	0.6
Magnesiogedrite	0.06	0.06	0.06	0.06
Orthoclase	0.2	0.21	0.3	0.22
Ankerite	0.29	0.35	0.49	0.33
Muscovite	0.05	0.05	0.07	0.05
Kaolinite	0.17	0.15	0.42	0.21
Quartz	2.7	3.1	4.32	3.07
Unclassified	0.98	1.01	1.2	1.04
Free surface	0.36	0.58	0.66	0.48
Total	5.53	6.31	8.74	6.26

Table E9: Kaolinite mineral locking in Colton Sandstone before and after reaction with chelating agents

Locking phase	Mass % of Kaolinite [%]			
	HEDTA	Initial	EDTA	GLDA
Albite	0.13	0.10	0.18	0.12
Orthoclase	0.04	0.04	0.06	0.05
Ankerite	0.06	0.06	0.09	0.07
Calcite	0.05	0.04	0.09	0.06
Quartz	0.61	0.49	0.8	0.6
Unclassified	0.23	0.18	0.24	0.22
Free surface	0.34	0.49	0.57	0.44
Total	1.53	1.45	2.1	1.62

Table E10: Magnesiogedrite mineral locking in Colton Sandstone before and after reaction with chelating agents

Locking phase	Mass % of Magnesiogedrite [%]			
	HEDTA	Initial	EDTA	GLDA
Albite	0.12	0.11	0.08	0.11
Quartz	0.58	0.55	0.38	0.57
Unclassified	0.22	0.2	0.11	0.2
Free surface	0.06	0.1	0.03	0.06
Total	1.2	1.18	0.77	1.18

Table E11: Grain size distribution of ankerite in Colton Sandstone before and after reaction with chelating agents

Size range (µm)	Number of grains of Ankerite					
	Initial	HEDTA	Initial	EDTA	Initial	GLDA
9.6<59	4197	3753	2717	2502	3903	3464
59<127	1741	1377	1402	1352	1692	1424
127<205	85	51	131	121	83	61
Total	6023	5181	4250	3975	5678	4949

Table E12: Grain size distribution of calcite in Colton Sandstone before and after reaction with chelating agents

Size range (µm)	Number of grains of Calcite					
	Initial	HEDTA	Initial	EDTA	Initial	GLDA

9.6<96	8691	7913	8359	8304	8990	8330
96<180	20	13	31	27	20	14
180<273	3	0	2	1	1	0
Total	8714	7926	8392	8332	9011	8344

Table E13: Grain size distribution of orthoclase in Colton Sandstone before and after reaction with chelating agents

Size range (µm)	**Number of grains of Orthoclase**					
	Initial	**HEDTA**	**Initial**	**EDTA**	**Initial**	**GLDA**
9.6<63	4579	4311	3881	3475	4656	4596
63<122	734	618	592	518	661	645
122<195	54	52	80	78	72	70
Total	5367	4981	4553	4071	5389	5311

Table E14: Grain size distribution of quartz in Colton Sandstone before and after reaction with chelating agents

Size range (µm)	**Number of grains of Quartz**					
	Initial	**HEDTA**	**Initial**	**EDTA**	**Initial**	**GLDA**
9.6<342	20567	18690	16307	14540	20654	19290
342<719	297	240	232	212	260	237
719<1124	35	31	50	48	52	42
Total	20899	18961	16589	14800	20966	19569

Table E15. Number of Particles in Colton Sandstone before and after reaction with chelating agents

Size Range (µm)	**Number of particles**					
	Reacted with HEDTA		**Reacted with EDTA**		**Reacted with GLDA**	
	Initial	**Reacted**	**Initial**	**Reacted**	**Initial**	**Reacted**
9.6<48	49624	34422	40625	27494	48833	37252
48<201	2539	1061	2554	718	2618	1231
201< 524	225	48	210	33	225	43
524< 994	59	10	49	15	44	10
994< 1607	128	108	104	97	124	118
Total	52575	35649	43542	28357	51844	38654

Table E16: Particles density distribution in Colton Sandstone before and after reaction with chelating agents

Density range (g/cm^3)	**Number of particles**					
	Reacted with HEDTA		**Reacted with EDTA**		**Reacted with GLDA**	
	Initial	**Reacted**	**initial**	**Reacted**	**Initial**	**Reacted**
2.0 < 2.4	85	50	87	53	85	38
2.4 < 2.8	49193	33422	41409	27082	48451	36472
2.8 < 3.7	2981	1987	1733	980	2982	1907
3.7 < 10	316	190	313	242	326	237
Total	52575	35649	43542	28357	51844	38654

Appendix F

Table F1: Elemental mass of Guelph dolomite before and after reaction with chelating agents

Element	Mass % of element [%]			
	EDTA	HEDTA	GLDA	Initial
Carbon	11.63	11.64	11.63	11.63
Oxygen	46.48	46.52	46.47	46.49
Magnesium	3.72	3.75	3.70	3.73
Silicon	0.02	0.02	0.01	0.01
Calcium	19.46	19.43	19.41	19.44
Manganese	2.58	2.58	2.60	2.60
Iron	15.77	15.78	15.87	15.83
Total	99.66	99.72	99.69	99.73

Table F2: Calcium deportment in Guelph dolomite before and after reaction with chelating agents

Primary phases	Mass % of Calcium in phase [%]			
	EDTA	HEDTA	GLDA	Initial
Ankerite	18.86	18.87	18.98	18.85
Calcite	0.11	0.03	0.01	0.07
dolomite	0.49	0.53	0.42	0.52
Total	19.45	19.43	19.41	19.44

Table F3: Magnesium deportment in Guelph dolomite before and after reaction with chelating agents

Primary phases	Mass % of Magnesium in phase [%]			
	EDTA	HEDTA	GLDA	Initial
Ankerite	3.43	3.43	3.45	3.44
dolomite	0.29	0.32	0.25	0.29
Total	3.72	3.75	3.7	3.73

Table F4: Mineral mass in Guelph dolomite before and after reaction with chelating agents

Minerals	Mass of phase [%]			
	EDTA	HEDTA	GLDA	Initial
Ankerite	97.12	97.18	97.71	97.81
Calcite	0.27	0.07	0.03	0.30
dolomite	2.24	2.42	1.92	1.79
Quartz	0.03	0.04	0.02	0.02
Unclassified	0.34	0.28	0.31	0.25
The rest	0.01	0.01	0.01	0.01
Total	100	100	100	100

Table F5: Calcite Mineral Locking in Guelph dolomite before and after reaction with chelating agents

Locking phase	Mass % of Calcite [%]			
	EDTA	HEDTA	GLDA	Initial
Ankerite	0.24	0.05	0.02	0.25
dolomite	0.01	0	0	0.02
Free surface	0.02	0.01	0.01	0.03
Total	0.27	0.07	0.03	0.3

Table F6: Dolomite Mineral Locking in Guelph dolomite before and after reaction with chelating agents

Locking phase	Mass % of Dolomite [%]			
	EDTA	HEDTA	GLDA	Initial
Ankerite	1.27	1.36	1.11	1.10
Unclassified	0.01	0.01	0.01	0.02
Free surface	0.95	1.05	0.79	0.67
Total	2.24	2.42	1.92	1.79

Table F7: Ankerite Mineral Locking in Guelph dolomite before and after reaction with chelating agents

Locking phase	Mass % of Ankerite [%]			
	EDTA	HEDTA	GLDA	Initial
Calcite	0.08	0.02	0.03	0.03
dolomite	3.14	3.33	2.94	2.96
Quartz	0.04	0.05	0.03	0.04
Unclassified	0.45	0.40	0.49	0.5
Free surface	93.38	93.34	94.22	94.28
Total	97.11	97.18	97.71	97.81

Table F8: Grain size distribution of ankerite in Guelph dolomite before and after reaction with chelating agents

Size range (µm)	Number of grains of Ankerite					
	EDTA	Initial	HEDTA	Initial	GLDA	Initial
9.6<435	41930	41955	45960	45987	34968	34979
435<964	155	160	116	125	89	95
964<1553	44	49	63	70	80	85
Total	42129	42164	46139	46182	35137	35159

Table F9: Grain size distribution of calcite in Guelph dolomite before and after reaction with chelating agents

Size range (µm)	Number of grains of Calcite					
	EDTA	**Initial**	**HEDTA**	**Initial**	**GLDA**	**Initial**
9.6<148	223	379	271	589	284	885
148<305	5	9	0	8	0	9
305<543	1	6	1	9	0	8
Total	229	394	272	606	284	902

Table F10: Grain size distribution of dolomite in Guelph dolomite before and after reaction with chelating agents

Size range (µm)	Number of grains of dolomite					
	EDTA	**Initial**	**HEDTA**	**Initial**	**GLDA**	**Initial**
9.6<18	17622	18011	19491	19801	16243	17896
18<35	4405	4701	4983	5120	3865	4210
35<50	39	70	53	75	44	88
Total	22066	22782	24527	24996	20152	22194

Table F11: Number of Particles in Guelph dolomite Sample before and after reaction with chelating agents

Size (µm)	Number of particles					
	Reacted with EDTA		**Reacted with HEDTA**		**Reacted with GLDA**	
	Initial	**Reacted**	**Initial**	**Reacted**	**Initial**	**Reacted**
9.6< 47	47874	43995	56012	51911	44428	40418
47< 199	3778	3543	4374	4085	3343	3024
199< 520	587	440	458	354	455	291

520< 985	189	116	125	81	139	62
985< 1590	57	46	75	64	96	80
Total	52485	48140	61044	56495	48461	43875

Table F12: Particles density distribution in Guelph dolomite before and after reaction with chelating agents

Density range (g/cm^3)	**Number of particles**					
	Initial	**EDTA**	**Initial**	**HEDTA**	**Initial**	**GLDA**
2.5<2.6	192	89	217	103	132	54
2.6<2.8	3456	1964	4375	2207	3957	1730
2.8<3.0	48814	46072	56426	54168	44351	42078
3.0<6.7	20	14	16	12	21	12
Total	52482	48139	61034	56490	48458	43874

Dear Umer,

As an Elsevier journal author, you retain the right to Include the article in a thesis or dissertation (provided that this is not to be published commercially) whether in full or in part, subject to proper acknowledgment; see https://www.elsevier.com/about/our-business/policies/copyright/personal-use for more information. As this is a retained right, no written permission from Elsevier is necessary.

If I may be of further assistance, please let me know.

Best of luck with your thesis and best regards,

Laura

Laura Stingelin

Permissions Helpdesk Associate

ELSEVIER | Global E-Operations Books

+1 215-239-3867 office

l.stingelin@elsevier.com

Contact the Permissions Helpdesk

+1 800-523-4069 x3808 | permissionshelpdesk@elsevier.com

Dear Mian Umer,

Good day! Welcome to the RightsLink service of Copyright Clearance Center.

Please be advised that "**Sandstone matrix acidizing knowledge and future development**" is an Open Access article published under a **Creative Commons Attribution 4.0 International License**. This allows you to reuse the material without having to obtain permission provided that the authors and original source of publication are properly acknowledged.

To know more, please contact the publisher directly or the following link:

https://creativecommons.org/licenses/by/4.0/

If you have any further questions please don't hesitate to contact a Customer Account Specialist at 855-239-3415 Monday-Friday, 24 hours/day.

Best regards,

Rose Cabudoc
Customer Account Specialist
Copyright Clearance Center
222 Rosewood Drive
Danvers, MA 01923
Error! Hyperlink reference not valid.
+1.855.239.3415
Facebook - Twitter - LinkedIn
ref:_00D30oeGz._5000c1bbFNs:ref

Dear Mian Umer,

Thank you for your request to reproduce content from:

M U Shafiq *et al* 2017 *IOP Conf. Ser.: Mater. Sci. Eng.* **206** 012010

Mian Umer Shafiq *et al* 2017 *IOP Conf. Ser.: Mater. Sci. Eng.* **217** 012023

Kind regards,

Christina

Copyright & Permissions Team
Gemma Alaway – Senior Rights & Permissions Adviser
Christina Colwell - Rights & Permissions Assistant

Contact Details
E-mail: permissions@iop.org

Hello Mian,

I am happy to confirm that all your co-authors agree that you can include your joint papers as part of your thesis.

Regards . . . Moses

Professor Moses Oludayo Tade
PhD HonFIEAust CPEng FIChemE CEng
John Curtin Distinguished Professor

Deputy Pro Vice Chancellor | Faculty of Science and Engineering
Past President | The Australian Council of Engineering Deans (ACED)
Editor-in-Chief apjChemEng (formerly DCEMPJ)

Curtin University
Tel | +61 8 9266 4800

Email | m.o.tade@curtin.edu.au
Web | curtin.edu.au